Railway Transition Zones

An Energy Approach for Design, Evaluation and Mitigation

Jain, A.

DOI
10.4233/uuid:a55a3145-b0e6-4d95-85bb-41a6f0239e66

Publication date
2024

Document Version
Final published version

Citation (APA)
Jain, A. (2024). *Railway Transition Zones: An Energy Approach for Design, Evaluation and Mitigation*. [Dissertation (TU Delft), Delft University of Technology]. https://doi.org/10.4233/uuid:a55a3145-b0e6-4d95-85bb-41a6f0239e66

Railway Transition Zones: An Energy Approach for Design, Evaluation and Mitigation

Railway Transition Zones: An Energy Approach for Design, Evaluation and Mitigation

Dissertation

for the purpose of obtaining the degree of doctor
at Delft University of Technology
by the authority of the Rector Magnificus Prof.dr.ir. T.H.J.J. van der Hagen

by

Avni JAIN

This dissertation has been approved by the promotors.

Composition of the doctoral committee:

Rector Magnificus,	chairperson
Prof. dr. A.V. Metrikine,	Delft University of Technology, promotor
Dr. ir. K.N. van Dalen,	Delft University of Technology, promotor
Dr. ir. M.J.M.M. Steenbergen,	Delft University of Technology, copromotor

Independent members:

Prof. dr. K. G. Gavin,	Delft University of Technology
Prof. dr. P. Galvin,	University of Seville, Spain
Prof. dr. ir. R.P.B.J Dollevoet,	Delft University of Technology
Prof. dr. Lars Vabbersgaard Andersen,	Aarhus University, Denmark

Reserve member:

Dr. A. Tsouvalas	Delft University of Technology

This research is supported by the Dutch Technology Foundation TTW (Project 15968), a part of the Netherlands Organisation for Scientific Research (NWO), and which is partly funded by the Ministry of Economic Affairs.

Printed by: Uitgeverij U2pi-The Hague, the Netherlands
Front & Back: Sketches in acrylic and charcoal by Avni Jain
Cover Design: on Inkscape by Avni Jain and Yuriy Marykovskiy

ISBN 9789493364974

An electronic version of this dissertation is available at
`https://repository.tudelft.nl/`.

To my teachers

Tunnel - Track Transition

Culvert - Track Transition

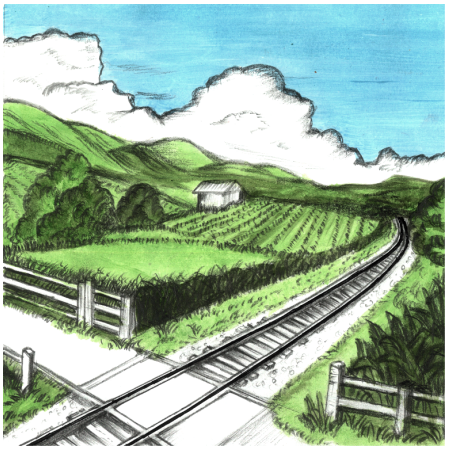

Road - Track Transition

Bridge- Track Transition

CONTENTS

Summary **xiii**

Samenvatting **xv**

1 Introduction **1**
1.1 Differential settlement and hanging sleepers . . . 3
1.2 Variation of vertical stiffness . . . 4
1.3 Design of track components . . . 6
1.3.1 Superstructure . . . 6
1.3.2 Substructure . . . 8
1.4 A comprehensive design methodology . . . 10
1.4.1 Chapter 2 . . . 12
1.4.2 Chapter 3 . . . 13
1.4.3 Chapter 4 . . . 13
1.4.4 Chapter 5 . . . 13
1.4.5 Chapter 6 . . . 13
1.4.6 Chapter 7 . . . 14
1.4.7 Chapter 8 . . . 14
1.4.8 Chapter 9 . . . 15

2 Design of railway transition zones: a novel energy-based criterion **17**
2.1 Introduction . . . 18
2.2 Methods . . . 20
2.2.1 Geometric model . . . 20
2.2.2 Numerical Model . . . 21
2.3 Results and Discussion . . . 24
2.3.1 Analysis of RTZs . . . 24
2.3.2 Design criterion . . . 31
2.4 Conclusions . . . 35

3 Evaluation of interventions: Substructure-level **37**
3.1 Introduction . . . 38
3.2 Methods . . . 40
3.3 Results and Discussion . . . 44
3.3.1 Standard embankment-bridge transition (case 1) versus horizontal approach slab (case 2) . . . 45
3.3.2 Standard embankment-bridge transition (case 1) versus inclined approach slab (case 3) . . . 47

3.3.3 Standard embankment bridge transition (case 1) versus transition wedge (case 4) . . . 48
3.3.4 Standard embankment bridge transition (case 1) versus new design: SHIELD (case 5) . . . 53
3.3.5 Transition wedge (case 4) versus SHIELD of railway transition zone (case 5) . . . 54
3.4 Conclusions . . . 57

4 Evaluation of interventions: Superstructure-level 61
4.1 Introduction . . . 62
4.2 Finite element model of an embankment-bridge transition . . . 64
4.3 Results and discussion . . . 66
4.3.1 Configuration of sleepers adjacent to the transition interface . . . 66
4.3.2 Sleeper layout . . . 68
4.3.3 Loss of contact between sleeper and ballast: hanging sleepers . . . 69
4.4 Conclusions . . . 71

5 Investigation of key phenomena governing design 73
5.1 Introduction . . . 74
5.2 Method . . . 74
5.3 Results . . . 76
5.4 Conclusion . . . 79

6 Material Optimisation: SHIELD 81
6.1 Introduction . . . 82
6.2 Evaluation of railway transition zones: Methods . . . 83
6.2.1 Finite Element Models . . . 83
6.2.2 Design space (input) . . . 86
6.2.3 Model response . . . 87
6.2.4 Polynomial Chaos Expansion (PCE) Surrogate Model . . . 88
6.2.5 Response Statistics . . . 90
6.3 Evaluation of railway transition zones: Results and Discussion . . . 91
6.3.1 Model 1 . . . 92
6.3.2 Model 2 . . . 95
6.3.3 Design Limits . . . 99
6.4 Conclusion . . . 101

7 Geometric Optimisation: SHIELD 103
7.1 Introduction . . . 104
7.2 Models . . . 107
7.2.1 Geometric model . . . 108
7.2.2 Numerical Model . . . 110
7.3 Results and Discussion . . . 115
7.3.1 Base Model . . . 115
7.3.2 Longitudinal profiles of SHIELD . . . 116
7.3.3 Transverse profiles of SHIELD . . . 117

7.3.4 Vertical profiles of SHIELD . . . 119
7.4 Summary of results . . . 120
7.5 Conclusions . . . 121

8 Evaluation for critical conditions: SHIELD 123
8.1 Introduction . . . 124
8.2 Models . . . 126
8.2.1 Geometry and zones under study . . . 126
8.2.2 Materials . . . 127
8.2.3 Mesh details . . . 127
8.2.4 Interface conditions . . . 127
8.2.5 Loads . . . 128
8.2.6 Cases studied . . . 129
8.3 Results and discussion . . . 129
8.3.1 Influence of velocity (speed and direction of moving load) . . . 131
8.3.2 Moving mass versus moving load . . . 133
8.3.3 Influence of track imperfections on SHIELD's performance . . . 134
8.3.4 Influence of vehicle . . . 136
8.4 Conclusions . . . 137

9 Evaluation: another transition type 139
9.1 Introduction . . . 140
9.2 Models . . . 140
9.2.1 Standard embankment-bridge transition without any transition structure . . . 141
9.2.2 Safe hull inspired energy limiting design: SHIELD . . . 142
9.3 Results . . . 143
9.3.1 Ballast . . . 143
9.3.2 Embankment . . . 144
9.3.3 Subgrade . . . 145
9.4 Discussion . . . 145
9.5 Conclusions . . . 147

10 Design of Experiment 149
10.1 Laboratorio de Geotecnia – CEDEX [1] . . . 149
10.2 Project description: . . . 151
10.2.1 Objectives . . . 151
10.2.2 Experimental Methodology . . . 152
10.2.3 Conclusion . . . 154
10.2.4 Current Status . . . 154

11 Conclusions and future scope of works 155

SUMMARY

Railway tracks are subjected to constant degradation in terms of geometry, and wear and tear of the track components (rails, sleepers, fasteners, trackbed layers, etc.). Over the years, trains have evolved immensely, but the track infrastructure has not kept pace. With rapid advancements in vehicle technologies, the design of rail infrastructure must cope with the challenges associated with the operation of railway tracks. In addition, railway transition zones (RTZs) degrade even faster (4-8 times) than normal tracks, leading to higher maintenance and operational costs. RTZs are areas where railway tracks cross stiffer structures (e.g., roads, bridges, culverts). The amplified degradation in RTZs is mainly attributed to abrupt changes in vertical stiffness and to differential settlement, resulting in amplified and non-uniform track responses. Even though the dynamic behavior of RTZs differs from that of normal tracks, the design of track components in these zones remains similar to normal tracks, with some modifications at the superstructure and/or substructure levels to mitigate the transition effects. There have been several attempts to mitigate the adverse effects of dynamic response amplification in RTZs, but they have proven either marginally effective or counterproductive. Therefore, a comprehensive design methodology for RTZs is needed that addresses the main degradation mechanisms leading to amplified degradation of these zones.

In this paper-based thesis, a novel methodology is proposed to design and evaluate railway transition zones. For this purpose, detailed analysis and design optimization is performed for a bridge-embankment transition using various two-dimensional and three-dimensional finite element models, different vehicle models, and surrogate models (using polynomial chaos expansion). Firstly, the proposed methodology establishes a robust design criterion to design and evaluate RTZs. The criterion relates the magnitude and uniformity (spatial and temporal) of the total strain energy in the trackbed layers to the permanent deformation of RTZs. This novel energy-based criterion is used to evaluate the most commonly used mitigation measures at the superstructure and substructure levels and to investigate the key phenomena governing RTZ design. Based on insights obtained from these analyses, a preliminary design of a novel transition structure called SHIELD (Safe Hull-Inspired Energy Limiting Design) is proposed. The second phase of the work is dedicated to identifying the most influential design parameters leading to optimized geometry of SHIELD and the desired material characteristics. The third phase involves the performance evaluation of optimized SHIELD subjected to critical loading conditions (e.g., critical and supercritical velocities, different directions of movement, hanging sleepers, non-straight rail) and SHIELD is shown to be a robust design solution for all conditions under study. In the end, the use of SHIELD is extended to another type of an embankment-bridge transition (with ballast running over the bridge) where it is shown to be equally (compared to embankment-bridge transition with no ballast layer

over the bridge) efficient in mitigating the transition effects, and a laboratory experiment is designed to test the effectiveness of the proposed design criterion and methodology.

A robust design methodology for RTZs is proposed in this work, which aims to minimize operation-induced degradation and can be adapted to different transition types and site-specific conditions. A preliminary optimized design of SHIELD is proposed, which has been shown to be effective in mitigating dynamic amplifications in RTZs under both ideal and non-ideal conditions. The results and conclusions presented in this work demonstrate the promise of SHIELD as an intervention for railway transition zones, outline the next steps toward its practical implementation, and highlight the challenges that need to be addressed in future research.

SAMENVATTING

Spoorwegen zijn onderhevig aan voortdurende degradatie van de spoorweggeometrie en aan slijtage van de spoorcomponenten (rails, dwarsliggers, railklemmen, de lagen in het baanlichaam, etc.). In de loop van de jaren zijn treinen enorm ontwikkeld, maar de ontwikkeling van de spoorweginfrastructuur is achtergebleven. Gegeven de snelle vooruitgang in voertuigtechnologieën moet het ontwerp van de spoorweginfrastructuur omgaan met de uitdagingen die gepaard gaan met het gebruik van de spoorwegen. Bovendien degraderen overgangszones (RTZs) in de spoorweginfrastructuur nog sneller (4-8 keer) dan de reguliere spoorweginfrastructuur, wat leidt tot hogere onderhouds- en operationele kosten. RTZs zijn zones waar spoorwegen stijvere constructies kruisen (bijv. die behorend bij wegen, bruggen, duikers). De versnelde degradatie in RTZs komt voornamelijk door abrupte veranderingen in de verticale stijfheid en door verschilzettingen, resulterend in vergrootte en ongelijkmatige responsies van de spoorweginfrastructuur. Hoewel het dynamische gedrag van RTZs verschilt van dat van de reguliere spoorweginfrastructuur, is het ontwerp van spoorcomponenten in RTZs vergelijkbaar gebleven met die van de componenten in de reguliere spoorweginfrastructuur, met enkele aanpassingen op het niveau van de bovenbouw en/of onderbouw om de overgangseffecten te beperken. Er zijn verschillende pogingen ondernomen om de nadelige effecten van dynamische responsievergroting in RTZs te verminderen, maar deze blekken ofwel een marginaal effectief of zelfs contraproductief. Er is daarom een omvattende ontwerpmethodologie voor RTZs nodig die de belangrijkste degradatiemechanismen leidend tot versnelde degradatie in deze zones in beschouwing neemt.

In dit proefschrift, wat is gebaseerd op artikelen, wordt een nieuwe methode voorgesteld voor het ontwerpen en evalueren van overgangszones in spoorwegen. Hiervoor worden een gedetailleerde analyse en ontwerpoptimalisatie uitgevoerd voor een overgang tussen een brug en baanlichaam met behulp van verschillende twee- en driedimensionale eindige-elementmodellen, verschillende voertuigmodellen en surrogaatmodellen (gebaseerd op zgn. polynomial chaos expansion). Ten eerste wordt in dit werk, als deel van de nieuwe ontwerpmethode, een robuust ontwerpcriterium voor het ontwerp en de evaluatie van RTZs opgesteld. Dit criterium relateert de grootte en uniformiteit (zowel ruimtelijk als in de tijd) van de totale energie in de verschillende lagen in het baanlichaam aan de permanente vervormingen in RTZs. Het nieuwe, op energie gebaseerde criterium wordt vervolgens gebruikt om de meest gangbare mitigatiemaatregelen, toegepast op het niveau van de bovenbouw en onderbouw, te evalueren en om de belangrijkste verschijnselen te onderzoeken die van invloed zijn op het ontwerp van RTZs. Op basis van de uit deze analyses verkregen inzichten wordt het voorlopig ontwerp van een nieuwe overgangsconstructie, genaamd SHIELD (Safe Hull-Inspired Energy Limiting Design), gepresenteerd. De tweede fase van het werk richt zich op het identificeren van de meest invloedrijke

ontwerpparameters die leiden tot een optimalisatie van de geometrie van SHIELD en van de materiaaleigenschappen. De derde fase omvat de prestatie-evaluatie van het geoptimaliseerde SHIELD onder kritische belastingscondities (bijv. kritische en superkritische snelheden, verschillende rijrichtingen, blinde vering, onvlakke rails). SHIELD blijkt een robuuste ontwerpoplossing te zijn onder alle bestudeerde omstandigheden. Tenslotte wordt SHIELD toegepast voor een ander type overgang tussen baanlichaam en brug (met ballastlaag op de brug), waarbij de nieuwe overgangsconstructie even effectief blijkt te zijn (als voor de baanlichaam-brug overgang zonder ballastlaag op de brug) in het beperken van de overgangseffecten. Ook wordt het ontwerp van een laboratoriumexperiment gepresenteerd dat als doel heeft de effectiviteit van het voorgestelde ontwerpscriterium en van de ontwikkelde methodologie te testen.

In dit werk is een robuuste ontwerpmethodologie voor RTZs opgevoerd die tot doel heeft de door gebruik veroorzaakte degradatie te minimaliseren. Deze kan worden aangepast voor verschillende overgangstypen en voor locatie-specifieke omstandigheden. Een voorlopig, geoptimaliseerd ontwerp van SHIELD is gepresenteerd, waarvan is aangetoond dat het effectief is in het beperken van dynamische vergrotingen in RTZs onder zowel ideale als niet-ideale omstandigheden. De resultaten en conclusies van dit werk tonen het potentieel van SHIELD aan als interventie voor overgangszones in spoorwegeg, schetsen de vervolgstappen richting praktische implementatie en belichten de uitdagingen die in toekomstig onderzoek moeten worden aangepakt.

1

INTRODUCTION

Railway tracks are subjected to constant degradation over the operational period. In addition to this, railway transition zones degrade about 4-8 [1] times faster than the open track leading to high maintenance and operation costs. Moreover, in the Netherlands, it is estimated that 40% of the maintenance costs are associated with preserving the geometry of railway tracks [1, 2]. Transition zones in railway tracks can be generally described as structural and geometrical variations along the track which are potentially vulnerable to deterioration causing an increase in the cost of maintenance of these zones. More specifically, transition zones are areas where the railway track crosses a different transportation modality (road, waterway, etc.) or where the rail experiences major changes in the type of track support structure. The most common types of transitions (Figure 1.1) are embankment - bridge transition [3–19], transition with culvert [20], embankment - bridge with approach slabs [10] and transition with culvert and approach slabs [1, 21, 22], embankment-bridge transition with a wedge-shaped backfill [7, 9, 23], railroad crossing [24, 25], and transition with underpass [26, 27].

Over the years, several studies [29–35] have suggested that strong amplifications in stresses and strains are induced by axles of the train moving over the inhomogeneity along the longitudinal direction of the railway track. This inhomogeneity can be attributed to changes in geometry, discontinuity in forces, the configuration of track components, and the constitutive properties of the materials. These variations are inherent characteristics of transition zones and are believed to be major reasons for rapid degradation in these zones. Track degradation has been defined and categorized in several works done in the past [36] and can be mainly described as damage of track components [2, 36–39] (rail surface defects, broken fasteners, cracks in concrete sleepers, breakage of ballast particles etc.) and deterioration of track geometry [37, 40–42]. The operation-induced dynamic response amplification leads to phenomena like but not limited to rapid compaction/ densification, abrasion and crushing of ballast, and increased settlement of embankment and subgrade layers, eventually leading to the occurrence of hanging sleepers in the vicinity of the transition interface. Several studies have related these phenomena in transition zones to two reasons [3, 13, 17]: uneven track stiffness and differential settlement. Some other detailed studies [10, 37, 38] on railway transition zones (RTZs) classify the factors as listed below:

Figure 1.1: Most common types of railway transitions zones [28].

- Primary factors: uneven track stiffness, geotechnical issues, subgrade failure, progressive shear failure, excessive plastic settlement, soil water response, wetting and shrinkage cycles.

- Secondary factors: height of embankment, type of bridge joint, type of abutment in the approaching structure, axle load, and train speed.

The primary factors listed above, in essence, can be reduced to uneven track stiffness and differential settlement. According to several studies, [3, 5, 17, 24, 30–33, 43, 44] the uneven track stiffness is one of the most influential factors leading to degradation in RTZs. The factors like soil water response, wetting and shrinkage cycles lead to changes in elasticity modulus and frictional properties of track components [4, 17] and eventually contribute to uneven track stiffness. Likewise, the remaining primary causes in the above-mentioned list namely geotechnical issues, subgrade failure, progressive shear failure, and excessive plastic settlement ultimately result in the differential settlement. The secondary factors listed above can be attributed to the type of transition and vehicle characteristics under consideration. These factors can be dealt with a robust design solution for specific site conditions.

To conclude the above discussion, the main factors that lead to an increased degradation in RTZs are uneven track stiffness and differential settlement. However, uneven track stiffness and differential settlement are not independent of each other [2] but lead to self-perpetuating mechanisms. In addition to this, the uneven track stiffness is claimed to be a reason for 'initiation' [3, 5, 17, 24, 30–33, 43, 44] mechanisms (transition radiation

[45–49]) that lead to the rapid degradation of railway transition zones. Several attempts have been made in past to minimize the degradation in transition zones. However, the track components or track-bed layers in the transition zones are designed similarly to open tracks with some interventions addressing the uneven track stiffness or differential settlement. Some of the most studied interventions to mitigate transition effects include auxiliary rails [43, 50–52], larger and closely spaced sleepers [43, 52–58], optimised rail pads [51, 53, 55, 59, 60], approach slabs [21, 22, 61–63], wedge-shaped backfills [64–69] etc. However, these measures proved to be inefficient as there is a lack of understanding of the design requirements for a robust mitigation measure aimed at minimizing the degradation in RTZs. An effective design solution demands the identification of the most influential parameters governing the design, an understanding of the key phenomena behind the amplified degradation of RTZs and a robust design/ evaluation criterion.

In the following sections, firstly, the two main factors (stiffness variation and differential settlement) discussed above will be elaborated based on the literature. Secondly, the existing practices adopted for the design of track components (rail, softening pads, sleepers, ballast, embankment and subgrade) in RTZs are discussed. Finally, the methodology proposed in this work to design RTZs is summarised.

1.1. DIFFERENTIAL SETTLEMENT AND HANGING SLEEPERS

One of the two major factors that contribute to the rapid degradation of railway transition zones is the phenomenon of differential settlement which leads to uneven track levels in these zones [70, 71]. This unevenness in track level is inevitable at transition zones as ballasted railway tracks will typically have a significant settlement as a result of permanent deformations (static) of the trackbed layers and a negligible settlement of the bridge or structure on pile foundation [72]. However, reducing the dynamic amplifications in these zones can delay the process of degradation and settlement (dynamic) resulting in less frequent maintenance and associated costs. Periodic measurements of relative transient and permanent vertical displacements were performed at various depths and locations along the vertical plane of the railway track [71]. The results in (Figure 1.2) show that the majority of permanent vertical displacements occur in the region between the sleepers and the bottom of the ballast layer. The amplified degradation in RTZs is mainly due to the occurrence of hanging sleepers as a consequence of differential settlement [70, 71]. Over the years several studies have been conducted both experimentally [73–75] and numerically [44, 72, 73, 76–78] to study the amplification of loads/ stresses due to hanging sleepers or voids between sleeper and ballast layer. Even though the hanging sleepers are found not only in transition zones but throughout the ballasted track, their occurrence is more likely in RTZs. In the study reported in [72, 78], it is found that one single hanging sleeper with a 1 mm gap between sleeper and ballast can cause the sleeper-ballast contact force at the sleeper adjacent to the hanging one to increase by 70% and the displacement by 40%. Consequently, this uneven loading of the ballast bed may induce non-uniform settlement of the trackbed worsening the problem even further. The worst case in an open track, considering the local settlement, was identified as when one supported sleeper was surrounded by two unsupported sleepers. Hanging sleepers also tend to increase the

stresses (nearing 40 %) experienced by the rail in the vicinity of the void [77]. The effect of hanging sleepers was proved to have a far more significant effect on the forces imposed on the track components than on the wheel-rail contact force.

To summarize this discussion in the context of transition zones, it can be concluded from the literature that the occurrence of hanging sleepers cannot be avoided but can be delayed by minimizing the operation-driven dynamic response amplification of the track components and hence delaying the process of differential settlement or unevenness in track level. In addition to this void identification methods can be helpful in determining the need for maintenance [73] and controlling the occurrence of hanging sleepers.

1.2. VARIATION OF VERTICAL STIFFNESS

Track stiffness is an important factor to consider when designing railway infrastructure since it impacts the loads transmitted to the track. On one hand, low stiffness leads to relatively large displacements, which in turn may lead to excessive settlement. On the other hand, very high stiffness values can lead to excessive dynamic overloads [79] and ultimately lead to track wear and fatigue. Hence, it is very important to find an optimal value of the vertical track stiffness for the speeds under consideration. In this section, firstly the importance of choosing an optimum track stiffness is discussed and then the influence of an abrupt change in vertical track stiffness on the track performance is highlighted.

It has been found that the subgrade soil condition (poor, moderate or good), ballast/ sub-ballast thickness and vertical stiffness of sleepers are the most influential factors that affect track stiffness whereas the track maintenance procedures like rail surfacing and ballast tamping have negligible effect in comparison. The effect of each track component on track modulus is studied in [80]. Track modulus is defined [80] as a measure of the vertical stiffness of the rail foundation. The correlations between track modulus and vertical deflections of rail, sleeper, and sub-grade have been studied in the past and it was found that an increase in track modulus results in a reduction of vertical deflections. The studies [80] also show that an increase in the track modulus results in an increase of the maximum vertical stress and the maximum deviator stress at the subgrade surface. Although the higher track modulus leads to higher stresses in the subgrade, it does not imply a poorer track performance as it depends not only on the generated stresses but also on the soil strength. A higher track modulus also implies a stiffer subgrade and hence a higher strength to resist the higher stresses. The value of track modulus that is optimum to ensure no excessive stresses and deformation depends on many factors which will be discussed in detail in the following sections.

The above discussion highlights the importance of choosing the appropriate track stiffness for optimal performance of a track and the associated challenges in doing so. In addition to this, RTZ design is even more sensitive to fluctuations in track stiffness as an abrupt stiffness variation in these zones is a major cause for initiation of the mechanisms leading to amplified degradation in these zones. Several attempts have been made in the

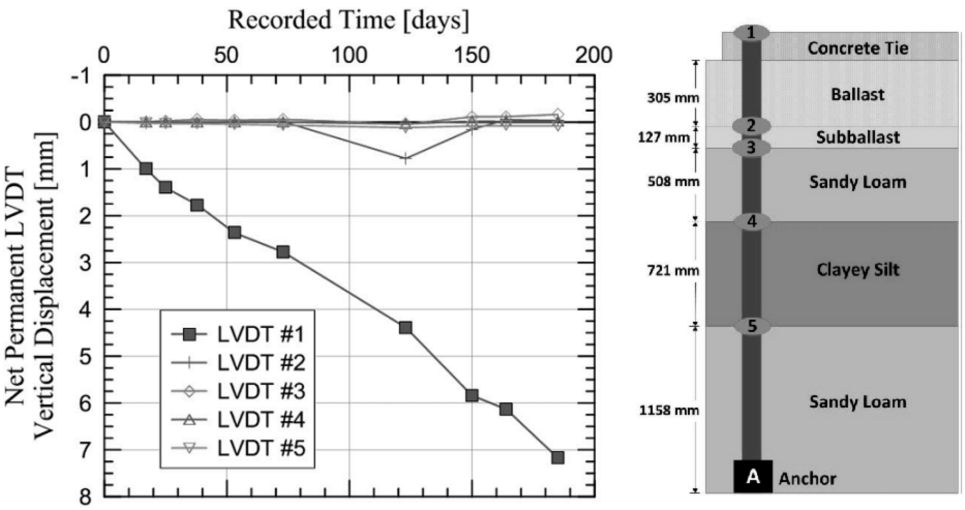

Figure 1.2: Net permanent vertical displacements for different depths (left), location of measurement devices (right) [71].

past to provide a gradual stiffness gradient in these zones to minimise the degradation. Despite these attempts at smoothening the variation [24] in vertical stiffness along the longitudinal direction of the track by either increasing the stiffness on the softer side or by decreasing the stiffness of the stiffer side, the benefits were limited. The approach that involves a decrease in stiffness on the stiffer side was not effective in the mitigation of excessive settlement of subgrade due to heavy axle load and other factors [10]. At the same time increasing the stiffness on the softer side led to a smoother stiffness transition and decrease in displacements but can lead to an increase in stresses. Moreover, there is a lack of understanding about the required uniformity of the system properties in the longitudinal direction to avoid or substantially reduce degradation. There have been some trials both at the site and in numerical models to propose and test the mitigation measures aiming at gradual change of stiffness along the longitudinal axis of the track. The most popular ones include transition wedges, improvement of foundation by insertion of piles and approach slabs. The transition wedges are aimed at smoothening the track transition [64–69] and were proved to be effective to some extent for embankment bridge type of transition zone [52]. But, for an effective implementation of transition wedges, a detailed analysis is required to make recommendations for thickness, slope, material and layer distribution of the wedge [81]. A comparative study of different wedge transitions based on material configuration and geometric shapes can be found in [65]. Some studies [82] have found an exponential increase in degradation after a year of operation for transition zones with wedges. In RTZs, ground improvement techniques include the insertion of piles which not only provide a gradual stiffness transition but also reduce the settlement on the softer side of these zones. The piles can be of different materials like concrete, steel, gravel, timber, sand or stone columns and depending on the length and material of these piles [55] the costs associated with this particular intervention can be very high. The

effectiveness of piles at a transition zone must be ensured by arranging them in a proper pattern and by varying their lengths depending on the requirements of the particular transition. This could possibly prove to be an effective mitigation measure provided that it is well-designed and implemented for each specific transition zone. The construction of horizontal or inclined approach slabs [21, 22, 61–63] on both sides of the structure in railway transition zones is the most common practice in Europe to achieve a smoother transition. However, recent research by [62] shows that the track on an approach slab has about four to eight times higher vertical displacements than on an embankment and culvert, respectively. It is reported [83] in a detailed study that these higher displacements could be due to hanging sleepers above the approach slab and the tracks rocking under train movement due to a pivoting action of the approach slabs around the edges of the stiff culverts, all of which leads to high impact loading.

A detailed overview of the above-mentioned mitigation measures can be found in [37, 38] and the authors in [37] conclude that these mitigation measures have been utilized without adequate theoretical reasoning, and therefore cannot overcome the need for frequent maintenance. Although these mitigation measures or design practices aim towards reducing the inhomogeneity in RTZs, they have been implemented without any knowledge of the required uniformity of the system properties or tolerance of the track components towards amplified stresses. An optimum solution must ensure that all the track components are within the allowable limits of stresses and deformations to insure a reduced degradation and maintenance in long term. The following section will discuss the current design practices and mitigation measures concerning each track components in detail.

1.3. DESIGN OF TRACK COMPONENTS

The following sections discuss the standard design practices for each track component, performance evaluation in the context of transition zones and mitigation measures implemented in the past related to each of these track components. The following critical components of railway tracks and more specifically transition zones will be discussed in this section:

1. Superstructure: rail, sleepers
2. Substructure: ballast, embankment, sub-grade or natural terrain

1.3.1. SUPERSTRUCTURE

RAIL

The rail behaves as a beam when low frequency (upto 100 Hz) deformations are considered and can be characterized through the bending stiffness and mass. The standard rail sections used in Europe are 54E1 and 60E1 (Figure 1.3). The mechanical properties of these standard rail profiles are listed in (Table: 1.1).

Table 1.1: Geometric and physical properties for the 54E1 and 60E1 rail profiles, EN13674-1, 2011.

Rail profile	**54E1**	**60E1**
Cross-sectional area [cm^2]	69.77	76.70
Linear mass [kg/m]	54.77	60.21
Moment of Inertia, x-x axis [cm^4]	2337.9	3038.3
Section modulus - head [cm^3]	278.7	333.6
Section modulus - base [cm^3]	311.2	375.5
Moment of Inertia, y-y axis [cm^4]	419.2	512.3
Section modulus, y-y axis [cm^3]	59.9	68.3

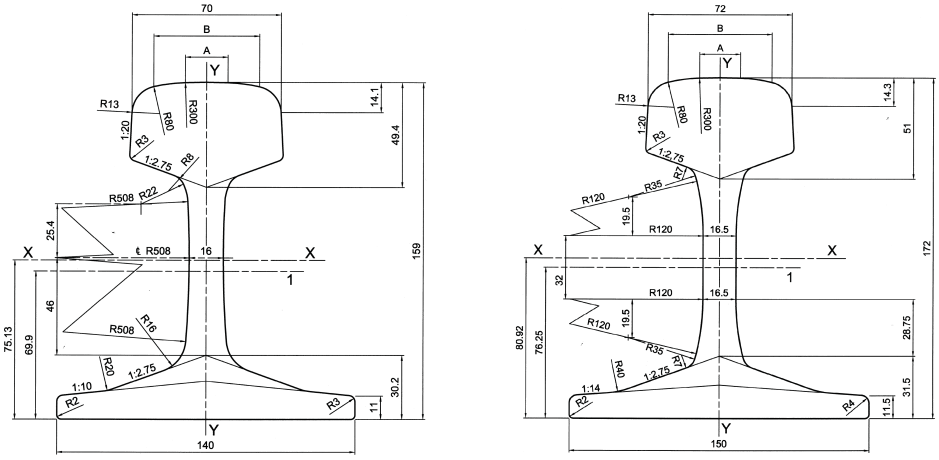

Figure 1.3: 54E1 (left) 60E1 (right) (EN 13674-1, 2011. Dimensions in millimetres)

Despite the fact that the stresses, deformations and wheel-rail interaction forces in transition zones at the rail level are much higher compared to the open tracks, the geometric and physical properties used to design the rail profiles in these zones are the same as in open tracks. An increase in the height of the rails can result in a higher bending stiffness which may imply a better distribution of loads, reducing the settlement of sleepers and the support layers (substructure) as suggested in the literature. Even so, it is not a common practice to adopt different rail sections.

Design modifications concerning rails that have been implemented include the use of auxiliary rails [43, 50, 51, 84] aimed at improving the bending stiffness of the track and reducing the stress in the ballast by guaranteeing a better distribution of loads over the sleepers [52]. A comparison of rail deflections for different numbers of auxiliary rails (0,2,4,6) was made and it was concluded that the use of two auxiliary rails leads to lower rail deflection variations for all analyzed speeds [51]. The addition of more than two auxiliary rails further decreases the rail deflection variation along the railway transition but the reduction is negligible. Numerical models suggest that the amplification of rail

deflections in transition zones relative to open tracks changed from 35-40% (low-high velocity) to 28-33% by the usage of auxiliary rails. However, site measurements show a negligible effect of auxiliary rail on the degradation of RTZs. Even though the studies suggest a reduction in vertical rail displacements by adding additional rails, its influence on the permanent deformations of the track-bed layers is minimal.

SLEEPERS

Sleeper dimensions of 2.6 m x 0.24 m x 0.24 m and a spacing of 0.6 m is a standard for railway tracks, and the same dimensions are also used in the case of transition zones most often. However, larger in size [43] and closely spaced sleepers were used in the transition area [55, 57, 58] to reduce the abrupt change in track stiffness. The larger sleepers were effective in reducing the ballast settlement and providing a better distribution (over a larger area) of contact force between sleeper and ballast [52, 57]. However, these design modifications did not affect dynamic load amplification in the transition zones [56]. An analysis of different sleeper configurations at a ballasted track-slab track transition was done to evaluate track support separation in the vicinity of the slab track while maintaining good track performance, which is assessed in terms of sleeper vertical displacements and stresses on ballast [54]. In addition to these, efforts have been made to minimize the maximum wheel-rail contact force and the maximum pressure between sleeper and foundation [53] so as to obtain the most efficient distributions of sleeper spacing (and rail pad stiffness) adjacent to the transition. These superstructure-level mitigation measures are of great interest as they are cost-effective and installation of such interventions is easy and straightforward. However, in all these studies, the solutions have not been studied or evaluated for long-term performance. Also, the effect of these measures is limited to reduced responses at the rail level or sleeper ballast interface and it does not necessarily ensure or verify reduced degradation in ballast, embankment and subgrade.

SOFTENING PADS

The other solutions that are easily implemented at the superstructure level are rail-pads and under sleeper-pads. The usage of rail pads improves the damping properties of the track [51, 53, 55, 59, 60] and under sleeper pads mitigate the transition effects by minimising the dynamic load impact [5, 39, 56, 58–60, 85–87]. Although both rail pads and under sleeper pads have been effective to some extent in reducing vertical rail displacements and/ or contact forces, their performance has been unsatisfactory based on a low benefit-cost ratio. Moreover, the influence of these pads on the permanent deformation of track-bed layers in RTZ is limited.

1.3.2. SUBSTRUCTURE

BALLAST

The ballast is the most vulnerable component of the track in transition zones, and unfortunately, the major part of the rail infrastructure consists of the ballasted track. Ballast is widely used in railway tracks due to the fact that it helps to distribute the loads to the underlying soil, dampens the dynamic loads and provides rapid drainage at low cost

[88]. The degradation of the ballast layer was found to be the primary source of track settlement based on an analysis of the track settlement data (or permanent deformation) at the instrumented sites. Generally, ballast layers accounted for over 50% of the transient deformations experienced by the track under train load, based on a quantitative analysis of each layer's contribution [89].

The required depth of the ballast beneath the sleepers depends on the track use and operation requirements [90]. As a general rule, the minimum acceptable depth of ballast is 150 mm [90] and the recommended depth is 250 mm to 300 mm [88, 90] but it can go up to 500 mm for high-speed trains. Moreover, to ensure the lateral stability of the track, shoulder width and slope are two important parameters that play a major role. For speeds lower than 160 km/h, the recommended width is between 450 mm-500 mm and larger widths (700 mm) must be adopted for higher speeds [91]. As for the slope of the ballast shoulder, an inclination of 2:3 (33 degrees) is recommended which is lower than the average angle of internal friction of crushed stone ballast, to ensure ballast bed stability. In the end, different depths of ballast result in different vertical track stiffness and improper geometry (width and slope) leads to running away of ballast and these must be checked for their influence on the performance of RTZs. Although these standards have been established for years now, they refer to specifications for normal track conditions and have not been particularly designed for transition zones.

In RTZs, design modifications that have aimed at reducing the dynamic effects on the ballast include concrete confinement walls and glued ballast. On one hand some studies [55, 92] have shown that these measures are effective in dealing with problems like reduction in lateral movement and loosening of ballast. On the other hand, some results [38] have proved them to be counterproductive as increased confinement leads to an increased ballast breakage. Also, some studies have claimed that the use of hot mix asphalt under the ballast [55, 67, 92, 93] reduces the stress in the ballast [94] and subgrade [95], increases drainage capacity of tracks [67], and hence reduces maintenance cycles. There is however no evidence of these measures being effective in mitigating the operation-induced amplified degradation in RTZs.

EMBANKMENT AND SUB-GRADE

The required depth of the embankment or sub-ballast beneath the ballast layer is 150 mm to 450 mm [88] and the minimum acceptable depth of sub-ballast is 100 mm. Underlying the ballast bed and embankment, there is natural soil at the site of the railway track or another granular material that can be used to replace natural soil for better track performance. The subgrade must have sufficient bearing strength and stiffness to support the weight of the rail track structure and the vehicle loads, and have high compactness to minimize the settlements due to these loads [88, 90].

The design standards and specifications mentioned above are the basis for the design of ballasted railway tracks but for the design requirements of transition zones specifically, a detailed analysis to determine the optimal material properties of these track bed layers

is lacking in the literature.

The authors in [96] have developed mathematical expressions to obtain vertical track stiffness as a function of height of the embankment (h_{EM}) and the modulus of elasticity of the embankment (E_{EM}) and natural ground (E_{NG}). This has been done by graphical analysis of results from a finite element simulation of the track using elastic rail, rail-pads and sleepers and perfectly elasto-plastic ballast, embankment and natural ground. In total 120 possible combinations of h_{EM} (3, 5, 7, 10 m), E_{EM} (25, 40, 60, 80, 160 MPa), E_{NG} (25, 40, 60, 80 MPa) with and without formation layer (E_{FL}) of 0.6 m and a fixed depth of 6 m for natural terrain were studied. The study concludes that the equivalent vertical stiffness depends on the height of the embankment and on the combination of the elasticity modulus of the embankment and natural soil. The results of [79, 96] emphasized the importance of geometric (depths and slopes) and physical properties (elasticity modulus) of ballast, embankment and natural terrain on the vertical track stiffness (static) and established important relationships and design recommendations. At the same time, these studies have been performed with an assumption that for stiffness (K) ranging from 50-60 kN/mm, the dynamic value of K is only 2% larger than the static value. Additionally, the identification of influential geometric and material parameters of the embankment and the subgrade layer that significantly affect the dynamic response of the RTZs is lacking and hence the choice of studied parameters has no basis. Moreover, the studies discussed above are all aimed at establishing standard height and elastic modulus of embankment and subgrade for ballasted railway tracks and the standard values of these parameters are unknown for RTZs. As these parameters eventually affect the vertical track stiffness, they are bound to influence the behaviour of RTZs and need to be investigated.

1.4. A COMPREHENSIVE DESIGN METHODOLOGY

To summarise the discussion presented thus far and establish a common ground for the subsequent work on developing a comprehensive design methodology, the following points can be drawn out:

- The abrupt change in vertical stiffness and differential settlement are the main reasons for amplified response in transition zones. On the one hand, the difference in autonomous settlement of the ballasted track and the concrete structure is unavoidable. On the other hand, the operation-driven dynamic amplifications due to abrupt changes in vertical stiffness can be controlled to a great extent with a robust design solution. The consequences of the autonomous differential settlement must be controlled by advanced monitoring systems and timely maintenance (ensuring straightness of the track).

- No existing design practices aim at a specialized design of all track components considering their interaction with each other, to address the mechanisms associated with amplified degradation of RTZs. The existing design involves mitigating the transition effects either at the substructure or superstructure level.

- Different track components affect the equivalent vertical track stiffness to various degrees. Geometry and material parameters of trackbed layers significantly affect the vertical track stiffness and the track performance. However, the effects of these are unknown for RTZs.
- There is no design methodology that aims towards the reduction of both induced stresses and deformations in "all" track components simultaneously for RTZs.
- There is a lack of clarity regarding the mechanisms leading to an amplified stress-strain state in transition zones.
- The current literature lacks consensus and required information on an appropriate criterion for the evaluation/ design of RTZs.
- A comprehensive evaluation of existing mitigation measures using one single criterion is missing in the literature.
- The behaviour of RTZs is sensitive to critical load states like changes in load velocity.

The objective of this work is to propose a comprehensive design methodology that establishes a robust design/ evaluation criterion, identifies the design parameters (material and geometric), and evaluates the performance of a railway transition zone equipped with the newly proposed transition structure for critical loading conditions.

Based on the points mentioned above and the insights obtained from the existing literature, it is established that there is a need for a comprehensive (involving formulation of design criterion and identification of influential parameters and the key phenomena governing design) design methodology to deal with the problem of amplified degradation in railway transition zones. Figure 1.4 shows the systematic methodology proposed in this work for the design of a transition structure aimed at minimizing the operation-driven degradation of RTZs. Moreover, it is highlighted that uniformity in the track response (leading to uniform track geometry) is desired for the optimum long-term performance of RTZs. In the following paragraphs, the work done in each step of the proposed design methodology is summarised. The first step (Chapter 2) in the proposed methodology is the formulation of a criterion for the design and evaluation of RTZs. A comprehensive criterion is proposed in Chapter 2, and it is used to evaluate the performance of the existing mitigation measures on both substructure (Chapter 3) and superstructure (Chapter 4) level. On one hand, the evaluation of existing mitigation measures on the superstructure level (large or closely spaced sleepers) prove them to be inefficient according to the proposed criterion. On the other hand, the evaluation of interventions aiming at gradual vertical stiffness change at the substructure level in RTZs like approach slabs and traditional transition wedge prove that smoothening the stiffness gradient only cannot lead to mitigation of dynamic amplifications in RTZs. It is found that these mitigation measures are inefficient as they channel energy to the different parts of the system that are prone to degradation. This motivates the investigation of key phenomena of energy absorption and uniform energy distribution within the trackbed layers in Chapter 5. The results of these above-mentioned investigations (Chapter 3, 4 and 5) are the basis of the

preliminary design of the transition structure. This preliminary design aims at guiding the energy away from the transition zones such that the energy is neither concentrated nor obstructed in any part of the system and maintains a smooth stiffness gradient at the same time. A two-dimensional model of an embankment-bridge transition equipped with a safe hull-inspired energy limiting design (SHIELD) is used to evaluate this new mitigation measure against the traditional mitigation measures for ideal (straight track) and non-ideal conditions (with hanging sleepers). SHIELD outperforms all the most commonly used mitigation measures like horizontal and inclined approach slabs, transition wedges and modified sleeper spacing and configurations. The preliminary design is then subjected to rigorous optimisation and verification processes. The optimisation is mainly carried out in two parts for parameters associated with material characterization (Chapter 6) and geometry (Chapter 7) using surrogate models obtained by polynomial chaos expansion and various three-dimensional finite element models respectively. Subsequently, the optimised design of SHIELD is subjected to critical loading conditions (Chapter 8) to propose the final design of the transition structure for the embankment-bridge transition under study. In Chapter 9, the proposed design methodology (Figure 1.4) is extended to another type of an embankment-bridge transition where the ballast layer continues over the bridge demonstrating a wider applicability of the proposed design methodology and the possibility of applying the same design principles and methods to the other types of railway transition zones. In the end, a design of the experiment (Chapter 10) is presented aimed at verification of the proposed design criteria and the final design of the transition structure (SHIELD).

The following subsections discuss briefly the contents of the chapters presented in this work.

1.4.1. CHAPTER 2

In this chapter, a two-step approach is presented for the formulation of a preliminary design criterion to delay the onset of processes leading to uneven track geometry in RTZs. Firstly, a systematic analysis of each track component in an RTZ is performed by examining spatial and temporal variations in kinematic responses, stresses and energies using a finite element model of an embankment-bridge transition. Secondly, the study proposes an energy-based criterion to be assessed using a model with linear elastic material behaviour and states that amplification in the total strain energy in the proximity of the transition interface is an indicator of increased (and thus non-uniform) degradation in RTZs compared to the open tracks. The correlation between the total strain energy (assessed in the model with linear material behaviour) and the permanent irreversible deformations is demonstrated using a model with non-linear elastoplastic material behaviour of the ballast layer. In the end, it is claimed that minimising the magnitude of total strain energy will lead to reduced degradation and a uniform distribution of total strain energy in each trackbed layer along the longitudinal direction of the track will ensure uniformity in the track geometry.

1.4.2. CHAPTER 3

This chapter aims to evaluate the efficacy of the most commonly used substructure-level mitigation measures and propose a novel Safe Hull-Inspired Energy Limiting Design (SHIELD) of a transition structure. Firstly, the traditional transition structures, including horizontal and inclined approach slabs and transition wedges are assessed, using commonly studied responses (kinematic response and stress) and the above-mentioned criterion based on total strain energy minimization. The second part of the chapter evaluates the preliminary design of a newly introduced transition structure (SHIELD) using the same criterion. A detailed investigation of existing and a new design using a 2-dimensional finite element model shows SHIELD's effectiveness in managing energy flow at transition zones and provides the reasoning behind the ineffectiveness of the other commonly used transition structures. The results in this chapter demonstrate the robustness and comprehensiveness of the recently developed energy-based criterion and its applicability to different types of transition zones. Moreover, it highlights the potential of SHIELD as a solution to address the complexities associated with the design of railway transition zones.

1.4.3. CHAPTER 4

In this chapter, the influence of different sleeper configurations in transition zones and reduced sleeper spacing on the operation-driven dynamic amplifications in railway transition zones is evaluated, employing the proposed criterion based on the total strain energy in the track-bed layers (ballast, embankment, and subgrade). In addition to this, the influence of the loss of contact between sleepers and ballast (i.e., hanging sleepers), which typically results from the differential settlement, is studied. The first part provides useful insights regarding the interventions (and/or initial design) in the sleeper configuration and spacing, whereas the second part of this chapter highlights the need for interventions to deal with the loss of contact between sleeper and ballast. The results show that it is not possible to mitigate the transition effects completely using the interventions involving sleeper spacing and configuration.

1.4.4. CHAPTER 5

In this chapter, several finite element models are employed to investigate the amplification of total strain energy due to the phenomena of reflection and redistribution of energy close to the transition interface. The models used in this chapter include non-reflective boundary (representing an energy sink) and homogeneous material along the vertical direction of the track, and the responses are studied for individual and combined effects in comparison to a benchmark case. The results show that eliminating the phenomena results in no dynamic amplification in total strain energy in railway transition zones and a potential design solution must aim at addressing these phenomena.

1.4.5. CHAPTER 6

In this chapter, the design challenges that arise due to variations in material properties in both the depth (trackbed layers composed of different materials) and longitudinal directions of the track, as well as temporal variations in mechanical properties of materials due

to several external factors over the operational period, are assessed. This chapter aims to investigate the effects of these variations in material properties (i.e., of the resulting stiffness distributions in vertical and longitudinal directions) on the behaviour of RTZs, assess from this perspective the performance of SHIELD, and establish a methodology for optimising material properties to minimise the dynamic amplifications in these zones. Results indicate that stiffness variations in both vertical and longitudinal directions significantly influence the dynamic behaviour of the RTZs. In the end, a permissible range of stiffness ratios to control the amplification of strain energy in the most critical components of RTZs, both in the initial state as well as during the operational phase (where material properties may vary over time), is suggested. Moreover, the proposed optimisation framework allows the applicability of the SHIELD design to a broad spectrum of material properties.

1.4.6. CHAPTER 7

In this chapter, a heuristic approach is adopted to optimise the geometry of SHIELD and investigate its influence on the strain energy distribution in railway transition zones. For this purpose, several three-dimensional finite element models are used to analyse different geometric profiles of SHIELD in a systematic manner. By altering SHIELD's geometry across longitudinal, transversal, and vertical directions, the influence of the different geometric profiles on the strain energy redistribution across the trackbed layers (ballast, embankment, and subgrade) is studied in terms of spatial and temporal distributions of total strain energy. It was found that the longitudinal geometric profile of SHIELD has the most significant impact on the strain energy distribution, while the transversal profile primarily influences the ballast layer, and the vertical profiles (i.e., in the plane perpendicular to both longitudinal and transverse planes) enhance the local distribution of strain energy in the vicinity of the transition interface. The preliminary optimisation presented in this chapter provides the starting point for full-scale optimisation to obtain tailored shapes of transition structures such that there is neither a concentration of energy nor an obstruction in the flow of energy in RTZs.

1.4.7. CHAPTER 8

In this chapter, SHIELD is evaluated for critical conditions arising due to different velocities (sub-critical, critical and super-critical), the direction of the moving load, the combination of inertial effects and track imperfections (non-straight rail and hanging sleepers), and passage of multiple axles (using a comprehensive vehicle model) using various vehicle models and finite element models of the RTZs. It was found that SHIELD effectively mitigates dynamic amplifications and results in smooth strain energy distribution across sub-critical, critical, and super-critical velocity regimes in both directions of movement implying that the expected operation-induced degradation will be as uniform as possible in longitudinal direction. Furthermore, even though SHIELD is designed to deal with initial track conditions (perfectly straight track), its superior performance is not confined to tracks in perfect condition; it also efficiently addresses adverse effects from track imperfections such as hanging sleepers and non-straight rail. Ultimately, the robustness of SHIELD is demonstrated for all the critical conditions under study.

1.4.8. CHAPTER 9

In this particular chapter, the scope of SHIELD is extended for an embankment-bridge transition with ballast running over the bridge and its performance is evaluated using a strain-energy criterion. It was concluded in the end, that the SHIELD can effectively mitigate the operation-induced dynamic amplification for more than one type of railway transition zone.

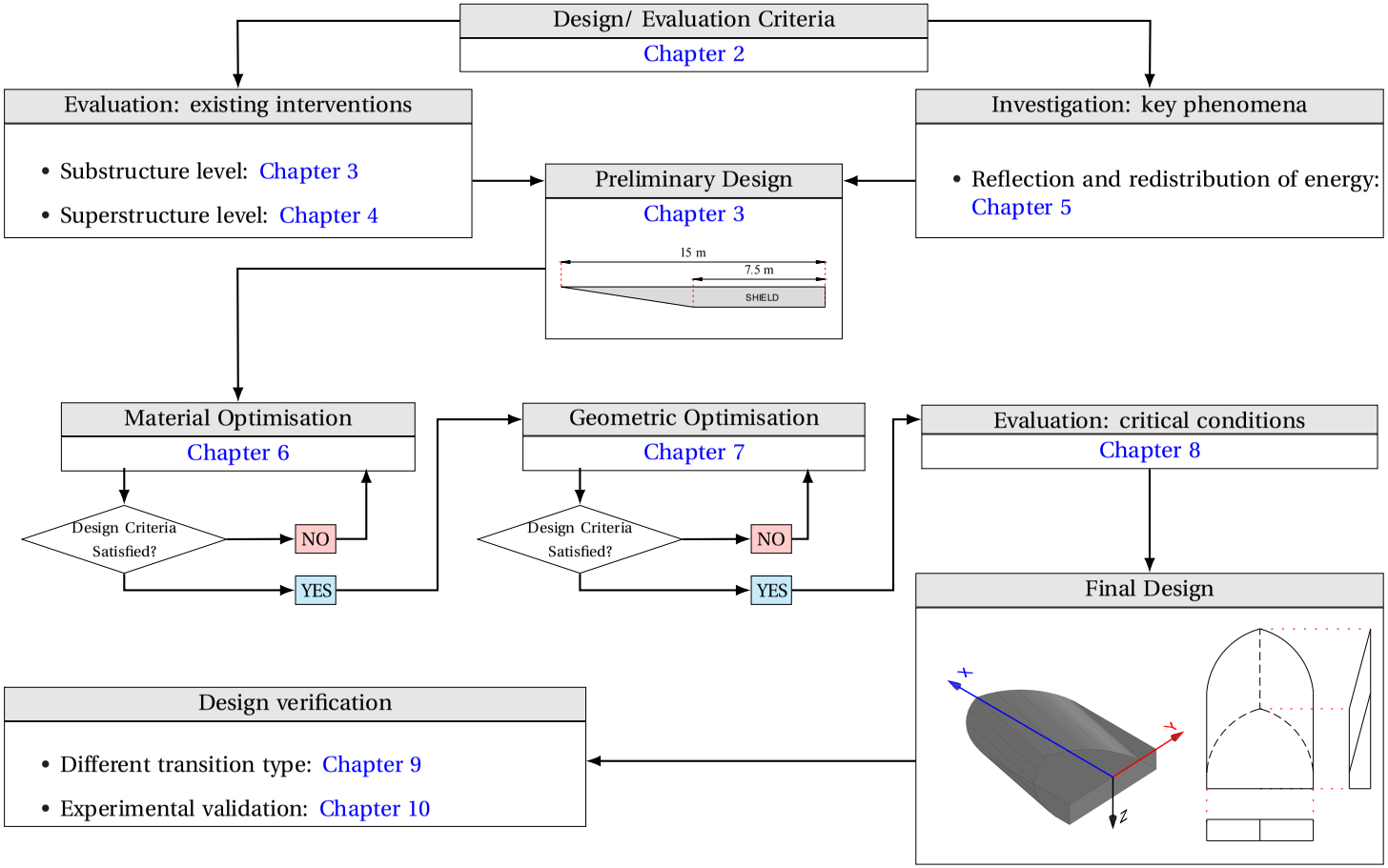

Figure 1.4: Methodology for evaluation and design of railway transition zones.

2

DESIGN OF RAILWAY TRANSITION ZONES: A NOVEL ENERGY-BASED CRITERION

This chapter (with minor changes) has been published as *A. Jain, Andrei V. Metrikine, Michael J.M.M. Steenbergen, and Karel N. van Dalen. Design of railway transition zones: a novel energy-based criterion. Transportation Geotechnics, page 101223, 2024. ISSN 2214-3912.*

ABSTRACT

Railway transition zones (RTZs) experience higher rates of degradation compared to open tracks, which leads to increased maintenance costs and reduced availability. Despite existing literature on railway track assessment and maintenance, effective design solutions for RTZs are still limited. Therefore, a robust design criterion is required to develop effective solutions. This paper presents a two-step approach for the formulation of a preliminary-design criterion to delay the onset of processes leading to uneven track geometry in RTZs. Firstly, a systematic analysis of each track component in a RTZ is performed by examining spatial and temporal variations in kinematic responses, stresses and energies using a finite element model of an embankment-bridge transition. Secondly, the study proposes an energy-based criterion to be assessed using a model with linear elastic material behavior and states that an amplification in the total strain energy in the proximity of the transition interface is an indicator of increased (and thus non-uniform) degradation in RTZs compared to the open tracks. The correlation between the total strain energy (assessed in the model with linear material behaviour) and the permanent irreversible deformations is demonstrated using a model with non-linear elastoplastic material behavior of the ballast layer. In the end, it is claimed that minimising the magnitude of total strain energy will lead to reduced degradation and a uniform distribution of total strain energy in each trackbed layer along the longitudinal direction of the track will ensure uniformity in the track geometry.

2.1. INTRODUCTION

Railway tracks are subject to constant degradation and require frequent maintenance which in turn leads to high maintenance costs and reduced availability of tracks for normal operations. Consequently, a large proportion (40-75%) of railway operating costs are spent on track maintenance [1] to ensure passenger comfort and safety. There is plenty of literature focused on assessment and maintenance of railway tracks. However, the problem at hand still remains and is even intensified in countries with soft soil [2]. The frequency and costs of maintenance in railway transition zones (RTZs) is even higher (4-8 times) compared to the open tracks [1, 2]. RTZs are areas where the railway track crosses a structure related to a different transportation modality (bridge, road, culvert, etc.) or where the rail experiences major changes in the type of track support structure. Although there have been several studies [3–7] pointing out the cause of increased degradation in these zones as mainly abrupt change in stiffness and differential settlement, there still is a lack of understanding to design an effective solution to this problem. The current approach to deal with the excessive degradation involves some proactive and reactive measures [6, 8–11] that have proved either not as efficient or even counterproductive in some cases. A robust design solution for RTZs is lacking in literature. RTZs are built similarly to regular railway tracks with some modifications addressing the stiffness jump and differential settlement but without a complete knowledge of the variation of dynamic response of each track component. In order to delay the onset of processes leading to uneven track geometry due to non-recoverable permanent deformations in RTZs, there is a need for an effective design solution. The formulation of an effective design solution demands mainly two steps as discussed below.

Firstly, there is a need to perform a systematic analysis of each track component in RTZs

which involves a detailed study of spatial and temporal variation of kinematic responses, stresses and energies. A railway track is composed of several components and each component serves a specific function in the system. The response of each track component experiences a variation in vertical (depth of the track), transversal (along the width of the track), and longitudinal (along the length of the track) directions. These variations affect the performance of the track components in the track which in turn drives non-uniform degradation and the failure process. In addition to this, the degradation or failure of one component has an effect on the performance of the other components in the track system. Therefore, the damage prediction requires a detailed and systematic study of the behavior of each track component and an in depth understanding of interactions between components. The current literature [10, 12–21] focuses either on any particular track component (mostly rail, sleepers or ballast) or on one particular track response (mainly vertical displacements or accelerations or stress in ballast layer). However, a detailed analysis of the spatial and temporal variation of the response of each track component in RTZs is lacking in the literature. Furthermore, an energy analysis of the track components in RTZs, which could help identify signs of degradation, has not yet been presented in the existing literature. The significance of energy variation will be discussed in the following paragraph, and this paper will investigate it in detail.

Secondly, the identification of an appropriate design criterion affecting the response of RTZs is essential to design an effective design solution. The current literature evaluates the performance of a RTZ mainly by assessing either permanent vertical track deformations or stresses in the ballast layer. However, the question can be asked whether the deformations or the stresses at this particular interface are sufficient to describe the onset of degradation in a RTZ. What precisely leads to faster degradation of these zones compared to the open tracks? The source, spacial extent and location of the degradation in these zones are still unknown. As indicated above, the literature lacks an insight into the spatial and temporal distribution of kinetic and potential energies in railway track components, while this is an indispensable information to answer the question posed. Studies conducted by different authors [22–24] have pointed out that both elastic and inelastic strain energy can be associated with material degradation and may aid in identifying potential failure mechanisms. In [22] authors have studied shakedown of soil in different test setups in terms of elastic and plastic strain energies. In [25] authors assessed the susceptibility of railway tracks to degradation by quantifying the mechanical energy dissipated under a moving train axle, but, due to its dimensional constraints, the model could neither demonstrate the variations of these energies in each layer of the substructure nor was focused on railway transition zones. Hence, the current work will investigate the mechanical energy distribution in space and time for RTZs using a model with linear elastic materials and demonstrate a correlation of the predicted responses with irreversible permanent deformation leading to uneven track geometry. In the end, this work will propose a strain-energy-based design criterion to minimize the degradation in RTZs.

This work is mainly divided into two parts addressing the points mentioned above. In the first part of this work, a 2-dimensional (2-D) model of an embankment bridge

transition with linear elastic materials is used to study the spatial and temporal distribution of the kinematic responses, stresses and energies for various track components. As the intent of this paper is to identify a possible design criterion for transition zones, the focus is not so much on the absolute values of the responses under study but on their variation in space and time; the 2-D model suffices for that purpose. The computational objective of the model used in the first part of the paper is to study the amplification in the above-mentioned responses of the track components in the approach zone (proximity of the transition interface) compared to the open tracks (far from the transition interface). In the second part of this work, the design criterion is proposed by evaluating the results obtained in the first part of the paper. Moreover, the validity of the proposed strain-energy-based criterion is demonstrated using another model with non-linear elastoplastic material. The only difference in the models used in the first (linear elastic materials) and the second (non-linear elastic material) parts of the paper is the material for the ballast layer. All models used in this paper are identical in geometry and loading conditions. Finally, it is to be noted that the proposed criterion only covers operation-driven permanent deformations resulting from dynamic amplifications and/or non-uniformity in the responses, and hence, autonomous settlements are not included in the paper.

2.2. METHODS

In this paper, a embankment-bridge transition is studied which consists of ballasted track and a concrete bridge. The ballasted track ("soft side") consists of track components namely rail, rail-pads, sleepers, ballast, embankment and sub-grade underneath. The ballast-less track ("stiff side") consists of rails connected to sleepers (with under sleeper pads) resting on the concrete bridge.

2.2.1. GEOMETRIC MODEL

The geometric model is 80 m (132 sleepers) long which consists of 60 m of ballasted track and 20 m of ballast-less track (concrete bridge). For this study, the geometrical model is divided into four zones (see Table-2.1) with additional 20 m at the beginning and 10 m at the end in order to eliminate the influence of boundaries (left and right extremes) on the results for the reasons discussed in section 2.2.2. Figure 2.1 shows the approach zones (AZ) on both sides that together constitute the transition zone (TZ), and open track (OT) on both sides are the zones that are practically free from any transition effects. In addition to this, Figure 2.1 shows materials (steel, concrete, ballast, sand, clay) of the track components in the legend and a magnified (scale 2:1) cross-section (section A) of the embankment-bridge transition under study with the depths of the trackbed layers (ballast, embankment and subgrade) marked in red. The length of each zone under study (OT-I, OT-II, AZ-I and AZ-II) is also marked in Figure 2.1. The geometric model mainly consists of following track components (Figure 2.1):

- Rail: rail profile 54E1 (UIC54) manufactured according European Standard EN

Table 2.1: Details of the zones under study

Zones	Length [m]	Description
OT-I	20	open track-soft side
AZ-I	20	approach zone-soft side
AZ-II	5	approach zone-stiff side
OT-II	5	open track-stiff side

13674-1

- Rail-pads: connecting rails to sleepers
- Sleepers: 240 mm x 240 mm, concrete
- Ballast: 0.3 m deep layer of ballast
- Embankment: 1 m deep dense sand under the ballast
- Natural terrain or subgrade: clayey soil of 1 m depth
- Under Sleeper pads (USPs) [26]: under sleeper pads of 0.01 m thickness under the sleepers on the stiff side
- Bridge: concrete bridge with fixed bottom of length 20 m

The sleeper spacing adopted is 0.6 m and the first sleeper next to the transition is located at 0.3 m from the interface of ballasted and ballastless track.

2.2.2. NUMERICAL MODEL

A 2-D Finite Element (FE) model was created using ABAQUS, with geometrical details mentioned in the previous section. The railway track components and the bridge were modelled using four-node plane-strain elements and the rail was modelled as a beam. Rayleigh damping (as suggested in [27]) for materials (see Table-2.2) was used to incorporate a realistic level of energy dissipation in the system; for more precise calculations, the damping formulation and its parameters might have to be changed or tuned. The length and depth of the model were chosen such that there is hardly any influence of the wave reflections from the boundaries (extreme right, left and bottom of the system) on results of the zones under study while restricting the vertical displacements to maintain a reasonable value as per literature [28, 29]. The depth of the layers under the sleepers was sufficient to reduce dynamic stresses at the bottom of the subgrade to less than 3% (this value was suggested to be less than 10% in [28] so as to eliminate artificial boundary effects) of their values at the bottom of the sleepers. However, for poorer subgrades, the depths at which the stress levels are below 10% might differ and the response must be verified accordingly based on the specific site conditions. It is recommended that an

additional analysis must be performed, comparing the results for two or three configurations of the system with different depths of the subgrade to validate the assumption. The following subsections describe the details regarding the numerical model used for FE analysis in terms of mesh properties, mechanical properties of materials, interactions between the track components, loads, constraints, boundary conditions and analysis procedures.

MESH

The sleeper, ballast, embankment, subgrade and the bridge were discretized [30] using linear quadrilateral elements of type CPE4R (12424 elements) and rail using two-node linear line elements of type B21 (7860 elements of size 0.01 m) to form a very regular mesh. The most critical zone (AZ-I) under study was meshed finer than rest of the model in order to obtain accurate results.

MECHANICAL PROPERTIES

The materials used for all track components are characterised by elastic properties (Young's modulus, Poisson's ratio), densities and Rayleigh damping factors [27, 31–33]. A static analysis was performed in order to tune the elasticity (Young's modulus) of the USP on the stiff side such that the static vertical displacements on soft and stiff sides are the same. The details of these parameters are mentioned in Table-2.2.

INTERFACE AND BOUNDARY CONDITIONS

The following key interface and boundary conditions were chosen with no separation allowed at any interface:

- Rail-sleeper: Rail was connected to the midpoints of the sleeper edges via railpads represented by vertical springs ($k = 1.2 \cdot 10^8$ N/m) and dashpots ($c = 5 \cdot 10^4$ N-s/m) [33].

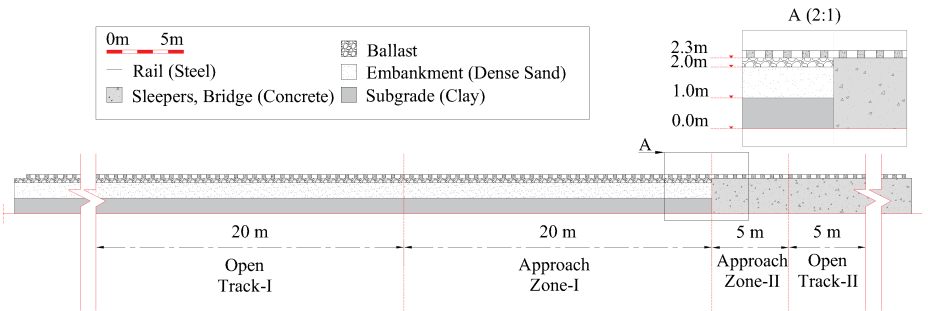

Figure 2.1: Cross-sectional details of the embankment-bridge transition and the division of zones (OT-I, AZ-I, AZ-II, OT-II) under study.

Table 2.2: Mechanical properties of the track components

Material	Elasticity Modulus E [MN/m^2]	Density ρ [kg/m^3]	Poisson's Ratio ν	Rayleigh damping α	β
Steel (rail)	210000	7850	0.3	-	-
Concrete (sleepers)	35000	2400	0.15	-	-
Ballast	150	1560	0.2	0.0439	0.0091
Sand (embankment)	80	1810	0.3	8.52	0.0004
Clay (subgrade)	25.5	1730	0.3	8.52	0.0029

- Sleeper-ballast, ballast-embankment, embankment-subgrade: surface-to-surface tie constraint (perfect matching of displacements and forces) was used for defining the conditions at these three interfaces.
- Vertical interface between ballast/ embankment/ subgrade and concrete bridge: a hard contact linear penalty method was used to define the normal behaviour and Coulomb's friction law was adopted to define the tangential behaviour with a frictional coefficient equal to 0.5 (details can be found in [30]). In the initial phase of model verification, it was found that inclusion of non-linearity for this particular interface was needed as surface-to-surface tie constraint led to an over-estimation of the responses of the track components.
- The bottom of the subgrade and the bridge were fixed.

The simulation was performed in two steps. Firstly a static step was performed to consider the effects of gravity in order to obtain the initial stress state of the model under self-weight. It was followed by a dynamic step (implicit solver using the Hilber-Hughes-Taylor time integration scheme combined with a Newton approach to achieve dynamic equilibrium) for 1.75 s with a time step of 0.005 s. The loads that have been considered are: gravity load for static analysis and one moving axle load of 90 kN with velocity of 144 km/hr for dynamic analysis. The load moving in the direction from soft side to stiff side of the transition was simulated using the DLOAD subroutine in ABAQUS [30, 34]. The moving load is a uniformly distributed line load of length 0.03 m (length of contact between wheel and rail). Note that the formulation of a design criterion, which is the ultimate objective of this paper, is not qualitatively influenced by the specific character of the moving load. Therefore, the simplest loading conditions have been adopted in this work as the main objective is to "formulate" a design criterion by comparing the responses of the track components in the approach zones to the open tracks and capturing the main mechanisms governing the dynamic amplifications in RTZs in the cleanest possible manner. The amplification of dynamic responses in the approach zone is expected to be higher for higher speeds and axle loads. Therefore, the designers must perform a sensitivity analysis for different vehicle characteristics (speeds, axle loads etc.) to achieve the most effective "use" of the proposed design criterion.

2.3. RESULTS AND DISCUSSION

In this section, the results are presented in two parts. Firstly a systematic analysis of the track components is performed by studying the kinematic responses (displacement, velocity and acceleration) of rail, sleepers and ballast, forces in rail pads, and maximum equivalent Von Mises stress at top and at the bottom of sleepers, ballast, embankment and subgrade (for a region of 0.6 m under each sleeper). The kinetic energy (KE) and strain energy (SE) variation in space and time is studied for the track bed layers (ballast, embankment and subgrade). Secondly, the analysis mentioned above is used to present a design criterion for RTZs, and its correlation with permanent deformations is demonstrated by comparing results of the analysis with linear elastic material to the one with a non-linear elastoplastic material behaviour of the ballast. It is to be noted that the discussion in this section related to the percentage increase of any of the responses (X) studied in this paper are calculated using the equation below:

$$\text{Percentage increase} = \frac{(X_{AZ} - X_{OT}) \cdot 100}{X_{OT}} \tag{2.1}$$

where X_{AZ} and X_{OT} are any of the responses under study (displacement, velocity, acceleration, stress, kinetic energy, strain energy) in the approach zone and open track respectively.

2.3.1. ANALYSIS OF RTZS

KINEMATICS OF TRANSITION ZONES

Rail: Figure 2.2 shows time history of displacement, velocity and acceleration for 10 control points each in AZ-I and AZ-II. The responses of the rail nodes above the sleepers on both sides right next to the transition show an increase when compared to nodes far from the transition. On one hand the increase in the maximum displacement under the load is only 5.4%, which can be attributed to the fact that only one axle is being studied. On the other hand, the increase in velocity (20%) and acceleration (15.5%) is much larger. Also, some permanent deformation can be seen (based on the final non-zero value of the displacements in Figure 2.2 and Figure 2.3 at time moment $t = 1.7s$) at locations (e.g., at sleeper 1) close to transition enabled by frictional sliding at the transition interface.

Sleepers: Figure 2.3 shows time history of displacement and accelerations for 10 control points each (midpoint of sleeper top and bottom) in AZ-I and AZ-II. It can be noticed that 0.114 mm of permanent deformation occurs at sleeper number 1 which can be again attributed to frictional sliding at the transition interface. Although the variation of the kinematic response from top to bottom of the sleepers is negligible, there is a significant increase in the displacements (9.5%) and accelerations (37.3%) of the sleepers on left (sleeper 1) and right (sleeper -1) of the transition interface when compared to the sleepers (10, -10, respectively) in far field.

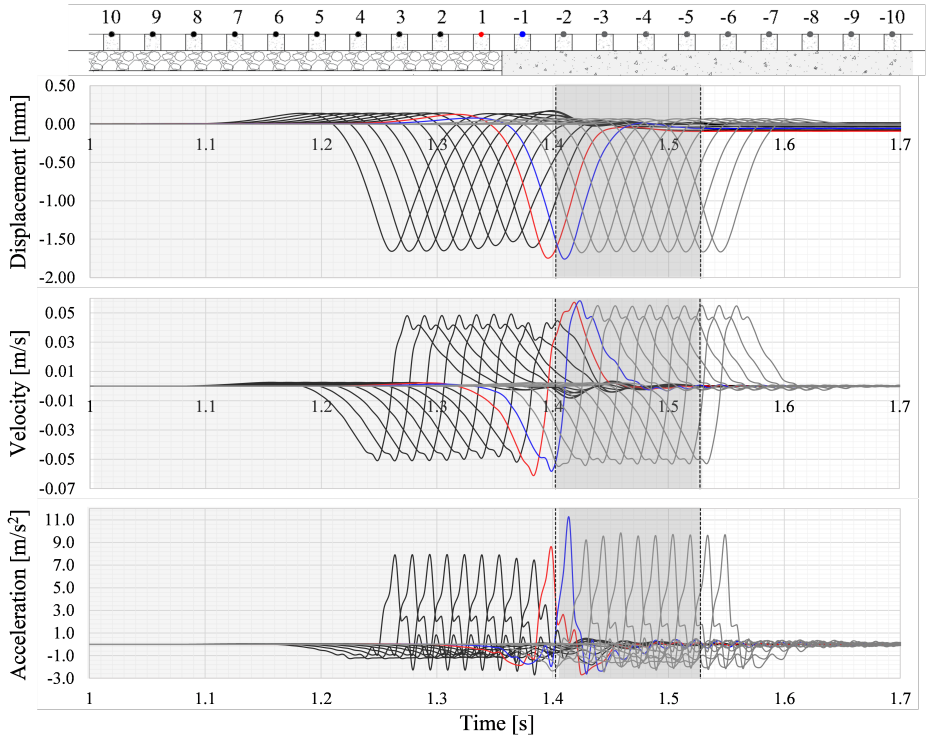

Figure 2.2: Time history of displacement, velocity and acceleration for 10 control points (on each side of transition interface) of the rail (above sleepers). The dashed lines show the time moments at which the moving load leaves the AZ-I and AZ-II. The red (soft side) and blue lines (stiff side) are the results for the control points above the first sleeper next to transition interface on both sides.

Ballast: The authors in [35] have associated breakage of ballast particle corners to load frequencies between 10-20 Hz, densification or compaction of ballast without much breakage was associated to load frequencies of 20-30 Hz and all load frequencies above 30 Hz can be associated with splitting of particles. Hence, the amplitude spectra of accelerations for ballast at different locations (under sleepers 1, 2, 10) are analyzed. A significant amplification (38.3%) is observed in the ballast acceleration under sleeper 1 (0.54g) compared to the ballast acceleration (0.39g) under sleeper 10. It can be clearly inferred from Figure 2.4 that the ballast in the approach zone (under the sleeper 1) is more susceptible to phenomena of corner breakage, compaction and splitting of particles compared to ballast in open tracks, which is in line with what has been observed in reality [36].

Clearly, the results in Figure 2.2 and Figure 2.3 show an increase in kinematic quantities at the locations of the first sleeper in AZ-I and AZ-II when compared to the open track on both sides. This is in agreement with the current literature [32, 36, 37] but site measurements show that the first three sleepers (in AZ-I) next to the transition interface

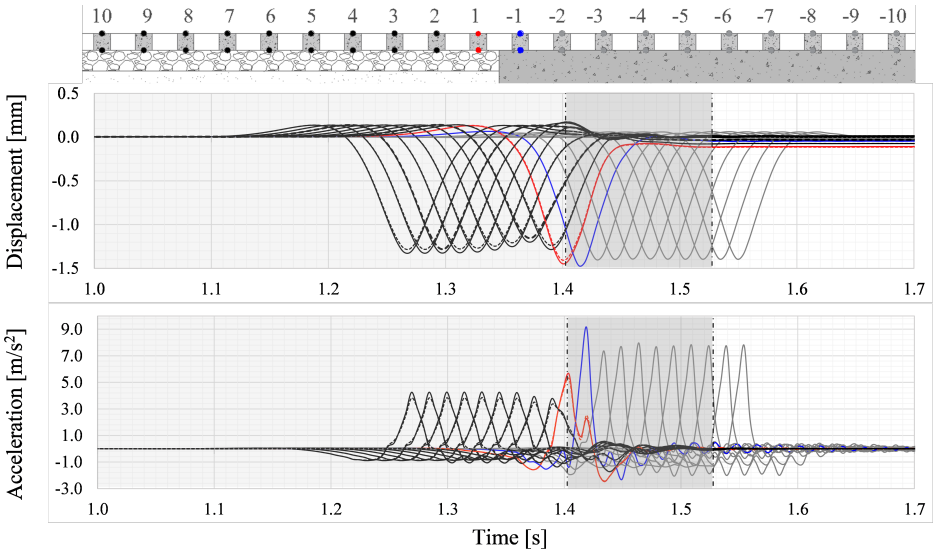

Figure 2.3: Time history of displacement and acceleration for 10 control points (on each side of transition interface) on top (solid lines) and bottom (dashed lines) of the sleepers. The dash-dotted lines show the time moments at which the moving load leaves the AZ-I and AZ-II. The red (soft side) and blue lines (stiff side) are the results for the first sleeper next to transition interface on both sides.

are critical in terms of observed damage. This shows that only kinematic studies are not adequate to predict damage in RTZs and for that reason we further investigate forces/ stresses and energies in the following sections.

STRESSES AND FORCES IN TRANSITION ZONES

Rail-sleeper interaction forces: Figure 2.5 shows a 5% increase in force (compressive) for the rail-pad connecting sleeper 2 to the rail compared to the force for rail-pad connecting sleeper 10 (in the open track) to the rail. Moreover, the rail-pad connecting sleeper 1 to the rail experiences a tensile force (with respect to the prestress in railpads which is typically present in practice) of approximately 4 kN. In the model, this is due to AZ-I and AZ-II deforming differently, which results in sleeper 1 hanging on the rail. In reality there might be a tensile force or reduction in prestress based on the conditions present at the site.

Maximum equivalent Von Mises stress: In this section the maximum equivalent Von Mises stresses at the top and bottom of each track component (sleepers, ballast, embankment, subgrade) are assessed in terms of their variation along the longitudinal direction (i.e., 'n' denotes the sleeper number). According to the Von Mises criterion, yielding of a material begins when the equivalent Von Mises stress exceeds the yield stress of the material. It is to be noted that the observed magnitude of the Von Mises stresses (Figure 2.6) is not close to the yield stresses of the materials as the system is studied only for

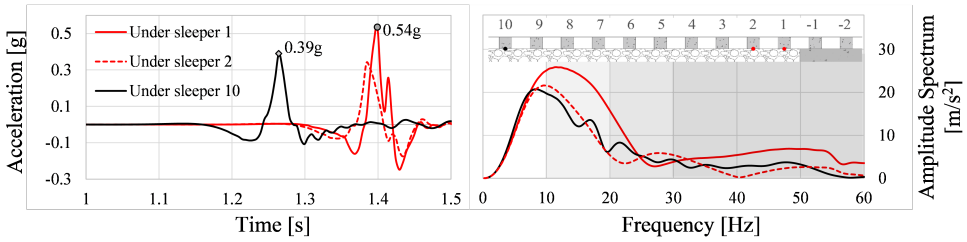

Figure 2.4: Time history of accelerations(left) and the amplitude spectra of accelerations (right) for two point on top of ballast layer under sleeper 1, 2 and 10.

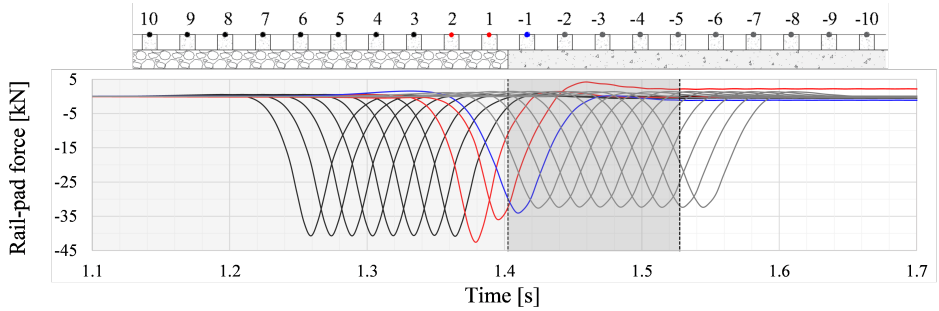

Figure 2.5: Time history of vertical forces in 10 rail-pads next to transition interface on each side. The red lines show the forces in first two rail-pads on the soft side and the blue line shows the force on first sleeper on the stiff side of the transition interface.

one axle load. However, the stress amplification in the AZ-I compared to OT-I can be clearly seen in Figure 2.6. This implies that AZ-I will yield earlier than OT-I. The stress amplifications are observed under the first three sleepers.

Figure 2.6 shows that the max. Von Mises stresses under the sleepers 4-10 are the same while there is an amplification under sleepers 1, 2 and 3 (similar to situation on top of the sleepers), which might lead to differential settlement in the long term. Also, a spike in stress can be seen on sleeper 2 and on the ballast under sleeper 2, which is consistent with the amplification in rail-pad force at this particular location (Figure 2.5). Moreover, the non-uniformity in max. Von Mises stress under sleepers 1, 2 and 3 for embankment and subgrade can be due to a combination of increased force in the rail-pad connecting sleeper 2 (Figure 2.5) to the rail and the boundary effects (reflection) at the transition interface. An amplification in max. Von Mises stress (Figure 2.6) in AZ-I compared to OT-I is clearly seen but minimizing these stress values does not necessarily assure that the materials do not fail at lower stresses. This is due to the fact that the Von-Mises criterion is essentially an energy criterion which only covers the maximum distortional energy density (it is proportional to the square of the maximum Von-Mises stress) expressed as follows:

$$U_d = \frac{1+\nu}{3E}\sigma_{VM}^2 \tag{2.2}$$

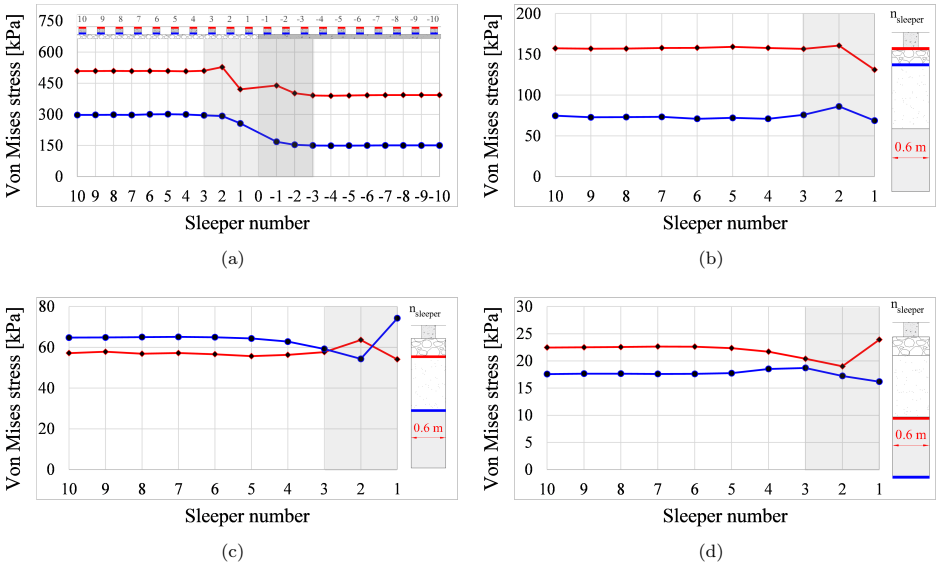

Figure 2.6: Maximum equivalent Von Mises stress at top (red) and bottom (blue) of (a) sleepers, (b) ballast, (c) embankment, and (d) subgrade for one sleeper bay.

where ν is Poisson's ratio, E is Young's modulus, σ_{VM} is the equivalent Von-Mises stress, and U_d is distortional energy density. The maximum distortion energy theory (Von Mises yield criterion) proposes that the total strain energy can be separated into two components: the volumetric strain energy and the distortional strain energy; failure is said to occur when the distortional component reaches the critical value. However, this criterion is most suitable for predicting the yielding conditions of metals and alloys. In RTZs the volumetric strain energy will also play a considerable role in phenomena like breakage, compaction and splitting of ballast particles, eventually resulting in a non-uniform transverse and longitudinal profile of the ballast layer. Although prediction of the type of failure is beyond the scope of this work, it is important to study the total strain energy (as used by authors in [22] to study the failure of soils) in order to assess the degradation in RTZs.

As shown in this section, the percentage increase in max. Von Mises stress for the layer of ballast in AZ-I compared to OT-I is 2.57% and the percentage increase in corresponding distortional energy is 5.2%. In the following sections, an increase in the total energy will be studied in terms of spatial and temporal variation and the percentage increase will be compared with that of Von Mises stress and distortional energy.

ENERGY VARIATION IN TRANSITION ZONES

Kinetic energy: Figure 2.7 shows the spatial variation of the kinetic energy (plotted for each element with maximum at marked time moments) in ballast (a) embankment (b)

and subgrade (c) in the AZ-I at 5 different time instances marked in the figure where a peak (t_2, t_4) or dip (t_3) can be seen in the total kinetic energy and a time instant where the energy is nearly constant (t_1). The colours shown in Figure 2.7 are associated with the values shown in the legend, where blue represents the lowest magnitude and red represents the highest magnitude of kinetic energy. The time instances t_2 and t_4, when the total kinetic energy has significantly increased, correspond to the load positions above the second sleeper on both sides of the transition interface. It is also interesting to observe that the increase of kinetic energy in the ballast layer is distributed all over the depth (Figure 2.7a for time instance t_2 and t_4) in the proximity of the transition interface. On the contrary, this increase is localized for the layers of embankment and soil in the top corner of these layers (also close to the transition interface); see Figure 2.7b and c. This concludes that the kinetic energy has more significant effect in the ballast layer compared to embankment and subgrade, which could be related to high wear of the ballast particles. Also, it is worth noticing that the elements next to the transition interface experience an increase in kinetic energy even after the load has left.

Figure 2.8 shows the temporal variation of the kinetic energy per unit depth in each track component (ballast, embankment, subgrade) in all the zones under study (OT-I, AZ-I, AZ-II, OT-II). The dash-dotted lines in the graphs show the time moments at which the load enters and exits the OT-I, AZ-I, AZ-II, OT-II. The total kinetic energy density decreases (approximately 5 times) in magnitude as we investigate deeper in the system whereas the total kinetic energy on soft side is approximately 100 times higher than that on the stiff side.

Strain energy: Figure 2.9 shows a spatial variation of strain energy (plotted for each element with maximum at marked time moments) in ballast (a) embankment (b) and subgrade (c) in the AZ-I at 3 different time instances marked in the figure where extremes (t_2, t_3) can be seen in the total strain energy in ballast layer and a time instant where the strain energy is constant (t_1). However, these critical time moments at which the strain energy curve exhibits extremes correspond to different load positions. In the ballast layer, the maximum total strain energy peak occurs at t_3, which is the time moment at which the load crosses the third sleeper (soft side). Similarly, a sharp local increase of strain energy can be seen at the bottom of the embankment layer (Figure 2.9b) at the time instance when the load passes over the second sleeper (soft side). In addition to this, a similar increase can be seen for the subgrade at the time moment when the load crosses the first sleeper (soft side). This shows correspondence to results obtained from both kinematic and stress studies combined together. Moreover, the locations of the strain energy peaks are restricted to regions next to the transition interface (for ballast) and the interfaces between the three track bed layers.

Figure 2.10 shows the temporal variation of the total strain energy (contribution only due to dynamic components) per unit depth in each track component (ballast, embankment, subgrade) in all the zones under study (OT-I, AZ-I, AZ-II, OT-II). The dash-dotted lines in the graphs show the time moments at which the load enters and exits the OT-I, AZ-I, AZ-II, OT-II. The total strain energy density increases (approximately 2.5 times) in

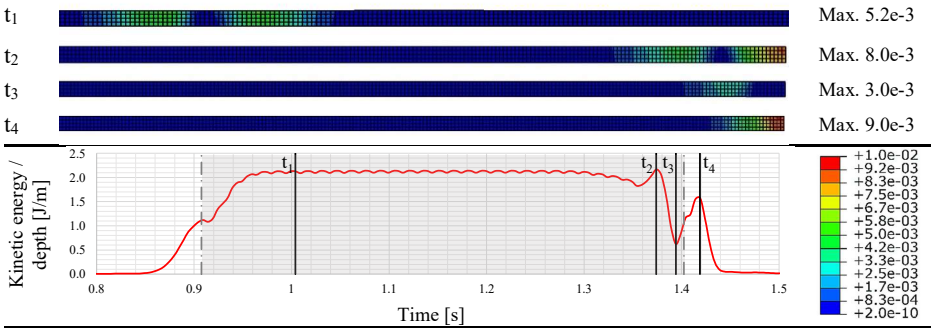

(a)

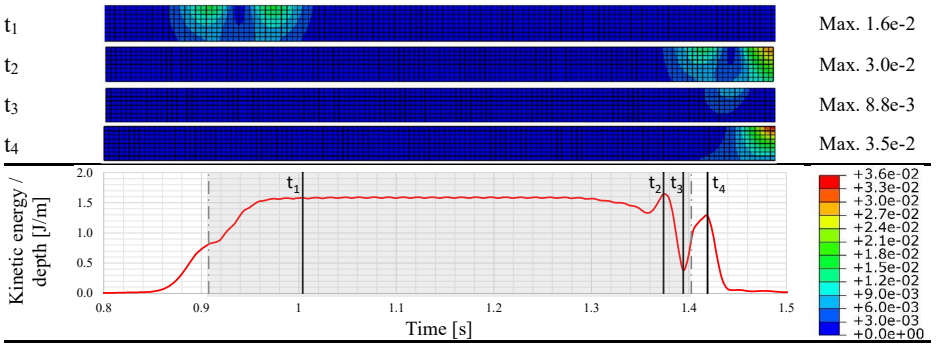

(b)

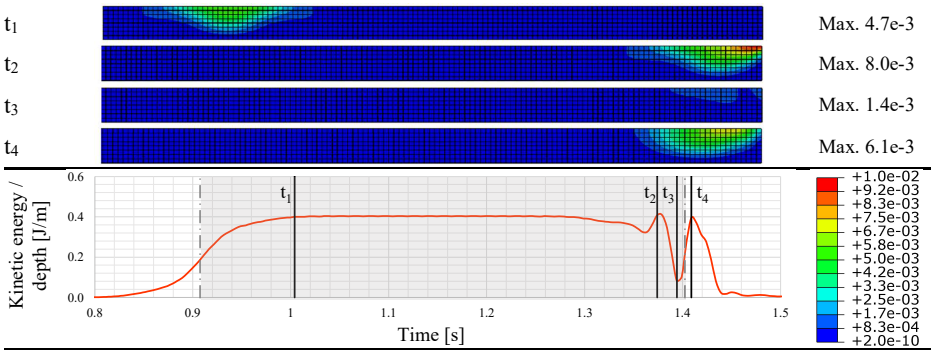

(c)

Figure 2.7: Spatial distribution of kinetic energy per unit depth in AZ-I in (a) ballast (b) embankment (c) subgrade at time instances t_{1-3}. The color map indicates the strain energy in each mesh element.

The graphs show the time moments (dashed lines) at which the load enters/exits the AZ-I and the time interval (grey shaded region) for which the load stays in the AZ-I.

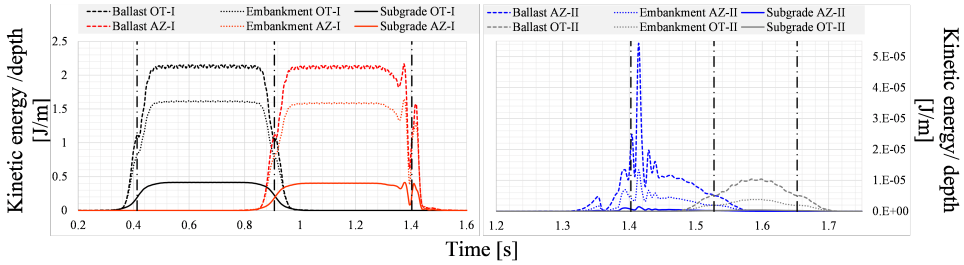

Figure 2.8: Temporal variation of total kinetic energy per unit depth in ballast, embankment and subgrade for each zone (OT-I, AZ-I, AZ-II, OT-II)

magnitude as we investigate deeper in the system whereas the total strain energy on soft side is approximately 300 times larger than that on the stiff side.

2.3.2. DESIGN CRITERION

A design criterion for RTZs can be proposed based on the comprehensive analysis presented in the first part of this work.

In the first phase of analysis in Section 2.3.1, the kinematic study suggested that there is a significant increase in displacements (5.4% to 9.5%) and accelerations (15.5% to 38.3%) for the track components (rail, sleepers and ballast) in the transition zone compared to open tracks. The location of the peak value of the kinematic responses under study for each of these track components was in the regions around the first sleeper on either side of the transition interface. The critical values of kinematic response occurred at the time moment when the load was passing over the location where the peak response was observed. In summary, a significant amplification in kinematic response was observed for each track component but it was localized to the region around the first sleeper only. Even though a kinematic response provide valuable information regarding dynamic amplifications in transition zones, it cannot be used as a valid design criterion to reduce degradation as site measurements [32, 36–38] suggest that the degradation in RTZs is observed at locations around the first 3 sleepers next to the transition interface. Therefore, the kinematic response can be a good criterion to evaluate the performance of the upper track components namely rail and sleepers but is insufficient to describe the degradation processes in the lower trackbed layers.

The second phase of analysis in Section 2.3.1 shows that there is a significant increase in max. equivalent Von Mises stress for each of the track components namely sleepers, ballast, embankment and subgrade in AZ-I compared to the OT-I. The location of the maximum Von Mises stress values for the ballast layer was under the second sleeper next to the transition interface on the soft side of the track. The peak value of the Von Mises stress in embankment layer was localized to the transition interface while in the subgrade layer the peak was in the region around the third sleeper (soft side) next to the

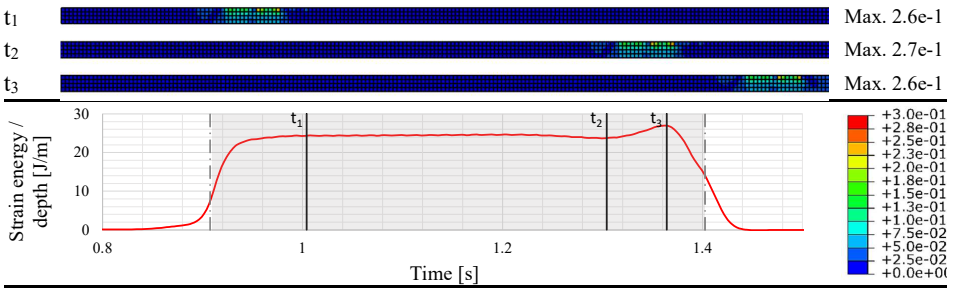

Figure 2.9: Spatial distribution of strain energy per unit depth in AZ-I in (a) ballast (b) embankment (c) subgrade at time instances t_{1-3}. The color map indicates the strain energy in each mesh element. The graphs show the time moments (dashed lines) at which the load enters/exits the AZ-I and the time interval (grey shaded region) for which the load stays in the AZ-I.

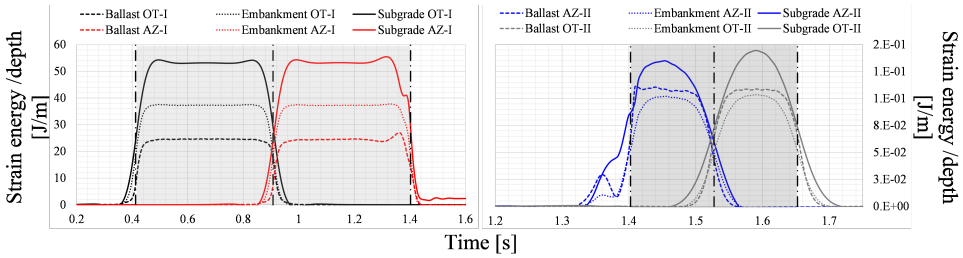

Figure 2.10: Temporal variation of total strain energy per unit depth in each track component for each zone (OT-I, AZ-I, AZ-II, OT-II)

transition interface. On one hand, the max. equivalent Von Mises stress shows that the critical locations are similar to those observed on many sites [32, 36–39]. However, on the other hand, based on the discussions above (see Section 2.3.1), the Von Mises criterion takes into account only the distortional component of strain energy and cannot explain all degradation mechanisms that are expected to occur in RTZs. Therefore, to assess or alleviate degradation mechanisms in RTZs, it is more comprehensive to consider the total strain energy, which comprises both distortional and volumetric components. Figure 2.11 summarises the comparison of percentage increase in max. Von Mises stress, distortional energy and total strain energy for the layer of ballast in AZ-I relative to the OT-I. Clearly, the total strain energy is significantly larger than the distortional energy.

The third phase of analysis in Section 2.3.1 was focused on the spatial and temporal variation of the mechanical energy. It can be clearly seen from Figure 2.7 and Figure 2.9 that both the total kinetic and strain energies increase by a significant amount for the top track-bed layer (ballast) in AZ-I compared to OT-I. This increase is less prominent in the lower layers (embankment and subgrade). The location of peak values of the energy is in the region around the first to the third sleeper on the soft side of the transition interface. The time moments at which these peak values are observed are when the load passes above sleeper 1 (for ballast), sleeper 2 (for embankment) and sleeper 3 (for subgrade). This shows that energy combines the information obtained from both kinematics and stresses and is therefore a more comprehensive quantity. Now that the magnitude of total kinetic energy is negligible compared to the total strain energy, the authors claim that the degradation of RTZs can be reduced by minimizing the increase in total strain energy in track-bed layers. It is to be noted that the increase in total strain energy for each track-bed layer will depend on various factors such as soil type, degree of compaction of the materials, magnitude and velocity of the load etc. This study shows a significant increase only in the ballast layer due to the choice of model and material parameters, but each layer should be monitored for any increase in total strain energy in the proximity of the transition interface.

Based on the above discussions and results shown in Section 2.3.1, it has been claimed that the total strain energy can be seen an indicator of potential damage in RTZs. In reality, a fraction of this total strain energy is recoverable (elastic) and the rest is dissi-

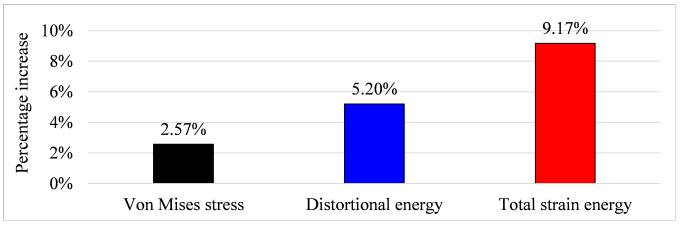

Figure 2.11: Comparison of percentage increase in Von Mises stress, distortional energy and total strain energy for the ballast layer in AZ-I relative to OT-I

pated through damage. This leads us to the conclusion that in order to minimise the degradation in RTZs, it is evident that there is a need to minimise the total strain energy in each of the track-bed layers. Moreover, a uniform distribution of the total strain energy along the longitudinal direction of track will ensure that there is no non-uniformity in degradation due to localised amplifications in the proximity of a transition interface. The validity of the proposed criterion can be demonstrated by establishing a correlation between permanent irreversible deformation (obtained from model 2) and total strain energy (obtained from model 1). This is done by comparing the results obtained from model 1, which includes linear elastic behaviour of the materials, and model 2, which includes a non-linear elastoplastic behaviour of the material representing the layer of ballast. The material model [40, 41], the stress-strain relationship and the damage parameters [42] used for simulating the non-linear elastoplastic material (model 2) comparable to ballast are adopted from literature and are used only for demonstration purposes. Hence, the authors do not claim that the absolute values of the quantities shown are fully representative of the railway track materials.

Figure 2.12 shows the permanent deformation observed at rail level above each sleeper (a) and the variation of the total strain energy for the layer of ballast (b) in OT-I and AZ-I for both linear elastic (model 1) and non-linear elastoplastic (model 2) material behaviour. It is to be noted that the rail deformation shown in Figure 2.12a is non-zero at all locations because of the static load due to gravity being active at all time moments. As for Figure 2.12, the total strain energy (for a finite volume) comprises solely recoverable strain energy for model 1, while for model 2, it accounts for both recoverable and dissipated strain energy resulting from damage. This explains the increasing trend of the total strain energy (in model 2) with the moving load progressing in the given volume. The dashed lines in Figure 2.12b represent the time moments at which the load enters and leaves OT-I and AZ-I. The locations of the strain-energy peaks (in AZ-I) predicted by both models are clearly the same, which shows the potential of model 1 to indicate damage. The increase in peak value of the total strain energy in AZ-I with respect to OT-I for model 1 is 1.28 J, and for model 2 is 0.57 J. This difference in the values is related to the non-linear material (model 2) undergoing permanent deformation (Figure 2.12a) in AZ-I, which is also reflected in the *final* strain energy difference (0.48 J) between OT-I and AZ-I, as seen in Figure 2.12b. In conclusion, the findings (Figure 2.12) indicate that the total strain energy peak observed in the model with linear elastic material behavior is

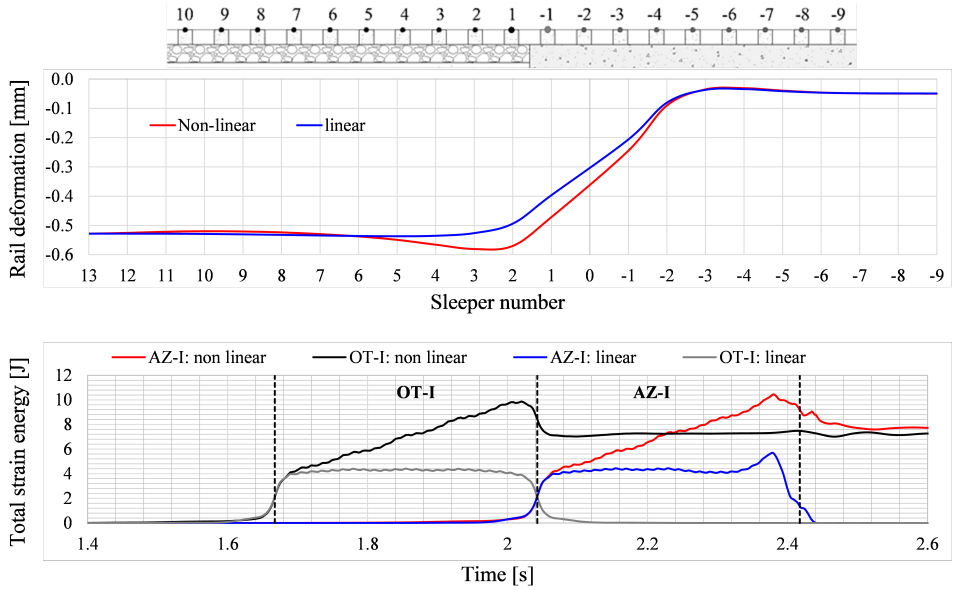

Figure 2.12: Comparison of (a) rail deformation and (b) total strain energy obtained from the model with linear elastic material behaviour (model 1) and non-linear elasto-plastic material behaviour (model 2) of ballast in RTZs for OT-I and AZ-I.

associated with a localized increase (compared to open track) in irreversible deformation in the vicinity of the transition interface (under sleepers 1, 2, 3; see Figure 2.12a) in the model with non-linear elastoplastic material. This demonstrates the validity of the design criterion proposed in this section.

It is to be noted that even though this paper proposes an energy-based criterion for the preliminary design of railway transition zones, the application is not limited to only design purposes [43, 44]. The proposed energy-based criterion can be used to evaluate the on-site condition (indicative) of a railway track or a transition zone by computing energy flux based on measured quantities (stress, strain etc.) that characterize the kinematic and dynamic responses of the system at critical points. However, in order to achieve full accuracy in the evaluation of the on-site condition using any approach (energy-based or other classical methods), detailed numerical models (tuned using measured data at monitoring points) must be used to predict the system's service situation.

2.4. CONCLUSIONS

In the first part of this paper, a systematic and detailed analysis of an embankment-bridge transition was conducted where the spatial and temporal distribution of displacements, velocities, accelerations, forces, stresses and mechanical energy were thoroughly studied

for the main track components. The investigation resulted in mapping the location and extent of the transition effects and formed the basis for the formulation of an energy-based design criterion that can be used in preliminary design to mitigate the amplified degradation of RTZs. The second part of the paper proposes the total strain energy based on a model with linear elastic materials as an indicator to predict degradation. The validity of this proposal was demonstrated and a clear correlation was found between the peak in the total strain energy (in the model with linear elastic material behaviour) and the localised increase in irreversible deformation (in a model with non-linear elastoplastic material behaviour) in the proximity of the transition interface. Therefore, it is concluded that the degradation in railway transition zones can be reduced by minimising the total strain energy in each track-bed layer in the approach zone or to the very least minimising the amplification and non-uniformity of the total strain energy in approach zones relative to the open track. It is claimed that minimising the magnitude of total strain energy will imply lesser permanent deformation and hence reduced degradation, and a uniform distribution of total strain energy along the longitudinal direction of the track will imply uniform degradation.

3

EVALUATION OF INTERVENTIONS: SUBSTRUCTURE-LEVEL

This chapter (with minor changes) has been published as *Jain, A., Metrikine, A. V., Steenbergen, M. J. M. M., van Dalen, K. N. (2023). Railway transition zones: evaluation of existing transition structures and a newly proposed transition structure. International Journal of Rail Transportation, 1–21.*

ABSTRACT

This comprehensive study addresses the persistent issue of railway transition zone degradation, evaluating the efficacy of the most commonly used mitigation measures and proposing a novel Safe Hull-Inspired Energy Limiting Design (SHIELD) of a transition structure. Firstly, this work assesses the traditional transition structures, including horizontal and inclined approach slabs and transition wedges, using commonly studied responses (kinematic response and stress) and a recently proposed criterion based on total strain energy minimization. The second part of the paper evaluates the newly introduced transition structure (SHIELD) using the same criterion as used for the evaluation of the traditional transition structures. A detailed investigation of existing and a new design using a 2-dimensional finite element model shows SHIELD's effectiveness in managing energy flow at transition zones and provides reasoning behind the ineffectiveness of the other commonly used transition structures. The study demonstrates the robustness and comprehensiveness of the recently developed energy-based criterion and its applicability to different types of transition zones. Moreover, it highlights the potential of SHIELD as a solution to address the complexities associated with the design of railway transition zones.

3.1. INTRODUCTION

The degradation of railway transition zones [1–6] has been a persistent problem for several years and despite the various mitigation measures [1, 2, 7–13] that have been adopted, a robust design solution has yet to be found. Approach slabs and transition wedges have been commonly used in railway transition zones to reduce the problem, but their effectiveness has been questionable. These measures have in some cases proved to be either inefficient or even counterproductive [2]. Therefore, it is necessary to evaluate the existing mitigation measures with a valid design criterion and understand the reasons behind their ineffectiveness. Factors such as the soil type [14, 15], the geometric parameters of the transition structure, the depth of the track-bed layers (ballast, embankment) [16, 17], and the speed of the passing trains also play a major role in determining the performance of these transition structures. However, the performance and sensitivity of the design solutions to the factors mentioned above can be controlled by engineers by carefully evaluating the transition structure using a reliable design criterion. In this work, keeping the abovementioned factors constant, different types of transition structures will be evaluated using the criterion discussed below. The purpose of this paper is twofold. Firstly, it aims to evaluate existing design solutions for railway transition zones using a robust design criterion and provide reasoning behind their inefficiency. Secondly, the paper proposes a novel, Safe Hull-Inspired Energy Limiting Design (SHIELD) of railway transition zones based on the study presented by the authors in [18] that highlights the importance of eliminating the obstruction of energy flow as much as possible in transition zones and by guiding it away from the trackbed layers that are prone to degradation.

Design criterion: The performance of existing mitigation measures in railway transition zones has been evaluated in various ways in the literature. The methods used to evaluate the performance of these measures include numerical simulations, field measurements, material testing, dynamic track testing, and inspection. The effectiveness of these methods in evaluating the performance of mitigation measures is dependent on the choice

of performance evaluation criterion. The most common dynamic responses that have been used for assessment of the railway transition zones are vertical displacements and accelerations for rail [19, 20] and/ or sleepers, vertical stresses in ballast or/ and subgrade or/ and the stress at sleeper-ballast interface [3, 6, 12]. In [21], authors have performed a systematic analysis and studied the dynamic responses of the track components in terms of displacements, accelerations, Von Mises stress and mechanical energy, and proposed a design criterion to minimise the amplified degradation of railway transition zones. It was claimed [21] that minimising the magnitude of total strain energy will imply lesser permanent deformation and hence reduced operation-induced degradation, and the total strain energy being as uniform as possible along the longitudinal direction (i.e., without an abrupt increase or decrease) will minimise non-uniform degradation. The evaluation of the extensively used mitigation measures in railway transition zones (the first aim of the paper as mentioned above), namely approach slabs and transition wedges, will be conducted using this recently developed criterion and the most widely investigated responses (vertical rail displacement and stress in ballast layer) in literature.

Current design solutions: The approach slabs [19, 20, 22–26] are most commonly used in areas (the Netherlands) with either soft or highly compressible soils, while transition wedges are used in areas (Spain, Portugal) with either stiffer or less compressible soils. Some numerical simulations [27–31] show that the transition wedges are effective in mitigating transition effects but site measurements contradict these claims [1, 2]. A case study [2] reports an exponential degradation of the approach wedge one year after its installation, and differential settlements were comparable to the pre-installation of the wedge. Another case study cite12 relating to a culvert transition with an inclined approach slab shows that the settlement of the subgrade under the slab activates an additional degradation mechanism being the sliding of particles over the inclined plate. In addition to this, the study also reported high degradation close to the extremities of the slab. Moreover, generally speaking, an assessment of the long-term performance of the mentioned mitigation measures is missing in the literature. Hence, there is no strong evidence supporting the effectiveness of these two most commonly used mitigation measures and the reasons behind the ineffectiveness are still not clear.

New Design (SHIELD): The above-mentioned new design of a transition structure (the second aim of the paper) is proposed to guide energy away from the trackbed layers that are prone to degradation so as to avoid energy concentrations inside these layers in the vicinity of the transition interface. The authors in [18] have demonstrated that avoiding energy concentrations in the vicinity of the transition interface mitigates the local dynamic amplifications (no abrupt increase within trackbed layers) in the approach zone. Thus, the geometry of SHIELD has been optimized to guide energy away from the track. In essence, SHIELD aims to minimise the total strain energy in approach zones (implying lesser degradation) and to avoid any local operation-induced amplification in total strain energy that could contribute to the processes leading to hanging sleepers. Consequently, SHIELD provides an effective solution to the challenges of managing energy flow at railway transition zones. The ideal 3-dimensional geometry of SHIELD resembles, in fact, a hull shape. However, in this paper, the effectiveness of this mitigation

concept will be evaluated, and for that reason, only the 2-dimensional (2-D) plane is considered. It is to be noted that SHIELD is not designed to counteract autonomous settlements, and additional measures may be needed for the optimal performance of SHIELD to deal with these situations (see Section 3.4). At the same time, the material properties of SHIELD have been optimised to ensure a gradual increase in equivalent track stiffness.

In this paper, the detailed investigation of existing designs of transition structures, namely approach slabs (horizontal and inclined) and a transition wedge, will therefore be performed using a 2-D finite element model (details in Section 3.2). The rail deformations, equivalent Von Mises stress and total strain energy in track bed layers will be compared for different scenarios, and the efficiency of these transition structures will be evaluated. In the end, the efficiency of the new design of the transition structure will be demonstrated in terms of the quantities mentioned above. All transition structures studied in this work are simulated with conditions for the most efficient performance. The approach slabs are modelled such that there is no rigid body rotation, the under-sleeper pads are tuned such that there are uniform static displacements throughout the system and the material geometry used for the transition wedge is chosen to deliver the best performance in the conditions under study. In summary, the inefficiency of the mitigation measures due to inappropriate design or installation has been eliminated in this study.

3.2. METHODS

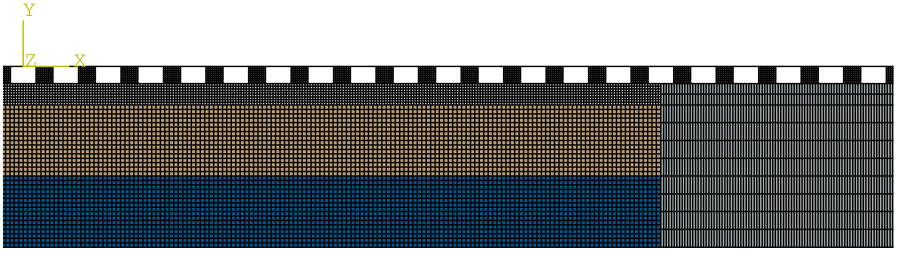

Figure 3.1: Finite element model of the standard embankment-bridge transition (see Figure 3.2 for cross-sectional details).

An embankment-bridge transition was simulated using a 2-dimensional plane-strain finite element model (see Figure 3.1). The model consists of 60 m of the ballasted track (soft side) and 20 m of the ballastless track (stiff side) The ballasted track comprises a beam representing the rail, connected using rail-pads (springs and dashpots) to the sleepers resting on a three-layered substructure. The top layer is 0.3 m of ballast with 1 m each of an embankment (dense sand) and the subgrade (clayey soil) layer underneath. The ballastless track comprises the rail, connected to sleepers with under-sleeper pads resting on a concrete structure with a depth of 2.3 m. The bridge was modelled as a solid block of concrete that is fixed at the base to provide a high stiffness contrast compared to

the ballasted track. A hard contact linear penalty method was used to define the normal behaviour and the Coulomb's friction law was adopted to define the tangential behaviour of the vertical interface between the ballasted and ballastless track. The sleeper (mesh size: 0.03 m), ballast (mesh size: 0.0375 m), embankment (mesh size: 0.0625 m), subgrade (mesh size: 0.0625 m) and the bridge (mesh size: 0.0375 m) were discretized using linear quadrilateral elements of type CPE4R and rail (mesh size: 0.01 m) using two-node linear beam elements of type B21 to form a regular mesh. The dynamic analysis was performed using implicit scheme time step integration (full Newton-Raphson method) for 1.75 s with a time step of 0.005 s. The details of the model can be found in [21] and the mechanical properties of the material are tabulated in Table 3.2 [32].

The previous paragraph describes the base model which is a standard embankment-bridge transition with no transition structure. The initial validation for this base model regarding the measured vertical rail displacements reported in [33] was performed in [21].This model was used to simulate three different types of most commonly used transition structures namely a transition wedge, a horizontal approach slab and an inclined approach slab. Additionally, a new transition structure (SHIELD) with a vertical cross-section of a trapezoid was also studied. Figure 3.2 shows the longitudinal-section details of these five modelling cases. The five cases studied in this paper are described in detail below. The under-sleeper pads (USP) on the stiff side were tuned such that the static rail deformations remain the same on both the stiff and soft sides of the track. A dynamic analysis with linear elastic material behaviour was performed using one axle load of 90 kN moving at a speed of 144 km/h for all the cases under study. It is to be noted that the vehicle effects are not accounted for in this work as the main objective is to compare the performance of each mitigation measure under study and capture the main mechanisms governing the dynamic amplifications under the simplest loading conditions and thus in the cleanest possible manner. A sensitivity analysis must be performed for different vehicle speeds, direction of movement and load configurations in order to achieve the most effective implementation of the design solution and this will be addressed in future investigations.

Each model is divided into five zones. Three zones on the soft side and two on the stiff side of the track. The details of these zones can be found in Figure 3.2 and Table 3.1. The zones that are affected by transition effects are referred to as the approach zones (AZ-I, AZ-II, AZ-III) and the zones that are unaffected by the transition effects are referred to as open track (OT-I, OT-II).

The responses (as discussed in Section 3.1) that will be studied for each of the cases mentioned above are:

- Rail displacements at nodes (see Figure 3.3) connected to sleepers in OT-I (26 to 30), AZ-I (14 to 25), AZ-II (1 to 14), AZ-III (-1 to -8), OT-II (-9)
- Maximum equivalent Von Mises stress in each zone for ballast.

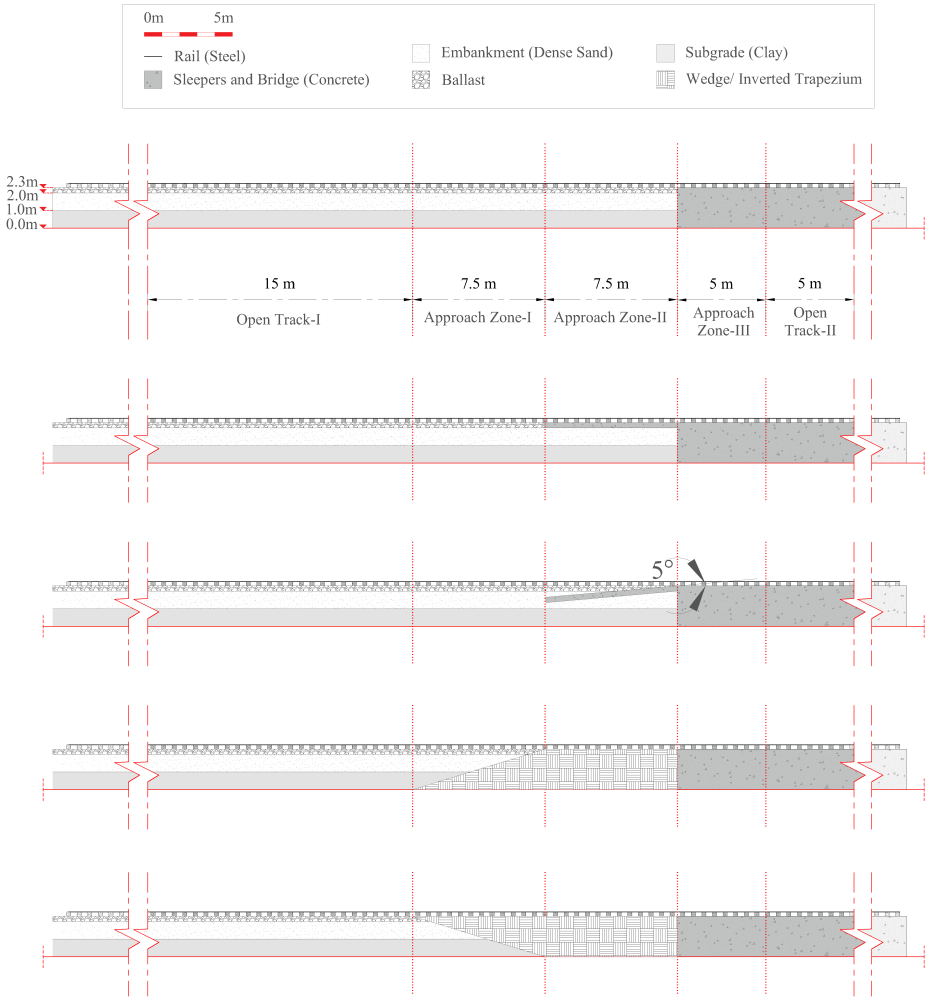

Figure 3.2: Cross-sectional details of the embankment-bridge transition under study with standard design, horizontal approach slab, inclined approach slab, transition wedge and the new design (in this order from top to bottom)

Table 3.1: Details of zones under study

Name of zone	Length (m)	Description
Open track 1 (OT-I)	15	Open track- soft side
Approach Zone 1 (AZ-I)	7.5	Approach zone to transition structure-soft side
Approach Zone 2 (AZ-II)	7.5	Approach zone from transition structure to bridge
Approach Zone 3 (AZ-III)	5	Approach zone-stiff side
Open track 2 (OT-II)	5	Open track- stiff side

- Total strain energy (in the volume considered) for each zone (as marked in Figure 3.2) in the track bed layers (ballast, embankment and subgrade). The strain energy due to only gravity is subtracted from all the results presented in the following sections. It is to be noted that kinetic energy magnitudes are negligible (approximately 10 times smaller) compared to strain energy magnitudes in each layer as shown in [21]. Therefore, the total mechanical energy in each layer is dominated by the strain energy.

In [21], the authors concluded that the total strain energy is the most comprehensive quantity to assess the degradation of railway transition zones and proposed an energy-based criterion to evaluate the performance of embankment-bridge transitions. Comparing the above-mentioned responses (incl. displacement, stress and strain energy) for different cases including transition structures, this paper will illustrate the comprehensiveness and robustness of the recently proposed energy criterion for different types of transition zones.

Table 3.2: Mechanical properties of the track components

Material	Elasticity Modulus E (N/m^2)	Density ρ (kg/m^3)	Poisson's Ratio ν	Rayleigh damping α	Rayleigh damping β
Steel (rail)	21 x 10^{10}	7850	0.3	-	-
Concrete (sleepers)	3.5 x 10^{10}	2400	0.15	-	-
Ballast	1.5 x 10^8	1560	0.2	0.0439	0.0091
Sand (embankment)	8 x 10^7	1810	0.3	8.52	0.0004
Clay (subgrade)	2.55 x 10^7	1730	0.3	8.52	0.0029
USP	1 x 10^6	500	0.1	-	-

Case 1 (Standard embankment-bridge transition): In this case, an embankment-bridge transition is studied without any transition structure to mitigate the dynamic amplifications. This case is used as a benchmark to evaluate the efficiency of currently used

mitigation measures presented in cases 2, 3 and 4 and of the newly proposed design presented in case 5. Figure 3.2 shows the geometrical details of this case.

Case 2 (Horizontal approach slab): In this case, a concrete slab of 7.5 m in length and 0.3 m in depth is used as a transition structure which is fixed at the bottom to restrict the rigid body rotation. In this case, the under-sleeper pads on the bridge are tuned such that the static displacements on the bridge are the same as on the approach slab.

Case 3 (Inclined approach slab): In this case, an inclined concrete slab of 7.5 m in length and 0.3 m in depth is used as a transition structure. It is inclined at 5 degrees with the longitudinal direction of the track and is fixed at the bottom to restrict the rigid body motion. The under-sleeper pads on the bridge and the approach slab are tuned similarly to case 2.

Case 4 (Transition Wedge): In this case, a wedge-shaped transition structure is used to mitigate the dynamic amplification in the RTZ. The geometric details of the wedge can be seen in Figure 3.2. The inclined-interface conditions are the same as mentioned above for the vertical transition interface in case 1. The mechanical properties of the wedge can be found in the Table 3.3.

Case 5 (New design-SHIELD): In this case, a new concept of design of transition structure is used to mitigate the dynamic amplifications in the RTZ. The behaviour of this transition structure is only studied in the longitudinal and vertical direction in this paper. The vertical cross-section of SHIELD in the longitudinal direction is a trapezoidal-shaped geometry with major base (top) of 15 m length and the minor base (bottom) is 7.5 m long, and other geometric details of the trapezium are given in Figure 3.2. The mechanical properties of the new transition structure can be found in Table 3.3.

Table 3.3: Mechanical properties of transition wedge and new transition structure

Transition structure	Elasticity modulus E (N/m^2)	Density ρ (kg/m^3)	Poisson's ratio ν
New design/ Wedge	3.6 x 10^8	1900	0.2

3.3. RESULTS AND DISCUSSION

This section presents the comparison of the standard embankment-bridge transition (case 1) with the horizontal approach slab (case 2), the inclined approach slab (case 3), the transition wedge (case 4), and the railway-transition SHIELD (case 5) with a trapezium-shaped cross-section, in terms of rail displacements, maximum equivalent Von Mises stress and total strain energies for the zones mentioned in Table 3.1. In addition to these comparative cases, a comparison of the two most promising solutions (case 4 and case 5) is presented at the end.

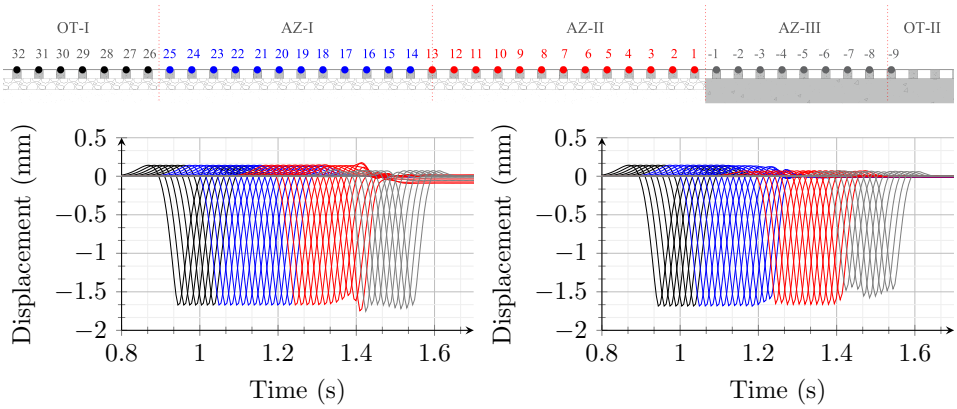

Figure 3.3: The time history of rail node displacements in OT-I (black), AZ-I (blue), AZ-II (red) and AZ-III (grey) for case 1 (left) and case 2 (right).

3.3.1. STANDARD EMBANKMENT-BRIDGE TRANSITION (CASE 1) VERSUS HORIZONTAL APPROACH SLAB (CASE 2)

Displacements: Figure 3.3 shows the time history of displacements for locations above the sleepers on the rail in the zones under study for cases 1 and 2. It can be seen that there is an increase in the magnitude of displacement under the load at locations 1 and -1 with respect to OT-I for case 1 but no increase for case 2 in any of the zones under study.

Maximum equivalent Von Mises stress: Figure 3.4 shows the maximum equivalent Von Mises stress for the ballast layer in OT-I (black), AZ-I (blue) and AZ-II (red) for case 1 and case 2. It can be verified that the increase in the max. Von Mises stress in AZ-II compared to OT-I in case 1 is observed around the transition interface. Although the horizontal approach slab leads to a reduction in the max. Von Mises stress in AZ-II (relative to OT-I), an amplification is seen in AZ-I.

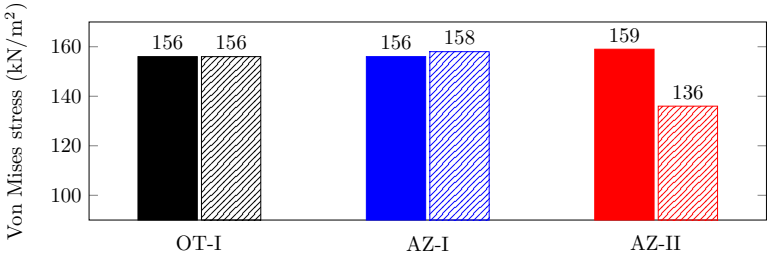

Figure 3.4: Max. Von Mises stress in the ballast layer in OT-I, AZ-I and AZ-II for case 1 (solid bars) and case 2 (striped bars).

Strain Energy: Figure 3.5 shows a comparison of total strain energy in the layers of ballast

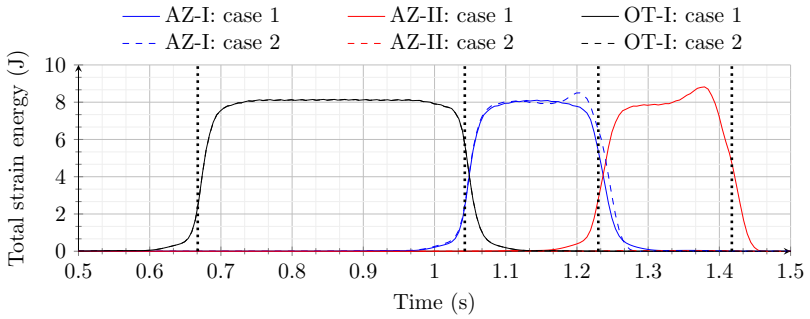

(a)

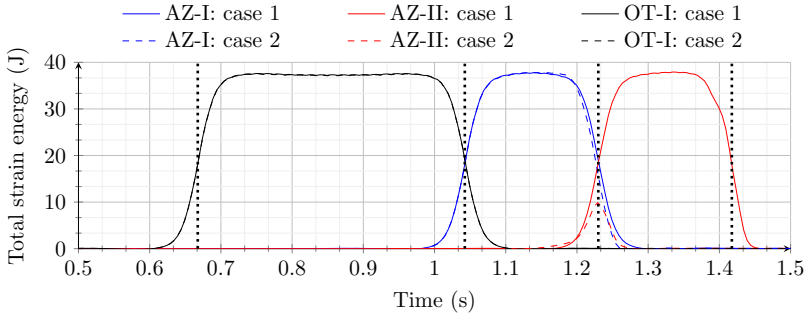

(b)

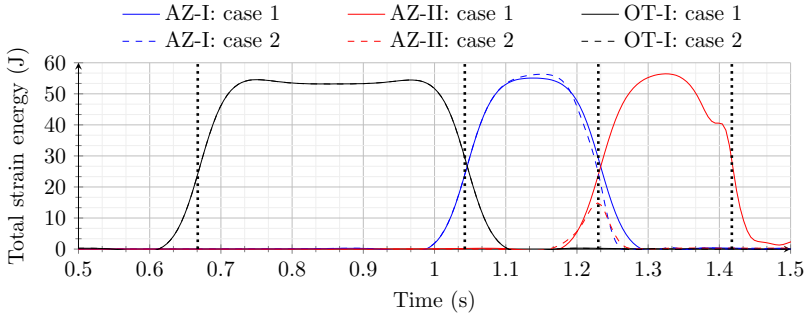

(c)

Figure 3.5: Total strain energy for the zones under study in the layers of (a) ballast, (b) embankment and (c) subgrade for case 1 and case 2. The vertical-dotted lines mark the time moments at which the load enters and exits each of the zones under study.

(a), embankment (b) and subgrade (c) in the zones shown in Figure 3.2 for case 1 and case 2. The total strain energy for case 2 in AZ-II cannot be seen in Figure 3.5 due to the magnitude being negligible compared to that in the other zones. It is evident from the results that the horizontal approach slab leads to a reduction of the total strain energy (in AZ-II relative to OT-I) in the layers of embankment and subgrade but does not lead to any significant reduction in the ballast layer. The amplification of total strain energy in the ballast layer that can be seen in AZ-II for case 1 simply shifts (it only gets slightly smaller) to AZ-I for case 2. This implies that adopting an approach slab creates a new transition zone at the end of the slab instead of mitigating the problem.

It is to be noted that, even though the horizontal approach slab shows no amplification in the kinematic response and only a minor increase in equivalent Von Mises stress, a clear amplification of the strain energy in the ballast layer is observed. The fact that the displacement decreases does not necessarily mean that the associated stress or the strain energy (combination of stress and strain) also diminishes. The strain energy amplification most clearly explains the inefficiency of this particular transition structure.

3.3.2. STANDARD EMBANKMENT-BRIDGE TRANSITION (CASE 1) VERSUS INCLINED APPROACH SLAB (CASE 3)

Displacements: Figure 3.6 shows the time history of displacements for locations above the sleepers on the rail in the zones under study for case 1 and case 3. The results shown on the left in Figure 3.6 are the same as shown previously. For case 3 the displacements are observed to reduce gradually in AZ-II compared to those in case 1.

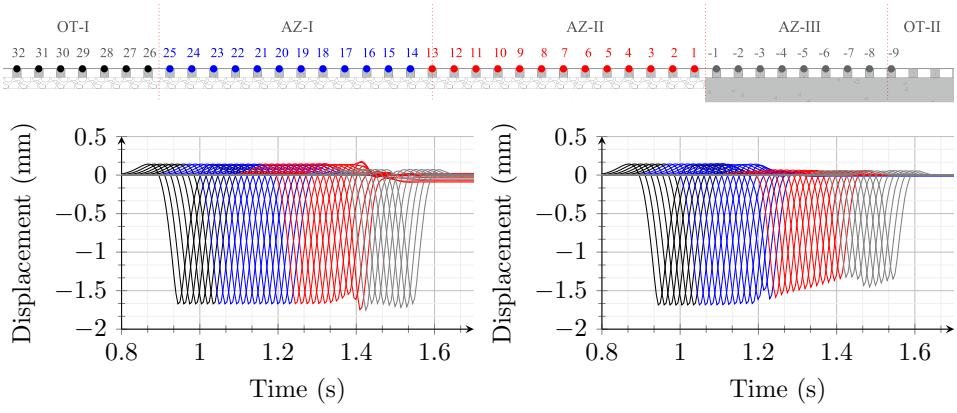

Figure 3.6: The time history of rail node displacements in OT-I (black), AZ-I (blue), AZ-II (red) and AZ-III (grey) for case 1 (left) and case 3 (right).

Maximum equivalent Von Mises stress: Figure 3.7 shows the maximum equivalent Von Mises stress for the ballast layer in OT-I (black), AZ-I (blue) and AZ-II (red) for case 1 and

case 3. Compared to case 1 and case 2 that both showed an increase in max. Von Mises stress in AZ-II and AZ-I, respectively, relative to OT-I, there is no amplification in stress for any of the zones under study for case 3. Moreover, there is a reduction in AZ-II for case 3 similar to what is observed for case 2, but the amount of reduction is higher.

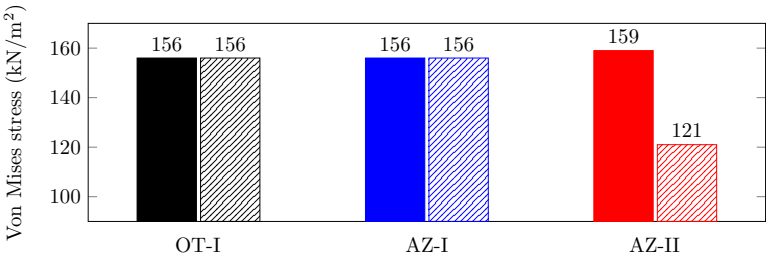

Figure 3.7: Max. Von Mises stress in the ballast layer in OT-I, AZ-I and AZ-II for case 1 (solid bars) and case 3 (striped bars).

Strain Energy: Figure 3.8 shows a comparison of total strain energy in the layers of ballast (a), embankment (b) and subgrade (c) for the zones shown in Figure 3.2, for case 1 and case 3. The total strain energy in all three track-bed layers in OT-I is the same for both the cases under study as expected. The total strain energy shows a peak in AZ-I for case 3 which is the same in magnitude as the peak observed for case 1 in AZ-II. Like for case 2, this implies that the transition effects are simply shifted but not mitigated by using an inclined approach slab. Moreover, a small increase in the total strain energy is also observed for the subgrade layer in case 3 compared to case 1. In summary, the use of an inclined approach slab could not reduce the dynamic amplifications in the RTZ under study but made it worse. It is important to highlight that the inclined approach slab seemed to be an efficient solution when evaluated using the kinematic response or the stress distribution as a criterion. However, the energy criterion clarifies the reason behind the inefficiency of this particular transition structure in reality.

3.3.3. STANDARD EMBANKMENT BRIDGE TRANSITION (CASE 1) VERSUS TRANSITION WEDGE (CASE 4)

Displacements: Figure 3.9 shows the time history of displacements for locations above the sleepers on the rail in the zones under study for case 1 and case 4. As mentioned above, the displacement at locations 1 and -1 for case 1 exhibits an increase, as is evident from the observation, but for case 4 the displacements gradually decrease in AZ-I and becomes constant in AZ-II and AZ-III. No abrupt changes were observed in any of the zones under study. Hence, the transition wedge seems to be a promising solution if the performance is evaluated solely based on vertical rail displacements.

Maximum equivalent Von Mises stress: Figure 3.10 shows the maximum equivalent Von Mises stress for the ballast layer in OT-I (black), AZ-I (blue) and AZ-II (red) for case 1 and

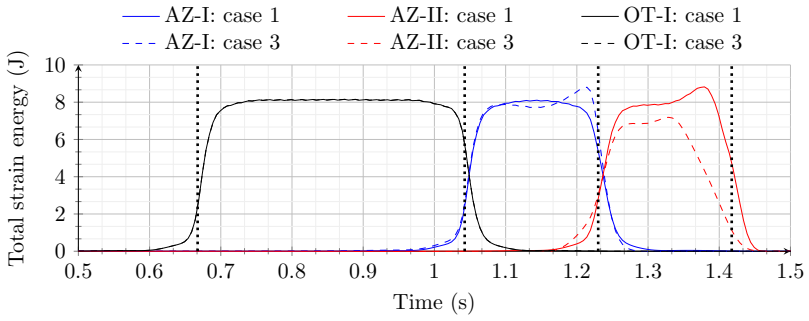

(a)

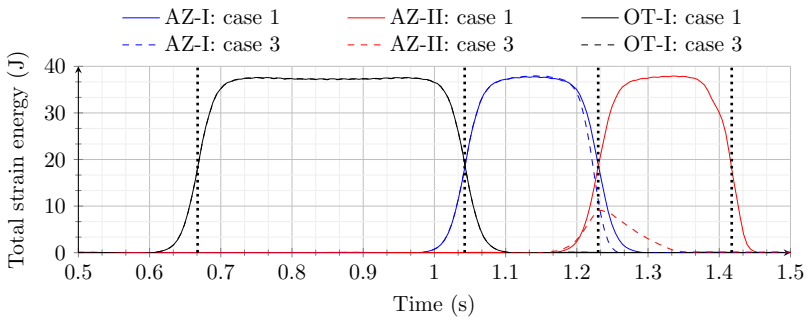

(b)

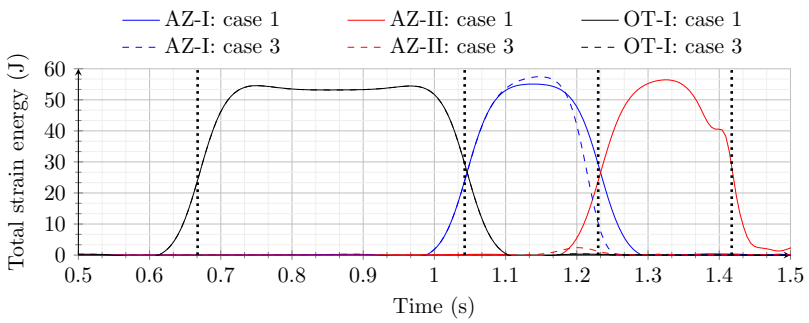

(c)

Figure 3.8: Total strain energy for the zones under study in the layers of (a) ballast, (b) embankment and (c) subgrade for case 1 and case 3. The vertical-dotted lines mark the time moments at which the load enters and exits each of the zones under study.

case 4. Although the displacement fields looks ideal for case 4, it can be verified that the Von Mises stress distribution across the zones is non-uniform and increases in AZ-I relative to OT-I (and then reduces again in AZ-II). This increase in stress indicates that the transition effects are not mitigated by the transition wedge but only moved further (on the soft side) from the previous location, like in case 1. The increase in case 4 is much higher than that observed in case 1 (compare Figure 3.4 and Figure 3.10), implying that the response is worse with this particular transition structure.

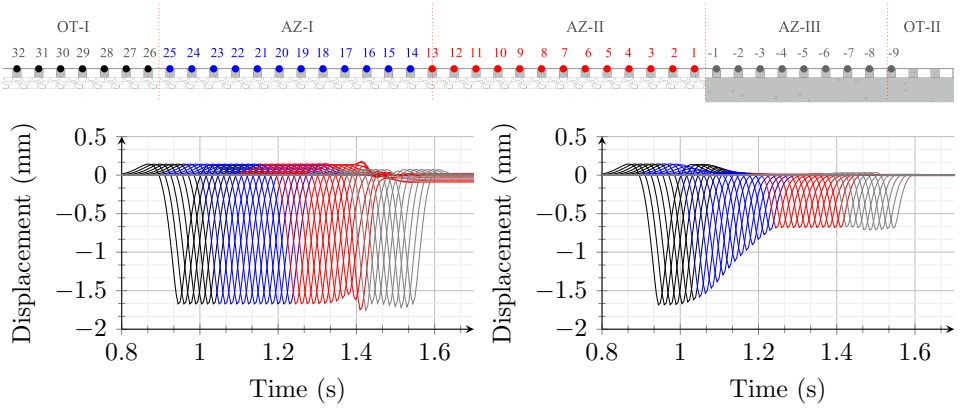

Figure 3.9: The time history of rail node displacements in OT-I (black), AZ-I (blue), AZ-II (red) and AZ-III (grey) for case 1 (left) and case 4 (right).

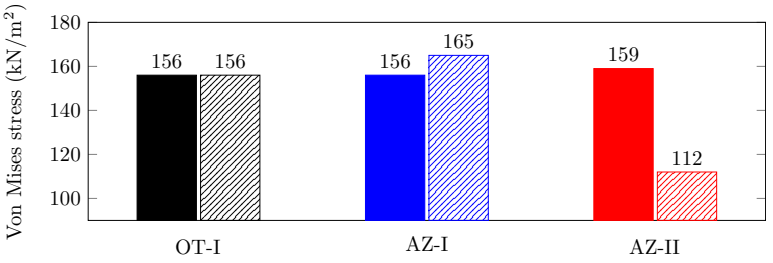

Figure 3.10: Max. Von Mises stress in the ballast layer in OT-I, AZ-I and AZ-II for case 1 (solid bars) and case 4 (striped bars).

Strain Energy: Figure 3.11 shows a comparison of total strain energy in the layers of ballast (a), embankment (b) and subgrade (c) for the zones shown in Figure 3.2 for case 1 and case 4. The transition wedge used in case 4 shows a significant reduction in total strain energy in the layers of embankment and subgrade. However, the total strain energy in the layer of ballast shows an increase towards the end of AZ-I compared to Figure 3.15a, where it smoothly decreases as a result of the added specific transition structure which provides the same change in overall (static) tracks stiffness as the current wedge structure.

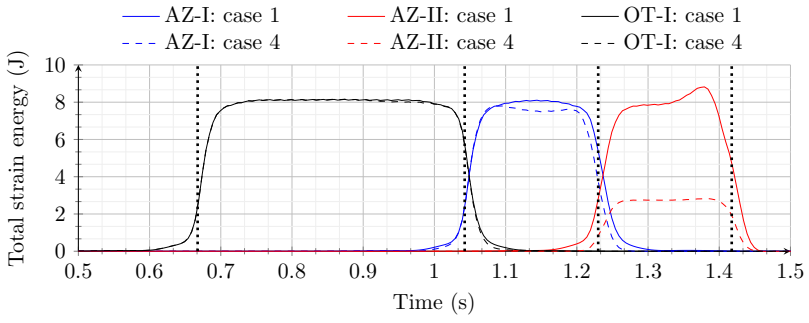

(a)

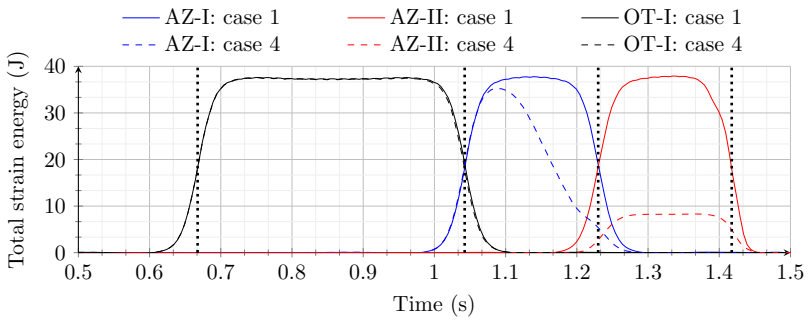

(b)

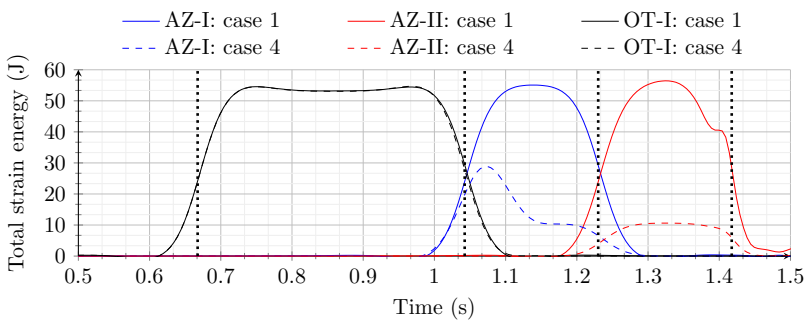

(c)

Figure 3.11: Total strain energy for the zones under study in the layers of (a) ballast, (b) embankment and (c) subgrade for case 1 and case 4. The vertical-dotted lines mark the time moments at which the load enters and exits each of the zones under study.

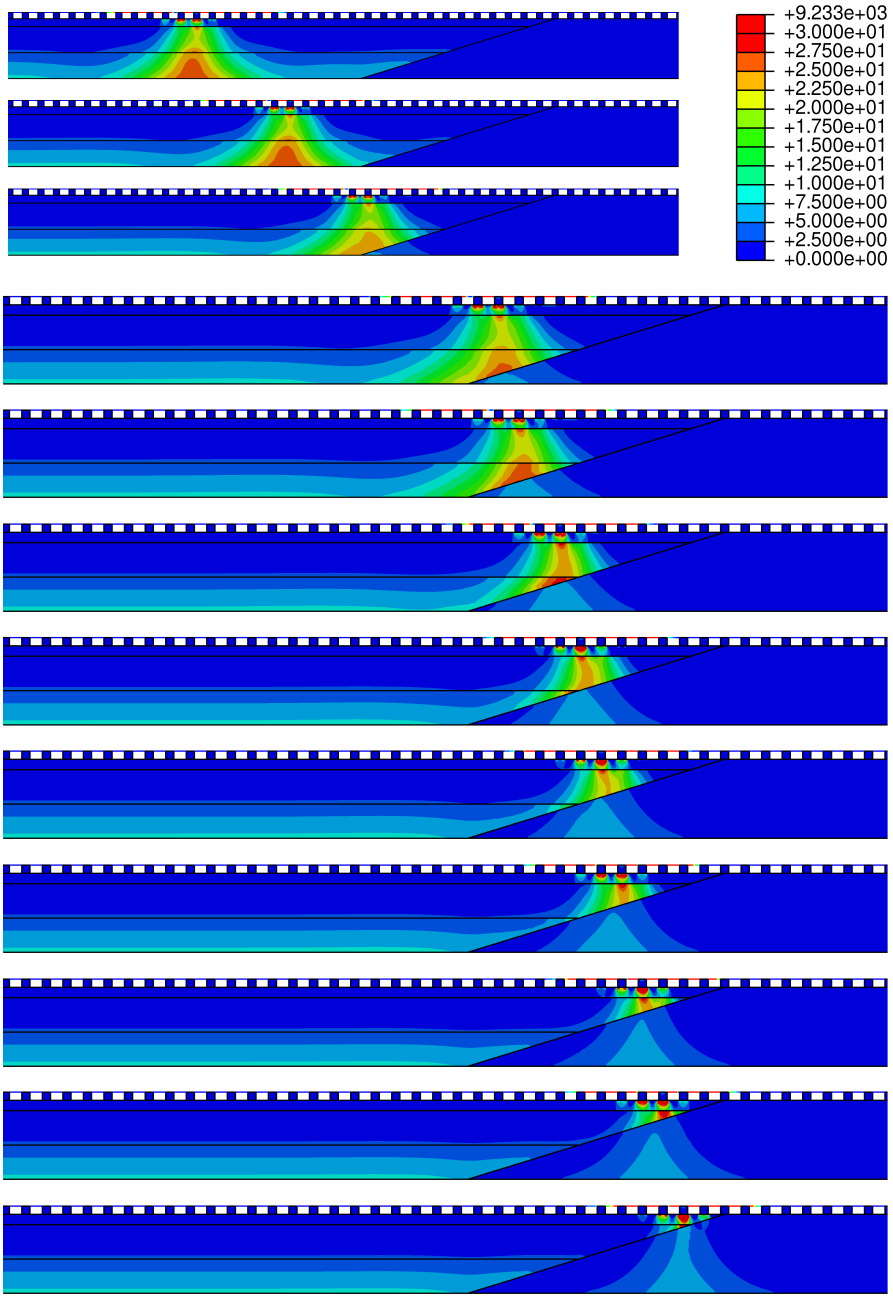

Figure 3.12: Contour plot of the strain energy in the system as the load approaches the transition wedge. Snapshots for time moments (from top to bottom) 0.8841 s, 0.9741 s, 1.049 s, 1.064 s, 1.079 s, 1.109 s, 1.129 s, 1.144 s, 1.154 s, 1.174 s, 1.184 s, 1.204 s.

Although the magnitude of total strain energy in AZ-I and AZ-II is less compared to the standard embankment-bridge transition (case 1), the reduction in AZ-I is not significant considering that the overall stiffness of this zone has increased considerably compared to OT-I which ideally should lead to a significant reduction in strain energy similar to case 5, as discussed in following sections. The inefficiency of the transition wedge can be attributed to guiding of strain energy (see Figure 3.12) from the bottom layers to the ballast layer due to the unfavourable geometry. The response will amplify even more in case of imperfections in the track, as demonstrated in Section 3.3.5.

3.3.4. STANDARD EMBANKMENT BRIDGE TRANSITION (CASE 1) VERSUS NEW DESIGN: SHIELD (CASE 5)

Displacements: Figure 3.13 shows the time history of displacements for locations above

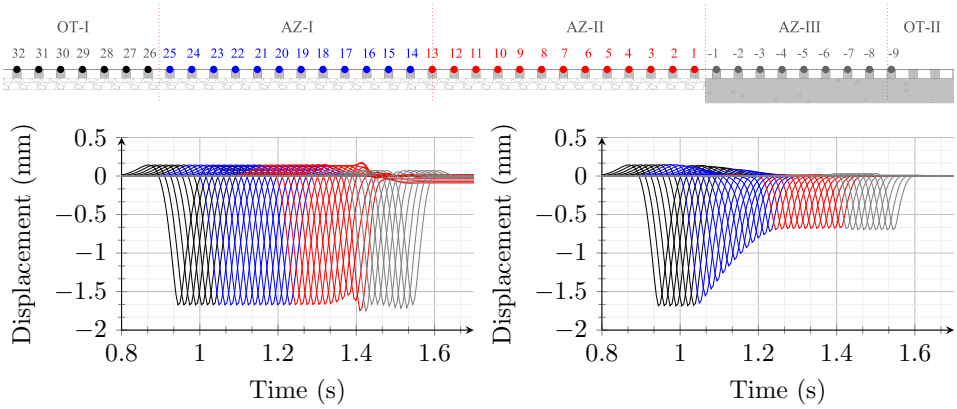

Figure 3.13: The time history of rail node displacements in OT-I (black), AZ-I (blue), AZ-II (red) and AZ-III (grey) for case 1 (left) and case 5 (right).

the sleepers on the rail in the zones under study for case 1 and case 5. Observing the results, it is apparent that the time history of displacements shows a resemblance to the case with a transition wedge due to the overall (static) track stiffness being the same. The displacements under the load gradually decrease in AZ-I, and becomes constant in AZ-II and AZ-III, and no abrupt changes were observed in any of the zones under study.

Maximum equivalent Von Mises stress: Figure 3.14 shows the maximum equivalent Von Mises stress for the ballast layer in OT-I (black), AZ-I (blue) and AZ-II (red) for case 1 and case 5. Case 5, which includes the new design of transition structure, demonstrates a gradual decrease in max. Von Mises stress in AZ-I and AZ-II relative to OT-I. No amplification is observed in any of the zones under study for case 5, unlike all the cases studied above. This indicates that the behaviour is promising, but the energy analysis (below) should obviously confirm that before conclusions can be drawn.

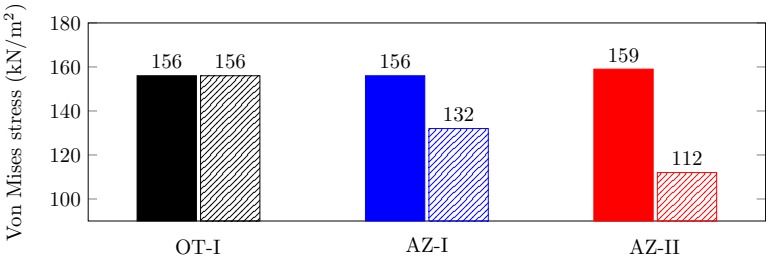

Figure 3.14: Max. Von Mises stress in the ballast layer in OT-I, AZ-I and AZ-II for case 1 (solid bars) and case 5 (striped bars).

Strain Energy: Figure 3.15 shows a comparison of total strain energy in the layers of ballast (a), embankment (b) and subgrade (c) for the zones shown in Figure 3.2 for case 1 and case 5. It is evident from the results that the new design leads to a gradual decrease in total strain energy in all three track-bed layers. No peaks are observed in AZ-I and AZ-II, and the magnitudes are much lower than in OT-I. Case 5 shows a significant reduction in the magnitude of the total strain energy in AZ-I and AZ-II relative to OT-I in the layers of ballast and embankment compared to all the cases with existing mitigation measures. In the subgrade layer, case 4 (Figure 3.15c) shows more reduction in total strain energy compared to case 5 in AZ-I. However, this can be attributed to the larger volume of stiffer material in AZ-I in case 4 compared to case 5, as the strain energy density is typically smaller for stiffer materials. In any case, SHIELD shows no amplification in any of the zones or layers under study and guides energy away from the upper track bed layers as seen in Figure 3.16. This is exactly the reason as to why case 5 outperforms case 4 (Figure 3.12), where the energy is guided towards the upper track bed layers, which leads to an energy concentration.

3.3.5. TRANSITION WEDGE (CASE 4) VERSUS SHIELD OF RAILWAY TRANSITION ZONE (CASE 5)

Figure 3.17 summarises the comparison of case 4 and case 5 in terms of equivalent stiffness (static) in AZ-I, rail displacements, equivalent Von-Mises stress and total strain energies. Figure 3.17a shows a gradual increase (same for case 4 and case 5) in equivalent trackbed stiffness from OT-I to AZ-II. Figure 3.17b shows a gradual decrease in rail displacements in AZ-I which is same for both case 4 and case 5. However, the equivalent Von Mises stress (Figure 3.17c) in AZ-I for case 4 is much higher than case 5 due to reasons discussed in Section 3.3.3, and this can be also seen in strain energy (Figure 3.17d) that combines the stress and strain fields over a volume. On one hand, despite a significant increase in stiffness, the max. Von Mises stress and the total strain energy in the AZ-I for the case with the transition wedge show no significant improvement in the ballast layer. On the other hand, case 5 shows a gradual decrease in Von Mises stress and total strain energy in AZ-I. Although case 4 shows no amplification in the total strain energy in AZ-I with respect to OT-I, it can be verified that the total strain energy increases locally in the

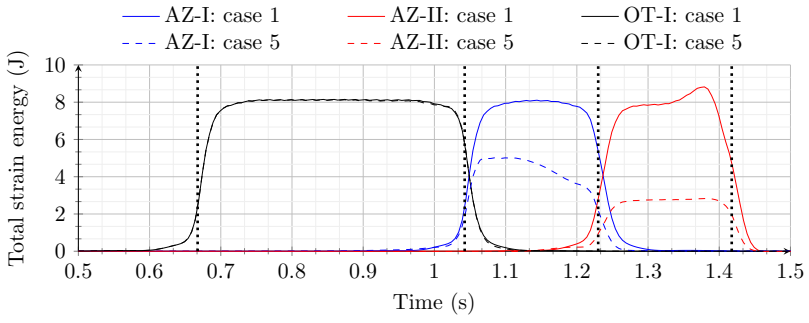

(a)

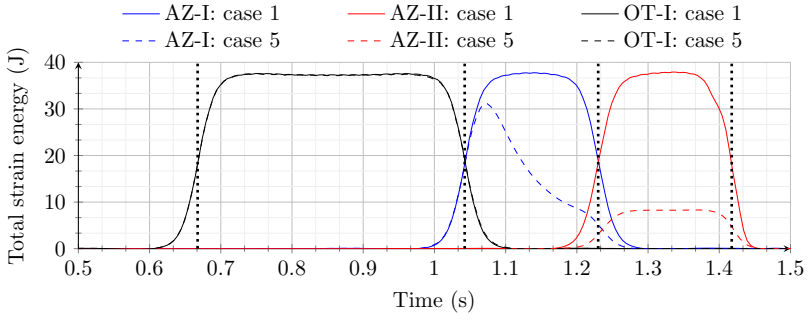

(b)

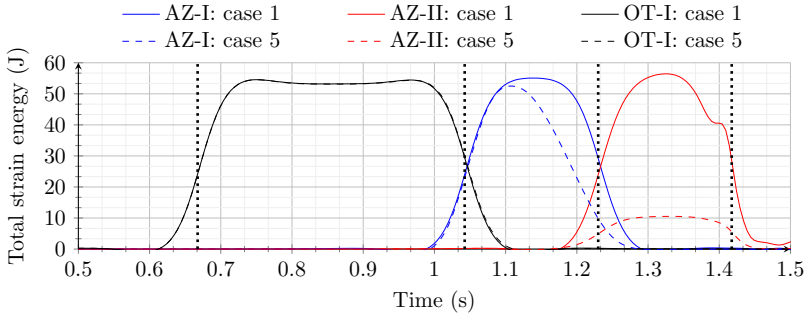

(c)

Figure 3.15: Total strain energy for the zones under study in the layers of (a) ballast, (b) embankment and (c) subgrade for case 1 and case 4. The vertical-dotted lines mark the time moments at which the load enters and exits each of the zones under study.

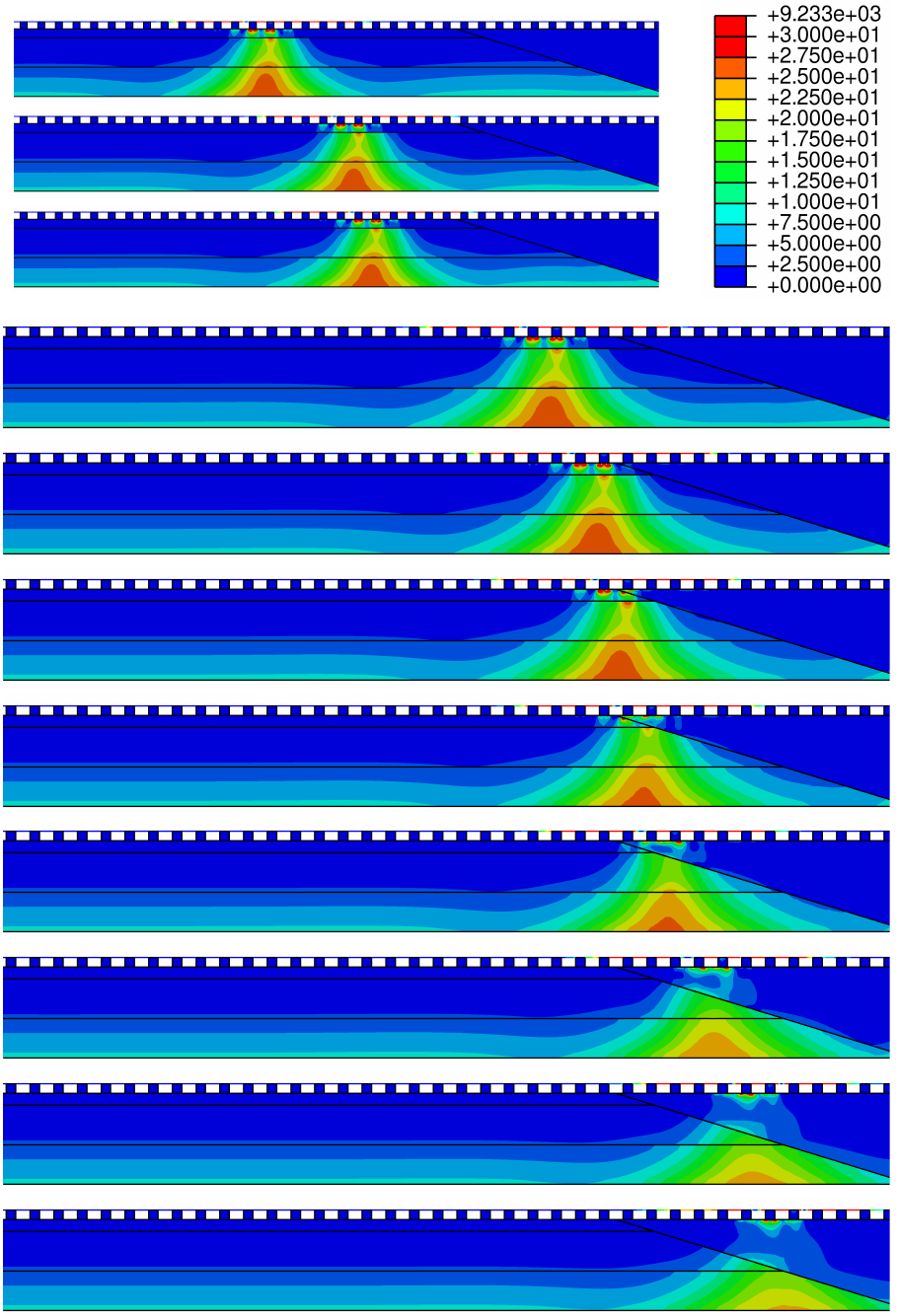

Figure 3.16: Contour plot of the strain energy in the system as the load approaches the new transition structure: SHIELD. Snapshots for time moments (from top to bottom) 0.8841 s, 0.9591 s, 0.9741 s, 1.004 s, 1.034 s, 1.049 s, 1.064 s, 1.079 s, 1.109 s, 1.134 s, 1.149 s.

proximity of interface between AZ-I and AZ-II in the ballast layer. Moreover, Figure 3.12 shows that the strain energy is guided towards the upper layers leading to an increase due to the unfavourable geometry of the transition wedge. This increase in strain energy can be worse in case of an imperfection along the track in this zone. Thus, in this section, the total strain energy for cases 4 and 5 will be compared to evaluate their performances in a non-ideal condition, i.e., a contact loss under sleeper 15 in AZ-I (refer to Figure 3.18 for the location of this sleeper) for case 4 and case 5.

Figure 3.18 shows the comparison of the total strain energy (OT-I, AZ-I, AZ-II) between case 4 and case 5 in the ballast layer under the non-ideal condition for both the cases. The total strain energy in the embankment and subgrade layers are not shown as amplifications due to the lost contact between sleeper 15 and the ballast layer are observed only in the ballast layer. Indeed, a significant amplification of total strain energy can be seen in AZ-I for case 4. A similar amplification takes place for case 5, but it is not high enough to exceed the energy level in OT-I. Hence, it is concluded that the case 5 outperforms case 4 not only in ideal conditions (Section 3.3.3 and Section 3.3.4) but especially in a non-ideal condition.

3.4. CONCLUSIONS

A comprehensive evaluation of existing transition structures and a new safe hull-inspired energy limiting design (SHIELD) for railway transition zones was performed.

Firstly, the existing transition structures, namely horizontal approach slab, inclined approach slab and transition wedge, were evaluated in terms of the most commonly studied responses (vertical rail displacement and stress in ballast) and the recently developed criterion based on total strain energy. None of the cases with transition structures led to local amplification in vertical rail displacements in the proximity of the transition interface, while the standard embankment-bridge transition case (with no transition structure) does. The maximum Von Mises stress in the zones under study showed a reduction for the cases with approach slabs (both horizontal and inclined) but an increase for the case with a transition wedge. In the end, looking at the total strain energy, which is the most comprehensive response quantity (and therefore the best damage indicator), a clear amplification was seen for all existing transition structures, which indicates the poor performance of these existing transition structures.

The second part of the paper evaluates the newly introduced transition structure (SHIELD) using the same criterion as used for the evaluation of the existing transition structures. The results presented in Section 3.3 make it evident that there is a gradual decrease in vertical rail displacements, max. equivalent Von Mises stress and, most importantly, in the total strain energy when moving from the open track to the transition interface. No local amplification was observed in any of the approach zones and, in addition to this, the magnitudes of all the responses were much lower than those in all other cases studied in this paper. Furthermore, the transition wedge was clearly outperformed by SHIELD under non-ideal conditions (loss of contact under the sleepers). Even

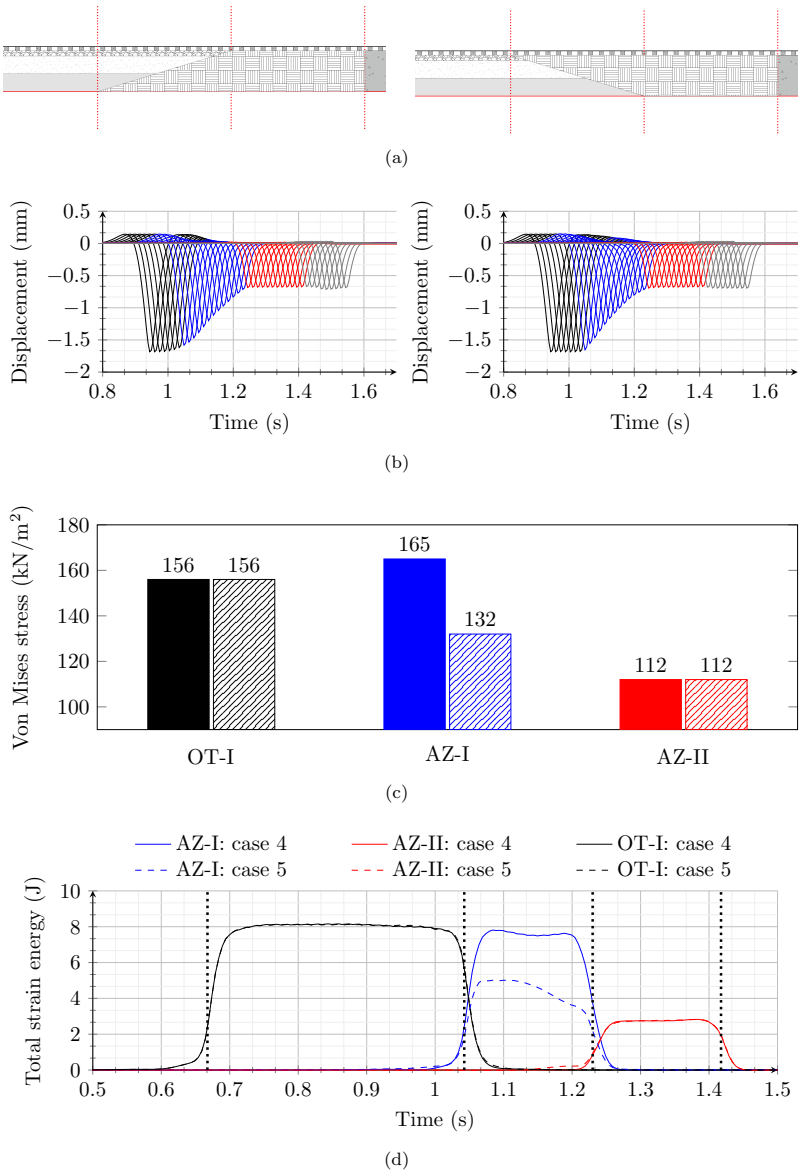

Figure 3.17: (a) cross-section details, (b) comparison of rail displacements for case 4 (left) and case 5 (right), (c) equivalent Von Mises stress and (d) time history of total strain energy

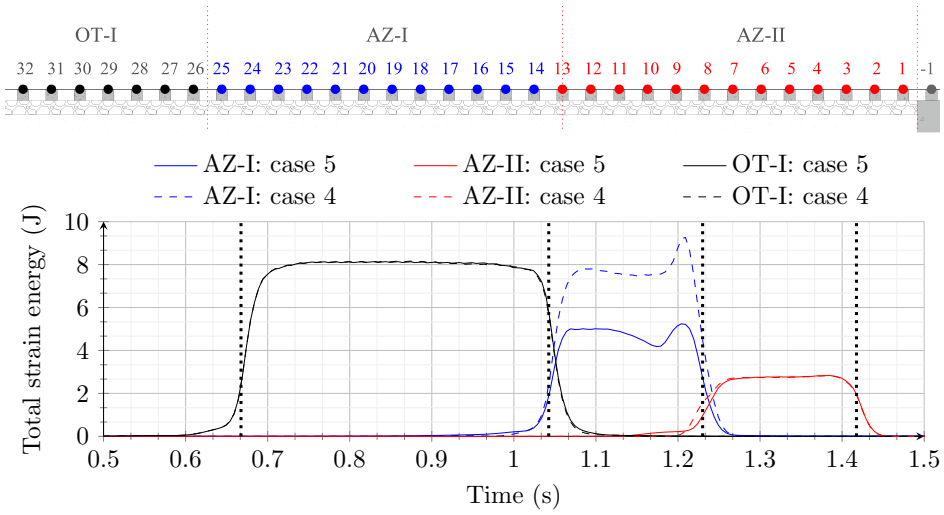

Figure 3.18: Total strain energy for the zones under study in the ballast layer for case 4 and case 5 accounting for the loss of contact under sleeper 15 in AZ-I for both the cases. The vertical-dotted lines mark the time moments at which the load enters and exits each of the zones under study.

though the SHIELD performs well under non-ideal conditions and is capable of dealing with consequences of autonomous settlement to some extent, it can be also combined with measures like adjustable sleepers [12] or wedge-shaped sleepers [13] to avoid loss of contact due to non-uniform settlement and reduce the maintenance requirements even more.

Future investigations related to this newly proposed transition structure must include the influence of the vehicle-structure interactions, three-dimensional response, material and geometric parameter sensitivities and experimental validation to lay out the guidelines regarding the choice of the parameters for effective and robust solutions.

4

EVALUATION OF INTERVENTIONS: SUPERSTRUCTURE-LEVEL

This chapter (with minor changes) has been published as *A. Jain, A. V. Metrikine, M. J. Steenbergen, K. N. van Dalen, Dynamic amplifications in railway transition zones: performance evaluation of sleeper configurations using energy criterion, Frontiers in Built Environment (2024).*

ABSTRACT

Railway transition zones present a major challenge in railway track design mainly due to abrupt jumps in stiffness and differential settlements that result from crossing stiffer structures such as bridges or culverts. Despite numerous efforts to mitigate these transition effects at both the superstructure and substructure levels, a comprehensive solution remains elusive. Substructure-level interventions have demonstrated some effectiveness but are often cost-prohibitive and challenging to implement in existing operational railway transition zones. In contrast, mitigation measures at the superstructure (rail, sleepers, rail-pads, under-sleeper pads) level can be easily installed but have shown limited improvement in site measurements. This study evaluates the influence of different sleeper configurations in transition zones and reduced sleeper spacings on the operation-driven dynamic amplifications in railway transition zones, employing a recently proposed criterion based on the total strain energy in the track-bed layers (ballast, embankment, and subgrade). In addition to this, the influence of the loss of contact between sleepers and ballast (i.e., hanging sleepers), which typically results from the differential settlement, is studied. The first part of the paper provides useful insights regarding the interventions (and/or initial design) in the sleeper configuration and spacing, whereas the second part of the work highlights the need for interventions to deal with the loss of contact between sleeper and ballast. A 2-dimensional finite element model of an embankment-bridge transition was used for the analysis. The results show that it is not possible to mitigate the transition effects completely using the interventions involving sleeper spacing and configuration.

4.1. INTRODUCTION

Railway transition zones (RTZs) are regions of inhomogeneity in railway tracks where the track crosses stiffer structures, such as bridges or culverts. This inhomogeneity [1] results in an abrupt jump in stiffness experienced by the moving load, causing significant dynamic amplification [2–4] and eventually contributing to differential settlement in RTZs. In addition to this, the differential settlement in transition zones is also due to differences in autonomous settlement of the foundations of the stiff and soft parts. Operation-driven dynamic amplifications in RTZs are the subject of this paper. These dynamic amplifications may not be very prominent when considering kinematics but can be clearly seen in terms of the strain energy of the trackbed layers [5]. Despite numerous attempts to alleviate these transition effects by gradually increasing stiffness at both the superstructure (rail, rail pads, sleepers, under-sleeper pads) and substructure levels (ballast, sub-ballast, embankment, subgrade), a comprehensive solution remains elusive.

Mitigation measures at the substructure level, including approach slabs [6–8], transition wedges [9–13], glued ballast, geotechnical improvements [14, 15], etc. have demonstrated some effectiveness; however, their cost-effectiveness ratio is unfavourable. Additionally, these measures are difficult to implement in existing, operational railway transition zones. In contrast, mitigation measures at the superstructure level [8, 15–17] can be easily installed for both old and new transition zones. Although the existing literature involving analytical/ numerical evaluations suggests that these measures may be efficient to some extent [5, 18], site measurements have not exhibited significant improvements from these interventions [19, 20].

Common superstructure-level interventions include auxiliary rails [15–17], under-sleeper pads, and large [21–23] or closely spaced sleepers [19, 20, 24, 25] made from modified materials [26, 27]. Sleepers are typically constructed from wood or reinforced concrete, with the latter requiring a C50/60 strength class as defined by the Eurocode, which specifies the Elastic modulus of 38 GPa and a Poisson's ratio of 0.2 (EN 1992-1-1, 2009). Alternative materials, such as plastic, rubber, and composites, have also been utilized in transition zones, with wood proving to be the most effective among them [28]. The average sleeper dimensions are 2.6m x 0.24m x 0.24m, and a standard spacing of 0.6m [29, 30] is commonly employed in railway tracks, including in transition zones. Large [21, 22, 31] or closely spaced sleepers [19, 20, 24] have been implemented in transition areas to reduce the abrupt change in track stiffness. These modifications have been effective in decreasing ballast settlement and improving the distribution of the contact force between sleeper and ballast over a larger area, but they have not reduced dynamic load amplification in transition zones. Various sleeper configurations have been analyzed [32] to evaluate track support separation and to maintain optimal track performance, as assessed by sleeper vertical displacements and stress on ballast. Efforts have also been made to minimize the maximum wheel-rail contact force and stress between the sleeper and foundation, seeking the most efficient distributions of sleeper spacing [32] adjacent to the transition. However, previous studies have not clearly stated the reasons behind the unsatisfactory performance of these solutions, nor have they assessed the broader implications of these measures on the degradation of ballast, embankment and subgrade. A recent study [5] presents a criterion based on total strain energy in the track bed layers as an indicator of potential irreversible permanent deformations, which can be employed to assess the influence of these solutions on the onset of degradation in different trackbed layers. A detailed analysis of all the track components was performed in [5] by analysing the kinematic responses, stresses, and kinetic and strain energies, concluding that the strain energy is the most comprehensive quantity to evaluate the railway transition as it comprises both distortional and volumetric components of strain energy, while Von Mises stress for instance only captures the distortional component of energy. The details of the criterion can be found in [5] and a valid application of this criterion can be found in a related study [33].

In this paper, the influence of various sleeper configurations and spacing on the dynamic behaviour of railway transition zones are investigated and the need for interventions to mitigate the loss of contact between sleepers and the ballast layer is highlighted, using the recently proposed criterion [5] based on total strain energy in trackbed layers. Firstly, the influence of the specific position of the first sleeper on both sides of the transition interface and the effect of overall and localised (i.e., only in the approach zone) reduced sleeper spacing is studied for the ideal geometric track profile. Secondly, the influence of non-ideal geometry (as a consequence of differential settlement) which entails the loss of contact [34, 35] between sleepers and ballast on the total strain energy distribution is investigated. The first part of the paper concerns the interventions (and/or design choices) at the superstructure level to avoid dynamic amplifications in transition zones, whereas the second part highlights the need for mitigation measures to deal with

the loss of contact.

4.2. FINITE ELEMENT MODEL OF AN EMBANKMENT-BRIDGE TRANSITION

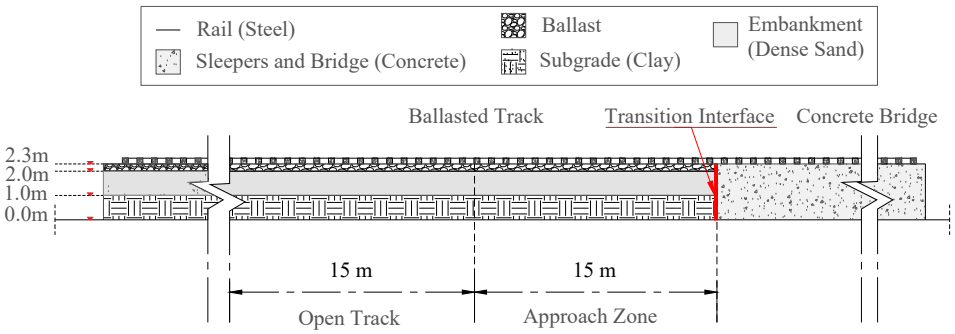

Figure 4.1: Geometric details of the embankment-bridge transition under study.

A two-dimensional (2-D), plane-strain finite element (FE) model of an embankment-bridge transition was created using ABAQUS, mainly comprising of ballasted track (soft side) of 60m in length and a ballastless track (stiff side) of 20 m length. The main components of the system under study as shown in Figure 4.1 namely rail, railpads, sleepers, under sleeper pads, ballast layer (0.3 m deep), embankment layer (1 m deep), subgrade (1 m deep), and a concrete bridge (2.3 m deep). The sleeper, ballast, embankment, subgrade, and bridge were meshed using linear plane strain quadrilateral elements (CPE4R), and the rail was discretized using two-node linear beam elements (B21). Materials for all components mentioned above were characterized by elastic properties (Elasticity modulus, Poisson's ratio, density, and Rayleigh damping factors) as tabulated in Table 4.1 [33]. Material properties tabulated in Table 4.1 have been adopted based on a detailed evaluation and design limits proposed in [36]. A static analysis was performed to tune the elastic properties of a thin layer of material under the sleepers referred to as under-sleeper pads (USP) on the stiff side, ensuring the same static vertical rail displacements throughout the track. It is to be noted that these are not conventional under sleeper pads but a way to insure the same static deformations throughout the track in order to study only dynamic effects of the moving load. The key interface and boundary conditions used in the model included vertical springs and dashpots connecting the rail and sleeper midpoint, surface-to-surface tie constraints between the sleeper-ballast, ballast-embankment, and embankment-subgrade, and a hard contact linear penalty method to define the normal behaviour combined with a Coulomb friction model for tangential behaviour at the vertical interface between the ballasted and the ballastless track. Firstly, a static analysis was performed to establish the initial stress state under self-weight, followed by a dynamic

analysis (full Newton-Raphson method) for a single moving axle load of 90 kN and a velocity of 144 km/hr, using a DLOAD subroutine in ABAQUS [37]. Only one axle load and speed (sub-critical) has been adopted as the main objective of this work is to compare the performance of different configurations (see Section 4.3) under study and capture the main mechanisms governing the dynamic amplifications under the simplest loading conditions and thus in the cleanest possible manner, to provide insight regarding efficiency or inefficiency of the superstructure level interventions. The effects are expected to be amplified for higher speeds and axle loads. The 2-D model used in this paper has been validated against a 3-D model and the details can be found in [5, 36] and Chapter 7. An ideal geometric track profile is used for evaluation of all the cases as the aim is to study the mechanisms (in isolation of other mechanisms) associated to the initial state of the track subjected to operation-induced loads. The strain energy distribution was found to be very similar in both 2D and 3D models (see Figure 4.2). For the purpose of this work, 2-D models are used as the cost of computation using the same resources was much higher for one iteration using a 3-D model (approximately 8 hours) compared to 2-D models (approximately 40 minutes). Moreover, the criterion [5] used for evaluation in this work claims to predict the onset of damage in non-linear models based on energy amplification in models with linear elastic materials.

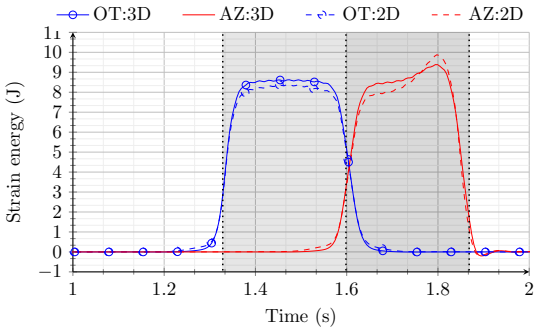

Figure 4.2: Comparison of the total strain energy in the ballast layer using a 2-D and a 3-D model.

For this study mainly two zones were studied to investigate the dynamic amplifications in railway transition zones (RTZs), namely the open track (OT) and the approach zone (AZ) on the ballasted track (soft side). Each of these zones is 15m in length. Figure 4.1 shows the zone unaffected by the transition effects (open track) and the zone next to the transition interface (approach zone) between the ballasted track and the concrete structure (stiff side), where significant dynamic amplifications are observed. The results studied in this paper are the temporal variation of total strain energy in each of the trackbed layers (ballast, embankment, and subgrade) for the open track and the approach zone. In addition, a percentage increase of the maximum total strain energy in AZ relative to the OT for each case is also presented.

Table 4.1: Mechanical properties of the track components

Material	Elasticity Modulus E [N/m^2]	Density ρ [kg/m^3]	Poisson's Ratio ν	Rayleigh damping α	β
Steel (rail)	21 x 10^{10}	7850	0.3	-	-
Concrete (sleepers)	3.5 x 10^{10}	2400	0.15	-	-
Ballast	1.5 x 10^{8}	1560	0.2	0.0439	0.0091
Sand (embankment)	8 x 10^{7}	1810	0.3	8.52	0.0004
Clay (subgrade)	2.55 x 10^{7}	1730	0.3	8.52	0.0029
USP	1 x 10^{6}	500	0.1	-	-

4.3. RESULTS AND DISCUSSION

This paper investigates six different configurations of the first sleeper on either side of the transition interface (Figure 4.3) and three different layouts of sleepers with reduced spacing (Figure 4.5). In the end, the influence of the number of hanging sleepers on the total strain energy amplification is studied. The following sections will describe all these scenarios in detail.

4.3.1. CONFIGURATION OF SLEEPERS ADJACENT TO THE TRANSITION INTERFACE

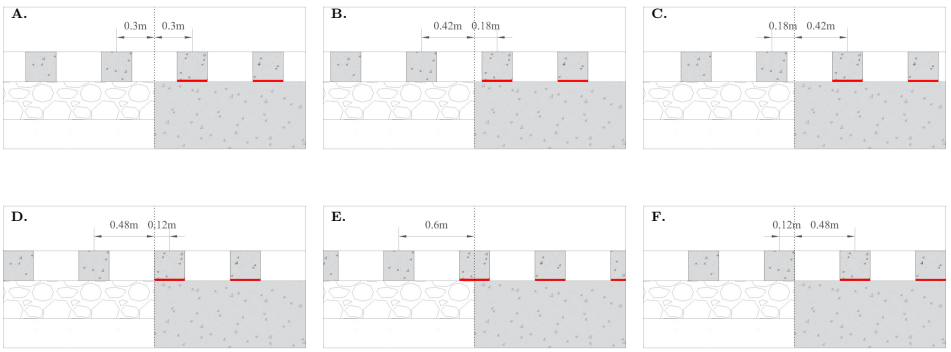

Figure 4.3: Study cases of different sleeper configurations (a) config 1, (b) config 2, (c) config 3, (d) config 4, (e) config 5, and (f) config 6 around the transition interface (the red layer represents the under-sleeper pads on the stiff side)

The six different sleeper configurations in the proximity of the transition interface as shown in Figure 4.3 are investigated. The six configurations can be broadly classified

into two categories; config.1-3 and config.4-6. Config.1-3 investigate the influence of 3 different spacing configurations of the first sleeper adjacent to the transition interface (on both sides) with respect to the interface, on the total strain energy in AZ compared with that in OT. Config.4-6 analyze the extreme scenarios where the edge/ mid-point of the sleeper is located at the transition interface.

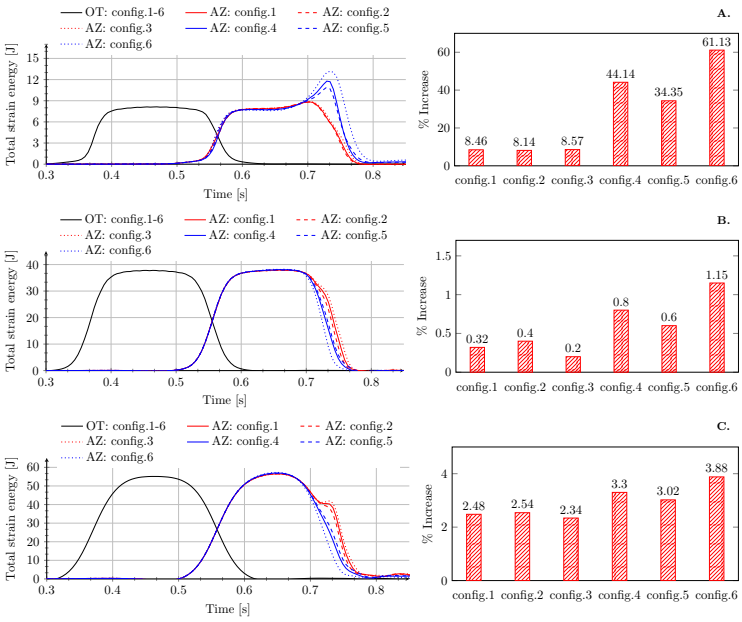

Figure 4.4: Time history of total strain energy (left) and percentage increase (right) of maximum total strain energy in AZ relative to OT for config.1-6 in ballast (a), embankment (b), and subgrade (c).

Figure 4.4 shows the time history of total strain energy in ballast (A.), embankment (B.), and subgrade (C.) for the open track and the approach zone, and the percentage increase in the maximum of the total strain energy in the approach zone relative to that in open track for all 6 configurations described above and shown in Figure 4.3. The results will be investigated in two broad categories of config.1-3 and config.4-6. Figure 4.4 shows that config.1, 2, and 3 do not exhibit any significant difference in the strain energy variations in ballast, embankment, or subgrade, implying that the position (with respect to the transition interface) of the first sleepers on both sides of the transition interface has negligible influence on the dynamic amplifications in RTZs. However, configurations (config.1-3) involving one of the sleepers being placed right next to the transition interface or on top of it do exhibit significantly larger amplifications in the total strain energy (approx. 5-7 times more than config. 4-6) for all track bed layers, implying that these extreme sleeper configurations must be avoided to achieve better performance of RTZs.

4.3.2. SLEEPER LAYOUT

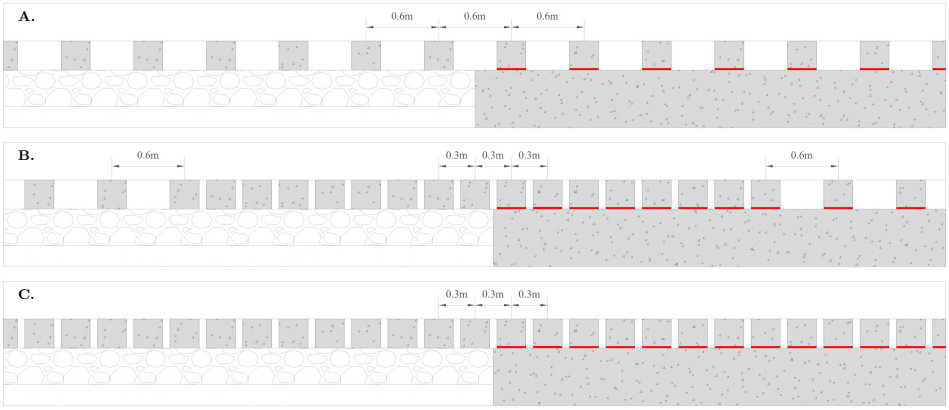

Figure 4.5: Sleeper layouts under study: (a) SL1 , (b) SL2, (c) SL3.

Three different sleeper layout (SL) scenarios (Figure 4.5) were investigated namely, SL1: standard sleeper spacing of 0.6 m throughout the track (OT and AZ), SL2: reduced sleeper spacing only in the transition zone (approach zone on the stiff and soft side of the track) and SL3: reduced sleeper spacing of 0.3 m throughout the track (OT and AZ).

Figure 4.6 shows the time history of total strain energy in the ballast (A.), embankment (B.), and subgrade (C.) for the open track and the approach zone, and the percentage increase in maximum total strain energy in the approach zone relative to that in the open track for sleeper layouts described above and shown in Figure 4.5. On the one hand, some authors [19, 20, 24, 25] have associated reduced sleeper spacing in the railway tracks with a reduction in ballast settlement and the results shown in Figure 4.6A. (left) for SL3 (when compared to SL1) can verify this claim for OT. On the other hand, the amplification of maximum total strain energy in AZ relative to OT is higher for SL3 in comparison to SL1 (which is the reference layout). Furthermore, although SL2 shows no amplification of maximum total strain energy in AZ relative to OT in the ballast layer, a significant increase is seen in the embankment layer. This implies that reduced sleeper spacing only in the transition zone is efficient in the reduction of permanent deformations in the ballast layer in the proximity of the transition interface. However, it is not an effective intervention to deal with transition effects in general as it leads to an increased degradation in the embankment layer. No significant change is observed in the behaviour of the subgrade layer for any of the sleeper layouts under study.

It is to be noted that a scenario with a smaller sleeper distance only on the ballasted track has not been investigated. However, it can be deduced from the results that the behaviour will be similar to SL2 as far as the energy in the soft side of the system is considered.

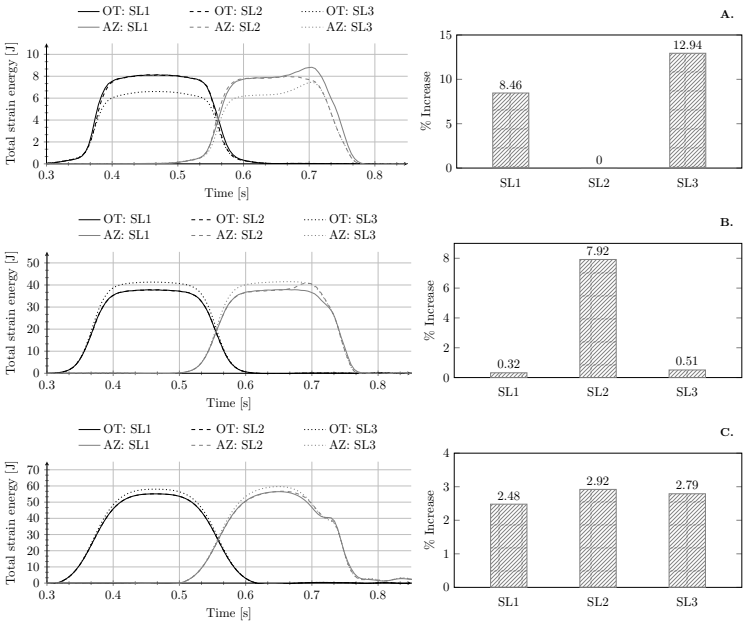

Figure 4.6: Time history of total strain energy (left) and percentage increase (right) of maximum total strain energy in AZ relative to OT for SL 1-3 in (a) ballast, (b) embankment, and (c) subgrade.

4.3.3. LOSS OF CONTACT BETWEEN SLEEPER AND BALLAST: HANGING SLEEPERS

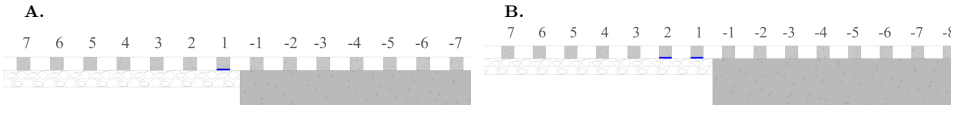

Figure 4.7: The embankment-bridge transition under study showing the locations of (a) one hanging sleeper and (b) two hanging sleepers marked in blue.

In RTZs, the difference in autonomous settlements on the soft and stiff side of the track together with the operation-driven dynamic amplifications lead to non-ideal geometric track configurations. As a consequence of these configurations, one or more sleepers in the vicinity of the transition interface typically lose contact with the ballast layer [34, 35]. Therefore, in this section, the influence of the number (1,2) of hanging sleepers is studied (Figure 4.7) and compared against the case with no hanging sleepers. No more than 2 hanging sleepers were analyzed as the tracks are necessarily maintained after the occurrence of the second hanging sleeper. It is to be noted that only extreme cases leading to

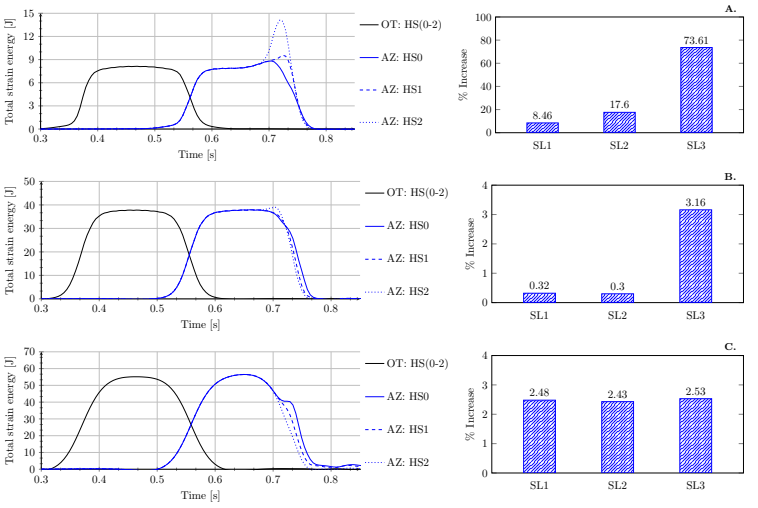

Figure 4.8: Time history of total strain energy (left) and percentage increase (right) of maximum total strain energy in AZ relative to OT for 0, 1, and 2 number of hanging sleepers next to transition interface for the **A.** ballast, **B.** embankment and **C.** subgrade.

complete loss of contact between the first two sleepers next to the transition interface are investigated.

Figure 4.8 shows the time history of total strain energy in ballast (A.), embankment (B.) and subgrade (C.) for open track and approach zone, and the percentage increase in the maximum of the total strain energy in the approach zone relative to that in the open track for the embankment-bridge transition with no hanging sleepers, one hanging sleeper and two hanging sleepers, as marked in Figure 4.8. It can be observed in the results that the occurrence of hanging sleepers affects mostly the top layers (ballast and embankment) and shows a small influence on the subgrade layer (and it does not lead to any amplification). In the embankment layer, one hanging sleeper has no influence, but some amplification in total strain energy can be seen with the occurrence of the second hanging sleeper. In the ballast layer, the presence of a single hanging sleeper in proximity to the transition interface leads to an approximate doubling of the strain energy amplification relative to situations without any hanging sleepers. It is to be noted that the occurrence of a second hanging sleeper has an even more pronounced effect, resulting in an approximately eightfold increase in total strain energy amplification when compared to the situation with no hanging sleepers. Thus, it can be concluded that the impact of hanging sleepers on total strain energy amplification is not merely additive but seemingly exponential, highlighting the need for meticulous monitoring and management of such conditions.

4.4. CONCLUSIONS

Despite certain studies advocating the efficacy of superstructure-based enhancements in railway transition zones (RTZs), site measurements have demonstrated limited efficiency. A recently developed energy-based criterion was used to highlight the potential shortcomings of some of these solutions, thus providing reasoning behind their ineffectiveness. A 2D finite element model was used to analyze the performance of railway transition zones (RTZs) for varying sleeper configuration in the proximity of the transition interface and varying sleeper spacing layouts using a recently developed strain energy-based criterion. Additionally, the loss of contact conditions (hanging sleepers) between the sleeper and ballast layer due to non-ideal geometry was also investigated. Firstly, various sleeper configurations around the transition interface were studied in terms of total strain energy amplifications and it was observed that the positioning of the first sleeper on both sides (soft and stiff) with respect to the transition interface has negligible influence on the performance of the RTZs. However, extreme positions of the sleepers (e.g., sleeper edge resting on the transition interface) must be avoided to limit the strain energy amplification in RTZs. Secondly, the effect of overall reduced sleeper spacing and reduced sleeper spacing only in the approach zones (both on the soft and stiff side) was compared with the standard sleeper spacing configuration (0.6 m). It was observed that even though an overall reduced sleeper spacing leads to lower total strain energy levels in the ballast layer, it does not reduce the strain energy amplification in approach zones with respect to the open track. Moreover, the layout with reduced sleeper spacing only for approach zones led to the mitigation of dynamic amplifications in the ballast layer but eventually resulted in an amplification of the strain energy within the embankment layer. Lastly, the study of the influence of hanging sleepers on the performance of RTZ showed that with an increase in the number of hanging sleepers, an exponential increase in strain energy amplification was observed in the approach zone. This highlights the need for interventions like adjustable sleepers [38], and wedge-shaped sleepers [39] to mitigate the loss of contact between sleepers and the ballast layer. In the end, it was concluded that optimizing the sleeper configuration (overall or in the proximity of the transition interface) does not lead to any significant improvement in the performance of railway transition zones in terms of strain energy amplifications. In addition, some critical configurations (sleeper edge on transition interface) or contact conditions (hanging sleepers) must be avoided or mitigated to prevent extreme strain energy amplifications in railway transition zones.

5

INVESTIGATION OF KEY PHENOMENA GOVERNING DESIGN

This chapter (with minor changes) has been published as *A. Jain, K.N. van Dalen, M.J.M.M. Steenbergen, and A.V.Metrikine. Dynamic amplifications in railway transition zones: investigation of key phenomena. Journal of Physics: Conference Series, 2647(15):152002, June 2024.*

ABSTRACT

The railway transition zone where the track transitions from a ballasted track to a slab track, is a crucial area that can experience amplified dynamic responses. This work aims to develop a deeper insight into the mechanisms leading to the amplified dynamic response in railway transition zones. The study employs a finite element model to investigate the amplification of total strain energy due to the phenomena of reflection and redistribution (i.e., among different layers) of energy close to the transition interface. The results of the study are obtained for three case studies involving non-reflecting boundary (representing an energy sink) and homogeneous material along the vertical direction of the track, and the responses are studied for individual and combined effects in comparison to a benchmark case. The findings of the study show that eliminating the phenomena of reflection and redistribution results in no dynamic amplification in total strain energy in railway transition zones. The conclusion highlights the importance of understanding these phenomena in order to design an efficient railway transition structure.

5.1. INTRODUCTION

Railway transition zones are subjected to increased degradation due to amplification of dynamic responses compared to the open tracks. The literature suggests that the dynamic amplification in transition zones can be associated mainly with stiffness variation and differential settlement [1], [2], [3]. However, there is a lack of understanding of the phenomena that initiate and govern the processes leading to these amplifications. The authors in this paper show that the phenomena of reflection and redistribution (i.e., among different layers) of energies close to the transition interface play a major role in defining the behaviour of railway transition zones (RTZs) described above. A vertical rigid boundary at the interface of a ballasted track and a concrete structure and an inhomogeneity in mechanical properties of materials in longitudinal and vertical directions are two inherent characteristics of typical RTZs. Over the years several mitigation measures have been adopted that aim to gradually minimize the material inhomogeneity in longitudinal direction but they have proved to be either inefficient or marginally effective in reducing the degradation in RTZs. In [4] authors proposed an energy-based criterion to design and evaluate the performance of railway transition zones. Hence, in this work the phenomena of reflection and redistribution of energy will be studied in the proximity of the transition interface in terms of total strain energy, and its importance will be highlighted in order to design an effective solution aimed at minimizing the dynamic response in RTZs. It is to be noted that the system under study is simplified in terms of geometry and material behaviour as the purpose of this work is to investigate the phenomena described above. The geometry of RTZs obviously is more complex and the material behaviour may be non-linear, but for the purpose of this study the simplified model is deemed sufficient.

5.2. METHOD

A two-dimensional (2-D) plane strain finite element (FE) model with linear elastic materials for the rail, concrete sleepers, ballast, embankment and sub-grade was used in this study. The properties of materials used are tabulated in Table 5.1 [5]. The system under study consists of the ballasted track (soft side), a concrete bridge (stiff side) and the inter-

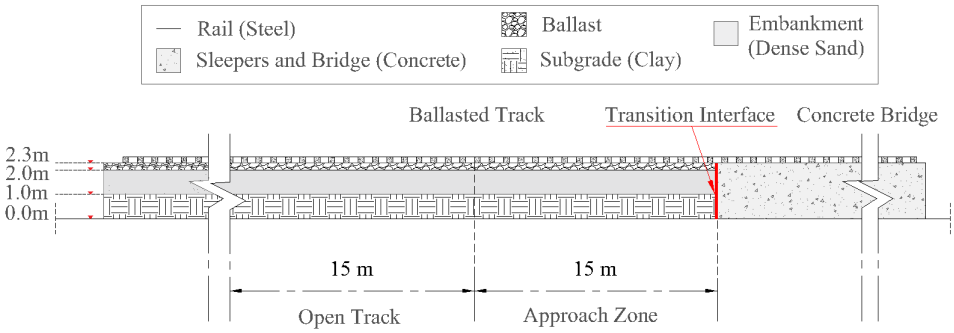

Figure 5.1: Geometric and cross-sectional details of the embankment-bridge transition under study.

face between these two parts, referred in this paper as transition interface. The geometric details of the system are shown in Figure 5.1 including the two zones under study. The first zone under study is open track (OT) which is far away from transition effects and the second zone is approach zone on ballasted track next to transition interface. For the purpose of this study 4 different cases were simulated as described below. A single axle load of 90 kN and velocity 144 km/h was used as dynamic loading for all the cases studied in this paper.

Case 1 - Base model: A standard bridge embankment transition was simulated in this case with cross-section details shown in Figure 5.1 with three track-bed layers namely ballast, embankment and sub-grade. The vertical interface of ballasted track and the concrete bridge allows frictional sliding in tangential direction based on Coulomb friction law and the concrete bridge acts as a rigid boundary in normal direction. The reflection coefficients (for 1D wave propagation) of shear and compressional waves based on the impedances were computed for preliminary checks and the reflection coefficients were close to 1 (i.e., 0.96 and 0.95, respectively). This demonstrates that the concrete provides a nearly rigid boundary.

Case 2 - Homogeneous foundation: The base model described above is studied with a different foundation for the ballasted part of the track. In this case instead of a three layered track-bed system, a homogeneous foundation (same mechanical properties as ballast) was used under the sleepers. The transition interface properties are the same as case 1. This case is representative of a condition with no redistribution of energy within the trackbed layers due to inhomogeneity of materials in vertical direction. The only material inhomogeneity in case 2 is along the longitudinal direction of the track.

Case 3 - Non-reflective boundary: In this case, the base model is modified where the mesh elements at the vertical boundary of the ballasted track at the transition interface was replaced by infinite elements. These elements (CINPE4) are continuum infinite,

Table 5.1: Mechanical properties of the track components

Material	Elasticity modulus E [N/m^2]	Density ρ [kg/m^3]	Poisson's ratio ν	Rayleigh damping α	β
Steel (rail)	21 x 10^{10}	7850	0.3	-	-
Concrete (sleepers)	3.5 x 10^{10}	2400	0.15	-	-
Ballast	1.5 x 10^8	1560	0.2	0.0439	0.0091
Sand (embankment)	8 x 10^7	1810	0.3	8.52	0.0004
Clay (subgrade)	2.55 x 10^7	1730	0.3	8.52	0.0029
USP	1 x 10^6	500	0.1	-	-

plane-strain and 4-node elements [6]. This case is representative of a system where we limit the reflections from the vertical rigid boundary of the concrete bridge.

5

Case 4 - Homogeneous foundation and non-reflective boundary: This case is a combination of case 2 and case 3, where the response will be studied for combined effects of no reflection and no redistribution of energies in the proximity of the transition interface. The above mentioned cases will be analyzed in terms of total strain energy variation in top most layer (ballast) and the bottom most layer (sub-grade) for open track and approach zone. Case 1 will be compared with cases 2, 3 and 4.

5.3. RESULTS

In this section, a comparison of total strain energy graphs are presented for ballast and sub-grade layer in open track and approach zone. It is to be noted that this a study of the phenomena and the focus is mainly on studying the amplifications in the railway transition zones with respect to the open tracks due to phenomena of reflection and redistribution of energy. Hence, the results presented in this section are normalized against the maximum values of total strain energy in the open tracks.

Case 1 versus Case 2: Comparison of case 1 and case 2 is performed such that the effects of the phenomenon of energy redistribution due to non-uniformity of materials in the vertical direction is studied. This phenomenon is studied in the proximity (AZ: approach zone) of the transition interface and far (OT: open track) from the transition effects. The results obtained from the base model with non-homogeneous foundation are compared against the results obtained by simulation of a homogeneous foundation. Figure 5.2 shows the comparison of normalized total strain energy (OT, AZ) in ballast (a) and sub-grade (b) for case 1 and case 2.

As seen in Figure 5.2, case 2 shows an increase of 2.21% in normalized total strain energy for the layer of ballast in approach zone relative to open track compared to case 1 where this increase is much higher (9%). This implies that inhomogeneity in foundation contributes significantly to the dynamic amplifications in railway transition zones. It

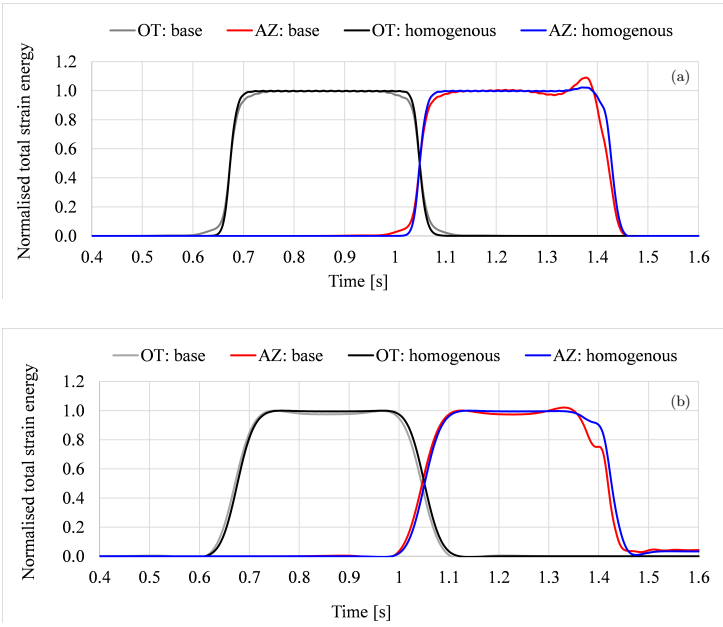

Figure 5.2: Comparison of normalized total strain energy in the layers of (a) ballast and (b) sub-grade for case 1 and case 2

is to be noted that the smaller amplification in total strain energy in case 2 could also be due to the fact that overall stiffness of the foundation is increased and the stiffness jump is lower than that in case 1. However, the effects of this difference in stiffness jump are negligible as ballast and subgrade both are approximately 230 times softer than the concrete bridge; this was verified in a simulation with a softer foundation. In any case, although the distribution of total strain energy in the approach zone for case 2 is not as uniform as in the open tracks, there is no significant increase in the magnitude of energy neither in ballast nor in sub-grade. Hence, the non-uniformity in strain energy distribution in case 2 is solely due to reflection of energy from the vertical boundary at the interface of ballasted track and the ballastless track.

Case 1 versus case 3: Comparison of case 1 and case 3 is performed such that the effects of the phenomenon of reflection at the vertical rigid boundary (concrete bridge) is studied. This phenomenon is studied in the proximity (AZ) of the transition interface and far (OT) from the transition effects. The results obtained from the base model with rigid boundary and frictional sliding at transition interface is compared against the results obtained by simulation of a non-reflective boundary at the transition interface. Figure 5.3 shows the comparison of normalized total strain energy (OT, AZ) in ballast (a) and sub-grade (b) for case 1 and case 3.

As seen in Figure 5.3, case 3 shows an increase of 2.43% in normalized total strain energy

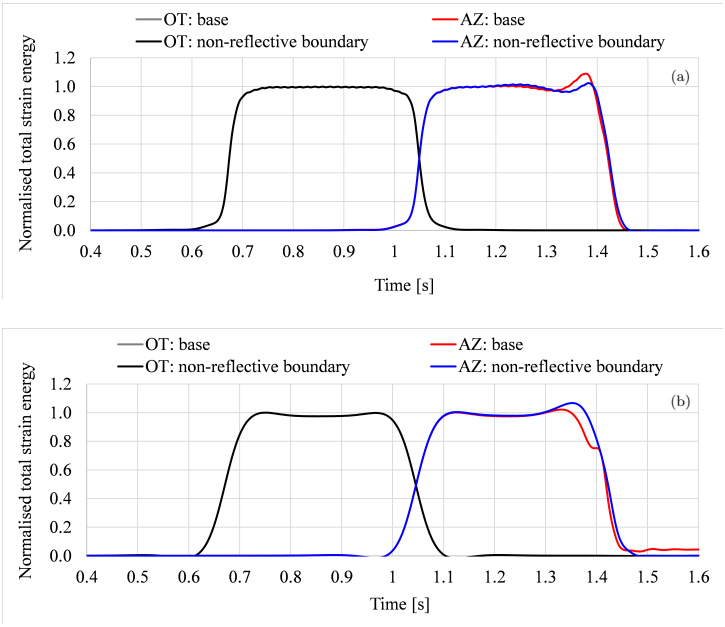

Figure 5.3: Comparison of normalized total strain energy in the layers of (a) ballast and (b) subgrade for case 1 and case 3

for the layer of ballast in approach zone relative to open track compared to case 1 where this increase was much higher (9%). This shows that reflection from the vertical boundary at the interface of ballasted track and the concrete structure contributes significantly to the dynamic amplifications in railway transition zones. In addition to this, an increase can be seen for the sub-grade layer which can be due to redistribution of energy between the three elastic layers of ballast, embankment and sub-grade. Moreover, the distribution of total strain energy in the proximity of transition interface is not uniform similar to case 1, 2 and 3. In this particular case the non-uniformity is expected due to redistribution of energy between track-bed layers.

Case 1 versus case 4: Comparison of case 1 and case 4 is performed such that the effects of the phenomenon of both energy redistribution and reflection is studied. This phenomenon is studied in the proximity (AZ) of the transition interface and far (OT) from the transition effects. The results obtained from the base model with non-homogeneous foundation and rigid vertical boundary with friction sliding at the transition interface is compared against the results obtained by adopting a homogeneous foundation and a non-reflective boundary. Figure 5.4 shows the comparison of normalized total strain energy (OT, AZ) in ballast (a) and sub-grade (b) for case 1 and case 4.

As seen in Figure 5.4, case 4 shows no increase at all in normalized total strain energy for the layer of ballast in approach zone relative to open track compared to all the other

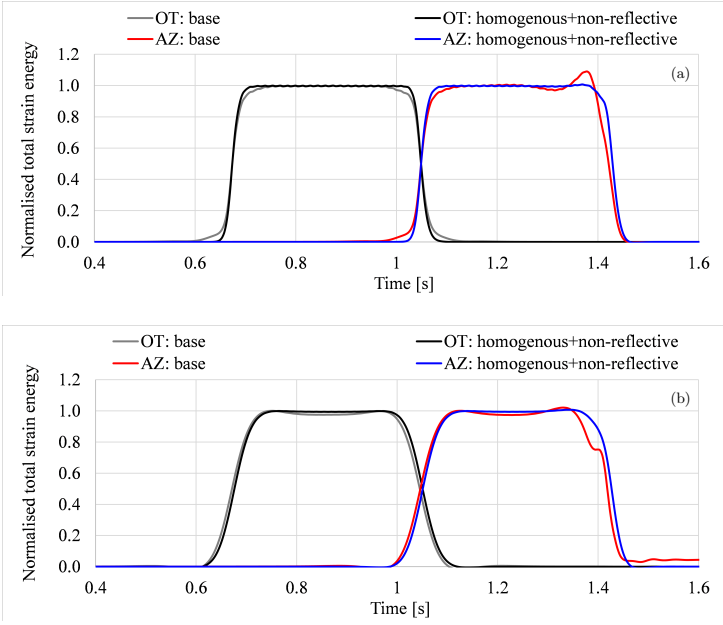

Figure 5.4: Comparison of normalized total strain energy in the layers of (a) ballast and (b) subgrade for case 1 and case 4

cases studied above. Moreover, there is no non-uniformity in the distribution of strain energy in approach zone and the energy variation curve is exactly the same as for open track.

5.4. CONCLUSION

This work highlights the need to mitigate the phenomena of reflection and redistribution of energies in the proximity of a transition interface. It is clearly seen in the results presented above that eliminating either of these two phenomena can lead to a significant reduction in energy amplifications in approach zones relative to open tracks. It was also shown that if a transition structure is designed such that the combined effects of reflection and redistribution of energies are mitigated, there will be no increase in the strain energy for any track-bed layer. Amplifications due to redistribution of energy can be dealt with by making the foundation as homogeneous as possible or gradually decreasing the inhomogeneity. Transition wedges are effective to some extent in achieving this but the problem due to the reflection of energy still remains. The energy reflection could be managed by trapping and dampening the energy in these zones using absorbing materials, or by ensuring that the reflected energy does not interfere with the main deformation field induced by the train (see Chapter 6).

6

MATERIAL OPTIMISATION: SHIELD

This chapter (with minor changes) has been published as *Avni Jain, YuriyMarykovskiy, Andrei V.Metrikine, and Karel N. van Dalen. Quantifying the impact of stiffness distributions on the dynamic behaviour of railway transition zones. Transportation Geotechnics, 45:101211, 2024. ISSN 2214-3912.*

ABSTRACT

Railway transition zones (RTZs) are regions where abrupt track stiffness changes occur that may lead to dynamic amplifications and subsequent track deterioration. The design challenges for these zones arise due to variations in material properties in both the depth (trackbed layers composed of different materials) and longitudinal directions of the track, as well as temporal variations in mechanical properties of materials due to several external factors over the operational period. This research aims to investigate the effects of these variations in material properties (i.e., of the resulting stiffness distributions in vertical and longitudinal directions) on the behaviour of RTZs, assess from this perspective the performance of a novel transition structure called the SHIELD, and establish a methodology for designing a robust solution to mitigate the dynamic amplifications in these zones. Results indicate that stiffness variations in both vertical and longitudinal directions significantly influence the dynamic behaviour of the RTZs. The study also suggests a permissible range of stiffness ratios to control the amplification of strain energy in the most critical components of RTZs, both in the initial state as well as during the operational phase (where material properties may vary over time). Moreover, the proposed methodology offers a valuable tool for the design and evaluation of RTZs and is applicable to various transition types and a broad spectrum of material properties.

6.1. INTRODUCTION

Railway transition zones (RTZs) are critical regions where the track stiffness changes abruptly, such as in the transition from a ballasted track to a track supported by a concrete structure. In these zones, dynamic amplification due to moving loads can lead to increased track deterioration and reduced service life [1]. In [2], a detailed literature review is presented, concerning the problem of amplified degradation in RTZs due to an abrupt stiffness variation in the foundation. Another detailed study [3] presents an overview of the existing mitigation measures (both preventive and corrective) on superstructure and substructure levels to deal with the dynamic amplifications in RTZs. Even though the influence of an abrupt increase in track stiffness in the longitudinal direction experienced by the moving load has been studied in the past [4–9], an effective design solution is lacking in practice. In addition to this, the trackbed layers (ballast, embankment and subgrade) are composed of materials with varying properties which adds to the complexity of the problem at hand [10, 11]. There have been some studies [12, 13] in the past on the influence of material parameters on the dynamic properties of railway transition zones. However, the current literature has no evidence of the influence of the distribution of material properties along the depth of the railway track on the behaviour of RTZs.

Even though transition structures like approach slabs [14–17] and transition wedges [18–21] are designed with an aim to achieve a gradual stiffness distribution in the longitudinal direction, it is difficult to maintain the robustness of the design of these transition structures as they are subjected to temporal variations in the mechanical properties of the materials due to environmental factors [22–24], geotechnical conditions [25], operation-induced wearing of materials etc. These factors lead to changes in the mechanical properties of the materials in terms of elastic moduli, densities and Poisson's ratios [24].

The influence of the variations in the mechanical properties of the materials on the performance of the transition structure is unknown. Therefore, a robust design solution for RTZs must take into account these variations in the above-mentioned material parameters and the related studies are lacking in the current literature.

This paper has three objectives. Firstly, the influence of the distribution of material properties along the depth and longitudinal directions of the track on the dynamic behaviour of a typical RTZ is investigated (Section 6.3.1). Secondly, the same analysis is performed for a specific transition structure, namely the safe hull-inspired energy limiting design (SHIELD) proposed by some of the authors in [26] (Section 6.3.2). The existing literature [2, 3, 18, 19, 27] shows that attempts have been made to mitigate the transition effects by providing a smoother stiffness transition (in the longitudinal direction) in the foundation, but it has been a challenge to quantify the permissible stiffness variation that is required to mitigate the dynamic amplifications in RTZs. Therefore, as a third objective, an appropriate set of material parameters for the design of the transition structure (SHIELD) to minimise the dynamic amplifications in RTZs is established. Based on that, the findings of this research will establish a methodology (Section 6.3.3) for designers to adopt an appropriate distribution of the material properties (in space and accounting for variation over the operation period) of the trackbed layers and to choose appropriate material parameters for the design of transition structures, ultimately improving their effectiveness and prolonging the service life of railway tracks in transition zones.

6.2. EVALUATION OF RAILWAY TRANSITION ZONES: METHODS

Figure 6.1 shows a flow diagram of the steps/ methods adopted for the evaluation of railway transition zones using a framework for sensitivity analysis [28]. Each of the steps mentioned in the figure is discussed in detail in the following subsections.

6.2.1. FINITE ELEMENT MODELS

The output from finite element simulations is used to create Polynomial Chaos Expansion (PCE) surrogate models. For this purpose, two finite element models are used in the present work. The first model (model 1) represents an embankment-bridge transition and the second model (model 2) incorporates a safe hull-inspired energy-limiting design of transition structure proposed by some of the authors in [26]. Both models include rail, sleepers, rail-pads, ballast, embankment and subgrade. Rails, rail-pads and sleepers have standard dimensions and material properties [8].

A 2-dimensional plane strain model (Figure 6.2) of an embankment bridge transition was used with linear elastic materials. An axle load of 90 kN moving with a velocity of 144 km/hr was simulated using the DLOAD subroutine in Abaqus [29]. The details of the model used can be found in [8, 26]. In accordance with the design criterion proposed in [8], the strain energy amplification in the approach zones (AZ) relative to the open track (OT) is studied for both models. In [8] authors presented a detailed analysis of kinematic

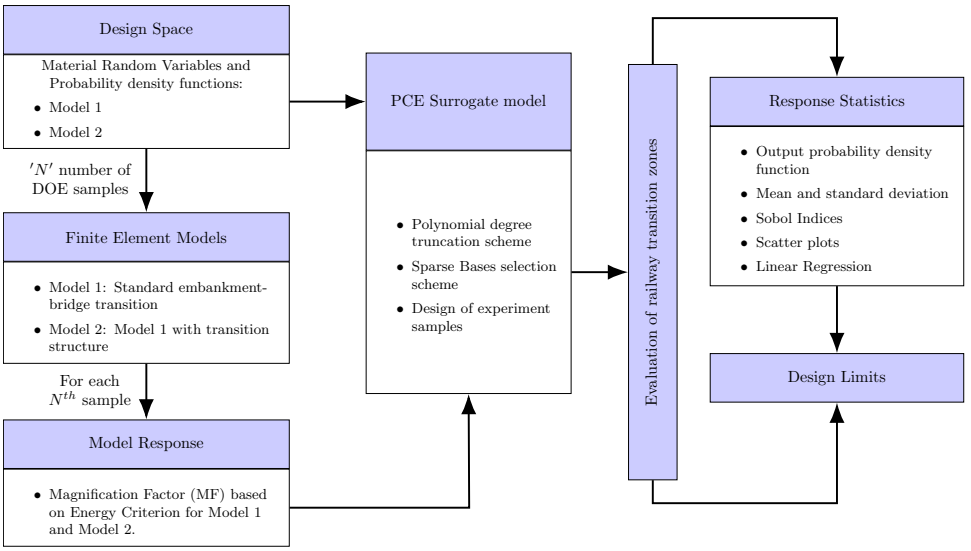

Figure 6.1: Framework for evaluation of railway transition zones

6

response, Von Mises stress and mechanical energy (kinetic and strain energy) variations in all track components (rail, sleepers, ballast, railpad, embankment and subgrade). The strain energy was shown to be the most comprehensive quantity to evaluate the railway transition as it comprises both distortional and volumetric components of the strain energy, while Von Mises stress for instance only captures the distortional component of energy. The total strain energy used for computations in this work is the volume integral of the strain energy density (only the dynamic contribution) in the zones under study. A detailed derivation of the expression for the total strain energy can be found in [30]. It is to be noted that the strain energy amplification is studied only for the ballast layer in both models as it is the most critical layer in terms of dynamic amplifications according to [8] (model 1) and [26] (model 2).

Bridge-embankment railway transition zone (model 1): A bridge-embankment transition is one of the most critical types of railway transition zones where the stiffness change is observed on multiple levels, i.e., the interaction of all trackbed layers (ballast, embankment and subgrade) with the concrete structure. In a detailed study [8] as mentioned above, it was concluded that the amplification in the total strain energy in the trackbed layers in the proximity of the transition interface relative to the open tracks can be associated with the non-uniformity in degradation observed along the longitudinal direction of the track. However, this study was performed for a specific set of mechanical properties of trackbed layer materials (Table 6.1). Therefore, this paper will assess the sensitivity of the dynamic response of the RTZ to the variation in the mechanical properties of trackbed materials in vertical and longitudinal directions.

For this purpose, the mechanical parameters used to define the material of ballast,

Table 6.1: Mechanical properties of the track components

Material	Elasticity Modulus E [N/m^2]	Density ρ [kg/m^3]	Poisson's Ratio ν	Rayleigh damping α	β
Steel (rail)	21 x 10^{10}	7850	0.3	-	-
Concrete (sleepers)	3.5 x 10^{10}	2400	0.15	-	-
Ballast	1.5 x 10^8	1560	0.2	0.0439	0.0091
Sand (embankment)	8 x 10^7	1810	0.3	8.52	0.0004
Clay (subgrade)	2.55 x 10^7	1730	0.3	8.52	0.0029

embankment and subgrade layers tabulated in Table 6.1 are varied as shown in Table 6.4. Figure 6.2 shows the time history of the total strain energy in the ballast layer in open track (7.5 m) and approach zones (7.5 m), with an amplification of approximately 9% in the vicinity of the transition interface for model 1. The sensitivity of this amplification to the variation in material properties of the trackbed layers is studied in terms of magnification factor (Y_{RTZ}) defined in 6.2.3.

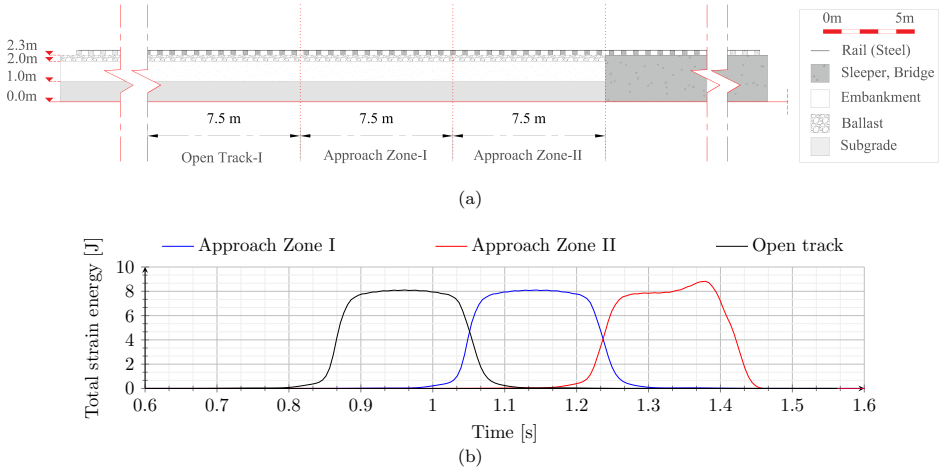

Figure 6.2: (a)Geometric details of an embankment-bridge transition, (b) time history of total strain energy in OT, AZ-I and AZ-II for an embankment-bridge transition

Bridge-embankment transition with SHIELD (model 2): This model is a modified version of model 1, as it has the transition structure proposed by the authors in [26]. This transition structure is placed between the ballasted track and the ballastless track to minimise the dynamic amplifications and guarantee a smooth variation of the total strain energy in

the longitudinal direction. However, in [26], the design and evaluation of this transition structure were performed using a particular set of material properties of trackbed layers (Table 6.1). Also, the mechanical properties of the transition structure (Table 6.2) were chosen to provide a smooth transition from certain materials in trackbed layers to a concrete structure. Hence, in this paper, the effect of variation in the material parameters of the trackbed layers on the choice of design parameters of the transition structure will be assessed.

Table 6.2: Mechanical properties of the transition structure

Transition structure	Elastic modulus E [N/m^2]	Density ρ [kg/m^3]	Poisson's ratio ν
SHIELD	3.6 x 10^8	1900	0.2

For this purpose, the mechanical parameters used to define the material of ballast, embankment, subgrade layers and the transition structure (TS) tabulated in Table 6.2 are varied as mentioned in Table 6.5. Figure 6.3 shows the time history of the total strain energy in the ballast layer in open track (7.5 m) and approach zones (7.5 m), with no amplification of total strain energy in any of the approach zones for the set of parameters used to design this particular transition structure (model 2). It can be seen that the total strain energy in AZ-II is much lower (65%) compared to OT. However, the total strain energy in AZ-I (38% lower compared to OT) can be sensitive to the variation in the material parameters of the trackbed materials listed in Table 6.3. Hence, the sensitivity of this response amplification (in AZ-I compared to OT) to the variation in material properties of the trackbed layers around the TS and the efficiency of TS is assessed in terms of magnification factor (Y_{TS}) defined in Section 6.2.3.

6.2.2. DESIGN SPACE (INPUT)

Design space is defined by the mechanical properties of materials (ballast, embankment, subgrade and transition structure) that are considered as random variables to account for the possible variations in their values. The mechanical parameters used to characterise the materials studied in this paper are tabulated in Table 6.3. The input domain of mechanical properties is defined by the probability density functions. Due to the lack of information in the current literature, uniform probability density functions denoted as $\mathcal{U}[a,b]$, were adopted for the majority of random variables. However, for the subgrade and embankment layers, preliminary investigations showed a very high sensitivity of the model response to the soil elasticity modulus. This was especially pronounced for soft soils. Adopting a fully inclusive input space of all soil types would result in soil elasticity having an overwhelming influence on the model response when compared to the effects of material properties in the remaining layers. Hence, for the purpose of this study, the distributions of soil material parameters were restricted to a single soil type (clayey soil for subgrade and sandy soil for embankment) and a normal probability density function

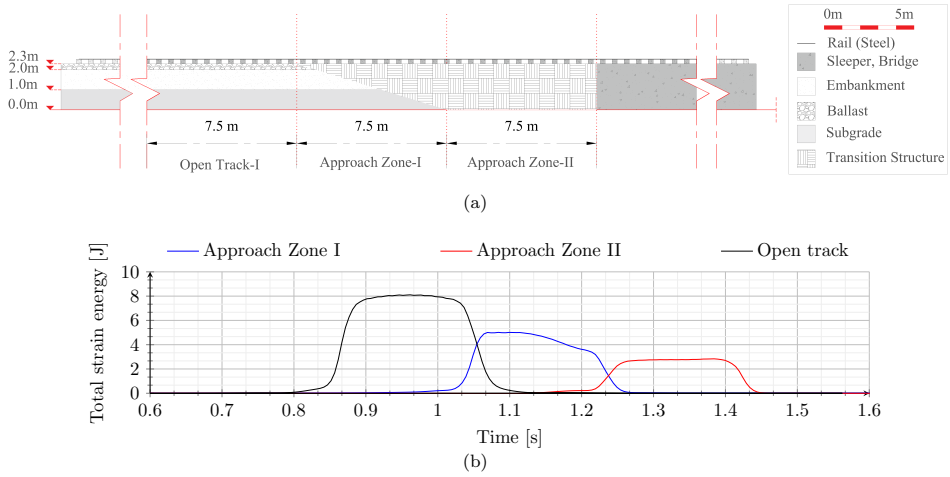

Figure 6.3: (a)Geometric details of an embankment-bridge transition with SHIELD, (b) time history of total strain energy in OT, AZ-I and AZ-II for an embankment-bridge transition with SHIELD

denoted as $\mathcal{N}(\mu,\sigma^2)$, was adopted for the elastic modulus. It is to be noted that a log-normal or any other suitable distribution could be adopted if more accurate data is available. A detailed discussion of the possible values of the mechanical properties of the materials (adopted across the literature for modelling purposes) constituting the trackbed layers (ballast, embankment and subgrade) was presented in [31]. The data presented in [31], combined with feedback from domain and industry experts has provided a starting point in establishing the lower and upper bounds of the uniform distributions (a and b, respectively) as well as the normal probability density function moments μ and σ. Constraints were imposed on the design space to avoid sampling of any negative values. It is to be noted that, the chosen input space is intentionally kept broad, in order not to restrict the analysis results to specific site conditions. Nevertheless, designers can apply the methodology outlined in this research to a specific transition zone by adopting statistical distributions that accurately reflect the site conditions.

The probability density functions used in this paper, for materials forming trackbed layers (ballast, embankment and subgrade) are presented in Table 6.4, and for the transition structure (SHIELD) are reported in Table 6.5.

6.2.3. MODEL RESPONSE

Magnification factor (MF): The amplification of the total strain energy in the approach zones relative to the open tracks is defined as the magnification factor, i.e., the ratio between the maximum total strain energy in each of these zones. The magnification factors for an embankment-bridge transition with (Y_{TS}) and without transition structure

Table 6.3: Random variables defined in Table 6.4 and Table 6.5

Layer	Elastic Modulus	Poisson's Ratio	Density
Ballast	E_b	ν_b	ρ_b
Embankment	E_e	ν_e	ρ_e
Subgrade	E_s	ν_s	ρ_s
Transition Structure	E_{TS}	ν_{TS}	ρ_{TS}

(Y_{RTZ}) are defined below.

- **MF for model 1:** Y_{RTZ} is the ratio of the maximum total strain energy in AZ-II to that in OT as shown in Figure 6.2. This magnification factor is expected to be always greater than 1 due to transition effects.
- **MF for model 2:** Y_{TS} is the ratio of the maximum total strain energy in AZ-I to that in OT as seen in Figure 6.3. This magnification factor is preferably smaller than 1 for an efficient design of a transition structure.

6.2.4. POLYNOMIAL CHAOS EXPANSION (PCE) SURROGATE MODEL

Given a rather wide range of possible transitions and a non-negligible computation cost of the FEM simulations, there is a need to efficiently sample the space of possible realisations. One such possibility is creating a PCE surrogate model with sparse bases. The advantages of PCE models as opposed to other surrogate model approaches are several. Firstly, these models are non-intrusive and do not require any modification to the underlying FEM simulations. Secondly, PCE models are transparent in terms of the theoretical underpinnings of their performance. Lastly, the post-processing of PCE model coefficients provides analytically computed Sobol indices, which can be used for global sensitivity analysis [32]. In the context of railway engineering the authors of [33] have recently demonstrated that PCE surrogates can be used instead of Monte Carlo simulations when modelling the response of railway embankments. Given the input space of random variables and the FEM model, a PCE surrogate model is an attractive alternative to the Monte Carlo sampling method, as it provides the benefits of faster computation, the prospect for adoption of higher fidelity, non-linear FEM models, and the capability to perform sensitivity analysis and optimization tasks more efficiently.

The PCE model in this work is built using UQlab, a framework developed at ETH Zurich [34]. This framework provides a high-level implementation of Uncertainty Quantification analysis. The details of the setup used to create PCE surrogate models employed in this work are described hereinafter.

Polynomial degree truncation scheme: It is often the case in applied science problems, that some terms in the polynomial basis have a marginal influence on the overall model response. This is known as the sparsity-of-effects principle. Based on this a hyperbolic (q-norm) polynomial degree truncation scheme [35] with $q = 0.75$ was chosen in the

Table 6.4: Probability density functions of random variables for bridge embankment transition

Layer	$E\,[\mathrm{N m^{-2}}]$	ν	$\rho\,[\mathrm{kg m^{-3}}]$
Ballast	$\mathcal{U}[a,b]$ 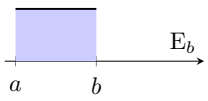 $a = 1.0 \cdot 10^8$ $b = 2.5 \cdot 10^8$	$\mathcal{U}[a,b]$ 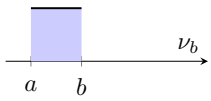 $a = 0.15$ $b = 0.25$	$\mathcal{U}[a,b]$ 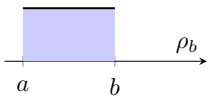 $a = 1.2 \cdot 10^3$ $b = 1.7 \cdot 10^3$
Embankment	$\mathcal{N}(\mu,\sigma^2)$ 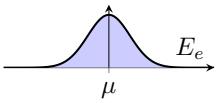 $\mu = 8.0 \cdot 10^7$ $\sigma = 5.0 \cdot 10^6$	$\mathcal{U}[a,b]$ 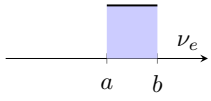 $a = 0.3$ $b = 0.4$	$\mathcal{U}[a,b]$ 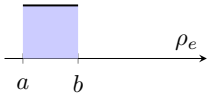 $a = 1.2 \cdot 10^3$ $b = 1.5 \cdot 10^3$
Subgrade	$\mathcal{N}(\mu,\sigma^2)$ 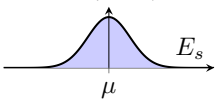 $\mu = 2.4 \cdot 10^7$ $\sigma = 4.0 \cdot 10^6$	$\mathcal{U}[a,b]$ 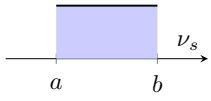 $a = 0.2$ $b = 0.4$	$\mathcal{U}[a,b]$ 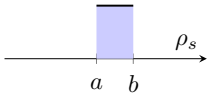 $a = 1.6 \cdot 10^3$ $b = 1.8 \cdot 10^3$

search of optimal basis.

Calculation of the coefficients for Sparse PCE Bases: In this study, the least angle regression algorithm [36] was used to create sparse bases and reduce the toll induced due to the high dimensionality of the input space. The minimum polynomial degree p was set to 3.

Design of Experiment (DOE) Samples: When the PCE model is built the input space is sampled at specific points, and the number of DOE samples (i.e. full FEM model evaluations) required to build the PCE surrogate model is proportional to the input space size and the degree of polynomial bases. For the standard truncation scheme, the cardinality is:

$$P = \frac{(M+p)!}{M!p!} \tag{6.1}$$

where M is the number of input variables and p is the polynomial expansion degree. In the case of least-square minimization, if the number of samples 'n' is smaller than P, it leads to an underdetermined system, while $n = P$ may lead to overfitting. As a rule of thumb,

$$n = k \cdot P \tag{6.2}$$

Table 6.5: Random variables for the transition structure of bridge embankment transition

Layer	$E\left[\mathrm{N\,m^{-2}}\right]$	ν	$\rho\left[\mathrm{kg\,m^{-3}}\right]$
	$\mathcal{U}[a,b]$	$\mathcal{U}[a,b]$	$\mathcal{U}[a,b]$
SHIELD	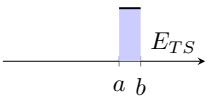	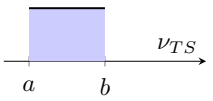	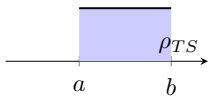
	$a = 3.5 \cdot 10^8$ $b = 4.0 \cdot 10^8$	$a = 0.15$ $b = 0.30$	$a = 1.5 \cdot 10^3$ $b = 2.0 \cdot 10^3$

with $k = 2 \sim 3$. By adopting the hyperbolic truncation scheme and the least angle regression algorithm, the number of evaluations can be significantly reduced. In fact, the common practice is to set the initial number of full model evaluations to $n = 10 \cdot M$. Leave One Out (LOO) error can serve as an indicator of the surrogate model accuracy when selecting the minimum polynomial degree and the number of DOE samples. For the present analysis, 100 FEM model evaluation resulted in ϵ_{LOO} of the order 10^{-3} for both model 1 and model 2. Generally, $\epsilon_{LOO} \leq 10^{-2}$ is sufficient for the purpose of global sensitivity analysis.

6

6.2.5. RESPONSE STATISTICS

The following results will be presented and analyzed in this paper (Section 6.3):

1. Probability density function (PDF): A log-normal distribution provided a good fit for the surrogate model responses. The log-normal distribution was chosen as opposed to a Gaussian, as model responses, represented by magnification factors, are always positive. The PDF of a log-normal distribution can be expressed as follows:

$$\psi(x, s, l, s_c) = \frac{1}{(x-l) \cdot s\sqrt{2\pi}} \cdot \exp\left(\frac{-\ln^2(x-l) + \ln^2(s_c)}{2s^2}\right) \tag{6.3}$$

   where x is the random variable and the shape (s), location (l), and scale (s_c) parameters are used to specify the particular log-normal distribution fitting the data. It is to be noted that no conclusions are drawn from the fitted curve and it was only provided to replicate the distribution by using the standard curves and associated parameters in equation 6.3.

2. Mean (μ) and standard deviation (σ): The upper and lower limits are marked in probability density function graphs as per the empirical rule in statistics to include 90% data. In mathematical notation, these facts can be expressed as follows, where Pr is the probability function [37, 38], X is an observation from a normally distributed random variable according to 6.4

$$\Pr(\mu - 1.6 \cdot \sigma < \mathrm{X} < \mu + 1.6 \cdot \sigma) = 90\% \tag{6.4}$$

3. Sobol indices: Sobol indices are used in sensitivity analysis to identify which variables have the greatest impact on the output of a system. They are calculated by partitioning the variance of the output into contributions from individual variables and combinations of variables. The first-order Sobol index measures the contribution of individual variables to the variance, while the total-effect Sobol index measures the contribution of the individual variables and all of their interactions to the variance. A comparison of Sobol indices of the most influential parameters is done for model 1 and model 2.

4. Scatter plots: The scatter plots are studied mainly for two types of parameters. Firstly, the parameters with the most significant contribution (in terms of Sobol indices) to the critical values of the magnification factor are investigated in detail. Secondly, as discussed in Section 6.1, even though the effects of stiffness variation in the longitudinal direction on the dynamic amplifications in RTZs is well known, there is no investigation on the influence of stiffness variation in the vertical direction on the dynamic behaviour of RTZs. Therefore, the influence of the stiffness ratios on the magnification factor will be analysed for all the cases under study. All scatter plots will be evaluated in terms of the quantities discussed below.
    - R-squared (strength): The coefficient of determination, also known as R-squared, is a statistical measure that represents the proportion of the variance for a dependent variable that's explained by an independent variable or variables in a regression model.
    - Spearman correlation coefficient: This coefficient is a measure of the strength and direction of the monotonic relationship between two variables. It measures how well the relationship between two variables can be described by a monotonic function, such as a straight line or a curve. Spearman correlation coefficient ranges from -1 to +1, where a value of -1 indicates a perfectly negative correlation, 0 indicates no correlation, and +1 indicates a perfectly positive correlation.
    - Linear regression line: This is a statistical method to find the best-fitting line through the data points in a scatter plot. This line can be used to predict the values of a variable based on the value of another variable.

6.3. EVALUATION OF RAILWAY TRANSITION ZONES: RESULTS AND DISCUSSION

An initial analysis was performed to compare the Sobol indices of the parameters under study to highlight the most influential parameters. It was observed that the densities of materials had no influence on the dynamic response of the system for both the models studied in this work. Therefore, in this section, the influence of elastic moduli and Poisson's ratios of different materials on the magnification factor is investigated, both for a typical transition zone without transition structure (Section 6.3.1) and with transition structure (Section 6.3.2). In addition, design limits are formulated for the latter to ensure that dynamic amplifications are avoided (Section 6.3.3).

6.3.1. MODEL 1

In this section, the results are presented for model 1 to study the dependence of the magnification factor (Y_{RTZ}) on the variation in the mechanical properties of the materials. It is to be noted that even though the variation in material properties is implemented in the vertical direction keeping the properties of the concrete bridge constant, there is a stiffness variation in both vertical and longitudinal directions (and the latter is affected as the stiffness of the layers in vertical direction, changes as per Table 6.4).

Probability density function (PDF): Figure 6.4 shows the probability density of the magnification factor Y_{RTZ} for the case without transition structure. It can be seen that 90% of the data belongs to the values of Y_{RTZ} lying between 1.12 and 1.3. This implies that for all combinations of parameters under study, the amplification in strain energy is approximately 12% to 30%. The mean (μ) and standard deviation (σ) of the distribution are 1.2 and 0.06, respectively. The probability density function of a log-normal distribution (Equation 6.3) can describe the obtained probability density (shown in Figure 6.4) when the following choices are made (Y_{RTZ} is the random variable): s is 0.27, l is 0.98 and s_c is 0.22.

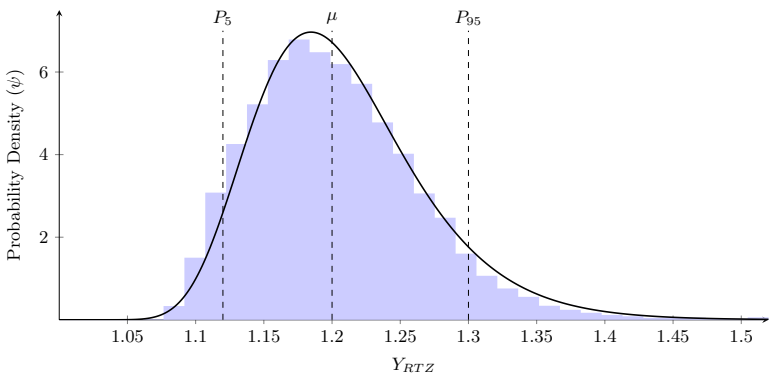

Figure 6.4: Probability density distribution of the amplification factor

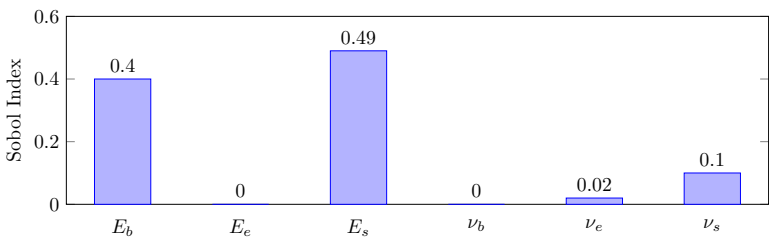

Figure 6.5: Total Sobol indices for input space parameters in model 1

Sobol indices: Figure 6.5 shows the Sobol indices for all the parameters (E_b, E_e, E_s, ν_b,

ν_e, ν_s) under study. It can be clearly seen that the elasticity modulus for ballast (E_b) and subgrade (E_s) are the most influential parameters. While the Poisson's ratio of the ballast and embankment layers shows no influence on Y_{RTZ}, the Poisson's ratio for the subgrade layer (ν_s) has a marginal influence on the magnification factor. Hence, in the following sections mainly E_b, E_s and ν_s will be investigated in detail. In addition to these parameters, as discussed in Section 6.2.5, the ratios of elastic moduli of the trackbed layers will be studied too.

Scatter of parameters (E_b, E_s): In the previous paragraph, Sobol indices (see Figure 6.5 show that E_b and E_s were the most influential parameters and ν_s was marginally influential. Therefore, in this paragraph, only these three parameters are investigated. Figure 6.6 presents the scatter plots of E_b (a) and E_s (b) with Y_{RTZ}, showing the influence of ν_s by means of colour gradient. Figure 6.6(c) shows a detailed investigation of these scatter plots in terms of strength and correlation coefficient. On one hand, a strong correlation of Y_{RTZ} is observed with both E_b (positive) and E_s (negative). On the other hand, ν_s shows some effect on Y_{RTZ} only for very low values (smaller than 0.3). Hence, the scatter plot of ν_s was not studied as the Spearman correlation coefficient and the R-squared coefficient of the scatter plot of ν_s is negligible compared to E_b and E_s.

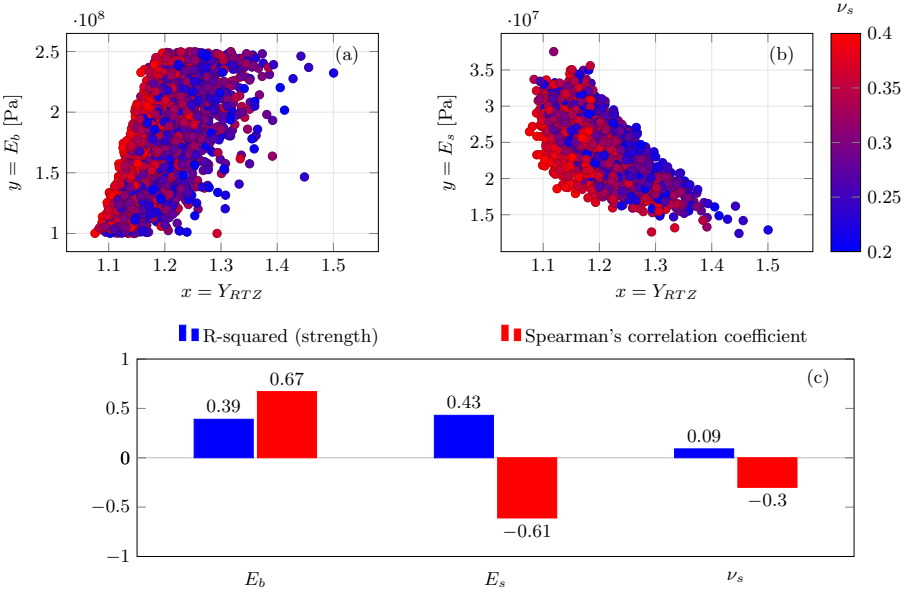

Figure 6.6: Scatter plot of (a) E_b and (b) E_s for model 1. (c)Bar chart showing the comparison of the R-squared (strength) and Spearman's correlation coefficient for the scatter plots.

Scatter of ratios ($E_b : E_s$, $E_b : E_e$, $E_e : E_s$): Figure 6.7 presents the scatter plots of the ratios $E_b : E_s$ (a), $E_b : E_e$ (b) and $E_e : E_s$ (c) with Y_{RTZ}, showing the influence of ν_s by means of colour gradient. A strong positive correlation is observed between $E_b : E_s$ and Y_{RTZ} in

the scatter plots with the highest R-squared strength (0.84) and Spearman's correlation coefficient (0.91) compared to $E_b : E_e$ and $E_e : E_s$ as shown in Figure 6.7 (d). In addition to these, the slope of the regression line for $E_b : E_s$ is significantly large, demonstrating a strong dependence of Y_{RTZ} on $E_b : E_s$ confirming the results shown in Figure 6.7(d).

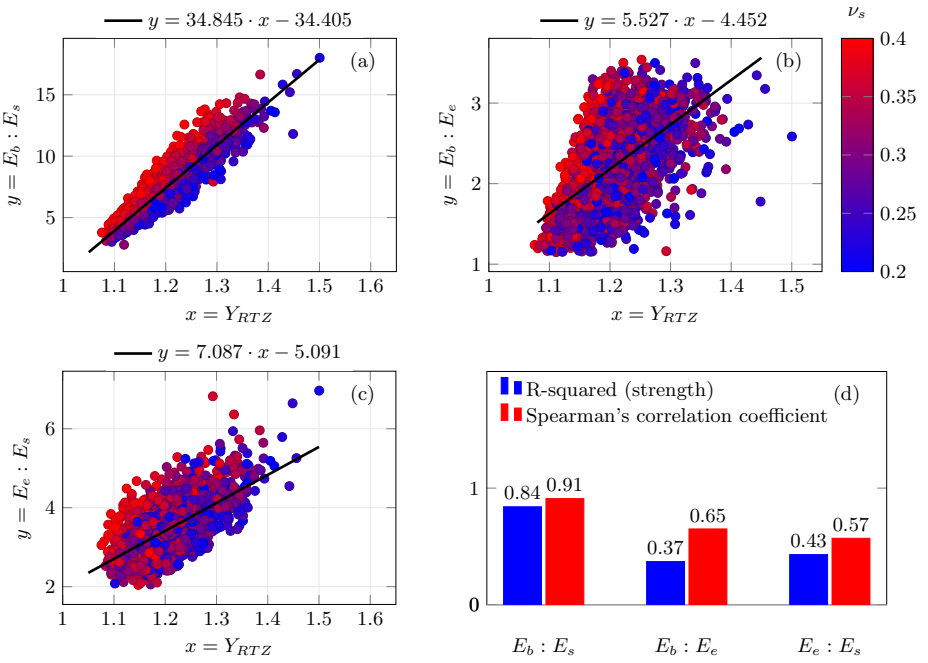

Figure 6.7: Scatter plot of the ratios (a) $E_b : E_S$, (b) $E_b : E_e$ and (c)$E_e : E_s$ for model 1. (d) Bar chart showing the comparison of the R-squared (strength) and Spearman's correlation coefficient for the scatter plots.

In summary, the most influential parameters that contribute to the amplification of the dynamic response in RTZs are the elastic moduli of the ballast (E_b) and subgrade (E_s). Additionally, the Poisson's ratio of the subgrade affects the response amplification to some extent only when the magnitude is less than 0.3. However, as seen in Figure 6.7(d), when compared to the influence of the stiffness ratios, the contribution of the individual parameters is surpassed by all the ratios under study in terms of both strength and correlation factor. Furthermore, the $E_b : E_s$ ratio dominates the comparison of all parameters and ratios under study, implying that a small change in this ratio can result in a large amplification of the dynamic response due to the reasons explained below. For completeness, it is noted that the vertical stiffness ratios do not only matter because they influence the stiffness ratio in the horizontal direction of the track, but also influence the magnification factor (Y_{RTZ}) even if the stiffness ratio in the horizontal direction of the track does not change (as shown in [26]).

The distribution of energy in a system (like the one under study in model 1) composed of three layers of different materials, where the load moves over a foundation of decreasing stiffness along the vertical direction (from stiffer to softer layers) and abruptly changing stiffness in the longitudinal direction, can be explained as follows:

1. Energy distribution in the open track response: The energy distribution over the different layers (in vertical direction) in the deformation field that moves with the load (in the open track) depends on the stiffness ratios. Generally, the stiffer a specific layer, the more energy gets concentrated in it. This can lead to a non-uniform energy distribution over the layers and energy can thus be concentrated in a relatively stiff layer (e.g., the ballast), which can become problematic in transition zones (see point 3).

2. Reflection and transmission of waves: Generally, when a wave encounters a boundary between two different materials, some of the energy carried by the wave is reflected back into the original material, and some is transmitted into the new material [39]. The proportion of energy that is reflected or transmitted depends on the difference in properties between the two materials; generally, the larger the contrast in stiffness (or more specifically, the impedance), the stronger the reflection. In the case under study, the ratios of stiffness ($E_b : E_s$, $E_b : E_e$, $E_e : E_s$) between two consecutive layers along the depth play a significant role.

3. Energy distribution in the RTZ: Amplifications in the response of the different track components and trackbed layers are the result of energy concentrations. As stated, large stiffness ratios will lead to energy concentrations in the open track response that approaches a RTZ (see point 1). The waves that are generated when the load enters and crosses the RTZ will not only be most energetic in the stiffer layers but most of the energy will also be trapped in these layers (in the form of guided waves [39, 40]) due to the large stiffness ratios (see point 2). This can lead to significant energy concentrations in stiff components.

The above-mentioned points explain the distribution of energy in the system under study and the actual behaviour therefore depends on the difference in stiffness between the layers, and how the stiffness changes from one layer to the other layer (gradually or abruptly). Hence, in order to obtain a uniform energy distribution along the depth of the trackbed layers, it is important to keep the ratios mentioned above under check and within permissible values such that the energy level in the stiffest layer (ballast) that is typically most prone to degradation does not exceed the critical values. In conclusion, a smoother stiffness variation in both vertical and longitudinal directions can ensure an uninterrupted energy flow and no trapping or concentration of energy at any particular location of the system. In all situations, energy concentrations should be avoided.

6.3.2. MODEL 2

In this section the results are presented for model 2, to study the influence of the variation in the mechanical properties of the materials on the strain energy amplification in the vicinity of the transition structure. The bounds of the material parameters for the

trackbed layers (ballast, embankment and subgrade) are exactly the same as case 1 with an addition of transition-structure material parameters as mentioned in Section 6.2.2.

Probability density function: Figure 6.8 shows the probability density of the magnification factor Y_{TS} for model 2. It can be seen that 90% of the data belongs to the values of Y_{TS} lying between 0.6 and 1.3. The mean and standard deviation of the distribution are 0.9 and 0.2 respectively. It is worth noting that by just introducing a transition structure, the mean is reduced from 1.2 (model 1) to 0.9 (model 2). The probability density function of a log-normal distribution shown in Figure 6.8 can be obtained by using Equation 6.3, where Y_{TS} is the random variable, s is 0.097, l is -1.2 and s_c is 2.15.

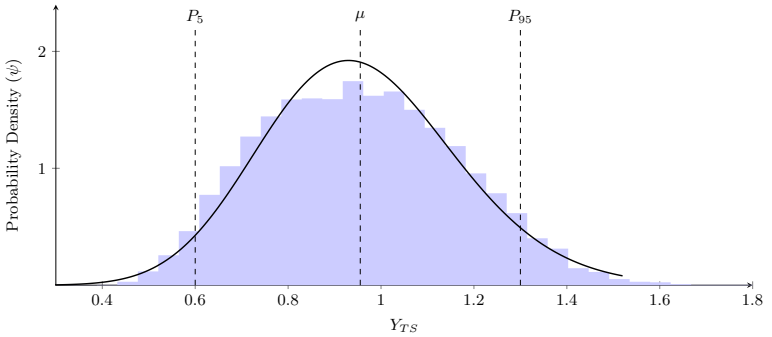

Figure 6.8: Probability density distribution of the amplification factor

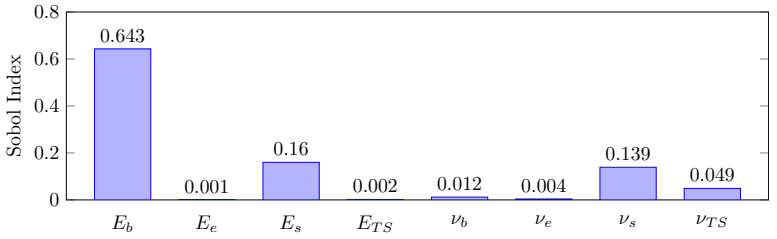

Figure 6.9: Total Sobol indices for input space parameters in model 2

Sobol indices: Figure 6.9 shows the Sobol indices for all the parameters (E_b, E_e, E_s, E_{TS}, ν_b, ν_e, ν_s, ν_{TS}) under study. It can be clearly seen that the elasticity modulus for ballast (E_b) is the most influential parameter. Other than E_b, material parameters associated with subgrade (E_s and ν_s) show a minor contribution to the amplification factor (Y_{TS}). Hence, in the following sections mainly E_b, E_s and ν_s will be investigated in detail similar to Section 6.3.1. In addition to these parameters, similar to model 1, the ratios of elastic moduli of trackbed layers and transition structure will be studied too. The ratios $E_b : E_s$, $E_b : E_e$ and $E_e : E_s$ will be investigated with an additional ratio ($E_{TS} : E_b$) representing the stiffness variation in the longitudinal direction of the track. It is to be noted that the

stiffness ratio in the longitudinal direction is studied for model 2 but not for model 1 as the material properties of the transition structure are varied (in model 2) according to Table 6.6 but the properties of the concrete bridge are kept constant in both model 1 and model 2.

Scatter of parameters (E_b and E_s): Figure 6.10 presents the scatter plots of E_b (a) and E_s (b) with Y_{TS}, showing the influence of ν_s by means of colour gradient. Figure 6.10(c) shows a detailed investigation of these scatter plots in terms of strength and Spearman's correlation coefficient associated with these scatter plots. Similar to model 1, a strong correlation is seen between E_b and Y_{TS}. In addition to these, a comparatively small influence of E_s is seen on Y_{TS}. Moreover, similar to model 1 ν_s is influential only for values smaller than 0.3.

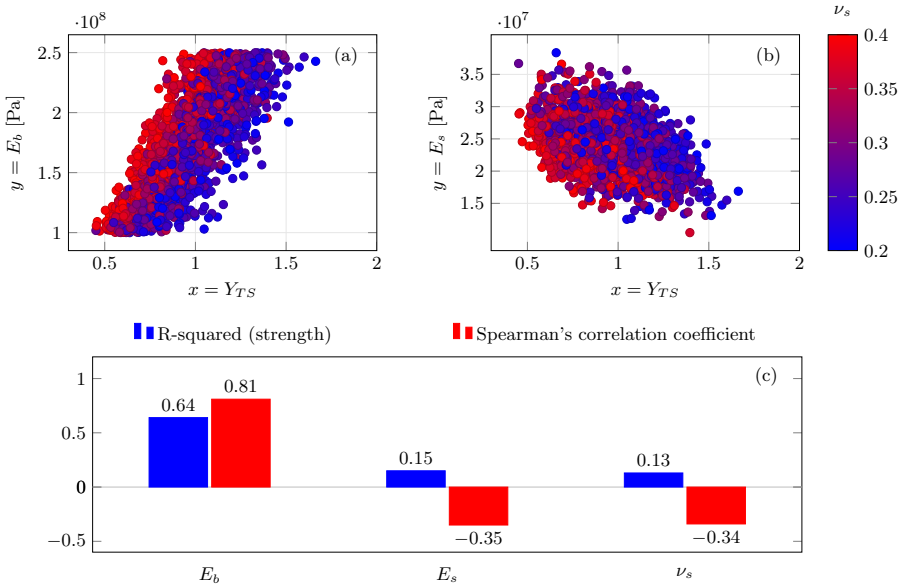

Figure 6.10: Scatter plot of (a) E_b and (b) E_s for model 2. (c) Bar chart showing the comparison of the R-squared (strength) and Spearman's correlation coefficient for the scatter plots.

Scatter of ratios ($E_b : E_s$, $E_b : E_e$, $E_e : E_s$, $E_{TS} : E_b$): Figure 6.11 presents the scatter plots of the ratios $E_b : E_s$ (a), $E_b : E_e$ (b), $E_e : E_s$ (c) and $E_{TS} : E_b$ (d) with Y_{TS}, showing the influence of ν_s by means of color gradient. A strong positive correlation of Y_{TS} is observed with $E_b : E_s$ (0.89) and $E_b : E_e$ (0.80) as shown in Figure 6.11(e). In addition to this, a strong negative correlation of Y_{TS} is observed with $E_{TS} : E_b$ (0.81). Figure 6.11 also shows the regression line for each scatter plot intersecting with the vertical line at Y_{TS}=1 (critical value of Y_{TS}) marking the critical allowable values of the ratios under study on the vertical axis of each of the plots.

The allowable ranges of the stiffness ratios identified based on observations discussed

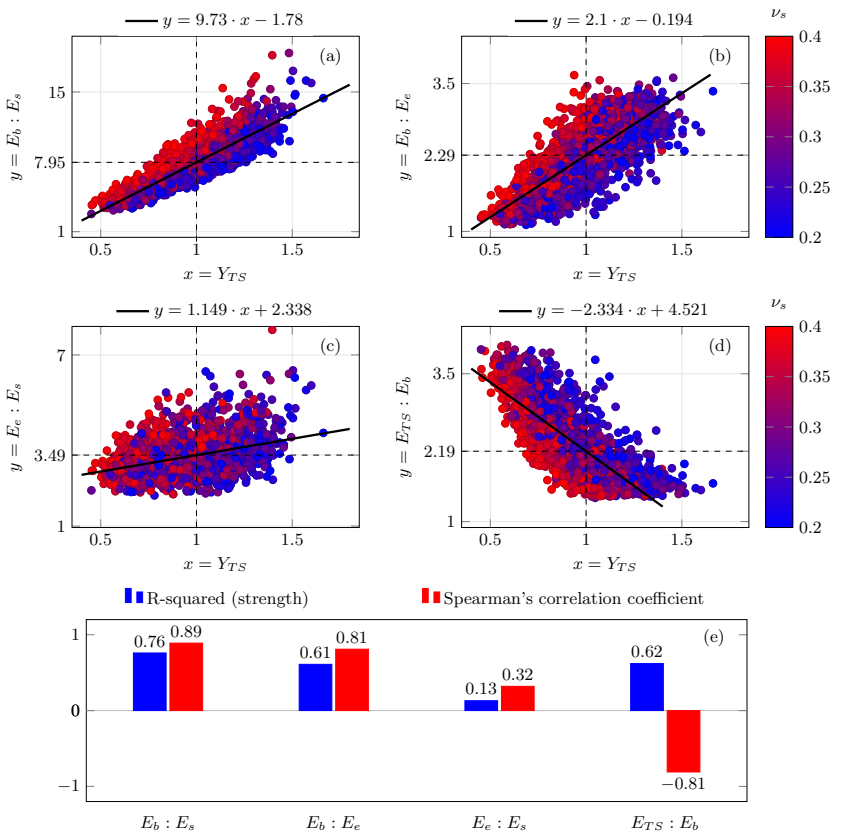

Figure 6.11: Scatter plot of the ratios (a) $E_b : E_S$, (b) $E_b : E_e$, (c)$E_e : E_s$ and (d) $E_{TS} : E_b$ for model 2. (e) Bar chart showing the comparison of the R-squared (strength) and Spearman's correlation coefficient for the scatter plots.

above and shown in Figure 6.11 can be summarised as follows:

- $E_b : E_s$ must be kept smaller than 8
- $E_b : E_e$ must be kept smaller than 2.3
- $E_e : E_s$ must be kept smaller than 3.5
- $E_{TS} : E_b$ must be kept larger than 2.2

The ratios of elastic moduli of materials of trackbed layers ($E_b : E_s$, $E_b : E_e$ and $E_e : E_s$) must be controlled for the same reasons as discussed in the previous section concerning model 1. As for the ratio $E_{TS} : E_b$, which represents a stiffness change in the longitudinal direction of the track, it is expected to be within certain limits as this ratio ($E_{TS} : E_b$) being too small implies that the transition structure is not stiff enough compared to ballast in

order to provide a smooth transition to the bridge. However, if this ratio is too high, it might lead to similar transition effects as in the case without any transition structure.

6.3.3. DESIGN LIMITS

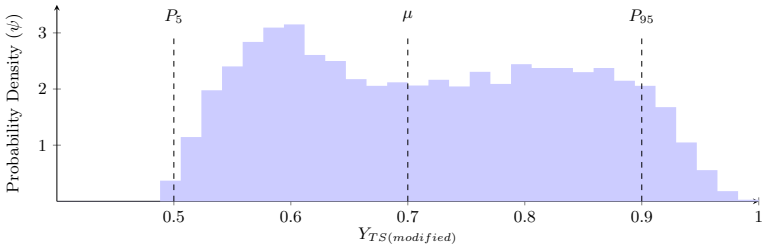

Figure 6.12: Probability density distribution of the magnification factor

This section summarises the conclusions obtained from model 1 and model 2 and in the end suggests a permissible range of the stiffness ratios to minimise the dynamic amplifications in the railway transition zones. The mean and standard deviation of the two cases under study provide useful insight into the behaviour of the two systems, particularly the central tendency (average dynamic amplification) and variability (consistency of the dynamic amplification).

System without transition structure (model 1): With a mean of 1.2 and a standard deviation of 0.06, this system shows a higher average dynamic amplification (mean in Figure 6.4) compared to model 2. The low standard deviation indicates that the amplification values are quite consistent - they tend to be close to the average value of 1.2. This could suggest that without a transition structure, the railway track consistently experiences a higher level of dynamic amplification and these dynamic amplifications are sensitive to variations in the mechanical properties of the materials in the system.

System with transition structure (model 2): With a mean of 0.9 and a standard deviation of 0.2, this system shows a lower average dynamic amplification (mean in Figure 6.8) compared to model 1, suggesting that the transition structures are effective in reducing the average dynamic amplification. However, the larger standard deviation indicates that the dynamic amplification values are more spread out and they vary more around the average. This could suggest that the effectiveness of the transition structures is not assured for all scenarios, reducing dynamic amplification significantly in some but less so in others. This is due to no active control over the relative stiffness or stiffness ratios when the materials present in the system are subjected to variations, leading to a non-uniform energy distribution within the system. This can be controlled by designing the trackbed layers around transition zones such that the relative stiffness of the materials in vertical and longitudinal directions stay within the ranges suggested in Section 6.3.2.

As mentioned in previous paragraphs, the designers must choose the material properties of the trackbed layers and the transition structure such that even though there is

Table 6.6: Design limits for ballast, embankment, subgrade and transition structure.

Layer	Design Limits	Distribution
Ballast (E_b)	$E_b > 150$ [MPa] $E_b < 250$ [MPa]	$E_b \sim \mathcal{U}[a,b]$ $a = 150$ [MPa] $b = 250$ [MPa]
Embankment (E_e)	$E_e > \frac{1}{2.3} \cdot E_b$ $E_e < 3.5 \cdot E_s$	$E_e = E_b\left(\frac{1}{2.3} + R_e\left(\frac{3.5}{R_s} - \frac{1}{2.3}\right)\right)$ $R_e \sim \mathcal{U}[a,b]$ $a = 0, b = 1$
Subgrade (E_s)	$E_s > \frac{1}{8} \cdot E_b$ $E_s < \frac{1}{2} \cdot E_b$	$E_s = R_s \cdot E_b$ $R_s \sim \mathcal{U}[a,b]$ $a = \frac{1}{8}, b = \frac{1}{2}$
Transition Structure (E_{TS})	$E_{TS} > 2 \cdot E_b$ $E_{TS} < 3 \cdot E_b$	$E_{TS} = R_{TS} \cdot E_b$ $R_{TS} \sim \mathcal{U}[a,b]$ $a = 2, b = 3$

a variation in the mechanical properties of the materials, the stiffness ratios are always kept in the permissible range. Therefore, based on the permissible ranges of these ratios proposed in Section 6.3.2, the mechanical properties of the materials are varied such that stiffness ratios R_e, R_s and R_{TS} are restricted (see Table 6.6) and the design space for model 2 is modified such that the stiffness ratios are bounded (similar to parameters in Table 6.4 and Table 6.5) with the aim to verify if the magnification factor is indeed minimized. The new design space is defined as described below.

The Poisson's ratios (ν_b, ν_e and ν_{TS}) are fixed for all the materials as they showed no significant influence on Y_{TS}. ν_s is kept constant at 0.3 as lower values are usually expected for fully unsaturated clayey soil which is unlikely to be found in reality. The elastic moduli of the materials for the trackbed layers and transition structure are defined as random variables with their relative distributions reported in Table 6.6.

Figure 6.12 shows the probability density of the magnification factor Y_{TS} for the case with a transition structure (SHIELD) and the material parameters bounded as defined in Table 6.6. In this case, the PDF resembles that of a uniform distribution, as opposed to a log-normal one. It can be seen that 90% of the data belongs to the values of Y_{TS} lying between 0.5 and 0.9. The mean and standard deviation of the distribution are 0.7 and 0.12 respectively. The mean is reduced from 0.9 to 0.7 when compared to case 2. Most importantly, all the values lie below the critical value (Y_{TS}=1) which is expected and desired for minimising the degradation in RTZs.

6.4. CONCLUSION

In this paper, a methodology to adopt an appropriate distribution (in space and accounting for the variation over the operation period) of the material properties in a railway transition zone is presented. The results of the study presented in this paper can be concluded as follows.

The behaviour of a standard embankment-bridge transition (model 1) subjected to variations in mechanical properties of the trackbed materials (ballast, embankment and subgrade) was investigated. While it is known that the stiffness variation in the longitudinal direction leads to dynamic amplification when the transition is subject to a moving load, this work has demonstrated that the stiffness variation in the vertical direction also significantly influences the dynamic behaviour of railway transition zones.

The efficiency of a recently proposed transition structure (SHIELD) was evaluated (model 2) when subjected to variations in the mechanical properties of the trackbed materials. Similar to model 1, the results for model 2 show that the stiffness ratios in longitudinal and vertical directions are the most influential parameters in determining the strain energy amplifications (strain energy is correlated to degradation) in railway transition zones. Moreover, for the system under study and the bounds adopted for the variation of material properties of the trackbed layers and SHIELD, a permissible range of design ratios is suggested to control the amplification of strain energy in all components of railway transition zones.

Lastly, based on the allowable range of stiffness ratios obtained from model 2, new bounds for the material properties of the ballast, embankment, subgrade and transition structure were formulated to ensure no amplification of strain energy. It was demonstrated that it is possible to mitigate the strain energy amplifications if the stiffness ratios in vertical and longitudinal directions are kept in check. We note that the stiffness ratios should be respected both in the design of the transition zone and structures (initial state) as well as during the operational phase (where the properties may vary over time).

The methodology adopted in this work to evaluate the behaviour of railway transition zones with or without a transition structure both in the initial design phase and when subjected to variation in material properties, and to establish the design limits on the material properties of the trackbed layers and the transition structure can be generalised for any type of transition zone and a wide set of material properties.

7

GEOMETRIC OPTIMISATION: SHIELD

This chapter (with minor changes) has been published as *A. Jain, A.V. Metrikine, and K.N. Dalen. Energy redistribution in railway transition zones by geometric optimisation of a novel transition structure. Transportation Geotechnics (2024), ISSN 2214-3912.*

ABSTRACT

Railway transition zones are critical regions in railway infrastructure that are subjected to excessive operation-driven degradation due to energy concentration within these zones. This work presents a heuristic approach to optimise the geometry of the transition structure and investigate its influence on the strain energy distribution in the railway transition zones (RTZs), with a specific focus on embankment-bridge transitions equipped with a newly proposed 'Safe Hull-Inspired Energy Limiting Design (SHIELD)' transition structure. For this purpose, a number of three-dimensional finite element models are used to analyze different geometric profiles of SHIELD in a systematic manner. By altering SHIELD's geometry across longitudinal, transversal, and vertical directions, the influence of the different geometric profiles on the total strain energy distribution across the trackbed layers (ballast, embankment, and subgrade) is studied in terms of spatial and temporal variations. The results establish the contribution of geometry to energy redistribution in all three directions and present an optimum geometry for the type of transition under study. It is found that among all the profiles, the longitudinal geometric profile of SHIELD has the most significant impact on the strain energy distribution, while the transversal profile primarily influences the ballast layer, and the alteration of vertical profiles enhance the local redistribution of strain energy in the vicinity of the transition interface. The preliminary optimisation (heuristic approach) presented in this work provides the starting point for full-scale optimisation to obtain tailored shapes of transition structures such that there is neither a concentration of energy nor an obstruction in the flow of energy in RTZs.

7.1. INTRODUCTION

Railway transition zones (RTZs), where track configurations change from one type of foundation to another (e.g., from a bridge onto an embankment or from slab track to ballasted track), represent critical sections in railway networks. Several studies [1–3] highlight the vulnerability of RTZs to geometry and material degradation leading to high maintenance costs [4]. In [5], a detailed overview of the problem in RTZs is presented highlighting the main causes behind the accelerated deterioration of track material and geometry in RTZs. Another study [6] provides a comprehensive review of various mitigation measures adopted to deal with the amplified degradation of RTZs. The zones are typically characterized by abrupt changes in track stiffness [7] and differential settlement [8–10] and are often subjected to dynamic amplifications. Over the years, these amplifications have been studied vastly in terms of kinematic responses or stresses in the track components such as rail, sleepers and trackbed layers (ballast, embankment, subgrade). However, in a recent study [11], the strain energy is proposed to be the most comprehensive quantity (as it includes both stress and strain) to study the operation-driven response amplifications in railway transition zones. Moreover, the total strain energy includes not only the distortional component (related to Von-Mises stress) but also the volumetric component of the strain energy. The study has concluded that "minimizing the magnitude of total strain energy (as the non-recoverable part of the strain energy contributes to the damage in material) will imply lesser permanent deformation and hence reduced operation-induced degradation, and the total strain energy being as uniform as possible along the longitudinal direction (i.e., without an abrupt increase or decrease) will mitigate non-uniform (operation-induced) degradation". The study performed to formulate this

design criterion clearly shows the amplification of strain energy in typical RTZs. However, this investigation was performed using a 2 dimensional (2-D) plane-strain finite element model. Even though some studies have shown that the amplified degradation in RTZs can be studied to some extent using equivalent 2-D models [12–15], the influence of the geometry in the transverse direction on the strain energy distribution is unknown. The investigation of strain energy variations in the trackbed layers using a 3-D model [16–19] is lacking in the literature.

There have been numerous attempts at designing an effective intervention to mitigate the effects of dynamic amplifications in railway transition zones. Some of the most commonly used interventions are transition structures such as approach slabs [20–23], transition wedges [24–27], auxiliary rails [28, 29] closely spaced sleepers [30], under-sleeper pads [31] and others [3, 32, 33]. Based on the recently proposed energy-based criterion mentioned above [11], it is shown in [30, 34] that most of these mitigation measures either have no effect on reducing energy amplifications close to the transition interface or may even amplify the strain energy elsewhere in the system. A novel Safe Hull-Inspired Energy Limiting Design (SHIELD) of a transition structure is adopted in [34] using the design principle of guiding energy away from the upper trackbed layers such that there is neither a concentration of energy in any part of the system nor an obstruction in the flow of energy in any of the trackbed layers. Figure 7.1 shows energy concentration in the upper trackbed layers due to geometry [34] and energy obstruction in the transition zone compared to the open tracks for an embankment-bridge transition discussed in Section 7.2. SHIELD as a name reflects that the transition structure design is 'safe' (as the transition structure safeguards the track from excessive degradation), 'hull-inspired' (as the geometry of the transition structure is inspired by the shape of a hull) and 'energy-limiting' (as the key phenomena governing design are based on limiting energy around the transition zones). However, these studies are based on a 2-D model of SHIELD. There is a need for comprehensive research targeting the effects of the various geometric profiles of this newly proposed design. The geometric profiles in longitudinal, transverse and vertical directions can play a pivotal role in the distribution of the strain energy in RTZs. A deeper understanding of this interplay between geometry and energy distributions can offer transformative insights into optimizing design, ensuring robustness, and extending the lifespan of RTZs. In this work, the influence of geometry on energy distributions is investigated, and the influence of energy distributions on geometry (permanent deformations in the vertical direction) is demonstrated in [11].

The role of geometry in guiding energy is paramount, especially in systems like RTZs where obstruction-free flow [35–37] and uniform distribution of energy are sought [38]. Geometry serves as a fundamental determinant in the path and characteristics of energy flow within a system. The role of geometry in energy distribution can be explained in terms of the following items:

- **Guiding energy using optimal pathways:** The shape and configuration of a structure can significantly influence the propagation of energy. For instance, certain geometric designs can ensure that wave energy gets distributed uniformly rather than concentrating in specific areas, preventing "hotspots" or areas of concen-

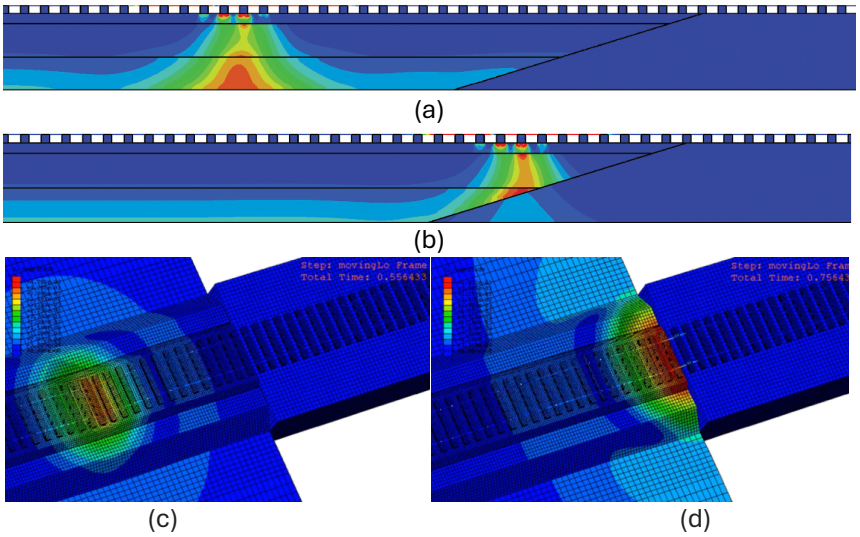

Figure 7.1: (a) 2-dimensional model showing energy flow in the open track in the longitudinal direction [34] and (b) energy concentration in upper trackbed layers [34] compared to open tracks due to geometry. (c) 3-dimensional model showing energy flow in the open track and (d) energy obstruction in the transition zone

trated energy. Geometry can be utilized to design optimal pathways such that the energy flow within railway transition zones can be guided to shield the most degradation-prone components from energy concentration or obstruction, thus preventing localized zones of high energy.

- **Scattering and reflection:** The geometry of a specific surface can determine how energy is reflected or scattered. Curved or angled surfaces, for instance, might scatter energy more effectively than flat ones, preventing energy concentration.
- **Mitigating stress concentrations:** Sharp corners or sudden changes in cross-section can lead to stress concentrations. By optimizing geometry, these concentrations can be minimized, ensuring a more uniform distribution of energy.

In summary, geometry serves as a blueprint for energy flow. By understanding the interplay between geometry and energy, designers and scientists can create systems that channel and distribute energy in desired and efficient ways.

This paper presents a detailed investigation of the influence exerted by geometry on the strain energy distributions induced by moving loads in RTZs. Firstly, a 3-D model of a standard embankment-bridge transition without any transition structure is studied to evaluate the distribution of total strain energy in the trackbed layers in the proximity of the transition interface and far from it. Secondly, the influence of different geometric profiles of SHIELD in longitudinal, transverse and vertical directions on the strain

energy distributions is studied using a number of 3-D finite element models (discussed in detail in Section 7.2). Lastly, based on the results (in Section 7.3) obtained for the above-mentioned cases, this paper presents an optimised geometry of the transition structure using a heuristic approach for energy redistribution in RTZs. It is to be noted that apart from the geometric profiles, all other parameters like mechanical properties of the materials, train speed and direction, type of transition etc., are kept constant in this work. The influence of mechanical properties of materials has been investigated in [39] and the influence of other parameters using more detailed models will be investigated in future works.

7.2. MODELS

In this paper, the dynamic behaviour of railway transition zones is studied for a standard embankment-bridge transition with and without a transition structure. For this purpose, a number of models are generated and will be discussed in detail in this section. It is to be noted that all materials used in this work are linear elastic as a correlation was demonstrated in [11] between strain energy amplifications and permanent deformations. The models studied in this work can be broadly classified into two categories as follows:

- **Standard embankment-bridge transition zone:** A three-dimensional (3-D) finite element model was developed using ABAQUS [40] to represent an embankment-bridge railway transition zone to study the influence of the geometry in all directions on the distribution of total strain energy in the trackbed layers. This model is referred to as the "base model" in this work. The improved behaviour of RTZs with the new transition structure (SHIELD; see category 2 below) is shown in comparison to this base model.

- **Embankment-bridge transition zone incorporating the "Safe Hull Inspired Energy Limiting Design" (SHIELD) transition structure:** The influence of longitudinal, transverse and vertical geometric profiles of SHIELD on the distribution of strain energy in each trackbed layer is studied using a variety of models. The geometric profiles shown in Figures 7.3, 7.4 and 7.5 are chosen such that the energy is guided away from the trackbed layers prone to degradation, there is no energy amplification due to adverse effects of reflection and scattering and there are no stress concentrations due to sharp geometric edges (based on discussions in Introduction). Firstly, five longitudinal profiles (see Figure 7.3 and Table 7.1 for details) of SHIELD are studied using two-dimensional plane-strain models. A two-dimensional model is used in this step to avoid the influence of out-of-plane geometry, which is investigated in the subsequent steps. Secondly, the longitudinal profile that shows the most promising dynamic behaviour according to the energy criterion (as discussed in the Introduction) is chosen as a basis for the generation of a 3-D shape of SHIELD with varying transversal cross-sections (see Figure 7.4 and Figure 7.5 for details). Lastly, the influence of the vertical cross-section (see Figure 7.6 and Figure 7.7 for details) is investigated using the longitudinal and transverse profiles that show the best performance according to the energy criterion.

7.2.1. GEOMETRIC MODEL

BASE MODEL

The geometric profiles (longitudinal, transverse, and vertical) of the base model are shown in Figure 7.2. In Figure 7.2, the longitudinal profile is in the X-Z plane, the transverse profile is in the X-Y plane and the vertical profile belongs to the Y-Z plane. The total length of the base model in the longitudinal direction is 80 m which is comprised of 60 m of ballasted track (soft side) and 20 m of ballast-less track (concrete bridge). The ballasted track is divided into three zones of 7.5 m each with an additional 22.5 m at the end in order to eliminate the influence of boundaries (extreme left and right) on the results of the zones under study. The first zone (see Figure 7.2 for zoning details) close to the transition interface is referred to as "Approach Zone - I (AZ-I)" which is the most influenced zone by transition effects. The last zone under study is referred to as "Open Track (OT)" as it is largely uninfluenced by transition effects. The second zone in between AZ-I and OT is referred to as "Approach Zone–II (AZ-II)" which might or might not be affected by transition effects. The geometric model mainly consists of the following track components:

- Rail with profile 54E1 (UIC54) according to European Standard EN 13674-1
- Rail-pads
- Sleepers
- Trackbed layers: Ballast, Embankment, Natural terrain or subgrade
- Concrete bridge

The sleeper spacing adopted is 0.6 m and the first sleeper next to the transition is located at 0.3 m from the transition interface.

SHIELD

The base model described above was modified by inserting various geometric shapes of SHIELD between the ballasted track and the concrete bridge. The different geometric profiles of SHIELD investigated in this paper are described in detail below.

Longitudinal profiles of SHIELD The longitudinal profile of SHIELD is a trapezoidal-shaped geometry with a major base (top) of length 'L_{top}' and a minor base (bottom) of length 'L_{bottom}' as shown in the schematic in Table 7.1. Five different longitudinal profiles (see Figure 7.3) are studied and listed below.

It is to be noted that models L1-L5 are studied to investigate the influence of the ratio of L_{top} to L_{bottom} of the transition structure. However, the design length 'L' mentioned in Table 7.1 will depend on several factors such as vehicle characteristics, material properties of the surrounding/environment, type of transition zone, etc. However, as the aim of this work is to demonstrate the influence of the geometric parameters of the longitudinal profile of the SHIELD on the strain energy distribution in the trackbed layers, all other

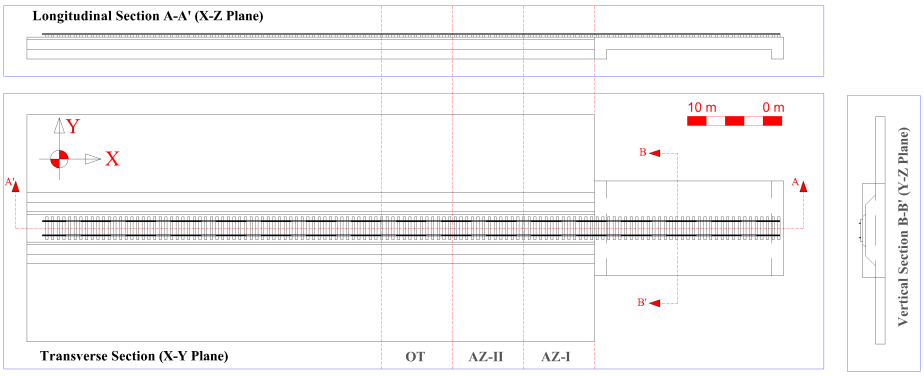

Figure 7.2: Cross-section details of a standard embankment-bridge transition used to generate a 3-D numerical model.

Table 7.1: Details of Longitudinal profiles of SHIELD studied in this paper.

Longitudinal Profiles	L_{top}	L_{bottom}	Schematic (models L1-L5)
Model-L1	L	$L/2$	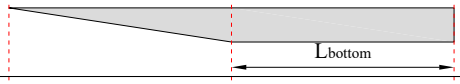
Model-L2	L	null	
Model-L3	L	L	
Model-L4	L	$L/4$	
Model-L5	L	$3L/4$	

parameters are kept constant. For a particular set of the above-mentioned factors considered in this work, $L = 15$ m was found to be the optimum length to mitigate the transition effects.

Transverse profiles of SHIELD The transverse profiles of SHIELD presented in this paragraph are based on the principle of guiding energy away from the trackbed layer (as discussed in the Introduction) in the transverse direction. As shown in Figure 7.4 and Figure 7.5, two extreme profiles of rectangular (model-T3) and triangular (model-T2) shaped geometry are considered. In addition to this, model-T4 (lanceolate-shaped) is a modification of model-T2 exhibiting curved edges around the apex and model-T1 (a combination of model-T3 and model-T4) has a rectangular-shaped bottom and lanceolate-shaped top. The transverse profiles of all the models are such that the volume of all the models is comparable, the vertical cross-section at the transition interface is rectangular and the longitudinal cross-section is similar to that of model-L1.

Vertical profiles of SHIELD Two vertical profiles of SHIELD are investigated to see the influence of tapering in the vertical plane on the energy distribution in the trackbed layers. The vertical profiles model-V1 (trapezoidal-shaped) and model-V2 (rectangular-shaped) are studied (see Figure 7.6 and Figure 7.7). It is to be noted that model-T1 was chosen to study the variation of the vertical-plane geometry of SHIELD as it shows the most

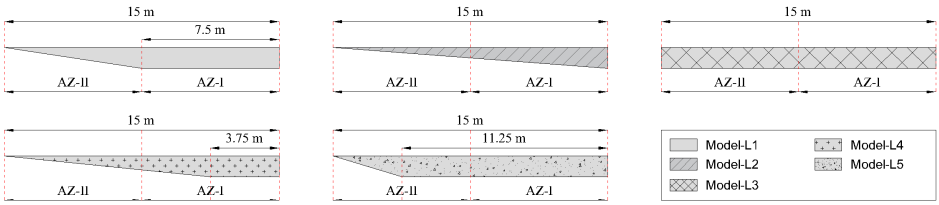

Figure 7.3: Longitudinal profiles of SHIELD (models L1 to L5 as shown in the legend).

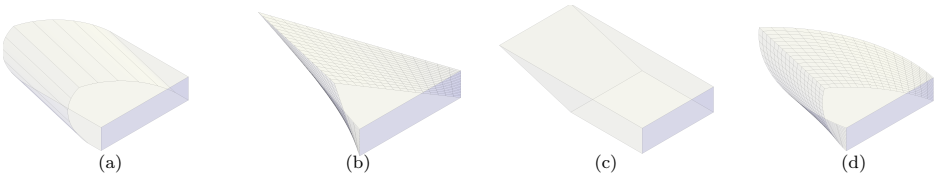

Figure 7.4: Three-dimensional (3-D) shapes of SHIELD with different transverse cross-sections for (a) Model-T1, (b) Model-T2, (c) Model-T3, (d) Model-T4.

favourable distribution of strain energy as per the criterion, as discussed later (in Section 7.2.2).

7

The total length of all the models described above is the same as the base model. However, the division of the zones is different in order to study the dynamic behaviour of the transition structure in detail. Each zone (AZ-I, AZ-II, AZ-III) is 7.5 m for all the above-mentioned cases with SHIELD. The open track behaviour is expected to be the same as that predicted by the base model. The first zone close to the transition interface between the bridge and transition structure is referred to as "Approach Zone-III (AZ-III)", and the last zone next to the interface between the ballasted track and transition structure is referred to as "Approach Zone–I (AZ-I)". The zone in between AZ-I and AZ-III is referred to as "Approach Zone–II (AZ-II)". All the track components remain the same as the base model, only the transition structure (SHIELD) is added. Figure 7.8 shows the zones of study for one of the models (model-V1) with SHIELD.

7.2.2. NUMERICAL MODEL

Several 3-D Finite Element (FE) models were created using ABAQUS, by modifying the base model (Figure 7.9) using geometrical details described in Section 7.2.1. To include realistic energy dissipation in the models, Rayleigh damping for materials was defined using parameters listed in Table 7.2 according to [39]. The dimensions (longitudinal and vertical direction) of the model were chosen to eliminate the influence of the wave reflections from the boundaries (extreme right, left and bottom of the system) on the results of the zones under study. The depth of the subgrade was limited to restrict the vertical displacements to maintain a reasonable value based on literature [41]. In addition

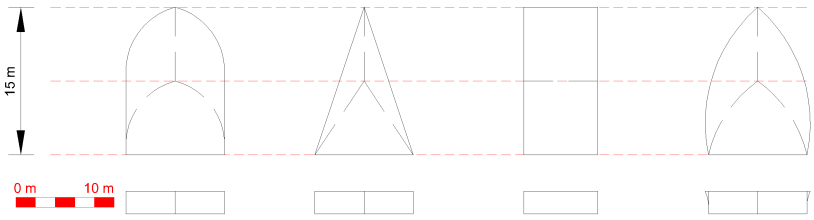

Figure 7.5: Transverse and vertical cross-sections of SHIELD for Model-T1, Model-T2, Model-T3, Model-T4 (left to right).

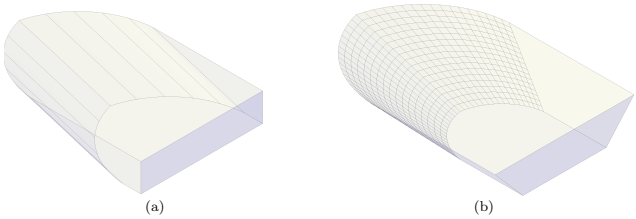

Figure 7.6: Three dimensional (3-D) shapes of SHIELD with different vertical cross-sections for (a) Model-V1, (b) Model-V2.

to this, the cumulative depth of the layers under the sleepers is maintained such that the dynamic stresses at the bottom of the subgrade are less than 3% (this value was suggested to be less than 10% in [12] so as to eliminate artificial boundary effects) of their values at the bottom of the sleepers. Moreover, the vertical rail displacements and stress in the ballast layer were verified with the data presented in [42] and [43] for a transition zone similar to the one under study, and values obtained from the base model (rail displacement = 1.47 mm) are comparable to the ones mentioned in the literature (rail displacement = 1.39 mm approx.) [42].

The following subsections describe the details regarding the FE models used in this paper in terms of mesh properties, mechanical properties of materials, interactions between the track components, loads and boundary conditions. A static step was performed to obtain the initial stress state of the model under self-weight, followed by a dynamic analysis (full Newton-Raphson method) for 2.5 s with a time step of 0.005 s. The loads that have been considered are the gravity load for the static analysis and one moving axle load of 90 kN with a velocity of 100 km/h for the dynamic analysis. It is to be noted that the simplest loading conditions have been adopted in this work as the main objective is to investigate the influence of geometry on the energy distributions, capturing the main mechanisms governing the dynamic amplifications in RTZs in the cleanest possible manner. The load moving in the direction from the soft side to the stiff side of the transition was simulated using the DLOAD subroutine in ABAQUS [44].

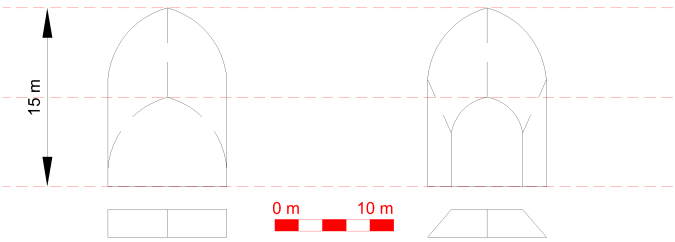

Figure 7.7: Transverse and vertical cross-sections of SHIELD for Model-V1 and Model-V2 (left to right).

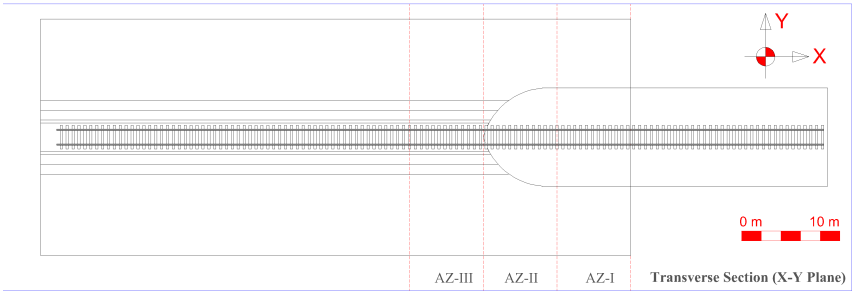

Figure 7.8: Transverse Cross-section of the model-V1 showing the zones (AZ-I, AZ-II, AZ-III) under study.

7

MATERIAL

The materials used for all track components in the models described in previous sections are characterised by elastic properties (Young's modulus, Poisson's ratio), densities and Rayleigh damping factors [45, 46]. A detailed analysis of the influence of material properties was performed in [39] and suggested stiffness ratios were used for optimal performance of SHIELD in this work. The mechanical properties of all the track components and the transition structure (SHIELD) are chosen as tabulated in Table 7.2 for this study.

INTERFACE AND BOUNDARY CONDITIONS

The infinite elements (CIN3D4R) are used on the vertical boundaries at extreme left and right to minimize reflections due to artificial boundaries. The interface conditions used in the models are defined below:

- Rail-sleeper: Rail was connected to the sleepers via rail-pads using vertical springs with stiffness (k = 1.2 x 10^8 N/m) and dashpots with coefficient (c = 5 x 10^4 N-s/m).
- Sleeper-ballast, ballast-embankment, and embankment-subgrade interfaces: surface-to-surface tie constraint was used for defining the conditions at these three interfaces.

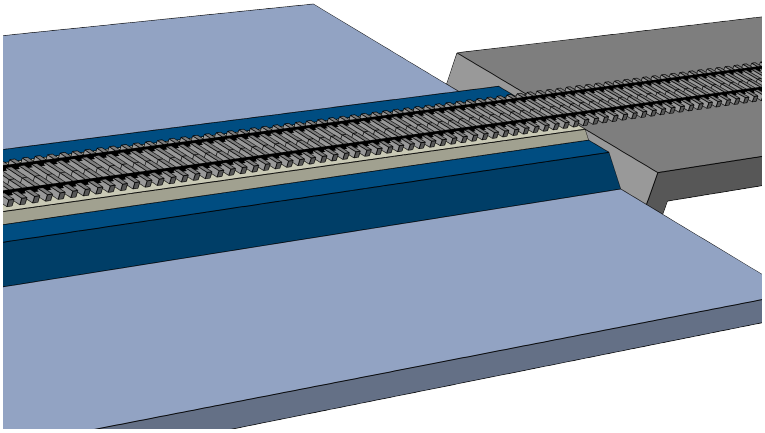

Figure 7.9: The 3-D finite element model (mesh elements are deactivated for better visualization) of a standard embankment-bridge transition (base model) generated using ABAQUS.

Table 7.2: Mechanical properties of the track components

Material	Elasticity Modulus E [N/m^2]	Density ρ [kg/m^3]	Poisson's Ratio ν	Rayleigh damping α	β
Steel (rail)	21 x 10^{10}	7850	0.3	-	-
Concrete (sleepers)	3.5 x 10^{10}	2400	0.15	-	-
Ballast	1.5 x 10^8	1560	0.2	0.0439	0.0091
Sand (embankment)	8 x 10^7	1810	0.3	8.52	0.0004
Clay (subgrade)	2.55 x 10^7	1730	0.3	8.52	0.0029
SHIELD	3.6 x 10^8	1900	0.2	0.0439	0.0091

- All vertical interfaces: a hard contact linear penalty method was used to define the normal behaviour and Coulomb's friction law was adopted to define the tangential behaviour with a frictional coefficient equal to 0.5. (details can be found in [40])
- The bottom of the bridge is fixed representing a rigid foundation.

MESH

In all the 3-D models, sleeper, ballast, embankment, subgrade, transition structure and bridge were discretized [40] using four-node tetrahedral elements (C3D4) the eight-node brick elements (C3D8). The rail was discretized using two-node linear beam elements of type B21 to form a very regular mesh. An initial mesh sensitivity analysis was performed for each of the models to ensure that there is no dependence of the results on the mesh size or quality.

OUTPUTS

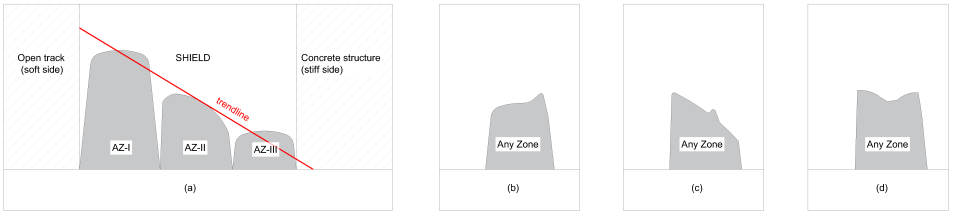

Figure 7.10: Schematic showing (a) spatial trend of the strain energy in zones from open track to concrete structure and its temporal trend within one zone: (b, c) abrupt local increase, (d) increase after decreasing trend.

The main outputs from the models studied in this paper are time histories of the total strain energy (only dynamic) in each of the zones under study for the layers of ballast, embankment and subgrade. In Abaqus [44], "ALLSE" provides a time history of the total strain energy within a considered volume (each zone for each trackbed layer). These outputs are compared for the different geometric profiles (Section 7.2.1 for details) of SHIELD and the base model under study.

The strain energy magnitude on the concrete structure (stiff side) is negligible (approximately 300 times smaller) compared to the ballasted tracks (soft side) as shown in [11] and a direct correlation was demonstrated between strain energy and permanent deformations. This implies a large difference in the permanent deformations on the soft and stiff side of the system. In order to avoid an abrupt drop of strain energy from the soft to the stiff side of the system, SHIELD was proposed [34, 39] to facilitate a gradual decrease in strain energy magnitudes (and thus in permanent deformation). In terms of magnitude (spatially), the ratio of maximum strain energy in consecutive zones shown in Figure 7.10 is desired to be always less than 1. In the temporal variation of strain energy, a monotonically decreasing trend is sought. Both of these requirements are directly inferred from the general criterion presented in [11]. The performance of different geometric profiles of SHIELD is assessed in terms of the following evaluation criteria (which directly follow from the design criterion referred to in the Introduction):

- Spatial trend: The variation of strain energy magnitudes from the open track to the concrete structure must demonstrate a gradual “decreasing trend”. This implies the strain energy magnitude must gradually decrease from one zone under study to another (from the largest in AZ-I to the lowest in AZ-III)) as shown in the schematic (Figure 7.10a).

- Temporal trend: Within each zone, the temporal variation of strain energy must demonstrate “smoothness”. This implies that the strain energy curve must not exhibit sharp spikes or drastic changes (increase or decrease) in a short span of time (Figure 7.10b,c). In addition to this, within each zone, ideally, the strain energy magnitude must never increase after a decreasing trend is observed at any

time moment (see Figure 7.10d). This type of local increase might lead to locally amplified degradation (e.g., hanging sleepers). It is to be noted that there is always an entrance effect or initial rise in strain energy magnitude due to the entrance of the deformation field carried by the moving load.

7.3. RESULTS AND DISCUSSION

7.3.1. BASE MODEL

As discussed in the Introduction, the investigation of strain energy variations in track components using a 3-D model is lacking in the literature. Therefore, in this section, the time histories of strain energy (Figure 7.11c) for the base case (described in Section 7.2) obtained using a 2-D model and a 3-D model are compared for the layers of ballast, embankment and subgrade in the zones under study (OT, AZ-I and AZ-II). It is observed that the plane-strain assumption of the 2-D model leads to an overestimation of the strain energy (given the same loading conditions) in the embankment and subgrade and shows a higher amplification of strain energy in the proximity of the transition interface in the ballast layer compared to that predicted by the 3-D model. The overestimation of responses can also be seen in a comparison of displacements (see Figure 7.12) obtained for 4 points (on rail, top of ballast, embankment and subgrade under rail) in the open track. The track components in the 2-D model deform much more than in the 3-D model. Even though the 2-D model captures the trends of strain energies in all the layers and zones under study, designers must rely on 3-D models for precise calculations.

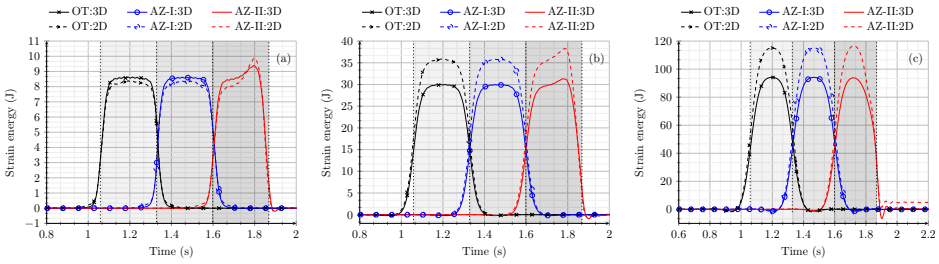

Figure 7.11: Time history of the strain energy obtained from the base model for the layers of (a) ballast, (b) embankment and (c) subgrade in all the zones under study (OT, AZ-I, AZ-II). The dotted lines mark the time moments at which the load enters and exits each zone.

In Figure 7.11, for the layers of ballast and embankment, it can be clearly seen that there is an amplification of strain energy in the AZ-II with respect to the OT in the proximity of the transition interface. Moreover, even though there is no strain energy amplification in AZ-II with respect to OT in the subgrade layer, the strain energy is non-zero (unlike other layers) even after the load has crossed the transition interface. In order to minimise the transition effects, it is necessary to minimise the strain energy amplifications in the affected trackbed layers. An effective intervention must ensure no amplification in strain energy in any of the trackbed layers under study in the proximity of the transition

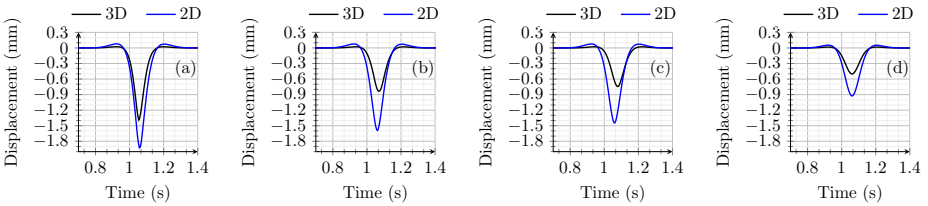

Figure 7.12: Time history of the displacements obtained from the base model for (a) rail, top of (b) ballast (c) embankment and (d)subgrade layers.

interface between the ballasted track and transition structure and between the transition structure and the concrete bridge. The following section will demonstrate the influence of geometric profiles on energy redistribution in the railway transition zone.

7.3.2. LONGITUDINAL PROFILES OF SHIELD

Ballast: Figure 7.13 shows a comparison of the time histories of strain energy in the ballast layer for the zones AZ-I, AZ-II and AZ-III for models L1-L5. It can be clearly seen that in AZ-I, model-L3 and model-L5 exhibit an amplification of strain energy at the time moment right before the load exits AZ-I. This is similar to AZ-II of the base model (Figure 7.11) as expected due to the rectangular shape of the transition structure in model-L3 and the very steep slope of the inclined interface for model-L5. In summary, models L3 and L5 are not suitable geometric profiles as they show strain energy amplification similar to the base model with the only difference of location. In the base model, this amplification is observed at the interface of ballast and the concrete structure, whereas, in models L3 and L5, the strain energy amplification is observed at the interface of ballast and SHIELD. Therefore, the study can be narrowed down to models L1, L2 and L4. In AZ-II, all these models show similar behaviour in terms of the magnitude of strain energy, but both a spatial (from one zone to the other as the load moves from AZ-I to AZ-III) and a temporal (within each zone) decreasing trend (as discussed in Section 7.2.2) can be seen only in model-L1. models L2 and L4 show unfavourable behaviour as they demonstrate a decrease after the time moment at which the load enters AZ-II (similar to Figure 7.10d) and an increase right before the load exits this zone. In AZ-III, none of the models show an abrupt increase in strain energy (temporal) but the spatially decreasing trend (from AZ-II to AZ-III) is observed only for model-L1. models L2 and L4 show a higher magnitude of strain energy compared to model L1 in AZ-III.

Embankment: Figure 7.14 shows a comparison of the time history of strain energy in the embankment layer for zones AZ-I, AZ-II and AZ-III for models L1-L5. Similar to the ballast layer, the embankment layer also shows an amplification of the strain energy for model-L3 in AZ-I. In AZ-II (Figure 7.14b), model-L1 shows the most promising behaviour because of both the decreasing spatial trend and the (temporal) smoothness (no abrupt increase or decrease) of the strain energy. In AZ-III (Figure 7.14c), however, all models result in similar strain energy curves.

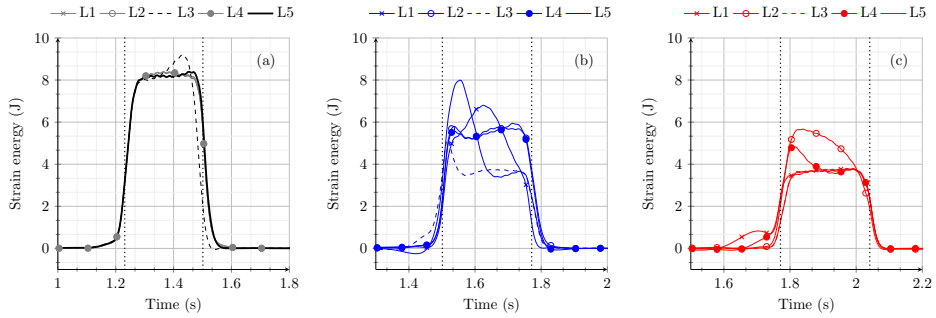

Figure 7.13: Time history of strain energy for different longitudinal profiles under study in the layer of ballast for (a) AZ-I, (b) AZ-II and (c) AZ-III. The dotted lines mark the time moments at which the load enters and exits each zone.

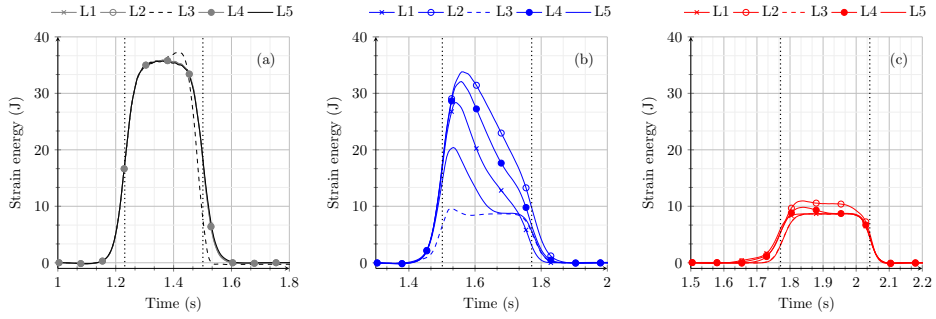

Figure 7.14: Time history of strain energy for different longitudinal profiles under study in the layer of the embankment for (a) AZ-I, (b) AZ-II and (c) AZ-III. The dotted lines mark the time moments at which the load enters and exits each zone.

Subgrade: Figure 7.15 shows a comparison of the time histories of strain energy in the subgrade layer for zones AZ-I, AZ-II and AZ-III, for models L1-L5. No amplification of strain energy is observed for any of the longitudinal profiles under study in AZ-I (Figure 7.15a). No spatial decreasing trend in the magnitude of the strain energy is observed for models L2 and L4 from AZ-I to AZ-II (Figure 7.15b). Models L1, L3 and L5 show a reduction in the magnitude of strain energy in AZ-II compared to that in AZ-I. However, model-L3 shows an abrupt decrease in the magnitude of strain energy in AZ-II compared to AZ-I. In the end, within zone AZ-II and AZ-III, all longitudinal profiles satisfy the strain energy criterion in terms of both spatial decreasing trend and smoothness.

7.3.3. TRANSVERSE PROFILES OF SHIELD

Ballast: Figure 7.16 shows a comparison of the time history of strain energy in the ballast layer for zones AZ-I (a), AZ-II (b) and AZ-III (c) for models T1-T4. In AZ-I, all the models illustrate the same strain energy distribution (no abrupt increase or decrease). In AZ-II, models T1 and T2 show the most smooth distribution of strain energy demonstrating a

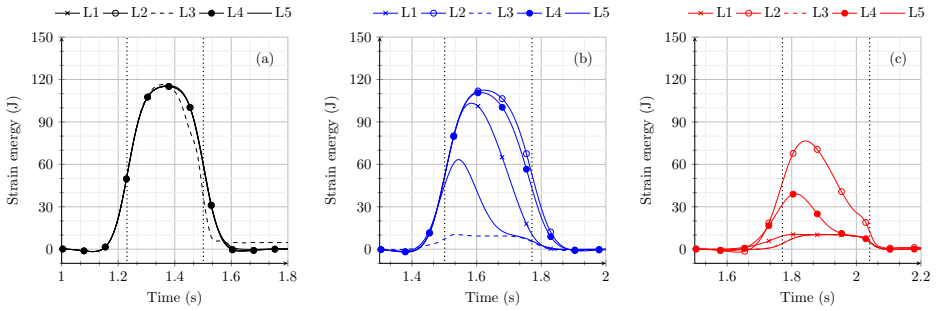

Figure 7.15: Time history of strain energy for different longitudinal profiles under study in the layer of subgrade for (a) AZ-I, (b) AZ-II and (c) AZ-III. The dotted lines mark the time moments at which the load enters and exits each zone.

gradual decrease in the magnitude of strain energy as the load approaches AZ-III (i.e., spatial trend). However, models T3 and T4 show a non-smooth (similar to Figure 7.10d) temporal trend of strain energy in AZ-II, which can be associated with the geometric profiles of these models guiding or reflecting (see Introduction) energy towards the ballast layer (similar to the case shown in [34]). In the end, model-T1 shows the smoothest strain energy distribution also for AZ-III, proving it to be the most efficient geometric profile of SHIELD in guiding the energy flow according to the criterion discussed in Section 7.2.2.

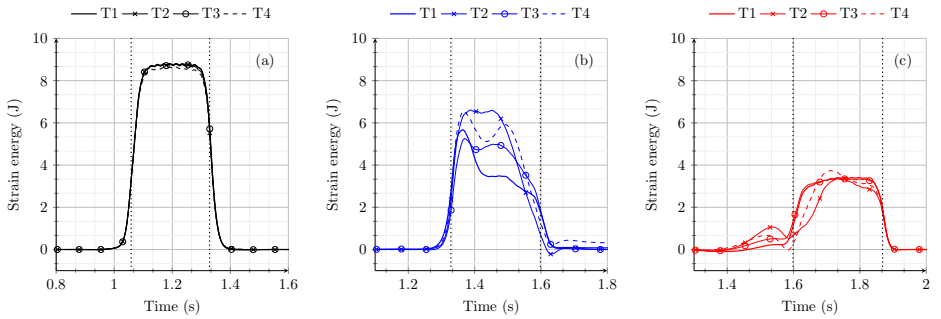

Figure 7.16: Time history of strain energy for different transverse profiles under study in the layer of ballast for (a) AZ-I, (b) AZ-II and (c) AZ-III. The dotted lines mark the time moments at which the load enters and exits each zone.

Embankment: Figure 7.17 shows a comparison of the time history of strain energy in the embankment layer for zones AZ-I (a), AZ-II (b) and AZ-III (c), for models T1-T4. It can be clearly seen that models T1 and T3 show a similar distribution of strain energy in all three zones for the embankment layer. Models T2 and T4 exhibit a higher strain energy magnitude in AZ-II and a less smooth distribution of strain energy in AZ-III compared to models T1 and T3. Nevertheless, none of the models show an amplification of strain energy in any of the zones under study.

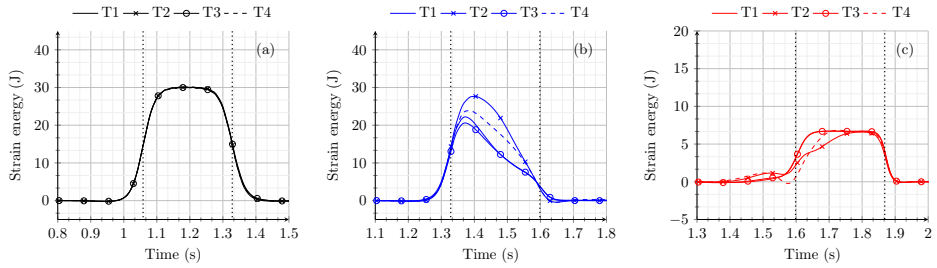

Figure 7.17: Time history of strain energy for different transverse profiles under study in the layer of the embankment for (a) AZ-I, (b) AZ-II and (c) AZ-III. The dotted lines mark the time moments at which the load enters and exits each zone.

Subgrade: Figure 7.18 shows a comparison of the time history of strain energy in the subgrade layer for zones AZ-I, AZ-II and AZ-III, for models T1-T4. In AZ-I (Figure 7.18a) and AZ-II (Figure 7.18b), all models show similar strain energy distributions. In AZ-III (Figure 7.18c), models T1 and T3 show a very similar strain energy distribution and models T2 and T4 show a non-smooth strain energy distribution compared to the other models due to the higher magnitude of strain energy at the time moment when the load enters this zone. In the end, models T1 and T3 demonstrate the most efficient distribution of strain energy in the subgrade layer.

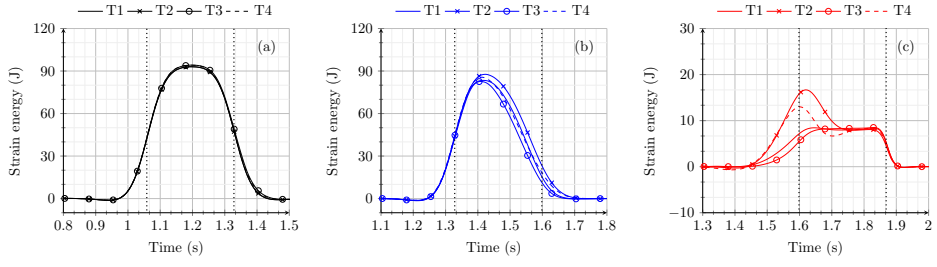

Figure 7.18: Time history of strain energy for different transverse profiles under study in the layer of ballast for (a) AZ-I, (b) AZ-II and (c) AZ-III. The dotted lines mark the time moments at which the load enters and exits each zone.

7.3.4. VERTICAL PROFILES OF SHIELD

The time history of the strain energy is compared for two vertical profiles of the shield (models V1 and V2) for the layers of ballast (Figure 7.19), embankment (Figure 7.20) and subgrade (Figure 7.21). For the layers of embankment and subgrade, both profiles show nearly the same strain energy distribution for each of the zones under study. In the ballast layer, both models have the same energy distribution in AZ-I, model-V2 shows higher magnitudes of strain energy in AZ-II compared to model-V1 but shows a smoother

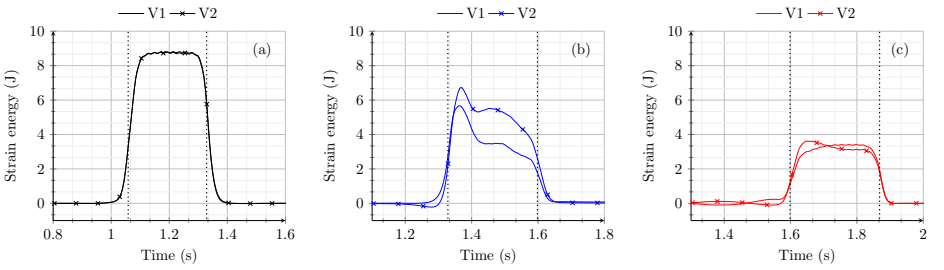

Figure 7.19: Time history of strain energy for different vertical profiles under study in the layer of ballast for (a) AZ-I, (b) AZ-II and (c) AZ-III. The dotted lines mark the time moments at which the load enters and exits each zone.

decreasing temporal trend in AZ-III compared to model-V1. This concludes that the vertical cross-section of the shield at the interface with the concrete bridge can be tuned to achieve a decreasing temporal trend of strain energy in the proximity of the concrete structure (AZ-III). In the end, models V1 and V2 both satisfy the criterion discussed in Section 7.2.2 in terms of both spatial and temporal trends. However, the final choice will depend on other factors such as type of transition, speed of vehicle etc. For the set of parameters chosen in this work, model-V1 outperforms V2 in terms of the smoothness of the temporal trend in AZ-II.

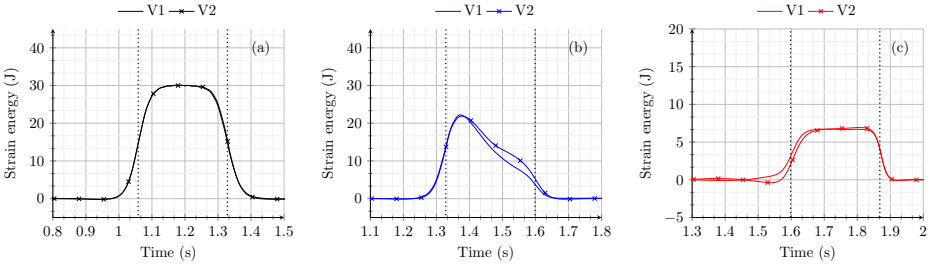

Figure 7.20: Time history of strain energy for different vertical profiles under study in the layer of embankment for (a) AZ-I, (b) AZ-II and (c) AZ-III. The dotted lines mark the time moments at which the load enters and exits each zone.

7.4. SUMMARY OF RESULTS

The results in the preceding section show the influence of geometry in the three principle planes (longitudinal, transverse and vertical) in redistributing energy in railway transition zones. The energy is directly correlated to permanent deformations in the vicinity of the transition interface and the non-uniformity of energy distribution is correlated to non-uniform permanent deformations. In summary, on one hand, this analysis concludes that model-L1 has the most promising longitudinal geometric profile that aids an efficient redistribution of strain energy in all the zones under study and for all the trackbed

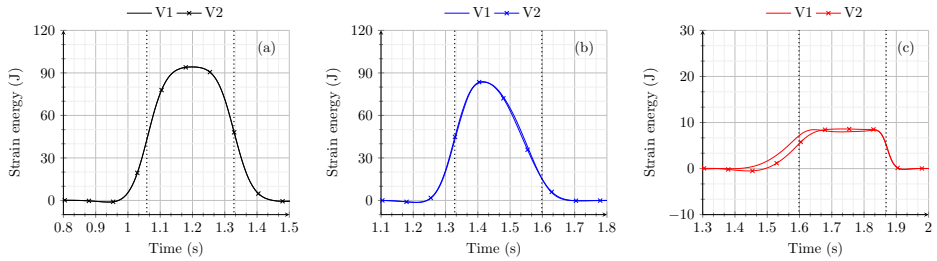

Figure 7.21: Time history of strain energy for different vertical profiles under study in the layer of subgrade for (a) AZ-I, (b) AZ-II and (c) AZ-III. The dotted lines mark the time moments at which the load enters and exits each zone.

layers (ballast, embankment and subgrade) according to the two-point evaluation criteria (spatial and temporal) discussed in Section 7.2.2. Moreover, considering the performance of all the transverse profiles studied in the previous section, model-T1 shows the optimum distribution of the strain energy in each of the trackbed layers (ballast, embankment and subgrade) according to the evaluation criteria. Therefore, the transverse profile of model-T1 is chosen as a starting point for the analysis of the influence of vertical profiles of SHIELD. In the end, when analysing vertical profiles, both models V1 and V2 satisfy the evaluation criteria in terms of both spatial and temporal trends. However, fine-tuning the vertical profiles can lead to a further smoothening of the temporal variation of strain energy curves in the vicinity of the transition interface. The current literature focuses only on longitudinal cross-sectional studies to minimise the degradation in railway transition zones. This work employs a novel energy-based criterion to highlight the need for the geometric optimisation of the transition structure in all geometric planes. Specifically, the role of optimising the transverse geometric profiles in energy redistribution was established through this work.

7.5. CONCLUSIONS

In this work, the effect of geometry on the spatial and temporal distribution of strain energy is studied for a standard embankment-bridge transition with and without a transition structure (SHIELD). The geometry of SHIELD is varied in longitudinal, transversal and vertical planes to investigate its influence on the redistribution of strain energy in the railway transition zones. In general, it is observed that the various zones and the trackbed layers of the railway transition zones react differently to different geometric profiles of SHIELD in terms of strain energy variations.

The ballast, embankment and subgrade layers demonstrate the highest sensitivity to the variation of the longitudinal profile of SHIELD compared to variations on the transverse and vertical profiles. The transverse profiles affect the ballast layer the most and optimising the vertical profile leads to a better distribution of strain energy in the zone next to the transition interface with the concrete structure. In the end, geometries in all directions (longitudinal, transverse and vertical) proved to be influential in one way or

another in redistributing the energy flow in the RTZs. For the parameters (speed, trackbed material properties and type of transition) considered in this work, model-V1 proved to be the most efficient geometrical shape (in all directions) of SHIELD according to the strain energy criterion that associates the strain energy distribution to the operation-driven degradation. Even though the geometric shape of SHIELD suggested in this work might not be optimal for all types of site conditions (as the best-suited profile will depend on the above-mentioned parameters), it definitely highlights the importance of geometry in tuning the spatial and temporal strain energy distributions. This study is a preliminary investigation that aims to guide the designers in optimising the geometric profiles of transition structures for their specific requirements (specific type of transition zones and/or site conditions) aimed at uninterrupted energy flow in RTZs.

In conclusion, the research substantiates that optimizing the geometric profiles of SHIELD in all directions is vital in redistributing strain energy effectively, thereby reducing operation-driven degradation and extending the lifespan of RTZs. This study not only reinforces the shift towards an energy-centric design of RTZs but also has practical implications for design and maintenance. This paper suggests that by fine-tuning geometric profiles, we can significantly improve the performance and durability of the transition structures. The insights developed in this work pave the way for robust, energy-efficient and resilient design solutions using geometry as a tool, establishing the stepping stone for an exploration into the intricate relationship between geometry, strain energy and the performance of railway transition zones subjected to operation-driven settlement. It is to be noted that for an effective implementation, the optimised geometric design will be verified for critical conditions arising due to track irregularities, impact wheel loading, and train-track interactions in future works concerning SHIELD.

8

EVALUATION FOR CRITICAL CONDITIONS: SHIELD

This chapter (with minor changes) has been published as *A. Jain, Andrei V. Metrikine, Michael J.M.M. Steenbergen, and Karel N. van Dalen (2024). Railway transition zones: energy evaluation of a novel transition structure for critical loading conditions. Journal of Vibration Engineering & Technologies.*

ABSTRACT

Railway transition zones (RTZs) are subjected to amplified degradation leading to high maintenance costs and reduced availability of tracks for operation. Over the years, several mitigation measures have been investigated to deal with the amplified degradation of these zones. However, to ensure the robustness of a design solution, it must be evaluated for critical conditions arising due to certain loading and track conditions. In this paper, the critical load conditions arising due to different velocities (sub-critical, critical and super-critical), the direction of the moving load, the combination of inertial effects and track imperfections (non-straight rail and hanging sleepers) and passage of multiple axles (using a comprehensive vehicle model) are investigated for an embankment-bridge transition. The results are then compared against the recently proposed design of a transition structure called SHIELD (Safe Hull Inspired Energy Limiting Design) to evaluate its performance under these critical conditions using various vehicle models and finite element models of the RTZs. It was found that the novel design of the transition structure effectively mitigates dynamic amplifications and results in smooth strain energy distribution across sub-critical, critical, and super-critical velocity regimes in both directions of movement implying that the expected operation-induced degradation will be as uniform as possible in longitudinal direction. Furthermore, even though this transition structure is designed to deal with initial track conditions (perfectly straight track), its superior performance is not confined to tracks in perfect condition; it also efficiently addresses adverse effects from track imperfections such as hanging sleepers and non-straight rail. In the end, this work demonstrates the robustness of the design solution for all the critical conditions under study.

8.1. INTRODUCTION

Railway tracks are subjected to continuous degradation over the operational period leading to high costs of operation and maintenance. In addition to this, some critical zones called railway transition zones (RTZs) experience even higher degradation than normal railway tracks. RTZs are the areas where a ballasted track typically crosses a stiff structure such as a bridge, culvert, road etc. leading to amplified dynamic response and/ or non-uniform response. In the Netherlands, the maintenance requirements at railway transitions are 4-8 times higher than in normal track [1]. A detailed overview of the problems associated with dynamic amplifications in RTZs is presented in [2–5]. The excessive material and geometry degradation in RTZs has been associated with the abrupt change in track stiffness and differential settlement. However, the severity of the degradation and maintenance requirement depends on several factors such as material properties of trackbed layers (ballast, embankment, subgrade), type of transition, load characteristics, track imperfections etc. Recently, the occurrence of operation-induced degradation (permanent vertical deformations) in the proximity of the transition interface was associated with strain energy amplifications [6]. Some of the above-mentioned factors (material of trackbed layers, type of transition) have been investigated in [7, 8] related to the performance of RTZs, using this strain energy-based criterion. Nevertheless, the influence of load characteristics and track imperfections leading to critical loading conditions for RTZs remain unexplored.

The abrupt stiffness variation was first associated with the phenomena of transition

radiation [9] by the authors of [10, 11] and transition radiation of waves in an elastic continuum was first theoretically described by the authors of [12]. In [13], it was shown that the transition radiation energy is small compared to the strain energy in the open tracks for small stiffness variation and small velocity of the load. It was proven that the transition radiation becomes powerful for velocities close to critical velocity [14]. Some dedicated studies have been performed associated with the influence of critical velocity related to the velocity of the load moving over a homogeneous foundation [15], for stratified media (layered soil configuration) [16] and for transition zones [17]. Therefore, it is clearly established that the influence of vehicle velocity [18–20] is a significant factor to be considered while designing a robust mitigation measure to deal with dynamic amplifications due to abrupt stiffness variation in RTZs. In the literature, the performances of a few mitigation measures have been evaluated for varying speeds. In [21, 22], the performance of a ballastless track in an embankment–tunnel transition using the resilient mats has been evaluated, with special attention regarding the critical speed. Other studies include a performance evaluation of RTZs [23] equipped with USP [24], adjustable sleepers [25], transition wedge [26], geogrid and pile configuration [27]. In a recent study [28, 29], a novel transition structure called Safe Hull Inspired Energy Limiting Design (SHIELD) was proposed and evaluated using a comprehensive criterion based on strain energy [6]. However, it was designed and evaluated for a specific vehicle speed and the influence of the vehicle speed relative to the critical speed on the performance of SHIELD is unknown while this may play a vital role in the performance of a robust mitigation measure.

The other major cause of excessive degradation in RTZs is differential settlement [30–33]. It is well known that the differential settlement in RTZs leads to hanging sleepers (void between sleepers and ballast) accelerating the degradation process to a great extent [34, 35] as they result in considerable increase in the dynamic wheel–rail interaction force and induced stress in the track-bed layers. Hanging sleepers can occur in open tracks [36–40] as well as in approach zones [41]. In open tracks, for example, one hanging sleeper can lead to 70% increase in sleeper-ballast contact force and 40% increase in the displacement of the adjacent sleepers [37]. Due to differential settlement, hanging sleepers are even more prominent in RTZs compared to open tracks. Another significant track imperfection arising due to differential settlement is non-straightness of the rail in the proximity of the transition interface. The evaluation of mitigation measures subjected to these track imperfections (hanging sleepers and non-straight rail) is missing in the literature. Moreover, in [42], it was concluded that accounting for the interaction between the wheel and the rail generally leads to stronger transition radiation compared to that induced by a simple moving constant load due to increased contact force. Therefore, when analyzing the influence of track imperfections, accounting for the wheel-rail interaction is important as track imperfections typically lead to an increased contact force.

The performance of the recently proposed transition structure called SHIELD will be evaluated in this work for critical loading conditions associated with critical speed effects and the combination of track imperfections and increased rail-wheel interaction forces. Firstly, a standard embankment-bridge transition with and without SHIELD will be evaluated in terms of strain energy variation for different velocities (speed and direction) of

the moving load. Secondly, the influence of using a moving load as an approximation of the moving mass for the evaluation of RTZs will be studied to highlight the importance of the interaction between rail and wheel for cases with and without track imperfections. Moreover, the performance of SHIELD will be evaluated for the critical load conditions arising due to combination of inertia effects and track imperfections. Lastly, the effectiveness of SHIELD will also be illustrated for a passage of a more comprehensive vehicle model (multiple axle loads) composed of a carbody, two bogies and four wheelsets.

8.2. MODELS

Two models (model 1 and model 2) of an embankment-bridge transition have been studied in this work. Model 1 is an embankment-bridge transition without any transition structure and model 2 is equipped with a transition structure called SHIELD. Both models are 2-dimensional and are identical in terms of geometry, materials, mesh and load conditions, interface conditions and division of zones under study. The validity of model 1 and model 2 used in this work has been already discussed in [6, 7, 28, 34].

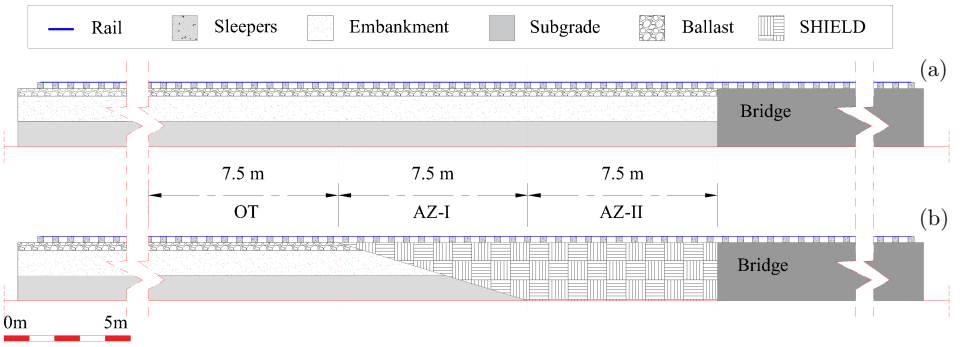

Figure 8.1: Cross-section details of (a) model 1 and (b) model 2 showing the division of zones under study.

8.2.1. GEOMETRY AND ZONES UNDER STUDY

The longitudinal profile cross-section details of model 1 and model 2 can be found in Figure 8.1, showing the main track components for both the models and the division of zones under study. Both models are broadly divided into “soft side” and “stiff side”. The soft side is composed of rail (profile 54E1), rail-pads, sleepers (240 mm x 240 mm), ballast (0.3 m depth), embankment (1 m depth), subgrade (1 m depth) for model 1 with an addition of transition structure called SHIELD for model 2. The stiff side is the same for both model 1 and model 2 and is comprised of rail, rail-pads, sleepers and a concrete structure. The total length of each model is 80 m which consists of 60 m of soft side and 20 m of stiff side. In this study, each of the three zones (see Figure 8.1) of interest are 7.5 m in length. The first zone called OT (open track) is practically free from the transition

effects as it is far from the transition interface between the soft side and the stiff side of the system. The last zone called AZ-II (approach zone-II) is in the vicinity of the transition interface and the zone called AZ-I lies between OT and AZ-II.

8.2.2. MATERIALS

The materials used for all track components in model 1 and model 2 are characterized by the elasticity modulus, Poisson's ratio, densities and Rayleigh damping factors as mentioned in Table 8.1. The material properties used in this paper are in accordance with those in [7] ensuring optimal performance of the RTZ. It was shown in [6] that there is a direct correlation between the strain energy peaks in the model with linear elastic materials and the permanent (operation-induced) deformations in the model with non-linear elasto-plastic material. Therefore, the behaviour of all the materials defined in Table 8.1 is assumed to be linear elastic for this study.

Table 8.1: Mechanical properties of the track components

Material	Elasticity Modulus	Density	Poisson's Ratio	Rayleigh damping	
	E [N/m^2]	ρ [kg/m^3]	ν	α	β
Steel (rail)	21 x 10^{10}	7850	0.3	-	-
Concrete (sleepers)	3.5 x 10^{10}	2400	0.15	-	-
Ballast	1.5 x 10^{8}	1560	0.2	0.0439	0.0091
Sand (embankment)	8 x 10^{7}	1810	0.3	8.52	0.0004
Clay (subgrade)	2.55 x 10^{7}	1730	0.3	8.52	0.0029
SHIELD	3.6 x 10^{8}	1900	0.2	0.0439	0.0091

8.2.3. MESH DETAILS

The sleeper, ballast, embankment, subgrade and the bridge were discretized using linear quadrilateral elements of type CPE4 and the rail using two-node linear beam elements of type B21 for both the models. The SHIELD was discretised using a combination of CPE4 and CPE3 elements. CPE4 and CPE3 are 4-node and 3-node plane strain elements (unit thickness) respectively (see ABAQUS manual for details [43, 44]).

8.2.4. INTERFACE CONDITIONS

Rail-pads are modelled using springs ($k = 1.2 \cdot 10^8$ N/m) and dashpots ($c = 5 \cdot 10^4$ Ns/m) to connect rail and sleepers. The vertical interface between ballast/ embankment/ subgrade and the bridge is defined using a hard contact linear penalty method (normal behaviour) and the Coulomb's friction law (tangential behaviour) using 0.5 as coefficient of friction.

The interface between the rail and wheel is defined by the contact spring of stiffness k_c (see Table 8.2) using the following equation [45]:

$$k_c = \sqrt[3]{\frac{3 \cdot E^2 \cdot Q \sqrt{R_{wheel} \cdot R_{railprof}}}{2 \cdot (1-\nu^2)^2}} \tag{8.1}$$

where E is the elasticity modulus and ν is the Poisson's ratio of the steel (wheel, rail), Q is the vertical wheel load, R_{wheel} is the radius of the wheel, $R_{railprof}$ is the radius of the railhead.

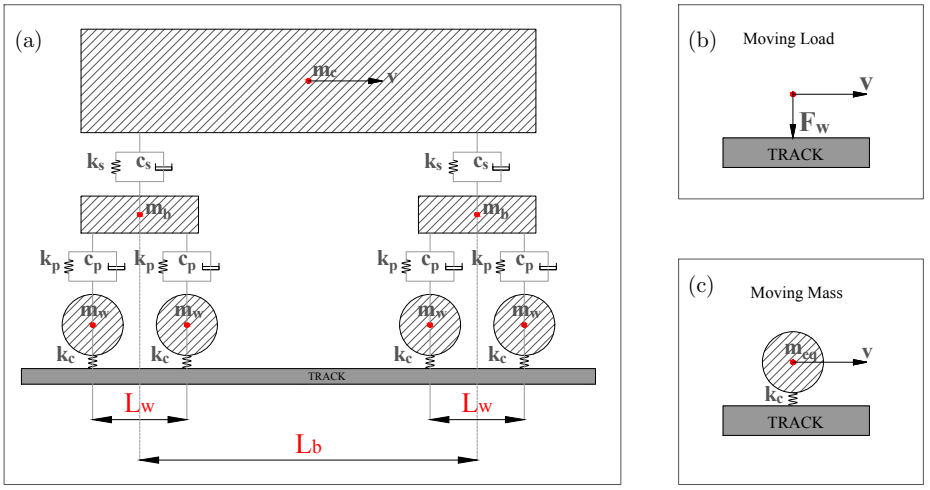

Figure 8.2: Schematic showing different types of vehicle models used in this study (a) vehicle, (b) moving load (ML) (c) moving mass (MM).

8

8.2.5. LOADS

An implicit scheme for dynamic analysis was used in Abaqus to simulate the cases studied in this work. Figure 8.2 shows different types of vehicle models used in this work representing a vehicle (a), moving load (ML) (b) and moving mass (MM) (c) with a velocity v. The vehicle is composed of a carbody of mass m_c connected to two bogies of mass m_b via a secondary suspension system (vertical spring k_s and dashpot c_s). Each bogie is connected to two wheelsets via the primary suspension system (vertical spring k_p and dashpot c_p). The values of vehicle parameters (masses [46], suspension stiffness and damping [47]) are tabulated in Table 8.2. The distance between two wheelsets of each bogie (L_w=2.5 m) and the distance between two bogies (L_b=20 m) have been adopted from [25] for a Dutch passenger train. For the cases with simplistic load condition representing only one wheel, a constant moving load F_w is considered and is compared against an equivalent moving mass m_{eq} as tabulated in Table 8.2.

8.2.6. CASES STUDIED

This section describes the three cases under study as discussed in Section 8.1. Figure 8.3 presents a schematic of the cases under study showing the zone of influence for each case, sleeper numbers on stiff and soft side and the geometric details of the track imperfections investigated in this work. Case 1 (Figure 8.3a) shows a perfectly straight track with no hanging sleepers or track imperfections where x_1 (x=0 m) is marked as the location of the transition interface. Case 2 (Figure 8.3b) shows three hanging sleepers (sleeper numbers 1, 2 and 3). The location x_2 (x=-1.8 m) marks the end of zone consisting of hanging sleepers. Lastly, case 3 (Figure 8.3c) depicts a non-straight geometric profile (possibly due to temperature effects or differential settlement) of the rail adopted from literature [33], where x_3 (x=-4.5 m) marks the end of the zone consisting of non-straight rail. The vertical dip D is assumed to be 10 cm based on one of the profiles studied in [33]. All the results presented in this work are in terms of total strain energies. In Abaqus [43], "ALLSE" provides a time history of the total strain energy within a considered volume (each zone for each trackbed layer).

Masses	m_c=28000 kg, m_b=1300 kg, m_w=900 kg
Equivalent mass	$m_{eq} = F_w/g$, g=9.81 ms^{-1}
Moving load	F_w =90 KN
Primary suspension	k_p=1.2 MNm^{-1} , c_p=4.0 KNsm^{-1}
Secondary suspension	k_s=0.43 MNm^{-1} , c_s=20 KNsm^{-1}
Contact stiffness	k_c=1200 MNm^{-1}

Table 8.2: Load characteristics shown in Figure 8.2

8.3. RESULTS AND DISCUSSION

This paper evaluates the performance of SHIELD systematically for critical loading conditions associated with critical speed effects and associated with the combination of track imperfections and increased rail-wheel interaction forces. Firstly, the influence of speeds and direction of the moving load is investigated for model 1 and model 2. Then the response of model 1 (in ballast layer) is investigated for the cases described in Section 8.2.6 when subjected to a constant moving load (ML) and the MM. It is found that the cases involving track imperfections are significantly influenced by the moving load approximation. Therefore, the response of model 1 and model 2 when subjected to the MM and track imperfections (cases described in Section 8.2.6) is studied for each of the trackbed layers (ballast, embankment and subgrade). Lastly, the influence of multiple axles on model 1 and model 2 is studied. The analyses in this section have been categorised in the points described below.

- Influence of velocity (speed and direction of moving load): An embankment-bridge transition is evaluated for speeds varying from 20 m/s to 150 m/s in both directions (soft-to-stiff and stiff-to-soft) without (model 1) and with SHIELD (model 2). The

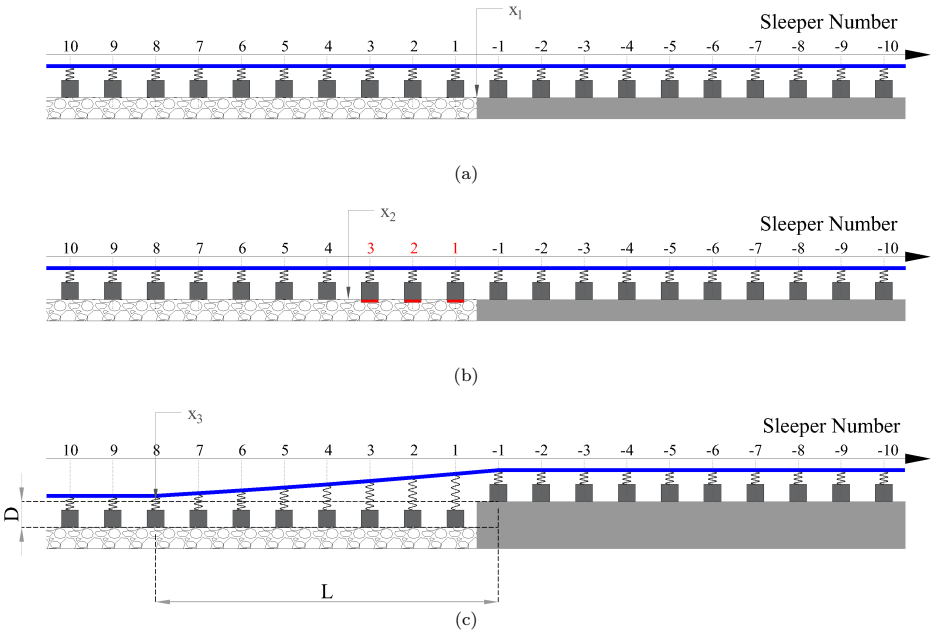

Figure 8.3: Schematic of the cases under study (a) case 1, (b) case 2 and (c) case 3.

evaluation is done in terms of maximum strain energy in each of the zones under study for the speeds in the range mentioned above. In addition to this, the magnification factor (MF) is studied for model 1 and model 2 for different speeds and zones under study. The magnification factor is defined as the ratio of maximum strain energy (SE) in the approach zones and the open track. In Section 8.3.1, the responses of model 1 and model 2 are studied (for case 1) for different speeds and directions of movement.

- Moving mass versus moving load: In Section 8.3.2, the response of model 1 to a moving load (F_w) and an equivalent moving mass (m_{eq}) is evaluated for cases 1, 2 and 3 in terms of strain energy distribution in the ballast layer.

- Influence of track imperfections: In Section 8.3.3, the conditions of cases 1, 2 and 3 (Section 8.2.6) are studied for model 1 and model 2 subjected to equivalent MM, in terms of strain energy distribution in the trackbed layers (ballast, embankment and subgrade).

- Influence of vehicle: In Section 8.3.4, the response of model 1 and model 2 subjected to a moving vehicle composed of a carbody, bogies and wheelsets (as shown in Table 8.2 and Figure 8.2) is studied for case 1 in terms of total strain energy distribution in the zones shown in Figure 8.1 for ballast, embankment and subgrade.

8.3.1. INFLUENCE OF VELOCITY (SPEED AND DIRECTION OF MOVING LOAD)

Soft to stiff: Figure 8.4 shows the maximum strain energy in open track (OT) and approach zones (AZ-I and AZ-II) for model 1 (Figure 8.4a) and model 2 (Figure 8.4b). The open track behaviour for both the models shows the same behaviour as expected with an increase in the peak value of strain energy with increasing speeds up to 110 m/s and starts a decrease after this critical value. Therefore, the system's (in open track) critical velocity (v_{cr}) can be identified based on maximum strain energy as 110 m/s.

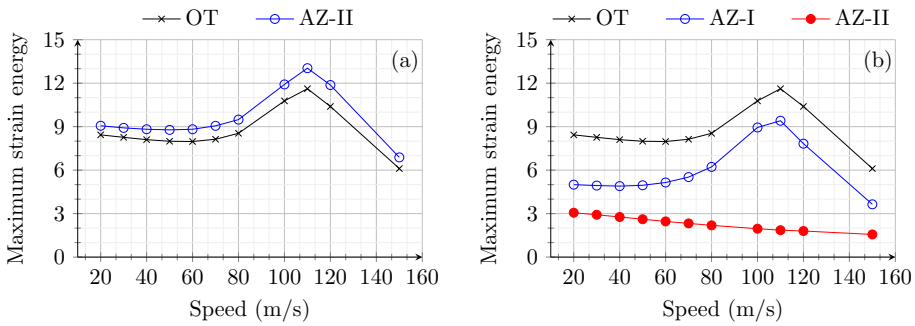

Figure 8.4: Maximum strain energy (Joules) in open track and approach zones for an embankment-bridge transition (a) without (model 1) and (b) with SHIELD (model 2) for different speeds of the load moving from soft to stiff side of RTZ.

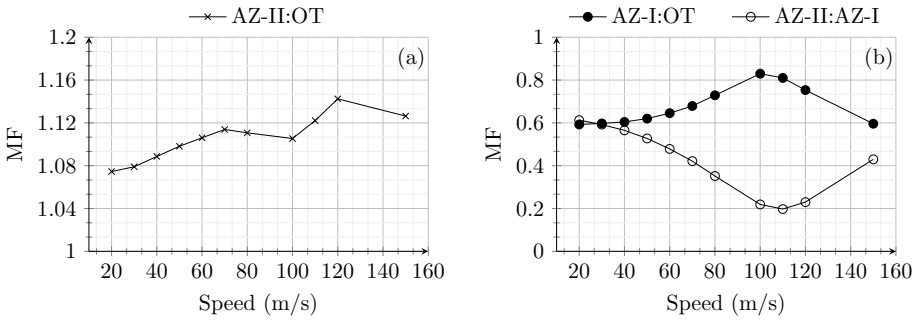

Figure 8.5: Magnification factor (MF) for an embankment-bridge transition (a) without (model 1) and (b) with SHIELD (model 2) for different speeds of the load moving from soft to stiff side of RTZ.

On one hand, for model 1, the strain energy distribution in AZ-I (not shown) is the same as in OT as there is no influence of transition effects in these zones. Only AZ-II shows a higher peak value of strain energy compared to the OT due to dynamic amplifications in the proximity of the transition interface. On the other hand, for model 2, the presence of SHIELD lowers the peak strain energy magnitude considerably for both AZ-I and AZ-II.

Moreover, AZ-II is much stiffer (more than 2 times) compared to OT and AZ-I as the material used for SHIELD is predominantly present in AZ-II. The wave speed in the SHIELD material is much higher than the velocities under consideration. Therefore, the strain energy magnitudes remain uninfluenced (no strain energy peaks for any speeds under study) by speed effects in AZ-II for model 2. Similarly, the magnification factor (MF) is compared for both models in Figure 8.5. The MF for model 1 is always greater than one implying dynamic amplification in the absence of SHIELD for all speeds (Figure 8.5 a). Conversely, the MF for model 2 is always lower than one 1 for all the speeds demonstrating the effectiveness of SHIELD in mitigating dynamic amplifications in railway transition zones. It is interesting to observe in Figure 8.5 that the MF for model 1 increases with increasing velocity upto 70 m/s then decreases until 100 m/s and then increases again. This is due to the fact that for velocities in the range 70-100 m/s, the increase in open track response is higher than the increase in approach zone response. In any case, Figure 8.4 and Figure 8.5 demonstrate the effectiveness of SHIELD for all speeds (in the range of 20-150 m/s) of the load moving from the soft to the stiff side of RTZs.

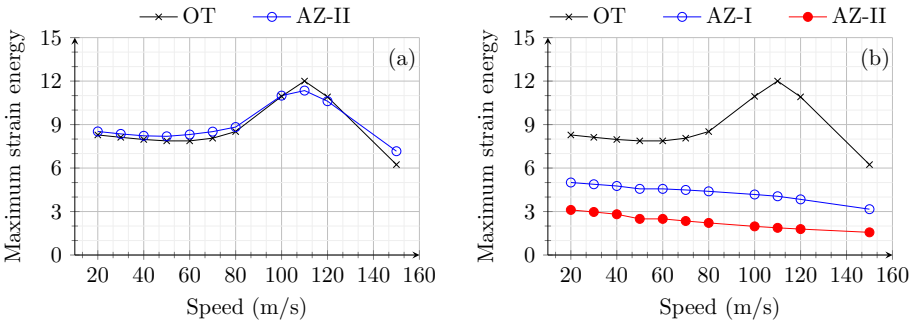

Figure 8.6: Maximum strain energy (Joules) in open track and approach zones for (a) model 1 and (b)model 2 for different speeds of the load moving from stiff to soft side of RTZ.

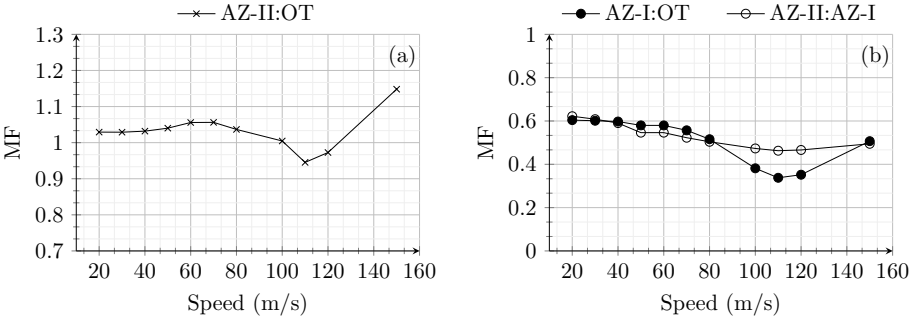

Figure 8.7: Magnification factor (MF) for (a) model 1 and (b)model 2 for different speeds of the load moving from stiff to soft side of RTZ.

Stiff to soft: Figure 8.6 shows the maximum strain energy in OT, AZ-I and AZ-II for a load moving from the stiff to the soft side of the system for speeds in the range 20-150 m/s. Unlike the response for soft-to-stiff direction, the response of model 1 in OT is similar (in magnitude) to that in AZ-II for all speeds. The critical speed is 110 m/s. Conversely, for model 2 (Figure 8.6b), no peaks are observed at all in AZ-I and AZ-II for increasing speeds. In summary, the influence of speed on the strain energy is negligible (no peaks observed) when the model 2 is subjected to a load moving from stiff to soft direction.

Figure 8.7 shows the magnification factor for model 1 (a) and model 2 (b) subjected to the load moving from the stiff to the soft side with speeds in range 20-150 m/s. Unlike the response of models to load moving from soft to stiff direction, the MF goes below one for speeds around 110 m/s (critical speed) for model 1. A similar dip in MF is observed for model 2 around the critical speed, at the same time also maintaining the MF always below 0.6. This shows that SHIELD is effective in mitigating dynamic amplifications for the loads moving with all speeds (in the range 20-150 m/s), also from stiff to soft side of the system.

In summary, even though the dynamic responses of the models are sensitive to the direction as well as the speed of the moving load, the presence of SHIELD is effective in mitigating dynamic amplifications in all scenarios.

8.3.2. MOVING MASS VERSUS MOVING LOAD

Figure 8.8 shows a comparison of the time history of total strain energy in OT, AZ-I and AZ-II for model 1 when subjected to a ML F_w and a MM m_{eq} for the three cases discussed in Section 8.2.6. For all three cases, the response of model 1 to the MM and the ML is practically the same in OT and AZ-I. It can be verified that the cases with the moving load have a smoother curve of strain energy in all the zones when compared to MM response. This is due to the presence of sleepers felt by the MM at every 0.6 m.

For case 1 (Figure 8.8 a), model 1 shows a small increase in peak strain energy when subjected to the MM compared to the ML in AZ-II. For case 2 (Figure 8.8 b), a significant difference in the response of model 1 is observed in the AZ-II when subjected to the MM and the ML. The strain energy peak in AZ-II for the ML is much higher than for the MM but the scenario with the MM leads to two strain energy peaks in AZ-II at time moments t_1 and t_2 (corresponding to locations x_1 and x_2 marked in Figure 8.3). In summary, for case 2, the ML approximation leads to an overestimation of strain energy amplifications in the proximity of the transition interface and does not provide accurate information in terms of the locations at which strain energy peaks. For case 3 (Figure 8.8 c), model 1 shows no influence of rail irregularity when subjected to the ML. This is due to the fact that when the system is subjected to the ML, the non-straight profile of rail does not lead to any change in the exerted force. However, a significant increase in strain energy in AZ-II is observed compared to OT in the time interval t_1 to t_3 that correspond to load positions at the onset and at the end of the zone with length L marked in Figure 8.3, respectively, when model 1 is subjected to the MM. The peak strain energy is observed at

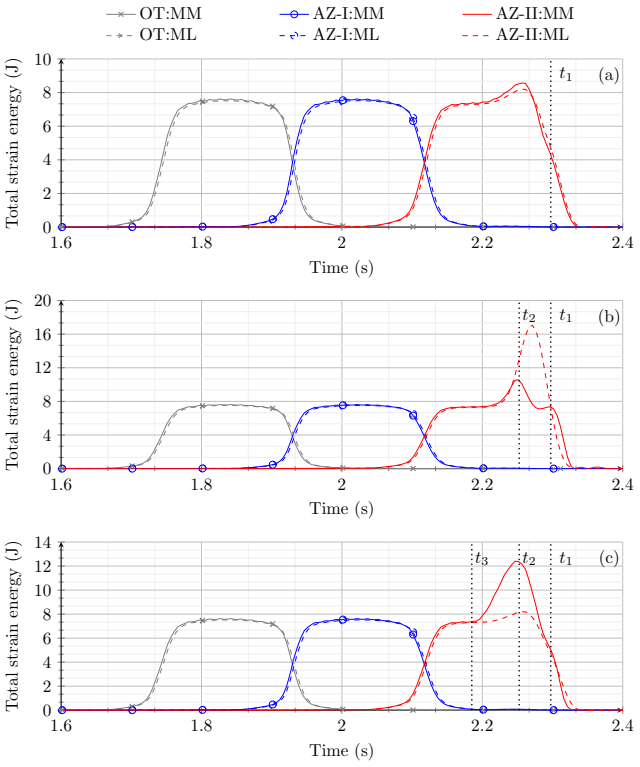

Figure 8.8: Comparison of total strain energy in the ballast layer for model 1 subjected to a MM and a MM for (a) case 1, (b) case 2 and (c) case 3.

8

time moment t_2. This implies that the ML response fails to capture the influence of the rail irregularity in case 3.

In the end, it can be concluded that ML is a good approximation of a MM if a perfectly straight track with no loss of contact condition needs to be studied. However, in cases with track imperfections like non-straight rail or hanging sleepers, the ML assumption might lead to incorrect prediction of the dynamic response of RTZs.

8.3.3. INFLUENCE OF TRACK IMPERFECTIONS ON SHIELD'S PERFORMANCE

From the results obtained in the previous section for model 1, a significant difference in the response is observed for the responses excited by the ML and the MM for cases 2 and 3. Therefore, model 1 and model 2 are subjected to MM and the time history of the total strain energy in each of the zones under study is compared for the two models in the layers of ballast (Figure 8.9 a,d), embankment (Figure 8.9 b,e) and subgrade (Figure

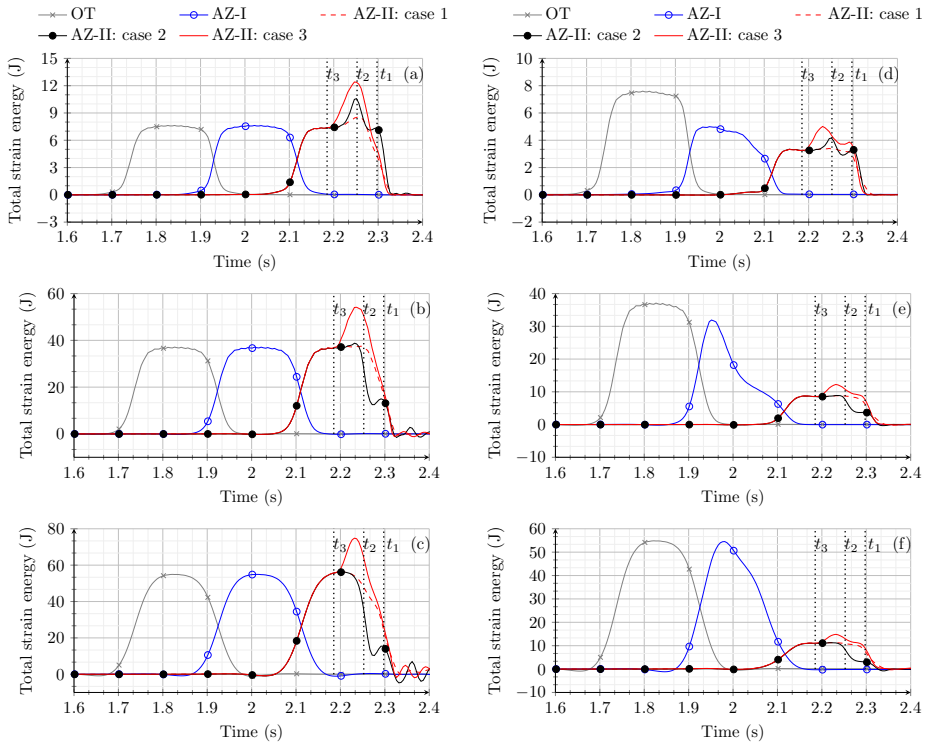

Figure 8.9: Time history of total strain energy for cases 1, 2 and 3 in the layers of (a) ballast (model 1), (b) embankment (model 1), (c) subgrade (model 1), (d) ballast (model 2), (e) embankment (model 2) and (f) subgrade (model 2).

8.9 c,f).

In the ballast layer, model 1 (Figure 8.9 a) shows a significant increase in strain energy in AZ-II compared to OT for case 2 (peaks at t_1 and t_2) and case 3 (peak at t_2) as also shown in Figure 8.8. Even though model 2 (Figure 8.9 d) shows small peaks for case 2 (peaks at t_1 and t_2) and case 3 (peak at t_1 and in interval t_2 to t_3) in AZ-II, the magnitude of strain energy in any of the zones (AZ-I, AZ-II) never exceeds the strain energy magnitude observed in OT. It is interesting to observe that for case 3, the presence of SHIELD not only lowers the strain energy magnitudes in AZ-II but also spreads it over a larger time interval (two small peaks in time interval t_1 to t_3) compared to model 1 (one extreme peak at t_2). The results shown in Figure 8.9 clearly demonstrate the efficiency of SHIELD in mitigating dynamic amplifications in the ballast layer of RTZ even in case of track imperfections (non-straight rail or hanging sleepers).

Similar to the ballast layer, for model 1, the embankment (Figure 8.9 b) and the subgrade (Figure 8.9 c) layers are subjected to a significant increase in strain energy magnitudes in

AZ-II compared to OT for cases 2 and 3 in the time interval t_1 to t_3. However, for model 2, no strain energy peaks are observed for case 2 in AZ-II and a very diminished peak is seen for case 3. In the end, this proves SHIELD to be a promising solution even in the embankment (Figure 8.9 e) and subgrade (Figure 8.9 f) layers.

It is to be noted that the preliminary design of SHIELD was proposed to mitigate the dynamic amplifications associated with the initial track conditions (perfectly straight track). However, SHIELD shows the capability to deal with dynamic amplification and maintain the strain energy magnitudes in approach zones much lower than in the open track also for non-straight rail and hanging sleepers, and within each layer under study.

8.3.4. INFLUENCE OF VEHICLE

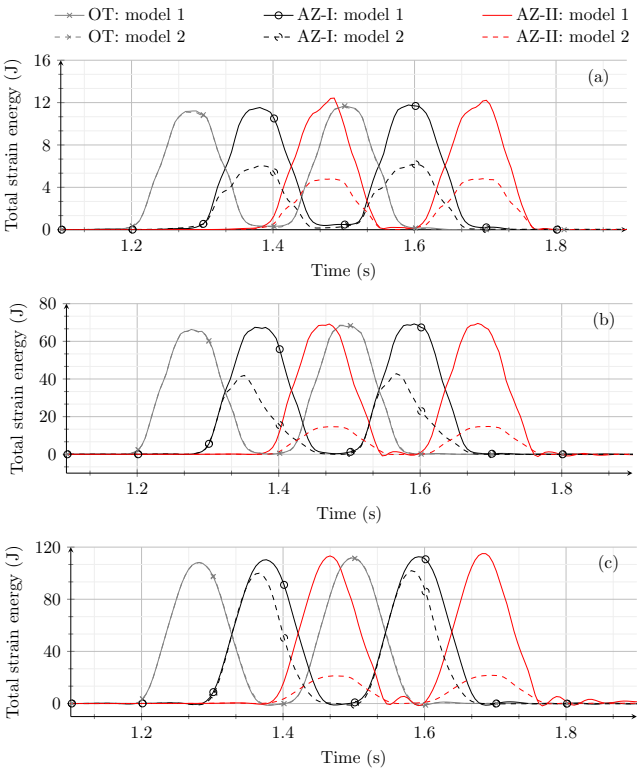

Figure 8.10: Time history of total strain energy obtained from model 1 and model 2 in the (a) ballast, (b) embankment and (c) subgrade layer

The influence of multiple axles of a vehicle consisting of a car-body, two bogies and 4 pairs of wheels is studied in the absence (model 1) and presence of SHIELD (model 2). This analysis is performed to verify if, for the straight track (for which SHIELD is designed),

any critical condition arises due to the presence of multiple axles (at the distances as shown in Figure 8.2) and if SHIELD still shows an optimal behaviour. Figure 8.10 shows the comparison of time histories of total strain energy in OT, AZ-I and AZ-II for model 1 and model 2 for initial track conditions (case 1). In the ballast layer (Figure 8.10 a), model 1 shows an amplification of strain energy in AZ-II compared to OT and AZ-I. In addition to this, the response of the front bogie is slightly amplified compared to the back bogie implying that the responses are not fully decoupled. Conversely, model 2 shows a gradual decrease in strain energy magnitude when the vehicle moves from OT to AZ-II. Moreover, unlike the response of model 1, model 2 shows a decoupled behaviour of the two bogies resulting in an identical distribution of strain energy for each bogie.

In the embankment (Figure 8.10 b) and subgrade (Figure 8.10 c) layer, both models show no amplification in approach zones compared to open track. However, model 2 shows a gradual decrease in strain energy magnitudes as the vehicle moves from the open track to the concrete structure. This gradual decrease in strain energy (in model 2) will imply a gradual decrease in permanent vertical deformations from the open track to the concrete structure. This is different from the response of model 1, where the strain energy drops abruptly from the open track to the concrete structure implying a large difference in permanent deformations on both sides of the transition interface.

Even though the coupling of responses for model 1 is not significant, combinations of certain speeds and track conditions might lead to more severe coupling. The responses are decoupled for the RTZ equipped with SHIELD for the initial track conditions (perfectly straight track), but this behaviour is not guaranteed for track imperfections and higher velocities. In any case, good track conditions must be maintained for an effective implementation of any design solution.

8.4. CONCLUSIONS

The efficiency of the safe hull-inspired energy limiting design (SHIELD) of transition structure for mitigating the operation-induced dynamic amplifications and/or non-uniform response in railway transition zones (RTZs) is demonstrated for critical load conditions. It was found that SHIELD was successful in mitigating the dynamic amplifications in sub-critical, critical and super-critical regimes of velocities in both the directions of movement. Moreover, the superior performance of SHIELD is not only limited to a track that is in a perfect condition but it also is efficient in mitigating the adverse effects of the track imperfections like hanging sleepers and non-straightness of the rail (e.g., due to differential settlements). Lastly, the response of model 1 (without SHIELD) and model 2 (with SHIELD) to a moving vehicle (two bogies and 4 wheelsets) was investigated. It was found, for ideal initial track conditions (perfectly straight track), SHIELD not only mitigates the dynamic amplifications in RTZs but also decouples the responses of the two bogies such that the load of the bogies act independently of each other, which is not the case in absence of SHIELD. In the end, this work shows the applicability of SHIELD as a robust mitigation measure to deal with dynamic amplifications in RTZs, even for critical loading conditions.

9

EVALUATION: ANOTHER TRANSITION TYPE

This chapter (with minor changes) has been published as *A. Jain, Andrei V. Metrikine, Michael J.M.M. Steenbergen, and Karel N. van Dalen. Evaluation of a novel mitigation measure for two different types of railway transition zones. In The Sixth International Conference on Railway Technology: Research, Development and Maintenance, Civil-Comp Conferences, United Kingdom, 2024.*

ABSTRACT

Railway transition zones are the most critical part of the railway infrastructures that experience 4-8 times more degradation compared to open tracks. Despite several attempts to reduce the maintenance and operation costs in these critical zones, a robust and comprehensive solution remains unknown. In recent studies, a robust safe hull-inspired energy limiting design (SHIELD) of a transition structure was proposed for an embankment-bridge transition (without ballast layer over the bridge) to deal with operation-induced degradation. However, this solution was investigated in detail for only this particular type of transition. In this work, the scope of this mitigation measure is extended for an embankment-bridge transition with ballast running over the bridge and its performance is evaluated using a strain-energy criterion. It was concluded that the SHIELD can effectively mitigate the operation-induced dynamic amplification for more than one type of railway transition zone.

9.1. INTRODUCTION

Railway transition zones (RTZs), where rail tracks undergo abrupt changes in foundation types, represent critical challenges in railway infrastructure due to their higher degradation rates compared to open tracks. A detailed overview of the problems and solutions associated to amplified degradation in RTZs is presented in [1, 2]. There are various types of RTZ such as an embankment-bridge transition, a culvert transition, level crossing etc. According to various studies, an embankment-bridge transition undergoes the most amount of degradation among all. Moreover, there can be two types of embankment-bridge transition, with and without the ballast layer over the bridge. The distribution of materials in these two types of railway transitions is different. This study utilises the insights from multiple research efforts [3–7] that have been made to propose robust design solutions for an embankment-bridge transition without a ballast layer over the bridge. In [3], a strain energy-based design criterion was proposed, asserting that minimizing and uniformly distributing total strain energy across the longitudinal track direction and in each trackbed layer can significantly mitigate uneven track geometry and reduce operation-induced degradation. In this work, an embankment-bridge transition with a ballast layer running over the bridge is evaluated without and with a transition structure called "safe hull-inspired energy limiting design (SHIELD)" using the above mentioned energy-based criterion proposed in [3]. Even though the mitigation measure used in this work was developed for a different type of transition [4, 6], the results demonstrate a wider application of SHIELD for other transition types as well. A comparison with the previous works associated to the embankment-bridge transition with the ballast layer discontinued over bridge is also presented.

9.2. MODELS

In this work, two three-dimensional (3-D) models are used to represent an embankment-bridge transition without (Figure 9.1a) and with SHIELD (Figure 9.1b). It is to be noted that the 3-D models used in this chapter are the same as the ones used in Chapter 7 with a minor modification of the ballast layer that continues over the concrete bridge (see Figure 9.1 for cross-section details). Both the models are divided into 5 zones. The zones

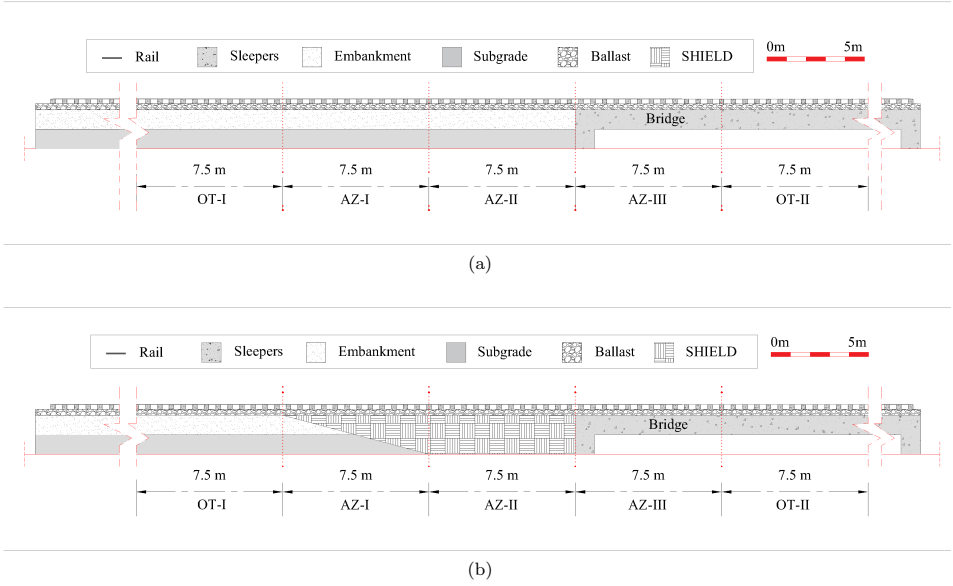

Figure 9.1: Cross-section details of a standard embankment-bridge transition (a) without and (b) with SHIELD.

are mainly categorised as open track (OT-I, OT-II) or approach zones (AZ-I, AZ-II, AZ-III). The open track is unaffected by transition effects and approach zones are in the vicinity of the transition interface showing dynamic amplifications due to transition effects. The soft-side (consists of ballast, embankment and subgrade) of the RTZ under study includes OT-I, AZ-I and AZ-II and the stiff-side (ballast layer running over the bridge) of the RTZ comprises AZ-III and OT-II. The cross-section details of both models are shown in Figure 9.1. The material properties of the track components (rail, sleepers, ballast, embankment, subgrade, SHIELD and bridge) are tabulated in Table 9.1. The models used in this work have been validated in [7]. The material properties used in this work are according to design limits proposed in [6]. A detailed description of the numerical models and the loading conditions can be found in [7].

9.2.1. STANDARD EMBANKMENT-BRIDGE TRANSITION WITHOUT ANY TRANSITION STRUCTURE

A standard embankment-bridge transition without a ballast layer running over the bridge was studied in detail in [3–7] and it was found that there are significant strain energy amplifications in the proximity of the transition interface in the track-bed layers (ballast, embankment and subgrade) on the soft side of the system. The strain energy magnitudes on the stiff side were an order of magnitude lower (negligible) compared to the soft side. However, this is expected to be different in the case of a standard embankment-bridge

Table 9.1: Mechanical properties of the track components.

Material	Elasticity Modulus E [N/m^2]	Density ρ [kg/m^3]	Poisson's Ratio ν	Rayleigh damping α	β
Steel (rail)	21 x 10^{10}	7850	0.3	-	-
Concrete (sleepers)	3.5 x 10^{10}	2400	0.15	-	-
Ballast	1.5 x 10^8	1560	0.2	0.0439	0.0091
Sand (embankment)	8 x 10^7	1810	0.3	8.52	0.0004
Clay (subgrade)	2.55 x 10^7	1730	0.3	8.52	0.0029
SHIELD	5.5 x 10^8	1900	0.15	0.0439	0.0091

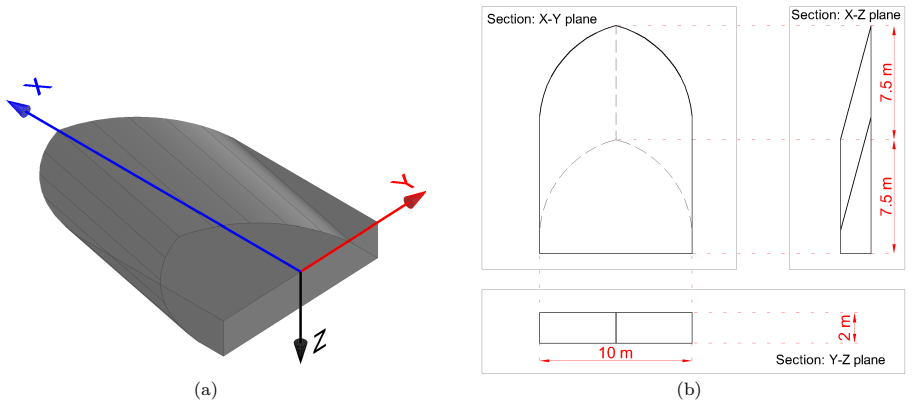

Figure 9.2: Geometric details of SHIELD (a) 3-D view and (b) cross-sections.

transition with the ballast layer continuing over the bridge.

9

9.2.2. SAFE HULL INSPIRED ENERGY LIMITING DESIGN: SHIELD

SHIELD was first proposed and evaluated using the strain-energy criterion in [4] using a 2-D plane strain model, and it was compared with the traditional transition structures like approach slabs and transition wedges. It was shown that SHIELD outperforms all other traditional transition structures in not only mitigating the dynamic amplifications in RTZs but also in obtaining a rather uniform strain-energy distribution. In [7], a detailed evaluation of different geometric profiles of SHIELD was performed to suggest an optimal geometry that aims at an optimal energy redistribution in RTZ according to the energy-criterion. However, all these studies were performed for an embankment-bridge transition where the ballast layer does not continue over the bridge. Therefore, in this paper the same geometric profile as proposed in [7] is used to mitigate dynamic amplifi-

cation for the case where the ballast layer continues over the bridge. Figure 9.2 shows the 3-D view and cross-section details of the SHIELD used in this work.

9.3. RESULTS

In this section, the time history of strain energy has been studied for an embankment-bridge transition without and with SHIELD for the layers of ballast, embankment and subgrade. In the ballast layer, 5 zones are studied as discussed in the above-mentioned sections. For the embankment and subgrade layers, only 3 zones on the soft-side are studied as the strain energy magnitudes are null on the stiff-side of the system.

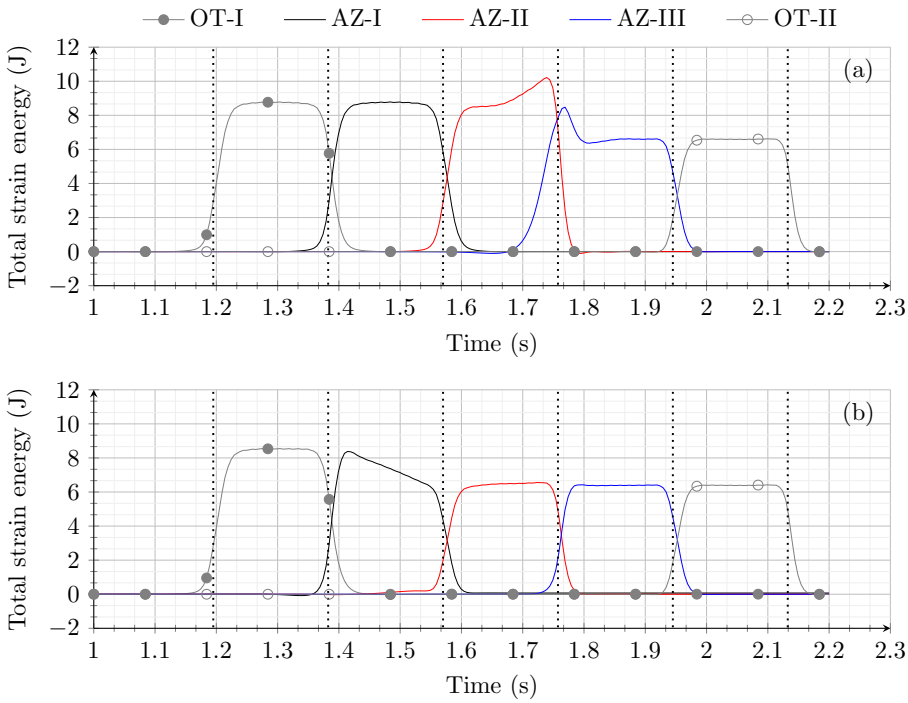

Figure 9.3: Time history of the total strain energy in the ballast layer for a standard embankment-bridge transition (a) without and (b) with SHIELD.

9.3.1. BALLAST

Figure 9.3a shows the time history of total strain energy in the 5 zones under study for the model without SHIELD. It can be clearly seen that there is a significant amplification of

strain energy in AZ-II on the soft-side and in AZ-III on the stiff-side of the transition structure compared to the open tracks on each side. In Figure 9.3b, the presence of SHIELD not only mitigates the local amplifications in the vicinity of the transition interface but also provides a gradual decrease in strain energy magnitudes from open track on the soft-side (OT-I) to the open track on the stiff-side (OT-II).

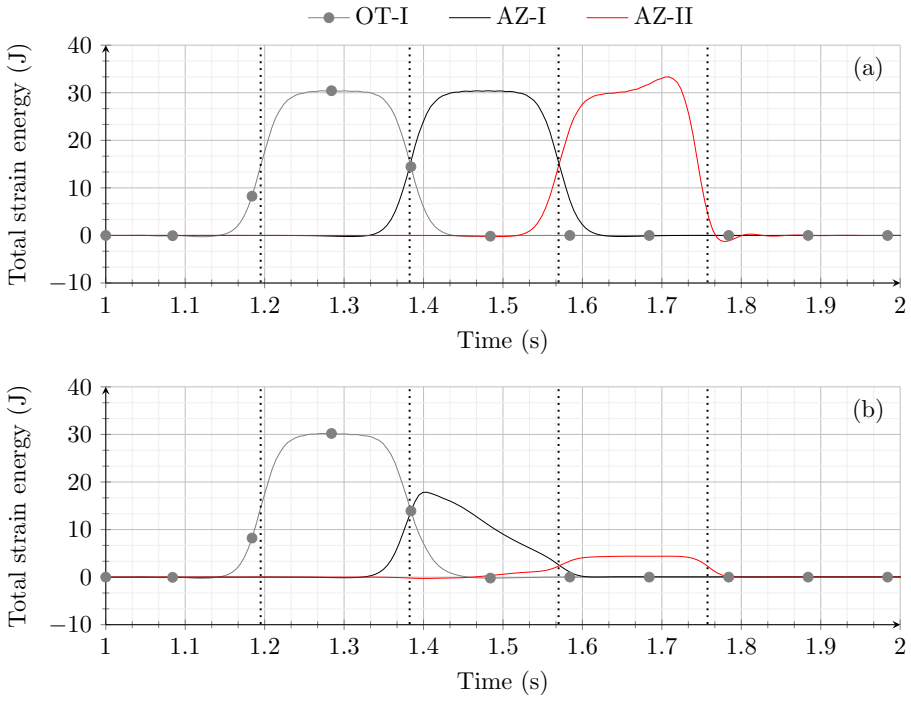

Figure 9.4: Time history of the total strain energy in the embankment layer for a standard embankment-bridge transition (a) without and (b) with SHIELD.

9.3.2. EMBANKMENT

Figure 9.4 shows the time history of strain energy in the embankment layer for a standard embankment-bridge transition without (Figure 9.4a) and with (Figure 9.4b) SHIELD. Figure 9.4a shows an amplification of strain energy in AZ-II compared to OT-I. Similar to ballast layer, also in the embankment layer the amplification of strain energy is mitigated (Figure 9.4b) by the presence of SHIELD showing a gradual decrease in the magnitude of strain energy from OT-I to AZ-I to AZ-II and finally to null on the concrete bridge implying a more uniform geometric profile (due to uniform degradation).

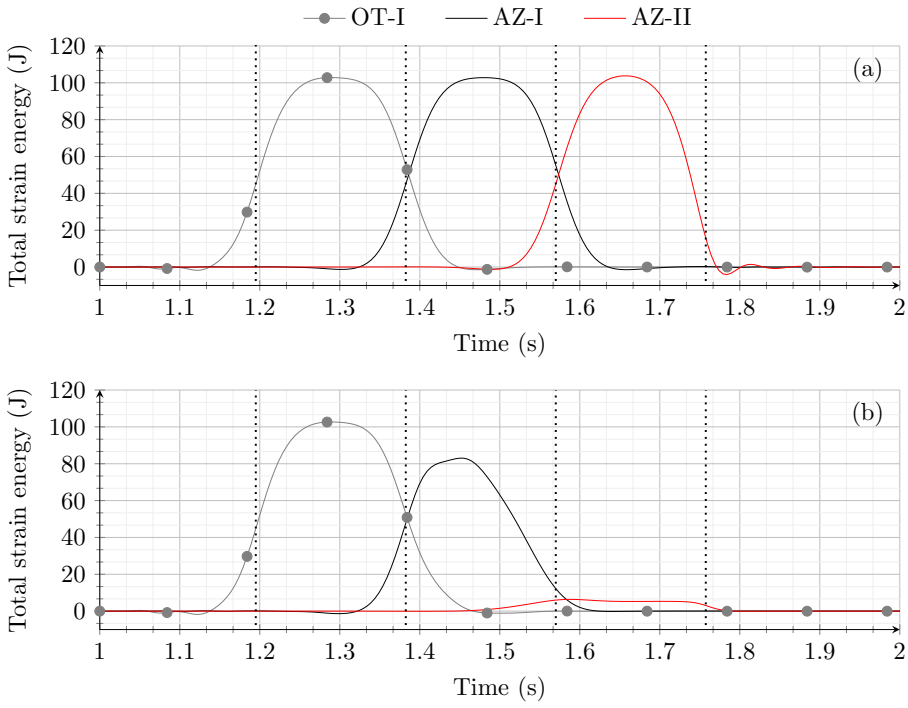

Figure 9.5: Time history of the total strain energy in the subgrade layer for a standard embankment-bridge transition (a) without and (b) with SHIELD.

9.3.3. SUBGRADE

Figure 9.5 shows the time history of strain energy in the subgrade layer for a standard embankment-bridge transition without (Figure 9.5a) and with (Figure 9.5b) SHIELD. Even though the model without SHIELD (Figure 9.5a) shows no amplification of strain energy in any of the zones under study, the presence of SHIELD provides a gradual decrease in strain energy (Figure 9.5b) from the soft-side (highest in the OT-I) of the system to the stiff-side (null).

9

9.4. DISCUSSION

In [7], the spatial and temporal distribution of strain energy is investigated in detail using various three-dimensional models of an embankment bridge transition (ballast layer discontinued over the bridge) without and with SHIELD. Figure 9.6 shows the time history of the strain energy in the (a) ballast, (b) embankment and (c) subgrade for that embankment-bridge transition. Unlike the results shown in previous sections, the strain energy magnitudes on the bridge are null. The only zone (AZ-II) that shows an amplifi-

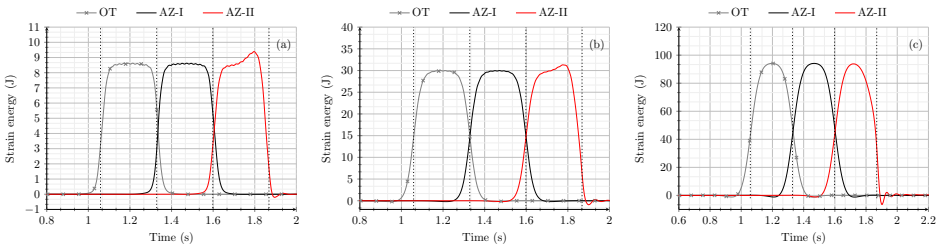

Figure 9.6: Time history of the total strain energy in the (a) ballast, (b) embankment and (c) subgrade layer for a standard embankment-bridge transition with ballast layer discontinued over the bridge.

cation of strain energy is on the soft side of the system. This amplification is mitigated using SHIELD as shown in the time history (see Figure 9.7) of the strain energy in the (a) ballast, (b) embankment and (c) subgrade for the embankment bridge transition without any ballast layer over the bridge. In comparison to the influence of SHIELD discussed in previous sections, only the ballast layer behaves differently. The embankment and the subgrade layers show almost the same behaviour when these two types of transitions are subjected to operation-induced dynamic loads. Additionally, it is observed that the strain energy distribution in the ballast layer is less uniform in the case of discontinued ballast layer (Figure 9.6a) than in the case of the continuous ballast layer (Figure 9.3b). This suggests that the operation-induced degradation will be even more uniform in the latter case.

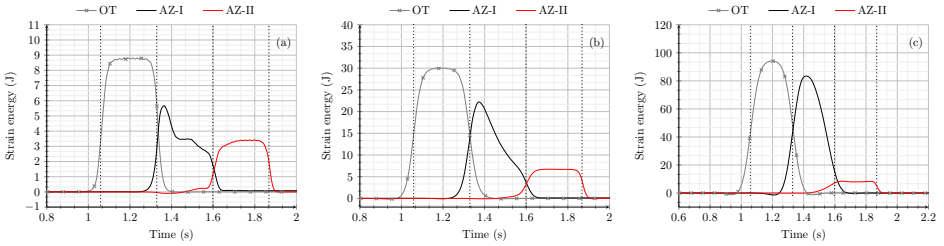

Figure 9.7: Time history of the total strain energy in the (a) ballast, (b) embankment and (c) subgrade layer for a standard embankment-bridge transition (equipped with SHIELD) without ballast layer over the bridge.

It is worth mentioning that efforts could be made to further optimise the strain energy distribution (shown in Figure 9.3(b)) by means of under ballast pads. A thin layer of relatively soft material can be used under the ballast layer aimed at an even more (compared to Figure 9.3) uniform distribution of strain energy (within ballast layer) in the zones under study; this way, the expected operation-induced degradation can be made even more uniform across the transition.

9.5. CONCLUSIONS

This work presents a detailed evaluation of a novel design of a transition structure that has been recently developed for an embankment-bridge transition (without ballast layer over the bridge) and in this work is extended to a transition zone where the ballast layer continues over the bridge. Even though the distribution of materials forming trackbed layers (ballast) in these two types of transitions are different, the safe hull-inspired energy-limiting design of the transition structure is equally efficient in mitigating the operation-induced dynamic amplification in both types of railway transition zones.

10

DESIGN OF EXPERIMENT

This work proposes an energy-based design methodology for railway transition zones but the insights offered in this work are not limited to only design purposes. For instance, the proposed energy-based criterion can be used to evaluate the on-site condition (indicative) of a railway track or a transition zone by computing energy flux based on measured quantities (stress, strain etc.) that characterize the kinematic and dynamic responses of the system at critical points. In order to achieve full accuracy in the design/ evaluation of the on-site condition using any approach (energy-based or other classical methods), detailed numerical models (tuned using measured data at monitoring points) must be used to predict the system's service situation. For this purpose, a full-scale laboratory experiment is planned to calibrate a high-fidelity model of an embankment-bridge transition. The detail of the experimental setup is described in the following sections. All the materials of track components in the 1:1 scale model will be tested in the laboratory to calibrate the material properties in the numerical model. This numerical model will be used to study the energy distribution in the proximity of the transition interface in the presence and absence of SHIELD for both short-term and long-term loading conditions. The experiment will contribute to new insights into the dynamic behaviour of the RTZs and the mechanisms leading to amplified degradation in these zones. Moreover, the experimentally validated numerical models will aid in the performance evaluation of the novel design of the transition structure (SHIELD) proposed in this work.

10.1. LABORATORIO DE GEOTECNIA – CEDEX [1]

CEDEX Track Box (CFC) is a 21 m long, 5 m wide and 4 m deep facility whose main objective is to test complete railway track sections (1:1 scale) of conventional and high-speed lines. The loading system (see Figure 10.1) consists of three pairs of servo-hydraulic actuators separated by a distance of 1.5m that can apply a maximum load of 250 kN (frequency 50 Hz). The loading system can reproduce the approaching, passing-by and departing of the passenger, freight and mixed traffic trains in a section moving with speeds up to 400 km/hr. The main advantage to this test setup is that the effect of the passing-by of trains for a year in a real section can be simulated in a time span of one week. This allows to study the long-term dynamic behavior of railway tracks in a very

short period of time.

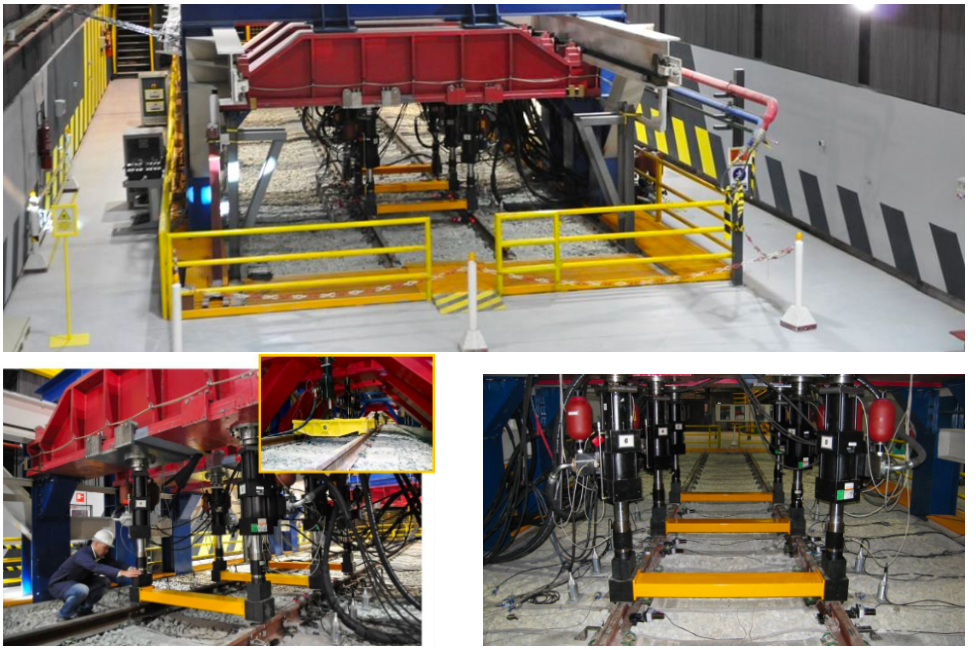

Figure 10.1: Loading system at CEDEX lab [1].

The test facility is equipped with advanced instrumentation (see Figure 10.2) for both the substructure and superstructure of railway track sections. The substructure response, in terms of displacements, velocities, accelerations and pressures, is collected from several linear variable differential transformers (LVDTs), geophones, accelerometers and pressure cells installed inside both the embankment and the bed layers (ballast, subballast and form layer) of the track. In addition to this, the railway superstructure response is recorded with mechanical displacement transducers, laser sensors, geophones and accelerometers installed on the different track components (rail, sleeper and railpad). The acquisition data unit can receive information from 150 sensors at the same time.

The proposed experiment at CEDEX lab has been accepted under the GEOLAB grant, a four-year Horizon 2020 project (2021 – 2025) funded by the European Union H2020 Research and Innovation Programme. The CEDEX test facility [1] has been previously used in the following projects:

- SUPERTRACK (2001-05) “Sustained performance of Railway Tracks” in the frame of 5th European Framework Program.
- INNOTRACK (2005-09) “Innovative Track Systems” in the frame of 6th European Framework Program.

Figure 10.2: Instrumentation at CEDEX lab [1]: laser sensors, geophones, accelerometers, displacement transducers, load cells.

- RIVAS (2009-13) “Railway Induced Vibration Abatement Solutions” in the frame of 7th European Framework Program.
- FASTRACK (2013-2014) “Nuevo sistema de vía en placa para alta velocidad sostenible y respetuoso con el medio ambiente” in the frame of Spanish CDTI Research Programs.
- CAPACITY4RAILS (2013-2017) “Increasing Capacity 4 Rail networks through enhanced infrastructure and optimized operations" in the frame of the 7th European Framework Program.

10.2. PROJECT DESCRIPTION:

10.2.1. OBJECTIVES

The proposed experiment has the following main objectives:

- Gain more insight into the long-term and short-term dynamic behaviour of railway transition zones in a controlled laboratory environment with perfectly maintained track conditions.
- Study the effects of environmental factors like water content in granular materials on the stiffness and on the behaviour of the transition zones.

- Calibration of the 3D numerical models.
- Evaluate the design methodology proposed in this work and the performance of a new design solution (SHIELD) to mitigate the dynamic amplifications in transition zones utilizing calibrated numerical models.

10.2.2. EXPERIMENTAL METHODOLOGY

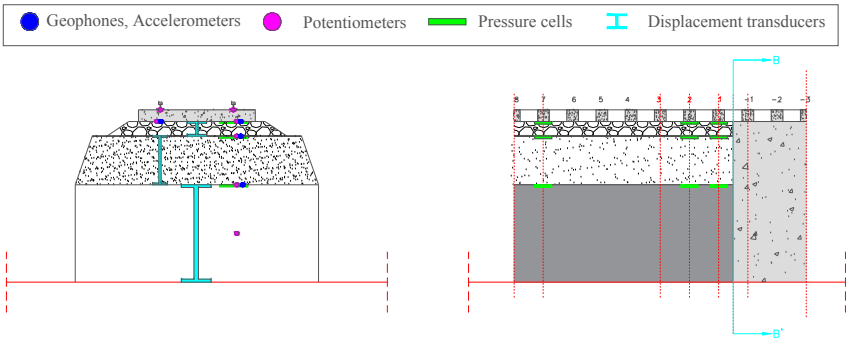

Figure 10.3: Longitudinal (a) and vertical (b) cross-section showing the locations for installation of measurement devices.

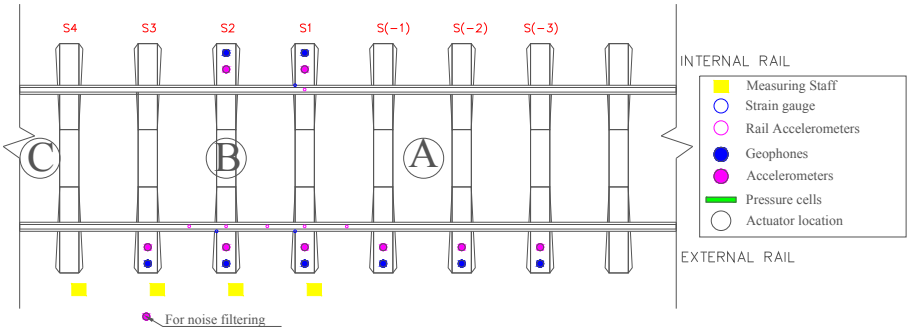

Figure 10.4: Top view of the laboratory setup showing the locations for installation of measurement devices and load simulators (A, B, C).

This experiment is designed to study the degradation process of an embankment-bridge transition subjected to a long-term loading using a 1:1 scale model in a controlled laboratory environment. The results of this test will be used to study the mechanisms leading to dynamic amplifications and amplified degradation in transition zones, validate the numerical models for further study and utilise the data and results for the evaluation/ verification of the novel design methodology for railway transition zones proposed in this work. The results in particular will be used for gaining more insight into the dynamics of the system, validation of the proposed design criteria and the design parameters for

an efficient and cost-effective design of railway transition zones. Also, the current literature does not provide any data on railway transition zones that have been collected at different stages of operation, i.e., from a perfectly straight track profile to a non-straight profile around the transition interface due to differential settlement. This experiment will also provide a detailed spatial and temporal mapping of the responses of the track components in the proximity of the transition interface and far from it.

Figure 10.4 and Figure 10.3 show the details of the track cross-section and instrumentation for the experimental setup.

RESULTS

The following output will be measured (See Figure 10.4 and Figure 10.3 for details):

1. Time history of accelerations using accelerometers
2. Time history of velocities using geophones
3. Time history of displacements using potentiometers
4. Permanent deformations: Displacement transducers (Figure 10.3 for location) to measure permanent settlement of each layer and measuring staff (Figure 10.4 for location) to plot the longitudinal profile of total permanent deformations.
5. Stress fields in granular materials using pressure cells.
6. Sliding at the interface (see Figure 10.3b section B-B' for location)
7. Force transferred to the sleepers at locations 1, 2, 3, -1, -2, -3 marked in Figure 10.3b.

The key equipment components for model building and testing, additional technical details and specifications to be provided by facility providers include the following:

1. Properties or type of geotechnical materials: The mechanical properties of the steel, concrete (sleeper, slab track), ballast, dense sand and clayey subgrade used for the experimental setup must be tested and provided for the calibration of finite element models.
2. Mixed traffic of the following trains is to be simulated in the experiment: Intercity trains (24 axles, axle load of 16 t and speed of 144 km/h) and Freight trains (24 axles, axle load of 22.5 t and speed of 85 km/h) 3. Expected number of load cycles: 1 year of operation
3. Location of load simulator: According to the FEM model that has been generated in line with the proposed experimental setup, the critical location is identified as S2 (Figure 10.4) next to the transition interface. Figure 10.4 shows the location of the load simulator to simulate the passage of trains.

10.2.3. CONCLUSION

The results will be used to calibrate the finite element models corresponding to the test setup. Calibrated 3D numerical models can be used in other types of studies related to railway transition zones. The data will be stored offline as well as online. The following are the outputs (expected publications) that will be derived from the experimental recording:

1. Experimental and numerical investigation of the long-term and short-term behaviour of an embankment-bridge railway transition using a controlled laboratory 1:1 scaled model.

2. Testing of a new design solution (SHIELD) for a railway transition utilizing experimentally calibrated models.

10.2.4. CURRENT STATUS

The project funding was granted in December 2023 and the experiment was scheduled for September 2024. However, due to technical problems in the laboratory, the project has been delayed and is scheduled to be completed in 2025.

11

CONCLUSIONS AND FUTURE SCOPE OF WORKS

This work proposes a novel energy-based approach to design railway transition zones (RTZs) in contrast to the traditional approaches that are based on either kinematic responses or stress fields mainly on the superstructure level. A comprehensive methodology is proposed to design RTZs, that is developed employing a multi-step approach. The first step involves a detailed investigation of all kinds of responses (spatially and temporally) of each track component to formulate the criterion that can be used to not only design a robust mitigation measure but also to evaluate why the current interventions are either counter-effective or only improve the performance marginally. The insights obtained from the evaluation of existing measures and investigation of key phenomena governing design are utilized to propose a new energy-based preliminary design of a transition structure.

The novelty of this work is threefold. Firstly, a novel design and evaluation criterion is introduced that not only describes the excessive degradation in RTZs but can also be used to design a robust mitigation measure that aims at reducing degradation in these zones. Secondly, a new design of a transition structure called SHIELD (Safe hull-inspired energy limiting design) is proposed and optimized based on limiting (minimising and ensuring a uniform distribution) energy within trackbed layers and around the transition interfaces. Lastly, a detailed methodology to design RTZs is developed in this work that establishes the design/ evaluation criterion (mentioned above) for an embankment-bridge transition, identifies design parameters (material and geometric), and evaluates the performance of RTZs for the most critical conditions that can occur due to operation over a period of time. This design methodology can be applied to different site-specific conditions and different types of transition zones.

The main conclusions of this work and the related future directions are discussed below:

Design criterion: The current evaluation criteria in the literature are based on kinematics and/or stresses and the criteria do not reflect a complete picture in terms of spatial

and temporal variation of dynamic responses of all the track components. In this work, energy is shown to be a more comprehensive criterion to describe the degradation in transition zones as it includes both stress and strain information for the track components. Furthermore, while looking at just the Von Mises stresses, the degradation due to only distortional energy is taken into account. The total strain energy criterion is more comprehensive as constitutes both distortional and volumetric components of strain energy. Throughout this work, the strain energy in the open tracks is considered as a benchmark, and the energies in the track components are minimized with respect to the magnitudes in the open track. However, for practical implementation of the energy approach proposed in this work, it is advisable that the strain energy associated with the failure of materials forming trackbed layers and the transition structure is identified via laboratory experiments. This will quantify the energy criterion proposed in this work for engineering practices.

Evaluation of existing mitigation measures and SHIELD: It is shown in this work that some mitigation measures like traditional transition wedges show significant improvement when looking at the vertical rail displacements but exhibit an increase in stresses. Similarly, using measures like approach slabs, the dynamic amplification is seen in terms of rail displacements but no significant amplification is observed in terms of stresses. Interestingly, the displacement fields for a traditional wedge and SHIELD looked exactly the same. However, a significant difference is seen in strain energy distribution (spatial and temporal) that explains the inefficiency of a traditional transition wedge in long-term performance and highlights the potential of SHIELD as a robust design solution. Another mitigation measure on the superstructure level (closely spaced sleepers) is proven to be inefficient when evaluating energy in the trackbed layers. Even though no dynamic amplifications are observed when considering rail displacements, there is a significant amplification of strain energy. Similar to approach slabs, this amplification is just moved to a different location.

Material optimisation: One of the most important conclusions is that not just the stiffness of materials but also stiffness ratios in longitudinal and vertical directions play a significant role in distributing energy spatially and temporally in the system. Therefore, it is not sufficient just to design the material of the SHIELD (providing gradual stiffness change from embankment to concrete structure) with appropriate stiffness to minimize the radiation due to load passing over the inhomogeneity but it is also necessary to maintain the ratios of stiffnesses in longitudinal (between embankment-SHIELD-concrete structure) and vertical directions (between trackbed layers). The relative stiffness of the ballast and the subgrade layers plays an important role in determining the performance of SHIELD in achieving uninterrupted energy flow. In this work, the bounds to the design ratios in longitudinal and vertical directions are proposed. In future works, investigations need to address the cases where there is a layer of subgrade under SHIELD to determine what kind of terrain is favourable for the foundation of SHIELD and ground improvement for what depths would guarantee optimum performance. Moreover, even though this work suggests the range of material properties in terms of elastic modulus, density, and Poisson's ratio that are desirable for the construction of SHIELD, a detailed investigation

must be performed to develop a constitutive model of the SHIELD material and it must be tested in the laboratory for cyclic loading. The range of optimized material properties proposed in this work could be achieved using chemically stabilized aggregates.

Geometric optimization: In this step of design methodology, the geometrical profiles in all three planes (longitudinal, transverse, and vertical directions) are investigated as the current literature does not highlight the role of geometry in the distribution of energy within the track bed layers in railway transition zones. Even though the longitudinal cross-section of SHIELD has the most significant contribution in channelling energy away from the trackbed layers, it is shown that poorly defined geometry of SHIELD in the transversal plane could still lead to local amplifications of strain energy. It is concluded that a 3-dimensional geometric optimization is necessary to ensure a smooth distribution of total strain energy in the trackbed layers and around the transition interface aiming at uninterrupted (no concentration or obstruction in any part of the system) energy flow in RTZs. However, future investigations related to SHIELD must include a detailed study regarding the long-term behaviour of the "nose" (the front tapered part) of the SHIELD. Depending on the chosen material and geometry, this particular part might be prone to breakage over a long period of operation and must be optimized further using the geometric profile proposed in this work as a preliminary design.

Evaluation of SHIELD for critical conditions: The formulation of the strain energy-based design criterion and the methodology proposed in this work is initially done using simplified vehicle models, fixed operation velocity (40 m/s), and ideal (perfectly straight track and no loss of contact between sleepers and ballast) track conditions. The variation of kinetic energies is insignificant compared to strain energy variation/ amplification for the operational velocities in the Netherlands. Future works must evaluate the sensitivity of the total mechanical energy (kinetic+strain) to the critical conditions (hanging sleepers, non-straight rail) for all velocity regimes (sub-critical, critical, and super-critical) using more detailed vehicle models. In this work, it is shown that the SHIELD design is promising for varying vehicle speeds in both directions of movement and also when subjected to detailed vehicle models. Moreover, the SHIELD design proves to be efficient also in dealing with non-ideal track conditions. In relation to this, the long-term performance of SHIELD (using non-linear models) should also be investigated in future works.

General conclusions: There are some critical conditions like moisture effects on material properties of aggregates, tracks subjected to extreme temperature variations, or other environmental factors that have not been investigated in this work. However, these critical conditions are evident in terms of variation (spatial and temporal) in the properties of trackbed materials and the influence of this variation (by implementing probabilistic distribution of elastic modulus, density and Poisson's ratio) is studied and dealt with (by proposing design limits) in this work. The implementation of the proposed energy-based criterion to evaluate the real-time performance of track conditions might be challenging as energy is a difficult quantity to measure on-site. However, with an increasing trend of adopting digital twins for monitoring real-time track conditions, the energy can be computed in the calibrated models and used as an evaluation criterion. Therefore, as a

part of this work, to calibrate numerical models for further investigations and to address some of the above concerns, a 1:1 scaled experiment (in a controlled environment) has been designed.

This work presents a preliminary design of a transition structure based on energy-limiting principles, that aims at mitigating the excessive degradation in railway transition zones. Any practical implementation of SHIELD must address the future scope of work suggested above and must be accompanied by detailed experiments and site measurements.

REFERENCES FOR CHAPTER 1

[1] B Coelho, P Hölscher, J Priest, W Powrie, and F Barends. An assessment of transition zone performance. *Proceedings of the Institution of Mechanical Engineers, Part F: Journal of Rail and Rapid Transit*, 225(2):129–139, February 2011. doi: 10.1177/09544097jrrt389. URL https://doi.org/10.1177/09544097jrrt389.

[2] B.E. Zuada Coelho. *Dynamics of railway transition zones in soft soils*. PhD thesis, May 2011. URL http://resolver.tudelft.nl/uuid:950e7ccd-1b18-4530-866d-5dd662fe0fa4.

[3] André Paixão, Eduardo Fortunato, and Rui Calçada. A numerical study on the influence of backfill settlements in the train/track interaction at transition zones to railway bridges. *Proceedings of the Institution of Mechanical Engineers, Part F: Journal of Rail and Rapid Transit*, 230(3):866–878, March 2015. doi: 10.1177/0954409715573289. URL https://doi.org/10.1177/0954409715573289.

[4] Haoyu Wang, Mika Silvast, Valeri Markine, and Bruce Wiljanen. Analysis of the dynamic wheel loads in railway transition zones considering the moisture condition of the ballast and subballast. *Applied Sciences*, 7(12):1208, November 2017. doi: 10.3390/app7121208. URL https://doi.org/10.3390/app7121208.

[5] Ricardo Insa, Pablo Salvador, Javier Inarejos, and Alejandro Roda. Analysis of the influence of under sleeper pads on the railway vehicle/track dynamic interaction in transition zones. *Proceedings of the Institution of Mechanical Engineers, Part F: Journal of Rail and Rapid Transit*, 226(4):409–420, December 2011. doi: 10.1177/0954409711430174. URL https://doi.org/10.1177/0954409711430174.

[6] Haoyu Wang and Valeri Markine. Corrective countermeasure for track transition zones in railways: Adjustable fastener. *Engineering Structures*, 169:1–14, August 2018. doi: 10.1016/j.engstruct.2018.05.004. URL https://doi.org/10.1016/j.engstruct.2018.05.004.

[7] André Paixão, Eduardo Fortunato, and Rui Calçada. Design and construction of backfills for railway track transition zones. *Proceedings of the Institution of Mechanical Engineers, Part F: Journal of Rail and Rapid Transit*, 229(1):58–70, August 2013. doi: 10.1177/0954409713499016. URL https://doi.org/10.1177/0954409713499016.

[8] Haoyu Wang and Valeri Markine. Dynamic behaviour of the track in transitions zones considering the differential settlement. *Journal of Sound and Vibration*, 459:114863, October 2019. doi: 10.1016/j.jsv.2019.114863. URL https://doi.org/10.1016/j.jsv.2019.114863.

[9] Miriam Labrado Palomo, Fernando Roca Barceló, Fran Ribes Llario, and Julia Real Herráiz. Effect of vehicle speed on the dynamics of track transitions. *Journal of Vibration and Control*, page 107754631774525, December 2017. doi: 10.1177/1077546317745254. URL https://doi.org/10.1177/1077546317745254.

[10] Chaminda Gallage, Biyanvilage Sampath Sri Sameer Dareeju, and Manicka Dhanasekar. State-of-the-art: track degradation at bridge transitions. In K P P Pathirana, editor, *Proceedings of the 4th International Conference on Structural Engineering and Construction Management 2013*, pages 40–52. Nethwin Printers Ltd, Sri Lanka, 2013. URL https://eprints.qut.edu.au/70153/.

[11] Haoyu Wang, Valeri Markine, and Xiangming Liu. Experimental analysis of railway track settlement in transition zones. *Proceedings of the Institution of Mechanical Engineers, Part F: Journal of Rail and Rapid Transit*, 232(6):1774–1789, December 2017. doi: 10.1177/0954409717748789. URL https://doi.org/10.1177/0954409717748789.

[12] Haoyu Wang and Valeri L. Markine. Methodology for the comprehensive analysis of railway transition zones. *Computers and Geotechnics*, 99:64–79, July 2018. doi: 10.1016/j.compgeo.2018.03.001. URL https://doi.org/10.1016/j.compgeo.2018.03.001.

[13] Haoyu Wang and Valeri Markine. Modelling of the long-term behaviour of transition zones: Prediction of track settlement. *Engineering Structures*, 156:294–304, February 2018. doi: 10.1016/j.engstruct.2017.11.038. URL https://doi.org/10.1016/j.engstruct.2017.11.038.

[14] D Li, D Otter, and G Carr. Railway bridge approaches under heavy axle load traffic: Problems, causes, and remedies. *Proceedings of the Institution of Mechanical Engineers, Part F: Journal of Rail and Rapid Transit*, 224(5):383–390, June 2010. doi: 10.1243/09544097jrrt345. URL https://doi.org/10.1243/09544097jrrt345.

[15] Timothy D Stark and Stephen T Wilk. Root cause of differential movement at bridge transition zones. *Proceedings of the Institution of Mechanical Engineers, Part F: Journal of Rail and Rapid Transit*, 230(4):1257–1269, June 2015. doi: 10.1177/0954409715589620. URL https://doi.org/10.1177/0954409715589620.

[16] Haoyu Wang, Ling Chang, and Valeri Markine. Structural health monitoring of railway transition zones using satellite radar data. *Sensors*, 18(2), 2018. ISSN 1424-8220. doi: 10.3390/s18020413. URL https://www.mdpi.com/1424-8220/18/2/413.

[17] Dingqing Li and David Davis. Transition of railroad bridge approaches. *Journal of Geotechnical and Geoenvironmental Engineering*, 131(11):1392–1398, November 2005. doi: 10.1061/(asce)1090-0241(2005)131:11(1392). URL https://doi.org/10.1061/(asce)1090-0241(2005)131:11(1392).

[18] André Paixão, Eduardo Fortunato, and Rui Calçada. Transition zones to railway bridges: Track measurements and numerical modelling. *Engineering Structures*,

80:435–443, December 2014. doi: 10.1016/j.engstruct.2014.09.024. URL https://doi.org/10.1016/j.engstruct.2014.09.024.

[19] Giacomo Ognibene, William Powrie, Louis Le Pen, and John Harkness. Analysis of a bridge approach: Long-term behaviour from short-term response. 07 2019.

[20] Cristina Alves Ribeiro, Rui Calçada, and Raimundo Delgado. Calibration and experimental validation of a dynamic model of the train-track system at a culvert transition zone. *Structure and Infrastructure Engineering*, 14(5):604–618, October 2017. doi: 10.1080/15732479.2017.1380674. URL https://doi.org/10.1080/15732479.2017.1380674.

[21] José N. Varandas, Paul Hölscher, and Manuel A.G. Silva. Dynamic behaviour of railway tracks on transitions zones. *Computers & Structures*, 89(13-14):1468–1479, July 2011. doi: 10.1016/j.compstruc.2011.02.013. URL https://doi.org/10.1016/j.compstruc.2011.02.013.

[22] J.N. Varandas, P. Hölscher, and M.A.G. Silva. Three-dimensional track-ballast interaction model for the study of a culvert transition. *Soil Dynamics and Earthquake Engineering*, 89:116–127, October 2016. doi: 10.1016/j.soildyn.2016.07.013. URL https://doi.org/10.1016/j.soildyn.2016.07.013.

[23] Julia Real-Herráiz, Clara Zamorano-Martín, Teresa Real-Herráiz, and Silvia Morales-Ivorra. New transition wedge design composed by prefabricated reinforced concrete slabs. *Latin American Journal of Solids and Structures*, 13(8):1431–1449, August 2016. doi: 10.1590/1679-78252556. URL https://doi.org/10.1590/1679-78252556.

[24] X Lei and B Zhang. Influence of track stiffness distribution on vehicle and track interactions in track transition. *Proceedings of the Institution of Mechanical Engineers, Part F: Journal of Rail and Rapid Transit*, 224(6):592–604, June 2010. doi: 10.1243/09544097jrrt318. URL https://doi.org/10.1243/09544097jrrt318.

[25] Louis Le Pen, Geoff Watson, William Powrie, Graeme Yeo, Paul Weston, and Clive Roberts. The behaviour of railway level crossings: Insights through field monitoring. *Transportation Geotechnics*, 1(4):201–213, December 2014. doi: 10.1016/j.trgeo.2014.05.002. URL https://doi.org/10.1016/j.trgeo.2014.05.002.

[26] André Paixão, Cristina Alves Ribeiro, Nuno Pinto, Eduardo Fortunato, and Rui Calçada. On the use of under sleeper pads in transition zones at railway underpasses: experimental field testing. *Structure and Infrastructure Engineering*, 11(2):112–128, January 2014. doi: 10.1080/15732479.2013.850730. URL https://doi.org/10.1080/15732479.2013.850730.

[27] Cristina Alves Ribeiro, André Paixão, Eduardo Fortunato, and Rui Calçada. Under sleeper pads in transition zones at railway underpasses: numerical modelling and experimental validation. *Structure and Infrastructure Engineering*, 11(11):1432–1449, October 2014. doi: 10.1080/15732479.2014.970203. URL https://doi.org/10.1080/15732479.2014.970203.

[28] A. Ramos, A. Gomes Correia, R. Calßada, and D.P. Connolly. Ballastless railway track transition zones: An embankment to tunnel analysis. *Transportation Geotechnics*, 33:100728, 2022. ISSN 2214-3912. doi: https://doi.org/10.1016/j.trgeo.2022.100728. URL https://www.sciencedirect.com/science/article/pii/S2214391222000125.

[29] Michaël J.M.M. Steenbergen. Physics of railroad degradation: The role of a varying dynamic stiffness and transition radiation processes. *Computers & Structures*, 124: 102–111, August 2013. doi: 10.1016/j.compstruc.2012.11.009. URL https://doi.org/10.1016/j.compstruc.2012.11.009.

[30] Andrei B. Fărăgău, Andrei V. Metrikine, and Karel N. van Dalen. Transition radiation in a piecewise-linear and infinite one-dimensional structure–a laplace transform method. *Nonlinear Dynamics*, 98(4):2435–2461, July 2019. doi: 10.1007/s11071-019-05083-6. URL https://doi.org/10.1007/s11071-019-05083-6.

[31] Andrei B. Fărăgău, Chris Keijdener, João M. de Oliveira Barbosa, Andrei V. Metrikine, and Karel N. van Dalen. Transition radiation in a nonlinear and infinite one-dimensional structure: a comparison of solution methods. *Nonlinear Dynamics*, 103(2):1365–1391, January 2021. doi: 10.1007/s11071-020-06117-0. URL https://doi.org/10.1007/s11071-020-06117-0.

[32] Andrei B. Fărăgău, Traian Mazilu, Andrei V. Metrikine, Tao Lu, and Karel N. vanDalen. Transition radiation in an infinite one-dimensional structure interacting with a moving oscillator—the green's function method. *Journal of Sound and Vibration*, 492:115804, February 2021. doi: 10.1016/j.jsv.2020.115804. URL https://doi.org/10.1016/j.jsv.2020.115804.

[33] João Manuel de Oliveira Barbosa, Andrei B. Fărăgău, and Karel N. van Dalen. A lattice model for transition zones in ballasted railway tracks. *Journal of Sound and Vibration*, 494:115840, March 2021. doi: 10.1016/j.jsv.2020.115840. URL https://doi.org/10.1016/j.jsv.2020.115840.

[34] João Manuel de Oliveira Barbosa and Karel N. van Dalen. Dynamic response of an infinite beam periodically supported by sleepers resting on a regular and infinite lattice: Semi-analytical solution. *Journal of Sound and Vibration*, 458:276–302, October 2019. doi: 10.1016/j.jsv.2019.06.014. URL https://doi.org/10.1016/j.jsv.2019.06.014.

[35] A.V. Metrikine, A.R.M. Wolfert, and H.A. Dieterman. Transition radiation in an elastically supported string. abrupt and smooth variations of the support stiffness. *Wave Motion*, 27(4):291–305, May 1998. doi: 10.1016/s0165-2125(97)00055-3. URL https://doi.org/10.1016/s0165-2125(97)00055-3.

[36] H. Wang. *Measurement, Assessment, Analysis and Improvement of Transition Zones in Railway Track*. PhD thesis, Mar 2019. URL https://doi.org/10.4233/uuid:73830b2c-deb1-4da9-b19c-5e848c5cfa4d.

[37] Buddhima Indraratna, Muhammad Babar Sajjad, Trung Ngo, António Gomes Correia, and Richard Kelly. Improved performance of ballasted tracks at transition zones: A review of experimental and modelling approaches. *Transportation Geotechnics*, 21:100260, December 2019. doi: 10.1016/j.trgeo.2019.100260. URL https://doi.org/10.1016/j.trgeo.2019.100260.

[38] R. Sañudo, L. dell'Olio, J.A. Casado, I.A. Carrascal, and S. Diego. Track transitions in railways: A review. *Construction and Building Materials*, 112:140–157, June 2016. doi: 10.1016/j.conbuildmat.2016.02.084. URL https://doi.org/10.1016/j.conbuildmat.2016.02.084.

[39] José Nuno Varandas da Silva Ferreira. *Long-term behaviour of railway transitions under dynamic loading application to soft soil sites*. PhD thesis, 2013. URL http://hdl.handle.net/10362/10145.

[40] Luís Coelho. Structure / embankment transitions in railway infrastructures behaviour and national and international practices. 2008.

[41] Ernest T. Selig and John M. Waters. *TRACK GEOTECHNOLOGY and SUBSTRUCTURE MANAGEMENT*. Thomas Telford Publishing, 1994. doi: 10.1680/tgasm.20139. URL https://www.icevirtuallibrary.com/doi/abs/10.1680/tgasm.20139.

[42] D Li, D Otter, and G Carr. Railway bridge approaches under heavy axle load traffic: Problems, causes, and remedies. *Proceedings of the Institution of Mechanical Engineers, Part F: Journal of Rail and Rapid Transit*, 224(5):383–390, 2010. doi: 10.1243/09544097JRRT345.

[43] Mojtaba Shahraki and Karl Josef Witt. 3d modeling of transition zone between ballasted and ballastless high-speed railway track. *Journal of Traffic and Transportation Engineering*, 3(4), April 2015. doi: 10.17265/2328-2142/2015.04.005. URL https://doi.org/10.17265/2328-2142/2015.04.005.

[44] Meysam Banimahd, Peter K. Woodward, Justin Kennedy, and Gabriela M. Medero. Behaviour of train–track interaction in stiffness transitions. *Proceedings of the Institution of Civil Engineers - Transport*, 165(3):205–214, August 2012. doi: 10.1680/tran.10.00030. URL https://doi.org/10.1680/tran.10.00030.

[45] A. I. Vesnitskii and A. V. Metrikin. Transition radiation in one-dimensional elastic systems. *Journal of Applied Mechanics and Technical Physics*, 33(2):202–207, 1992. ISSN 1573-8620. doi: 10.1007/bf00851588. URL http://dx.doi.org/10.1007/BF00851588.

[46] Andrei V. Metrikine and A.C.W.M. Vrouwenvelder. Surface ground vibration due to a moving train in a tunnel: Two-dimensional model. *Journal of Sound and Vibration*, 234(1):43–66, June 2000. ISSN 0022-460X. doi: 10.1006/jsvi.1999.2853. URL http://dx.doi.org/10.1006/jsvi.1999.2853.

[47] A.V. Metrikine, A.R.M. Wolfert, and H.A. Dieterman. Transition radiation in an elastically supported string. abrupt and smooth variations of the support stiffness. *Wave*

Motion, 27(4):291–305, May 1998. ISSN 0165-2125. doi: 10.1016/s0165-2125(97)00055-3. URL http://dx.doi.org/10.1016/S0165-2125(97)00055-3.

[48] Karel N. van Dalen and Andrei V. Metrikine. Transition radiation of elastic waves at the interface of two elastic half-planes. *Journal of Sound and Vibration*, 310(3):702–717, 2008. ISSN 0022-460X. doi: https://doi.org/10.1016/j.jsv.2007.06.007.

[49] Karel N. van Dalen, Apostolos Tsouvalas, Andrei V. Metrikine, and Jeroen S. Hoving. Transition radiation excited by a surface load that moves over the interface of two elastic layers. *International Journal of Solids and Structures*, 73-74:99–112, 2015. ISSN 0020-7683. doi: https://doi.org/10.1016/j.ijsolstr.2015.07.001.

[50] Mojtaba Shahraki, Chanaka Warnakulasooriya, and Karl Josef Witt. Numerical study of transition zone between ballasted and ballastless railway track. *Transportation Geotechnics*, 3:58–67, June 2015. doi: 10.1016/j.trgeo.2015.05.001. URL https://doi.org/10.1016/j.trgeo.2015.05.001.

[51] H. Heydari-Noghabi, J. N. Varandas, M. Esmaeili, and J. Zakeri. Investigating the influence of auxiliary rails on dynamic behavior of railway transition zone by a 3d train-track interaction model. *Latin American Journal of Solids and Structures*, 14(11):2000–2018, 2017. doi: 10.1590/1679-78253906. URL https://doi.org/10.1590/1679-78253906.

[52] Mojtaba Shahraki, Chanaka Warnakulasooriya, and Karl Josef Witt. Numerical study of transition zone between ballasted and ballastless railway track. *Transportation Geotechnics*, 3:58–67, June 2015. doi: 10.1016/j.trgeo.2015.05.001. URL https://doi.org/10.1016/j.trgeo.2015.05.001.

[53] Emil Aggestam and Jens C.O. Nielsen. Multi-objective optimisation of transition zones between slab track and ballasted track using a genetic algorithm. *Journal of Sound and Vibration*, 446:91–112, April 2019. doi: 10.1016/j.jsv.2019.01.027. URL https://doi.org/10.1016/j.jsv.2019.01.027.

[54] Roberto Sañudo, Mikel Cerrada, Borja Alonso, and Luigi dell'Olio. Analysis of the influence of support positions in transition zones. a numerical analysis. *Construction and Building Materials*, 145:207–217, August 2017. doi: 10.1016/j.conbuildmat.2017.03.204. URL https://doi.org/10.1016/j.conbuildmat.2017.03.204.

[55] David Read and Dingqing Li. *Design of Track Transitions*. The National Academies Press, Washington, DC, 2006. doi: 10.17226/23228. URL https://www.nap.edu/catalog/23228/design-of-track-transitions.

[56] Jennifer Elizabeth Nicks. *The Bump at the End of the Railway Bridge*. PhD thesis, Dec 2009. URL https://oaktrust.library.tamu.edu/handle/1969.1/ETD-TAMU-2009-12-7432.

[57] Akira NAMURA and Takahiro SUZUKI. Evaluation of countermeasures against differential settlement at track transitions. *Quarterly Report of RTRI*, 48(3):176–182, 2007. doi: 10.2219/rtriqr.48.176.

[58] Akira NAMURA, Yukihiro KOHATA, and Seiichi MIURA. Effect of sleeper size on ballasted track settlement. *Quarterly Report of RTRI*, 45(3):156–161, 2004. doi: 10.2219/rtriqr.45.156.

[59] T. Dahlberg. Railway track settlements - a literature review. 2004.

[60] Miguel Sol-Sánchez, Fernando Moreno-Navarro, and Mª Carmen Rubio-Gámez. The use of elastic elements in railway tracks: A state of the art review. *Construction and Building Materials*, 75, 2015. doi: 10.1016/j.conbuildmat.2014.11.027.

[61] C. S. Cai, X. M. Shi, G. Z. Voyiadjis, and Z. J. Zhang. Structural performance of bridge approach slabs under given embankment settlement. *Journal of Bridge Engineering*, 10(4):482–489, 2005. doi: 10.1061/(ASCE)1084-0702(2005)10:4(482).

[62] Bruno Zuada Coelho, Jeffrey Priest, and Paul HÄ¶lscher. Dynamic behaviour of transition zones in soft soils during regular train traffic. *Proceedings of the Institution of Mechanical Engineers, Part F: Journal of Rail and Rapid Transit*, 232(3):645–662, 2018. doi: 10.1177/0954409716683078.

[63] D. Sasaoka and D. Davis. Implementing track transition solutions for heavy axle load service. 2005.

[64] B Coelho, P Hölscher, J Priest, W Powrie, and F Barends. An assessment of transition zone performance. *Proceedings of the Institution of Mechanical Engineers, Part F: Journal of Rail and Rapid Transit*, 225(2):129–139, February 2011. doi: 10.1177/09544097jrrt389. URL https://doi.org/10.1177/09544097jrrt389.

[65] E. Fortunato, A. Paixão, and R. Calçada. Railway track transition zones: Design, construction, monitoring and numerical modelling. *International Journal of Railway Technology*, 2(4):33–58, 2013. doi: 10.4203/ijrt.2.4.3. URL https://doi.org/10.4203/ijrt.2.4.3.

[66] Ping Hu, Chunshun Zhang, Sen Wen, and Yonghe Wang. Dynamic responses of high-speed railway transition zone with various subgrade fillings. *Computers and Geotechnics*, 108:17–26, April 2019. doi: 10.1016/j.compgeo.2018.12.011. URL https://doi.org/10.1016/j.compgeo.2018.12.011.

[67] Dingqing Li and David Davis. Transition of railroad bridge approaches. *Journal of Geotechnical and Geoenvironmental Engineering*, 131(11):1392–1398, November 2005. doi: 10.1061/(asce)1090-0241(2005)131:11(1392). URL https://doi.org/10.1061/(asce)1090-0241(2005)131:11(1392).

[68] André Paixão, Eduardo Fortunato, and Rui Calçada. A numerical study on the influence of backfill settlements in the train/track interaction at transition zones to railway bridges. *Proceedings of the Institution of Mechanical Engineers, Part F: Journal of Rail and Rapid Transit*, 230(3):866–878, March 2015. doi: 10.1177/0954409715573289. URL https://doi.org/10.1177/0954409715573289.

[69] André Paixão, José Nuno Varandas, Eduardo Fortunato, and Rui Calçada. Numerical simulations to improve the use of under sleeper pads at transition zones to railway bridges. *Engineering Structures*, 164:169–182, June 2018. doi: 10.1016/j.engstruct.2018.03.005. URL https://doi.org/10.1016/j.engstruct.2018.03.005.

[70] H E M and HUNT. Settlement of railway track near bridge abutments. (third paper in young railway engineer of the year (1996) award). *Proceedings of the Institution of Civil Engineers - Transport*, 123(1):68–73, 1997. doi: 10.1680/itran.1997.29182. URL https://doi.org/10.1680/itran.1997.29182.

[71] Timothy D Stark and Stephen T Wilk. Root cause of differential movement at bridge transition zones. *Proceedings of the Institution of Mechanical Engineers, Part F: Journal of Rail and Rapid Transit*, 230(4):1257–1269, June 2015. doi: 10.1177/0954409715589620. URL https://doi.org/10.1177/0954409715589620.

[72] A Lundqvist and T Dahlberg. Load impact on railway track due to unsupported sleepers. *Proceedings of the Institution of Mechanical Engineers, Part F: Journal of Rail and Rapid Transit*, 219(2):67–77, March 2005. doi: 10.1243/095440905x8790. URL https://doi.org/10.1243/095440905x8790.

[73] Mykola Sysyn, Michal Przybylowicz, Olga Nabochenko, and Lei Kou. Identification of sleeper support conditions using mechanical model supported data-driven approach. *Sensors*, 21(11):3609, May 2021. doi: 10.3390/s21113609. URL https://doi.org/10.3390/s21113609.

[74] J. Y. Zhu, D. J. Thompson, and C. J.C. Jones. On the effect of unsupported sleepers on the dynamic behaviour of a railway track. *Vehicle System Dynamics*, 49(9):1389–1408, September 2011. doi: 10.1080/00423114.2010.524303. URL https://doi.org/10.1080/00423114.2010.524303.

[75] Ryutaro Takahashi, Kimitoshi Hayano, Takahisa Nakamura, and Yoshitsugu Momoya. Integrated risk of rail buckling in ballasted tracks at transition zones and its countermeasures. *Soils and Foundations*, 59(2):517–531, April 2019. doi: 10.1016/j.sandf.2018.12.013. URL https://doi.org/10.1016/j.sandf.2018.12.013.

[76] Guoqing Jing, Qi Luo, Zijie Wang, and Yonggang Shen. Micro-analysis of hanging sleeper dynamic interactions with ballast bed. *Journal of Vibroengineering*, Feb 2015. URL https://www.jvejournals.com/article/15698.

[77] Y Bezin, S D Iwnicki, M Cavalletti, E de Vries, F Shahzad, and G Evans. An investigation of sleeper voids using a flexible track model integrated with railway multi-body dynamics. *Proceedings of the Institution of Mechanical Engineers, Part F: Journal of Rail and Rapid Transit*, 223(6):597–607, June 2009. doi: 10.1243/09544097jrrt276. URL https://doi.org/10.1243/09544097jrrt276.

[78] Mykola Sysyn, Olga Nabochenko, and Vitalii Kovalchuk. Experimental investigation of the dynamic behavior of railway track with sleeper voids. *Railway Engineering Science*, 28(3):290–304, August 2020. doi: 10.1007/s40534-020-00217-8. URL https://doi.org/10.1007/s40534-020-00217-8.

[79] Inmaculada Gallego Giner and A López Pita. Numerical simulation of embankment—structure transition design. *Proceedings of the Institution of Mechanical Engineers, Part F: Journal of Rail and Rapid Transit*, 223(4):331–343, January 2009. doi: 10.1243/09544097jrrt234. URL https://doi.org/10.1243/09544097jrrt234.

[80] E. Selig and Dingqing Li. Track modulus: Its meaning and factors influencing it. *Transportation Research Record*, 1994.

[81] Inmaculada Gallego Giner, Andrés López Pita, Eduardo W. Vieira Chaves, and Ana María Rivas Álvarez. Design of embankment structure transitions for railway infrastructure. *Proceedings of the Institution of Civil Engineers - Transport*, 2012. doi: 10.1680/tran.8.00037.

[82] Andrea Fara. Transition zones for railway bridges : A study of the sikån bridge. Master's thesis, 2014. Validerat; 20140917 (global_studentproject_submitter).

[83] Diego Froio, Egidio Rizzi, Fernando M.F. Simões, and António Pinto Da Costa. Universal analytical solution of the steady-state response of an infinite beam on a pasternak elastic foundation under moving load. 132-133:245–263, February 2018. doi: 10.1016/j.ijsolstr.2017.10.005. URL https://doi.org/10.1016/j.ijsolstr.2017.10.005.

[84] A.B. Fărăgău, A. Jain, J.M. de Oliveira Barbosa, A.V. Metrikine, and K.N. van Dalen. Auxiliary rails as a mitigation measure for degradation in transition zones. In J. Pombo, editor, *Proceedings of The Fifth International Conference on Railway Technology: Research, Development and Maintenance*, volume CCC 1 of *Civil-Comp Conferences*, United Kingdom, 2023. Civil-Comp Press. doi: 10.4203/ccc.1.19.4.

[85] Taufan Abadi, Louis Le Pen, Antonis Zervos, and William Powrie. Effect of sleeper interventions on railway track performance. *Journal of Geotechnical and Geoenvironmental Engineering*, 145(4):04019009, 2019. doi: 10.1061/(ASCE)GT.1943-5606.0002022.

[86] Ricardo Insa, Pablo Salvador, Javier Inarejos, and Alejandro Roda. Analysis of the influence of under sleeper pads on the railway vehicle/track dynamic interaction in transition zones. *Proceedings of the Institution of Mechanical Engineers, Part F: Journal of Rail and Rapid Transit*, 2012. doi: 10.1177/0954409711430174.

[87] Sinniah K. Navaratnarajah, Buddhima Indraratna, and Ngoc Trung Ngo. Influence of under sleeper pads on ballast behavior under cyclic loading: Experimental and numerical studies. *Journal of Geotechnical and Geoenvironmental Engineering*, 2018. doi: 10.1061/(ASCE)GT.1943-5606.0001954.

[88] C Esveld. *Modern railway track, second edition.*, pages 1–653. MRT productions, 2001.

[89] Debakanta Mishra, Erol Tutumluer, Huseyin Boler, James P. Hyslip, and Theodore R. Sussmann. Railroad track transitions with multidepth deflectometers and strain gauges. *Transportation Research Record*, 2448(1):105–114, 2014. doi: 10.3141/2448-13.

[90] C. Bonnett. Practical railway engineering. 2005.

[91] André Filipe da Silva Rodrigues. *Viability and Applicability of Simplified Models for the Dynamic Analysis of Ballasted Railway Tracks*. PhD thesis, Jun 2017. URL http://hdl.handle.net/10362/21663.

[92] Stephen T Wilk, Timothy D Stark, and Jerry G Rose. Evaluating tie support at railway bridge transitions. *Proceedings of the Institution of Mechanical Engineers, Part F: Journal of Rail and Rapid Transit*, 230(4):1336–1350, 2016. doi: 10.1177/0954409715596192.

[93] Miriam Labrado Palomo, Fernando Roca Barceló, Fran Ribes Llario, and Julia Real Herráiz. Effect of vehicle speed on the dynamics of track transitions. *Journal of Vibration and Control*, 24(21):5118–5128, 2018. doi: 10.1177/1077546317745254.

[94] J G Rose, L A Walker, and Duo Li. Heavy-haul asphalt (hma) underlayment trackbeds: Pressures/deflections/materials properties measurements. Nov 2001. URL https://trid.trb.org/view/745182.

[95] Md. Abu Sayeed and Mohamed A. Shahin. Design of ballasted railway track foundations using numerical modelling. part i: Development. *Canadian Geotechnical Journal*, 55(3):353–368, 2018. doi: 10.1139/cgj-2016-0633.

[96] Inmaculada Gallego Giner, J Muñoz, A Rivas, and S Sánchez-Cambronero. Vertical track stiffness as a new parameter involved in designing high-speed railway infrastructure. *Journal of Transportation Engineering*, 137(12):971–979, December 2011. doi: 10.1061/(asce)te.1943-5436.0000288. URL https://doi.org/10.1061/(asce)te.1943-5436.0000288.

REFERENCES FOR CHAPTER 2

[1] B Coelho, P Hölscher, J Priest, W Powrie, and F Barends. An assessment of transition zone performance. *Proceedings of the Institution of Mechanical Engineers, Part F: Journal of Rail and Rapid Transit*, 225(2):129–139, February 2011. doi: 10.1177/09544097jrrt389. URL https://doi.org/10.1177/09544097jrrt389.

[2] José N. Varandas, Paul Hölscher, and Manuel A.G. Silva. Dynamic behaviour of railway tracks on transitions zones. *Computers & Structures*, 89(13-14):1468–1479, July 2011. doi: 10.1016/j.compstruc.2011.02.013. URL https://doi.org/10.1016/j.compstruc.2011.02.013.

[3] Jens CO Nielsen, Eric G Berggren, Anders Hammar, Fredrik Jansson, and Rikard Bolmsvik. Degradation of railway track geometry – correlation between track stiffness gradient and differential settlement. *Proceedings of the Institution of Mechanical Engineers, Part F: Journal of Rail and Rapid Transit*, 234(1):108–119, December 2018. doi: 10.1177/0954409718819581. URL https://doi.org/10.1177/0954409718819581.

[4] Buddhima Indraratna, Muhammad Babar Sajjad, Trung Ngo, António Gomes Correia, and Richard Kelly. Improved performance of ballasted tracks at transition zones: A review of experimental and modelling approaches. *Transportation Geotechnics*, 21:100260, December 2019. doi: 10.1016/j.trgeo.2019.100260. URL https://doi.org/10.1016/j.trgeo.2019.100260.

[5] R. Sañudo, L. dell'Olio, J.A. Casado, I.A. Carrascal, and S. Diego. Track transitions in railways: A review. *Construction and Building Materials*, 112:140–157, June 2016. doi: 10.1016/j.conbuildmat.2016.02.084. URL https://doi.org/10.1016/j.conbuildmat.2016.02.084.

[6] Transportation Research Board and National Academies of Sciences, Engineering, and Medicine. *Design of Track Transitions*. The National Academies Press, Washington, DC, 2006. doi: 10.17226/23228.

[7] Dingqing Li and David Davis. Transition of railroad bridge approaches. *Journal of Geotechnical and Geoenvironmental Engineering*, 131(11):1392–1398, nov 2005.

[8] Cristina Alves Ribeiro, André Paixão, Eduardo Fortunato, and Rui Calçada. Under sleeper pads in transition zones at railway underpasses: numerical modelling and experimental validation. *Structure and Infrastructure Engineering*, 11(11):1432–1449, October 2014. doi: 10.1080/15732479.2014.970203. URL https://doi.org/10.1080/15732479.2014.970203.

[9] André Paixão, Eduardo Fortunato, and Rui Calçada. Transition zones to railway bridges: Track measurements and numerical modelling. *Engineering Structures*, 80:435–443, December 2014. doi: 10.1016/j.engstruct.2014.09.024. URL https://doi.org/10.1016/j.engstruct.2014.09.024.

[10] André Paixão, Eduardo Fortunato, and Rui Calçada. A numerical study on the influence of backfill settlements in the train/track interaction at transition zones to railway bridges. *Proceedings of the Institution of Mechanical Engineers, Part F: Journal of Rail and Rapid Transit*, 230(3):866–878, March 2015. doi: 10.1177/0954409715573289. URL https://doi.org/10.1177/0954409715573289.

[11] Haoyu Wang and Valeri Markine. Corrective countermeasure for track transition zones in railways: Adjustable fastener. *Engineering Structures*, 169:1–14, August 2018. doi: 10.1016/j.engstruct.2018.05.004. URL https://doi.org/10.1016/j.engstruct.2018.05.004.

[12] Mojtaba Shahraki and Karl Josef Witt. 3d modeling of transition zone between ballasted and ballastless high-speed railway track. *Journal of Traffic and Transportation Engineering*, 3(4), April 2015. doi: 10.17265/2328-2142/2015.04.005. URL https://doi.org/10.17265/2328-2142/2015.04.005.

[13] Haoyu Wang, Mika Silvast, Valeri Markine, and Bruce Wiljanen. Analysis of the dynamic wheel loads in railway transition zones considering the moisture condition of the ballast and subballast. *Applied Sciences*, 7(12):1208, November 2017. doi: 10.3390/app7121208. URL https://doi.org/10.3390/app7121208.

[14] Ricardo Insa, Pablo Salvador, Javier Inarejos, and Alejandro Roda. Analysis of the influence of under sleeper pads on the railway vehicle/track dynamic interaction in transition zones. *Proceedings of the Institution of Mechanical Engineers, Part F: Journal of Rail and Rapid Transit*, 226(4):409–420, December 2011. doi: 10.1177/0954409711430174. URL https://doi.org/10.1177/0954409711430174.

[15] Meysam Banimahd, Peter K. Woodward, Justin Kennedy, and Gabriela M. Medero. Behaviour of train–track interaction in stiffness transitions. *Proceedings of the Institution of Civil Engineers - Transport*, 165(3):205–214, 2012. doi: 10.1680/tran.10.00030. URL https://doi.org/10.1680/tran.10.00030.

[16] Julia Real-Herráiz, Clara Zamorano-Martín, Teresa Real-Herráiz, and Silvia Morales-Ivorra. New transition wedge design composed by prefabricated reinforced concrete slabs. *Latin American Journal of Solids and Structures*, 13(8):1431–1449, August 2016. doi: 10.1590/1679-78252556. URL https://doi.org/10.1590/1679-78252556.

[17] André Paixão, Cristina Alves Ribeiro, Nuno Pinto, Eduardo Fortunato, and Rui Calçada. On the use of under sleeper pads in transition zones at railway underpasses: experimental field testing. *Structure and Infrastructure Engineering*, 11(2):112–128, January 2014. doi: 10.1080/15732479.2013.850730. URL https://doi.org/10.1080/15732479.2013.850730.

[18] Cristina Alves Ribeiro, André Paixão, Eduardo Fortunato, and Rui Calçada. Under sleeper pads in transition zones at railway underpasses: numerical modelling and experimental validation. *Structure and Infrastructure Engineering*, 11(11):1432–1449, October 2014. doi: 10.1080/15732479.2014.970203. URL https://doi.org/10.1080/15732479.2014.970203.

[19] J.N. Varandas, P. Hölscher, and M.A.G. Silva. Three-dimensional track-ballast interaction model for the study of a culvert transition. *Soil Dynamics and Earthquake Engineering*, 89:116–127, October 2016. doi: 10.1016/j.soildyn.2016.07.013. URL https://doi.org/10.1016/j.soildyn.2016.07.013.

[20] Md. Abu Sayeed and Mohamed A. Shahin. Design of ballasted railway track foundations using numerical modelling. part i: Development. *Canadian Geotechnical Journal*, 55(3):353–368, March 2018. doi: 10.1139/cgj-2016-0633. URL https://doi.org/10.1139/cgj-2016-0633.

[21] Akira Aikawa. Dynamic characterisation of a ballast layer subject to traffic impact loads using three-dimensional sensing stones and a special sensing sleeper. *Construction and Building Materials*, 92:23–30, September 2015. doi: 10.1016/j.conbuildmat.2014.06.005. URL https://doi.org/10.1016/j.conbuildmat.2014.06.005.

[22] Wojciech Sas, Andrzej Głuchowski, Bartłomiej Bursa, and Alojzy Szymański. Energy-based analysis of permanent strain behaviour of cohesive soil under cyclic loading. *Acta Geophysica*, 65(2):331–344, April 2017. doi: 10.1007/s11600-017-0028-7. URL https://doi.org/10.1007/s11600-017-0028-7.

[23] R. T. Qu, Z. J. Zhang, P. Zhang, Z. Q. Liu, and Z. F. Zhang. Generalized energy failure criterion. *Scientific Reports*, 6(1), March 2016. doi: 10.1038/srep23359. URL https://doi.org/10.1038/srep23359.

[24] Bjorn Birgisson, Jianlin Wang, Reynaldo Roque, and Boonchais Sangpetngam. Numerical implementation of a strain energy-based fracture model for HMA materials. *Road Materials and Pavement Design*, 8(1):7–45, January 2007. doi: 10.1080/14680629.2007.9690065. URL https://doi.org/10.1080/14680629.2007.9690065.

[25] Mehran Sadri, Tao Lu, and Michaël Steenbergen. Railway track degradation: The contribution of a spatially variant support stiffness - local variation. *Journal of Sound and Vibration*, 455:203–220, September 2019. doi: 10.1016/j.jsv.2019.05.006.

[26] André Paixão, José Nuno Varandas, Eduardo Fortunato, and Rui Calçada. Numerical simulations to improve the use of under sleeper pads at transition zones to railway bridges. *Engineering Structures*, 164:169–182, June 2018. doi: 10.1016/j.engstruct.2018.03.005. URL https://doi.org/10.1016/j.engstruct.2018.03.005.

[27] Piyush Punetha, Krijan Maharjan, and Sanjay Nimbalkar. Finite element modeling of the dynamic response of critical zones in a ballasted railway track. *Frontiers in Built Environment*, 7, April 2021. doi: 10.3389/fbuil.2021.660292.

[28] Giacomo Ognibene, William Powrie, Louis Le Pen, and John Harkness. Analysis of a bridge approach: Long-term behaviour from short-term response. 07 2019.

[29] Haoyu Wang, Valeri Markine, and Xiangming Liu. Experimental analysis of railway track settlement in transition zones. *Proceedings of the Institution of Mechanical Engineers, Part F: Journal of Rail and Rapid Transit*, 232(6):1774–1789, December 2017. doi: 10.1177/0954409717748789. URL https://doi.org/10.1177/0954409717748789.

[30] *ABAQUS/Standard User's Manual, Version 6.9*. Dassault Systèmes Simulia Corp, United States.

[31] A. Jain, K. N. van Dalen, A. V. Metrikine, Andrei Fărăgău, and M. J. M. M. Steenbergen. Comparative analysis of the dynamic amplifications due to inhomogeneities at railway transition zones. In J. Pombo, editor, *Proceedings of The Fifth International Conference on Railway Technology: Research, Development and Maintenance*, Edinburgh, UK, 2022. Civil-Comp Press.

[32] Haoyu Wang and Valeri Markine. Modelling of the long-term behaviour of transition zones: Prediction of track settlement. *Engineering Structures*, 156:294–304, February 2018. doi: 10.1016/j.engstruct.2017.11.038.

[33] H. Wang. *Measurement, Assessment, Analysis and Improvement of Transition Zones in Railway Track*. PhD thesis, 2019.

[34] *ABAQUS Online Documentation: Version 6.6-1*. Dassault Systèmes Simulia Corp, United States.

[35] Buddhima Indraratna, Pramod Kumar Thakur, and Jayan S. Vinod. Experimental and numerical study of railway ballast behavior under cyclic loading. *International Journal of Geomechanics*, 10(4):136–144, August 2010. doi: 10.1061/(asce)gm.1943-5622.0000055. URL https://doi.org/10.1061/(asce)gm.1943-5622.0000055.

[36] Haoyu Wang, Ling Chang, and Valeri Markine. Structural health monitoring of railway transition zones using satellite radar data. *Sensors*, 18(2):413, January 2018. doi: 10.3390/s18020413. URL https://doi.org/10.3390/s18020413.

[37] Haoyu Wang and Valeri L. Markine. Methodology for the comprehensive analysis of railway transition zones. *Computers and Geotechnics*, 99:64–79, July 2018. doi: 10.1016/j.compgeo.2018.03.001. URL https://doi.org/10.1016/j.compgeo.2018.03.001.

[38] Mojtaba Shahraki, Chanaka Warnakulasooriya, and Karl Josef Witt. Numerical study of transition zone between ballasted and ballastless railway track. *Transportation Geotechnics*, 3:58–67, June 2015. doi: 10.1016/j.trgeo.2015.05.001. URL https://doi.org/10.1016/j.trgeo.2015.05.001.

[39] Timothy D Stark and Stephen T Wilk. Root cause of differential movement at bridge transition zones. *Proceedings of the Institution of Mechanical Engineers,*

Part F: Journal of Rail and Rapid Transit, 230(4):1257–1269, June 2015. doi: 10.1177/0954409715589620. URL https://doi.org/10.1177/0954409715589620.

[40] Avni Jain, Maurizio Acito, and Claudio Chesi. Seismic sequence of 2016–17: Linear and non-linear interpretation models for evolution of damage in san francesco church, amatrice. *Engineering Structures*, 211:110418, May 2020. doi: 10.1016/j.engstruct.2020.110418. URL https://doi.org/10.1016/j.engstruct.2020.110418.

[41] A. Jain, M. Acito, C. Chesi, and E. Magrinelli. The seismic sequence of 2016–2017 in central italy: a numerical insight on the survival of the civic tower in amatrice. *Bulletin of Earthquake Engineering*, 18(4):1371–1400, November 2019. doi: 10.1007/s10518-019-00750-w. URL https://doi.org/10.1007/s10518-019-00750-w.

[42] Maurizio Acito, Eleonora Magrinelli, Gabriele Milani, and Simone Tiberti. Seismic vulnerability of masonry buildings: Numerical insight on damage causes for residential buildings by the 2016 central italy seismic sequence and evaluation of strengthening techniques. *Journal of Building Engineering*, 28:101081, March 2020. doi: 10.1016/j.jobe.2019.101081. URL https://doi.org/10.1016/j.jobe.2019.101081.

[43] A. Jain, A.V. Metrikine, M.J.M.M. Steenbergen, and K.N. van Dalen. Railway transition zones: evaluation of existing transition structures and a newly proposed transition structure. *International Journal of Rail Transportation*, pages 1–21, 2023. doi: 10.1080/23248378.2023.2272668. URL https://doi.org/10.1080/23248378.2023.2272668. (Note: Included as Chapter 3).

[44] Avni Jain, Yuriy Marykovskiy, Andrei Metrikine, and Karel van Dalen. Quantifying the impact of stiffness distributions on the dynamic behaviour of railway transition zones. 2023. doi: 10.2139/ssrn.4649163. URL http://dx.doi.org/10.2139/ssrn.4649163. (Note: Included as Chapter 6).

REFERENCES FOR CHAPTER 3

[1] Buddhima Indraratna, Muhammad Babar Sajjad, Trung Ngo, António Gomes Correia, and Richard Kelly. Improved performance of ballasted tracks at transition zones: A review of experimental and modelling approaches. *Transportation Geotechnics*, 21:100260, December 2019. doi: 10.1016/j.trgeo.2019.100260.

[2] R. Sañudo, L. dell'Olio, J.A. Casado, I.A. Carrascal, and S. Diego. Track transitions in railways: A review. *Construction and Building Materials*, 112:140–157, June 2016. doi: 10.1016/j.conbuildmat.2016.02.084.

[3] Haoyu Wang, Ling Chang, and Valeri Markine. Structural health monitoring of railway transition zones using satellite radar data. *Sensors*, 18(2):413, January 2018. doi: 10.3390/s18020413.

[4] E. Fortunato, A. Paixão, and R. Calçada. Railway track transition zones: Design, construction, monitoring and numerical modelling. *International Journal of Railway Technology*, 2(4):33–58, 2013. doi: 10.4203/ijrt.2.4.3.

[5] Akira Namura and Takahiro Suzuki. Evaluation of countermeasures against differential settlement at track transitions. *Quarterly Report of RTRI*, 48(3):176–182, 2007. doi: 10.2219/rtriqr.48.176.

[6] Yue Shang, Maria Nogal, Haoyu Wang, and A. R. M. (Rogier) Wolfert. Systems thinking approach for improving maintenance management of discrete rail assets: a review and future perspectives. *Structure and Infrastructure Engineering*, 19(2): 197–215, June 2021. doi: 10.1080/15732479.2021.1936569.

[7] Karmen Fifer Bizjak, Friderik Knez, Stanislav Lenart, and Katja Slanc. Life-cycle assessment and repair of the railway transition zones of an existing bridge using geocomposite materials. *Structure and Infrastructure Engineering*, 13(3):331–344, 2017. doi: 10.1080/15732479.2016.1158288.

[8] Cristina Alves Ribeiro, André Paixão, Eduardo Fortunato, and Rui Calçada. Under sleeper pads in transition zones at railway underpasses: numerical modelling and experimental validation. *Structure and Infrastructure Engineering*, 11(11):1432–1449, 2015. doi: 10.1080/15732479.2014.970203.

[9] H. Heydari-Noghabi, J. N. Varandas, M. Esmaeili, and J. Zakeri. Investigating the influence of auxiliary rails on dynamic behavior of railway transition zone by a 3d train-track interaction model. *Latin American Journal of Solids and Structures*, 14 (11):2000–2018, 2017. doi: 10.1590/1679-78253906.

[10] A.B. Fărăgău, A. Jain, J.M. de Oliveira Barbosa, A.V. Metrikine, and K.N. van Dalen. Auxiliary rails as a mitigation measure for degradation in transition zones. In J. Pombo, editor, *Proceedings of The Fifth International Conference on Railway Technology: Research, Development and Maintenance*, volume CCC 1 of *Civil-Comp Conferences*, United Kingdom, 2023. Civil-Comp Press. doi: 10.4203/ccc.1.19.4.

[11] Morteza Esmaeili, Hamidreza Heydari-Noghabi, and Mehdi Kamali. Numerical investigation of railway transition zones stiffened with auxiliary rails. *Proceedings of the Institution of Civil Engineers - Transport*, 173(5):299–308, October 2020. doi: 10.1680/jtran.17.00035.

[12] Haoyu Wang and Valeri Markine. Corrective countermeasure for track transition zones in railways: Adjustable fastener. *Engineering Structures*, 169:1–14, August 2018. doi: 10.1016/j.engstruct.2018.05.004.

[13] Wenli Jia, Valeri Markine, Mario Carvalho, David P. Connolly, and Yunlong Guo. Design of a concept wedge-shaped self-levelling railway sleeper. *Construction and Building Materials*, 386:131524, July 2023. doi: 10.1016/j.conbuildmat.2023.131524.

[14] P. Chumyen, D.P. Connolly, P.K. Woodward, and V. Markine. The effect of soil improvement and auxiliary rails at railway track transition zones. *Soil Dynamics and Earthquake Engineering*, 155:107200, April 2022. doi: 10.1016/j.soildyn.2022.107200.

[15] Ping Hu, Chunshun Zhang, Sen Wen, and Yonghe Wang. Dynamic responses of high-speed railway transition zone with various subgrade fillings. *Computers and Geotechnics*, 108:17–26, April 2019. doi: 10.1016/j.compgeo.2018.12.011.

[16] Piyush Punetha and Sanjay Nimbalkar. An innovative rheological approach for predicting the behaviour of critical zones in a railway track. *Acta Geotechnica*, 18 (10):5457–5483, May 2023.

[17] Ernest T. Selig and Dingqing Li. Track modulus: Its meaning and factors influencing it. *Transportation Research Record*, 1994. URL `http://onlinepubs.trb.org/Onlinepubs/trr/1994/1470/1470-006.pdf`.

[18] Avni Jain, Andrei Metrikine, Michael Steenbergen, and Karel van Dalen. Dynamic amplifications in railway transition zones: investigation of key phenomena. Journal of Physics: Conference Series. IOP Publishing, 2023. (Note: Included as Chapter 5).

[19] H Heydari-Noghabi, JA Zakeri, M Esmaeili, and JN Varandas. Field study using additional rails and an approach slab as a transition zone from slab track to the ballasted track. *Proceedings of the Institution of Mechanical Engineers, Part F: Journal of Rail and Rapid Transit*, 232(4):970–978, May 2017. doi: 10.1177/0954409717708527.

[20] Khosrow Asghari, Saeed Sotoudeh, and Jabbar-Ali Zakeri. Numerical evaluation of approach slab influence on transition zone behavior in high-speed railway track. *Transportation Geotechnics*, 28:100519, May 2021. doi: 10.1016/j.trgeo.2021.100519.

[21] A. Jain, A. V. Metrikine, M. J. M. M. Steenbergen, and K. N. van Dalen. Design of railway transition zones: a novel energy-based criterion, 2023. URL `https://arxiv.org/abs/2310.07956`. (Note: Included as Chapter 2).

[22] J.N. Varandas, P. Hölscher, and M.A.G. Silva. Three-dimensional track-ballast interaction model for the study of a culvert transition. *Soil Dynamics and Earthquake Engineering*, 89:116–127, October 2016. doi: 10.1016/j.soildyn.2016.07.013.

[23] Kamil Laco and Viktor Borzovič. Reliability of approach slabs and modelling of transition zones of bridges. *Applied Mechanics and Materials*, 821:741–746, January 2016. doi: 10.4028/www.scientific.net/amm.821.741.

[24] Giacomo Ognibene, William Powrie, Louis Le Pen, and John Harkness. Analysis of a bridge approach: long-term behaviour from short-term response. In *15th Railway Engineering Conference, Edinburgh, U.K.*, pages 1–15, July 2019.

[25] Bruno Zuada Coelho and Michael A Hicks. Numerical analysis of railway transition zones in soft soil. *Proceedings of the Institution of Mechanical Engineers, Part F: Journal of Rail and Rapid Transit*, 230(6):1601–1613, October 2015. doi: 10.1177/0954409715605864.

[26] Akshay Sakhare, Hafsa Farooq, Sanjay Nimbalkar, and Goudappa R. Dodagoudar. Dynamic behavior of the transition zone of an integral abutment bridge. *Sustainability*, 14(7):4118, March 2022. doi: 10.3390/su14074118.

[27] André Paixão, Eduardo Fortunato, and Rui Calçada. A numerical study on the influence of backfill settlements in the train/track interaction at transition zones to railway bridges. *Proceedings of the Institution of Mechanical Engineers, Part F: Journal of Rail and Rapid Transit*, 230(3):866–878, March 2015. doi: 10.1177/0954409715573289.

[28] André Paixão, Eduardo Fortunato, and Rui Calçada. Design and construction of backfills for railway track transition zones. *Proceedings of the Institution of Mechanical Engineers, Part F: Journal of Rail and Rapid Transit*, 229(1):58–70, August 2013. doi: 10.1177/0954409713499016.

[29] Miriam Labrado Palomo, Jesús Herminio Alcañiz Martínez, Adrian Zornoza Arnoa, and Juan José Catalán Medina. Structural and vibration performance in different scenarios of a prefabricated wedge for railway transition zones. *Journal of Vibration Engineering &amp Technologies*, 9(7):1657–1668, May 2021. doi: 10.1007/s42417-021-00319-5.

[30] Cristina Alves Ribeiro, Rui Calçada, and Raimundo Delgado. Calibration and experimental validation of a dynamic model of the train-track system at a culvert transition zone. *Structure and Infrastructure Engineering*, 14(5):604–618, October 2017. doi: 10.1080/15732479.2017.1380674.

[31] André Paixão, Eduardo Fortunato, and Rui Calçada. Transition zones to railway bridges: Track measurements and numerical modelling. *Engineering Structures*, 80:435–443, December 2014. doi: 10.1016/j.engstruct.2014.09.024.

[32] A. Jain, K.N. van Dalen, A.V. Metrikine, A.B. Faragau, and M.J.M.M. Steenbergen. Comparative analysis of the dynamic amplifications due to inhomogeneities at railway transition zones. In J. Pombo, editor, *Proceedings of The Fifth International Conference on Railway Technology: Research, Development and Maintenance*, volume CCC 1 of *Civil-Comp Conferences*, United Kingdom, 2023. Civil-Comp Press. doi: 10.4203/ccc.1.19.1.

[33] Haoyu Wang, Valeri Markine, and Xiangming Liu. Experimental analysis of railway track settlement in transition zones. *Proceedings of the Institution of Mechanical Engineers, Part F: Journal of Rail and Rapid Transit*, 232(6):1774–1789, 2018. doi: 10.1177/0954409717748789. PMID: 30662168.

REFERENCES FOR CHAPTER 4

[1] A. Jain, K.N. van Dalen, A.V. Metrikine, A.B. Faragau, and M.J.M.M. Steenbergen. Comparative analysis of the dynamic amplifications due to inhomogeneities at railway transition zones. In J. Pombo, editor, *Proceedings of The Fifth International Conference on Railway Technology: Research, Development and Maintenance*, volume CCC 1 of *Civil-Comp Conferences*, United Kingdom, 2023. Civil-Comp Press. doi: 10.4203/ccc.1.19.1.

[2] André Paixão, José Nuno Varandas, and Eduardo Fortunato. Dynamic behavior in transition zones and long-term railway track performance. *Frontiers in Built Environment*, 7, 2021. ISSN 2297-3362. doi: 10.3389/fbuil.2021.658909.

[3] Giacomo Ognibene, William Powrie, Louis Le Pen, and John Harkness. Analysis of a bridge approach: long-term behaviour from short-term response. In *15th Railway Engineering Conference, Edinburgh, U.K.*, pages 1–15, July 2019.

[4] C. Charoenwong, D.P. Connolly, A. Colaço, P. Alves Costa, P.K. Woodward, A. Romero, and P. Galvín. Railway slab vs ballasted track: A comparison of track geometry degradation. *Construction and Building Materials*, 378:131121, 2023. ISSN 0950-0618. doi: https://doi.org/10.1016/j.conbuildmat.2023.131121.

[5] A. Jain, A.V. Metrikine, M.J.M.M. Steenbergen, and K.N. van Dalen. Design of railway transition zones: A novel energy-based criterion. *Transportation Geotechnics*, 46: 101223, 2024. ISSN 2214-3912. doi: https://doi.org/10.1016/j.trgeo.2024.101223. (Note: Included as Chapter 2).

[6] J.N. Varandas, P. Hölscher, and M.A.G. Silva. Three-dimensional track-ballast interaction model for the study of a culvert transition. *Soil Dynamics and Earthquake Engineering*, 89:116–127, October 2016. doi: 10.1016/j.soildyn.2016.07.013.

[7] Kamil Laco and Viktor Borzovič. Reliability of approach slabs and modelling of transition zones of bridges. *Applied Mechanics and Materials*, 821:741–746, January 2016. doi: 10.4028/www.scientific.net/amm.821.741.

[8] H Heydari-Noghabi, JA Zakeri, M Esmaeili, and JN Varandas. Field study using additional rails and an approach slab as a transition zone from slab track to the ballasted track. *Proceedings of the Institution of Mechanical Engineers, Part F: Journal of Rail and Rapid Transit*, 232(4):970–978, May 2017. doi: 10.1177/0954409717708527.

[9] André Paixão, Eduardo Fortunato, and Rui Calçada. A numerical study on the influence of backfill settlements in the train/track interaction at transition zones to railway bridges. *Proceedings of the Institution of Mechanical Engineers, Part*

F: Journal of Rail and Rapid Transit, 230(3):866–878, March 2015. doi: 10.1177/0954409715573289. URL https://doi.org/10.1177/0954409715573289.

[10] André Paixão, Eduardo Fortunato, and Rui Calçada. Design and construction of backfills for railway track transition zones. *Proceedings of the Institution of Mechanical Engineers, Part F: Journal of Rail and Rapid Transit*, 229(1):58–70, August 2013. doi: 10.1177/0954409713499016. URL https://doi.org/10.1177/0954409713499016.

[11] Miriam Labrado Palomo, Jesús Herminio Alcañiz Martínez, Adrian Zornoza Arnoa, and Juan José Catalán Medina. Structural and vibration performance in different scenarios of a prefabricated wedge for railway transition zones. *Journal of Vibration Engineering and Technologies*, 9(7):1657–1668, May 2021. doi: 10.1007/s42417-021-00319-5. URL https://doi.org/10.1007/s42417-021-00319-5.

[12] Cristina Alves Ribeiro, Rui Calçada, and Raimundo Delgado. Calibration and experimental validation of a dynamic model of the train-track system at a culvert transition zone. *Structure and Infrastructure Engineering*, 14(5):604–618, October 2017. doi: 10.1080/15732479.2017.1380674.

[13] André Paixão, Eduardo Fortunato, and Rui Calçada. Transition zones to railway bridges: Track measurements and numerical modelling. *Engineering Structures*, 80:435–443, December 2014. doi: 10.1016/j.engstruct.2014.09.024. URL https://doi.org/10.1016/j.engstruct.2014.09.024.

[14] Ping Hu, Chunshun Zhang, Sen Wen, and Yonghe Wang. Dynamic responses of high-speed railway transition zone with various subgrade fillings. *Computers and Geotechnics*, 108:17–26, April 2019. doi: 10.1016/j.compgeo.2018.12.011. URL https://doi.org/10.1016/j.compgeo.2018.12.011.

[15] P. Chumyen, D.P. Connolly, P.K. Woodward, and V. Markine. The effect of soil improvement and auxiliary rails at railway track transition zones. *Soil Dynamics and Earthquake Engineering*, 155:107200, April 2022. doi: 10.1016/j.soildyn.2022.107200. URL https://doi.org/10.1016/j.soildyn.2022.107200.

[16] H. Heydari-Noghabi, J. N. Varandas, M. Esmaeili, and J. Zakeri. Investigating the influence of auxiliary rails on dynamic behavior of railway transition zone by a 3d train-track interaction model. *Latin American Journal of Solids and Structures*, 14 (11):2000–2018, 2017. doi: 10.1590/1679-78253906. URL https://doi.org/10.1590/1679-78253906.

[17] A. B. Fărăgău, A. Jain, J.M. de Oliveira Barbosa, A.V. Metrikine, and K.N. van Dalen. Auxiliary rails as a mitigation measure for degradation in transition zones. In J. Pombo, editor, *Proceedings of The Fifth International Conference on Railway Technology: Research, Development and Maintenance*, volume CCC 1 of *Civil-Comp Conferences*, United Kingdom, 2023. Civil-Comp Press. doi: 10.4203/ccc.1.19.4.

[18] Akira Namura and Takahiro Suzuki. Evaluation of countermeasures against differential settlement at track transitions. *Quarterly Report of RTRI*, 48(3):176–182, 2007. doi: 10.2219/rtriqr.48.176.

[19] Buddhima Indraratna, Muhammad Babar Sajjad, Trung Ngo, António Gomes Correia, and Richard Kelly. Improved performance of ballasted tracks at transition zones: A review of experimental and modelling approaches. *Transportation Geotechnics*, 21:100260, December 2019. doi: 10.1016/j.trgeo.2019.100260. URL https://doi.org/10.1016/j.trgeo.2019.100260.

[20] R. Sañudo, L. dell'Olio, J.A. Casado, I.A. Carrascal, and S. Diego. Track transitions in railways: A review. *Construction and Building Materials*, 112:140–157, June 2016. doi: 10.1016/j.conbuildmat.2016.02.084. URL https://doi.org/10.1016/j.conbuildmat.2016.02.084.

[21] Mojtaba Shahraki and Karl Josef Witt. 3d modeling of transition zone between ballasted and ballastless high-speed railway track. *Journal of Traffic and Transportation Engineering*, 3(4), April 2015. doi: 10.17265/2328-2142/2015.04.005. URL https://doi.org/10.17265/2328-2142/2015.04.005.

[22] Mojtaba Shahraki, Chanaka Warnakulasooriya, and Karl Josef Witt. Numerical study of transition zone between ballasted and ballastless railway track. *Transportation Geotechnics*, 3:58–67, June 2015. doi: 10.1016/j.trgeo.2015.05.001. URL https://doi.org/10.1016/j.trgeo.2015.05.001.

[23] Stephen T Wilk, Timothy D Stark, and Jerry G Rose. Evaluating tie support at railway bridge transitions. *Proceedings of the Institution of Mechanical Engineers, Part F: Journal of Rail and Rapid Transit*, 230(4):1336–1350, July 2015. doi: 10.1177/0954409715596192. URL https://doi.org/10.1177/0954409715596192.

[24] José María Galván Giménez. Estudio por elementos finitos de la transición vía con balasto-vía en placa. 2011.

[25] David Read and Dingqing Li. Design of track transitions. *TCRP research results digest*, (79), 2006.

[26] Transportation Research Board and National Academies of Sciences, Engineering, and Medicine. *Design of Track Transitions*. The National Academies Press, Washington, DC, 2006. doi: 10.17226/23228. URL https://nap.nationalacademies.org/catalog/23228/design-of-track-transitions.

[27] Anand Raj, Chayut Ngamkhanong, Lapyote Prasittisopin, and Sakdirat Kaewunruen. Nonlinear dynamic responses of ballasted railway tracks using concrete sleepers incorporated with reinforced fibres and pre-treated crumb rubber. *Nonlinear Engineering*, 12(1):20220320, 2023. doi: doi:10.1515/nleng-2022-0320. URL https://doi.org/10.1515/nleng-2022-0320.

[28] Nicks and Jennifer Elizabeth. *The Bump at the End of the Railway Bridge*. PhD thesis, Texas AM University., 2009. URL https://hdl.handle.net/1969.1/ETD-TAMU-2009-12-7432.

[29] Roberto Sañudo, Marina Miranda, Borja Alonso, and Valeri Markine. Sleepers spacing analysis in railway track infrastructure. *Infrastructures*, 7(6):83, June

2022. doi: 10.3390/infrastructures7060083. URL https://doi.org/10.3390/infrastructures7060083.

[30] Roberto Sañudo Ortega, Joao Pombo, Stefano Ricci, and Marina Miranda. The importance of sleepers spacing in railways. *Construction and Building Materials*, 300:124326, 2021. ISSN 0950-0618. doi: https://doi.org/10.1016/j.conbuildmat.2021.124326. URL https://www.sciencedirect.com/science/article/pii/S0950061821020857.

[31] Akira Namura, Yukihiro Kohata, and Seiichi Miura. Effect of sleeper size on ballasted track settlement. *Quarterly Report of RTRI*, 45(3):156–161, 2004. doi: 10.2219/rtriqr.45.156.

[32] Roberto Sañudo, Mikel Cerrada, Borja Alonso, and Luigi dell'Olio. Analysis of the influence of support positions in transition zones. a numerical analysis. *Construction and Building Materials*, 145:207–217, August 2017. doi: 10.1016/j.conbuildmat.2017.03.204. URL https://doi.org/10.1016/j.conbuildmat.2017.03.204.

[33] A. Jain, A.V. Metrikine, M.J.M.M. Steenbergen, and K.N. van Dalen. Railway transition zones: evaluation of existing transition structures and a newly proposed transition structure. *International Journal of Rail Transportation*, 0(0):1–21, 2023. doi: 10.1080/23248378.2023.2272668. (Note: Included as Chapter 3).

[34] Timothy D Stark and Stephen T Wilk. Root cause of differential movement at bridge transition zones. *Proceedings of the Institution of Mechanical Engineers, Part F: Journal of Rail and Rapid Transit*, 230(4):1257–1269, June 2015. doi: 10.1177/0954409715589620. URL https://doi.org/10.1177/0954409715589620.

[35] Mohammad Siahkouhi, Junyi Wang, Xiaodong Han, Peyman Aela, Yi-Qing Ni, and Guoqing Jing. Railway ballast track hanging sleeper defect detection using a smart cnt self-sensing concrete railway sleeper. 2023. doi: 10.2139/ssrn.4414996. URL https://doi.org/10.2139/ssrn.4414996.

[36] Avni Jain, Yuriy Marykovskiy, Andrei V. Metrikine, and Karel N. van Dalen. Quantifying the impact of stiffness distributions on the dynamic behaviour of railway transition zones. *Transportation Geotechnics*, 45:101211, 2024. ISSN 2214-3912. doi: https://doi.org/10.1016/j.trgeo.2024.101211. URL https://www.sciencedirect.com/science/article/pii/S2214391224000321. (Note: Included as Chapter 6).

[37] ABAQUS/Standard User's Manual. *ABAQUS/Standard User's Manual, Version 6.9*, 2009. URL http://130.149.89.49:2080/v6.9/books/usb/default.htm.

[38] Haoyu Wang and Valeri Markine. Corrective countermeasure for track transition zones in railways: Adjustable fastener. *Engineering Structures*, 169:1–14, August 2018. doi: 10.1016/j.engstruct.2018.05.004.

[39] Wenli Jia, Valeri Markine, Mario Carvalho, David P. Connolly, and Yunlong Guo. Design of a concept wedge-shaped self-levelling railway sleeper. *Construction and Building Materials*, 386:131524, July 2023. doi: 10.1016/j.conbuildmat.2023.131524.

REFERENCES FOR CHAPTER 5

[1] B Coelho, P Hölscher, J Priest, W Powrie, and F Barends. An assessment of transition zone performance. *Proceedings of the Institution of Mechanical Engineers, Part F: Journal of Rail and Rapid Transit*, 225(2):129–139, February 2011. doi: 10.1177/09544097jrrt389. URL https://doi.org/10.1177/09544097jrrt389.

[2] R. Sañudo, L. dell'Olio, J.A. Casado, I.A. Carrascal, and S. Diego. Track transitions in railways: A review. *Construction and Building Materials*, 112:140–157, June 2016. doi: 10.1016/j.conbuildmat.2016.02.084. URL https://doi.org/10.1016/j.conbuildmat.2016.02.084.

[3] Buddhima Indraratna, Muhammad Babar Sajjad, Trung Ngo, António Gomes Correia, and Richard Kelly. Improved performance of ballasted tracks at transition zones: A review of experimental and modelling approaches. *Transportation Geotechnics*, 21: 100260, December 2019. doi: 10.1016/j.trgeo.2019.100260. URL https://doi.org/10.1016/j.trgeo.2019.100260.

[4] A. Jain, A.V. Metrikine, M.J.M.M. Steenbergen, and K.N. Dalen. Design of railway transition zones: a novel energy-based criterion. *Transportation Geotechnics*, page 101223, 2024. ISSN 2214-3912. doi: https://doi.org/10.1016/j.trgeo.2024.101223. URL https://www.sciencedirect.com/science/article/pii/S2214391224000448. (Note: Included as Chapter 2).

[5] A. Jain, K. N. van Dalen, A. V. Metrikine, Andrei Fărăgău, and M. J. M. M. Steenbergen. Comparative analysis of the dynamic amplifications due to inhomogeneities at railway transition zones. In J. Pombo, editor, *Proceedings of The Fifth International Conference on Railway Technology: Research, Development and Maintenance*, Edinburgh, UK, 2022. Civil-Comp Press.

[6] *ABAQUS/Standard User's Manual, Version 6.9*. Dassault Systèmes Simulia Corp, United States.

REFERENCES FOR CHAPTER 6

[1] Akira Namura and Takahiro Suzuki. Evaluation of countermeasures against differential settlement at track transitions. *Quarterly Report of RTRI*, 48(3):176–182, 2007. doi: 10.2219/rtriqr.48.176.

[2] Buddhima Indraratna, Muhammad Babar Sajjad, Trung Ngo, António Gomes Correia, and Richard Kelly. Improved performance of ballasted tracks at transition zones: A review of experimental and modelling approaches. *Transportation Geotechnics*, 21:100260, December 2019. doi: 10.1016/j.trgeo.2019.100260.

[3] R. Sañudo, L. dell'Olio, J.A. Casado, I.A. Carrascal, and S. Diego. Track transitions in railways: A review. *Construction and Building Materials*, 112:140–157, June 2016. doi: 10.1016/j.conbuildmat.2016.02.084.

[4] Bruno Zuada Coelho and Michael A Hicks. Numerical analysis of railway transition zones in soft soil. *Proceedings of the Institution of Mechanical Engineers, Part F: Journal of Rail and Rapid Transit*, 230(6):1601–1613, October 2015. doi: 10.1177/0954409715605864.

[5] Ernest T. Selig and Dingqing Li. Track modulus: Its meaning and factors influencing it. *Transportation Research Record*, 1994. URL `http://onlinepubs.trb.org/Onlinepubs/trr/1994/1470/1470-006.pdf`.

[6] E. Fortunato, A. Paixão, and R. Calçada. Railway track transition zones: Design, construction, monitoring and numerical modelling. *International Journal of Railway Technology*, 2(4):33–58, 2013. doi: 10.4203/ijrt.2.4.3.

[7] Jabbar Ali Zakeri and He Xia. Sensitivity analysis of track parameters on train-track dynamic interaction. *Journal of Mechanical Science and Technology*, 22(7):1299–1304, July 2008. ISSN 1976-3824. doi: 10.1007/s12206-008-0316-x. URL `http://dx.doi.org/10.1007/s12206-008-0316-x`.

[8] A. Jain, A. V. Metrikine, M. J. M. M. Steenbergen, and K. N. van Dalen. Design of railway transition zones: a novel energy-based criterion, 2023. URL `https://arxiv.org/abs/2310.07956`. (Note: Included as Chapter 2).

[9] João M. de Oliveira Barbosa, Andrei B. Fărăgău, Karel N. van Dalen, and Michael J.M.M Steenbergen. Modelling ballast via a non-linear lattice to assess its compaction behaviour at railway transition zones. *Journal of Sound and Vibration*, 530:116942, 2022. ISSN 0022-460X.

[10] Avni Jain, Andrei Metrikine, Michael Steenbergen, and Karel van Dalen. Dynamic amplifications in railway transition zones: investigation of key phenomena. Journal of Physics: Conference Series. IOP Publishing, 2023. (Note: Included as Chapter 5).

[11] A. Jain, K.N. van Dalen, A.V. Metrikine, A.B. Faragau, and M.J.M.M. Steenbergen. Comparative analysis of the dynamic amplifications due to inhomogeneities at railway transition zones. In J. Pombo, editor, *Proceedings of The Fifth International Conference on Railway Technology: Research, Development and Maintenance*, volume CCC 1 of *Civil-Comp Conferences*, United Kingdom, 2023. Civil-Comp Press. doi: 10.4203/ccc.1.19.1.

[12] Yao Shan, Yao Shu, and Shunhua Zhou. Finite-infinite element coupled analysis on the influence of material parameters on the dynamic properties of transition zones. *Construction and Building Materials*, 148:548–558, 2017. ISSN 0950-0618. doi: https://doi.org/10.1016/j.conbuildmat.2017.05.071.

[13] Yao Shan, Xinran Li, and Shunhua Zhou. Multi-objective optimisation methodology for stiffness combination design of bridge-embankment transition zones in high-speed railways. *Computers and Geotechnics*, 155:105242, 2023. ISSN 0266-352X. doi: https://doi.org/10.1016/j.compgeo.2022.105242.

[14] J.N. Varandas, P. Hölscher, and M.A.G. Silva. Three-dimensional track-ballast interaction model for the study of a culvert transition. *Soil Dynamics and Earthquake Engineering*, 89:116–127, October 2016. doi: 10.1016/j.soildyn.2016.07.013.

[15] Giacomo Ognibene, William Powrie, Louis Le Pen, and John Harkness. Analysis of a bridge approach: long-term behaviour from short-term response. In *15th Railway Engineering Conference, Edinburgh, U.K.*, pages 1–15, July 2019.

[16] H Heydari-Noghabi, JA Zakeri, M Esmaeili, and JN Varandas. Field study using additional rails and an approach slab as a transition zone from slab track to the ballasted track. *Proceedings of the Institution of Mechanical Engineers, Part F: Journal of Rail and Rapid Transit*, 232(4):970–978, May 2017. doi: 10.1177/0954409717708527.

[17] Bruno Zuada Coelho and Michael A Hicks. Numerical analysis of railway transition zones in soft soil. *Proceedings of the Institution of Mechanical Engineers, Part F: Journal of Rail and Rapid Transit*, 230(6):1601–1613, October 2015. doi: 10.1177/0954409715605864.

[18] André Paixão, Eduardo Fortunato, and Rui Calçada. A numerical study on the influence of backfill settlements in the train/track interaction at transition zones to railway bridges. *Proceedings of the Institution of Mechanical Engineers, Part F: Journal of Rail and Rapid Transit*, 230(3):866–878, March 2015. doi: 10.1177/0954409715573289.

[19] André Paixão, Eduardo Fortunato, and Rui Calçada. Design and construction of backfills for railway track transition zones. *Proceedings of the Institution of Mechanical Engineers, Part F: Journal of Rail and Rapid Transit*, 229(1):58–70, August 2013. doi: 10.1177/0954409713499016.

[20] Miriam Labrado Palomo, Jesús Herminio Alcañiz Martínez, Adrian Zornoza Arnoa, and Juan José Catalán Medina. Structural and vibration performance in different scenarios of a prefabricated wedge for railway transition zones. *Journal of Vibration Engineering &amp Technologies*, 9(7):1657–1668, May 2021. doi: 10.1007/s42417-021-00319-5.

[21] Cristina Alves Ribeiro, Rui Calçada, and Raimundo Delgado. Calibration and experimental validation of a dynamic model of the train-track system at a culvert transition zone. *Structure and Infrastructure Engineering*, 14(5):604–618, October 2017. doi: 10.1080/15732479.2017.1380674.

[22] Lei Zhang, Xin Jiang, Zhenkun Li, Zhonghao Yang, Gang Liu, Zhichen Dong, and Yanjun Qiu. Influence of the attenuation of subgrade elastic modulus caused by precipitation on ballasted track structure. *Construction and Building Materials*, 352: 128971, October 2022. ISSN 0950-0618. doi: 10.1016/j.conbuildmat.2022.128971. URL http://dx.doi.org/10.1016/j.conbuildmat.2022.128971.

[23] Xiaopei Cai, Yanke Liang, Tao Xin, Chaozhi Ma, and Haoyu Wang. Assessing the effects of subgrade frost heave on vehicle dynamic behaviors on high-speed railway. *Cold Regions Science and Technology*, 158:95–105, 2019. ISSN 0165-232X. doi: https://doi.org/10.1016/j.coldregions.2018.11.009.

[24] Haoyu Wang, Mika Silvast, Valeri Markine, and Bruce Wiljanen. Analysis of the dynamic wheel loads in railway transition zones considering the moisture condition of the ballast and subballast. *Applied Sciences*, 7(12):1208, November 2017. ISSN 2076-3417. doi: 10.3390/app7121208. URL http://dx.doi.org/10.3390/app7121208.

[25] I. Gallego, J. Muñoz, A. Rivas, and S. Sánchez-Cambronero. Vertical track stiffness as a new parameter involved in designing high-speed railway infrastructure. *Journal of Transportation Engineering*, 137(12):971–979, December 2011. ISSN 1943-5436. doi: 10.1061/(asce)te.1943-5436.0000288. URL http://dx.doi.org/10.1061/(ASCE)TE.1943-5436.0000288.

[26] A. Jain, A. V. Metrikine, M. J. M. M. Steenbergen, and K. N. van Dalen. Railway transition zones: evaluation of existing transition structures and a newly proposed transition structure. *International Journal of Rail Transportation*, pages 1–21, 2023. doi: 10.1080/23248378.2023.2272668. (Note: Included as Chapter 3).

[27] A.B. Fărăgău, A. Jain, J.M. de Oliveira Barbosa, A.V. Metrikine, and K.N. van Dalen. Auxiliary rails as a mitigation measure for degradation in transition zones. In J. Pombo, editor, *Proceedings of The Fifth International Conference on Railway Technology: Research, Development and Maintenance*, volume CCC 1 of *Civil-Comp Conferences*, United Kingdom, 2023. Civil-Comp Press. doi: 10.4203/ccc.1.19.4.

[28] Stefano Marelli and Bruno Sudret. Uqlab: A framework for uncertainty quantification in matlab. In *Vulnerability, Uncertainty, and Risk*. American Society of Civil Engineers, June 2014. doi: 10.1061/9780784413609.257. URL http://dx.doi.org/10.1061/9780784413609.257.

[29] *ABAQUS/Standard User's Manual, Version 6.9*. Dassault Systèmes Simulia Corp, United States.

[30] *Abaqus Theory Manual (V6.6)*. Dassault Systèmes Simulia Corp, United States. URL https://classes.engineering.wustl.edu/2009/spring/mase5513/abaqus/docs/v6.6/books/stm/default.htm?startat=ch01s05ath12.html.

[31] Rodrigues André Filipe da Silva. Viability and Applicability of Simplified Models for the Dynamic Analysis of Ballasted Railway Tracks, 2017. URL http://hdl.handle.net/10362/21663.

[32] Bruno Sudret. Global sensitivity analysis using polynomial chaos expansions. *Reliability Engineering and System Safety*, 93(7):964–979, 2008. doi: https://doi.org/10.1016/j.ress.2007.04.002.

[33] Mohammadreza Mohammadi, Araliya Mosleh, Mehran Razzaghi, Pedro Alves Costa, and Rui Calçada. Stochastic analysis of railway embankment with uncertain soil parameters using polynomial chaos expansion. *Structure and Infrastructure Engineering*, 2022. doi: 10.1080/15732479.2022.2033277.

[34] Stefano Marelli and Bruno Sudret. Uqlab: A framework for uncertainty quantification in matlab. *Vulnerability, Uncertainty, and Risk*, pages 2554–2563, 2014. doi: 10.1061/9780784413609.257. URL https://ascelibrary.org/doi/abs/10.1061/9780784413609.257.

[35] Géraud Blatman. *Adaptive sparse polynomial chaos expansion for uncertainty propagation and sensitivity analysis*. PhD thesis, Blaise Pascal University - Clermont, 2009.

[36] Géraud Blatman and Bruno Sudret. Adaptive sparse polynomial chaos expansion based on least angle regression. *Journal of Computational Physics*, 230(6):2345–2367, 2011. ISSN 0021-9991. doi: https://doi.org/10.1016/j.jcp.2010.12.021.

[37] F. Huber. *A Logical Introduction to Probability and Induction*. Oxford University Press, 2018. ISBN 9780190845414.

[38] Robert V. Hogg and Allen T. Craig. *Introduction to Mathematical Statistics*. 1959. URL https://api.semanticscholar.org/CorpusID:122755063.

[39] W. Maurice Ewing, Wenceslas S. Jardetzky, and Frank Press. *Elastic Waves in Layered Media*. McGraw-Hill Publishing Co., 1957.

[40] J.D.Achenbach. *Wave Propagation in Elastic Solids*. Applied Mathematics and Mechanics Series. North-Holland Publishing Company, 1973. ISBN 9780720403251.

REFERENCES FOR CHAPTER 7

[1] E. Fortunato, A. Paixão, and R. Calçada. Railway track transition zones: Design, construction, monitoring and numerical modelling. *International Journal of Railway Technology*, 2(4):33–58, 2013. doi: 10.4203/ijrt.2.4.3.

[2] *Design of Track Transitions*. Transportation Research Board, October 2006. ISBN 9780309436670. doi: 10.17226/23228. URL http://dx.doi.org/10.17226/23228.

[3] Akira NAMURA and Takahiro SUZUKI. Evaluation of countermeasures against differential settlement at track transitions. *Quarterly Report of RTRI*, 48(3):176–182, 2007. doi: 10.2219/rtriqr.48.176.

[4] B Coelho, P Hölscher, J Priest, W Powrie, and F Barends. An assessment of transition zone performance. *Proceedings of the Institution of Mechanical Engineers, Part F: Journal of Rail and Rapid Transit*, 225(2):129–139, February 2011. ISSN 2041-3017. doi: 10.1177/09544097jrrt389. URL http://dx.doi.org/10.1177/09544097JRRT389.

[5] Buddhima Indraratna, Muhammad Babar Sajjad, Trung Ngo, António Gomes Correia, and Richard Kelly. Improved performance of ballasted tracks at transition zones: A review of experimental and modelling approaches. *Transportation Geotechnics*, 21:100260, December 2019. doi: 10.1016/j.trgeo.2019.100260.

[6] R. Sañudo, L. dell'Olio, J.A. Casado, I.A. Carrascal, and S. Diego. Track transitions in railways: A review. *Construction and Building Materials*, 112:140–157, June 2016. doi: 10.1016/j.conbuildmat.2016.02.084.

[7] A.V. Metrikine, A.R.M. Wolfert, and H.A. Dieterman. Transition radiation in an elastically supported string. abrupt and smooth variations of the support stiffness. *Wave Motion*, 27(4):291–305, 1998. ISSN 0165-2125. doi: https://doi.org/10.1016/S0165-2125(97)00055-3. URL https://www.sciencedirect.com/science/article/pii/S0165212597000553.

[8] H E M and HUNT. Settlement of railway track near bridge abutments. (third paper in young railway engineer of the year (1996) award). *Proceedings of the Institution of Civil Engineers - Transport*, 123(1):68–73, 1997. doi: 10.1680/itran.1997.29182. URL https://doi.org/10.1680/itran.1997.29182.

[9] Timothy D Stark and Stephen T Wilk. Root cause of differential movement at bridge transition zones. *Proceedings of the Institution of Mechanical Engineers, Part F: Journal of Rail and Rapid Transit*, 230(4):1257–1269, June 2015. ISSN

2041-3017. doi: 10.1177/0954409715589620. URL http://dx.doi.org/10.1177/0954409715589620.

[10] Jens CO Nielsen, Eric G Berggren, Anders Hammar, Fredrik Jansson, and Rikard Bolmsvik. Degradation of railway track geometry – correlation between track stiffness gradient and differential settlement. *Proceedings of the Institution of Mechanical Engineers, Part F: Journal of Rail and Rapid Transit*, 234(1):108–119, December 2018. ISSN 2041-3017. doi: 10.1177/0954409718819581. URL http://dx.doi.org/10.1177/0954409718819581.

[11] A. Jain, A.V. Metrikine, M.J.M.M. Steenbergen, and K.N. Dalen. Design of railway transition zones: a novel energy-based criterion. *Transportation Geotechnics*, page 101223, 2024. ISSN 2214-3912. doi: https://doi.org/10.1016/j.trgeo.2024.101223. URL https://www.sciencedirect.com/science/article/pii/S2214391224000448. (Note: Included as Chapter 2).

[12] Giacomo Ognibene, William Powrie, Louis Le Pen, and John Harkness. Analysis of a bridge approach: long-term behaviour from short-term response. In *15th Railway Engineering Conference, Edinburgh, U.K.*, pages 1–15, July 2019.

[13] Akshay Sakhare, Hafsa Farooq, Sanjay Nimbalkar, and Goudappa R. Dodagoudar. Dynamic behavior of the transition zone of an integral abutment bridge. *Sustainability*, 14(7):4118, March 2022. doi: 10.3390/su14074118.

[14] R. Calçada A. Ramos, A. Gomes Correia and P. Alves Costa. Stress and permanent deformation amplification factors in subgrade induced by dynamic mechanisms in track structures. *International Journal of Rail Transportation*, 10(3):298–330, 2022. doi: 10.1080/23248378.2021.1922317. URL https://doi.org/10.1080/23248378.2021.1922317.

[15] Ana Ramos, António Gomes Correia, Pedro Alves Costa, and Rui Calçada. Influence of track irregularities in the stress levels of the ballasted and ballastless tracks. In Erol Tutumluer, Xiaobin Chen, and Yuanjie Xiao, editors, *Advances in Environmental Vibration and Transportation Geodynamics*, pages 601–612, Singapore, 2020. Springer Singapore.

[16] J.N. Varandas, P. Hölscher, and M.A.G. Silva. Three-dimensional track-ballast interaction model for the study of a culvert transition. *Soil Dynamics and Earthquake Engineering*, 89:116–127, 2016. ISSN 0267-7261. doi: https://doi.org/10.1016/j.soildyn.2016.07.013. URL https://www.sciencedirect.com/science/article/pii/S0267726116300926.

[17] Yao Shan, Bettina Albers, and Stavros A. Savidis. Influence of different transition zones on the dynamic response of track–subgrade systems. *Computers and Geotechnics*, 48:21–28, 2013. ISSN 0266-352X. doi: https://doi.org/10.1016/j.compgeo.2012.09.006. URL https://www.sciencedirect.com/science/article/pii/S0266352X12001887.

[18] P. Galvín, A. Romero, and J. Domínguez. Fully three-dimensional analysis of high-speed train–track–soil-structure dynamic interaction. *Journal of Sound and Vibration*, 329(24):5147–5163, 2010. ISSN 0022-460X. doi: https://doi.org/10.1016/j.jsv.2010.06.016. URL https://www.sciencedirect.com/science/article/pii/S0022460X10004062.

[19] Meysam Banimahd, Peter K. Woodward, Justin Kennedy, and Gabriela M. Medero. Behaviour of train–track interaction in stiffness transitions. *Proceedings of the Institution of Civil Engineers - Transport*, 165(3):205–214, 2012. doi: 10.1680/tran.10.00030. URL https://doi.org/10.1680/tran.10.00030.

[20] Kamil Laco and Viktor Borzovič. Reliability of approach slabs and modelling of transition zones of bridges. *Applied Mechanics and Materials*, 821:741–746, January 2016. doi: 10.4028/www.scientific.net/amm.821.741.

[21] H Heydari-Noghabi, JA Zakeri, M Esmaeili, and JN Varandas. Field study using additional rails and an approach slab as a transition zone from slab track to the ballasted track. *Proceedings of the Institution of Mechanical Engineers, Part F: Journal of Rail and Rapid Transit*, 232(4):970–978, May 2017. doi: 10.1177/0954409717708527.

[22] Bruno Zuada Coelho and Michael A Hicks. Numerical analysis of railway transition zones in soft soil. *Proceedings of the Institution of Mechanical Engineers, Part F: Journal of Rail and Rapid Transit*, 230(6):1601–1613, October 2015. doi: 10.1177/0954409715605864.

[23] Khosrow Asghari, Saeed Sotoudeh, and Jabbar-Ali Zakeri. Numerical evaluation of approach slab influence on transition zone behavior in high-speed railway track. *Transportation Geotechnics*, 28:100519, May 2021. doi: 10.1016/j.trgeo.2021.100519.

[24] Ping Hu, Chunshun Zhang, Sen Wen, and Yonghe Wang. Dynamic responses of high-speed railway transition zone with various subgrade fillings. *Computers and Geotechnics*, 108:17–26, April 2019. doi: 10.1016/j.compgeo.2018.12.011.

[25] André Paixão, Eduardo Fortunato, and Rui Calçada. A numerical study on the influence of backfill settlements in the train/track interaction at transition zones to railway bridges. *Proceedings of the Institution of Mechanical Engineers, Part F: Journal of Rail and Rapid Transit*, 230(3):866–878, March 2015. doi: 10.1177/0954409715573289.

[26] André Paixão, Eduardo Fortunato, and Rui Calçada. Design and construction of backfills for railway track transition zones. *Proceedings of the Institution of Mechanical Engineers, Part F: Journal of Rail and Rapid Transit*, 229(1):58–70, August 2013. doi: 10.1177/0954409713499016.

[27] Miriam Labrado Palomo, Jesús Herminio Alcañiz Martínez, Adrian Zornoza Arnoa, and Juan José Catalán Medina. Structural and vibration performance in different scenarios of a prefabricated wedge for railway transition zones. *Journal of Vibration Engineering &amp Technologies*, 9(7):1657–1668, May 2021. doi: 10.1007/s42417-021-00319-5.

[28] Morteza Esmaeili, Hamidreza Heydari-Noghabi, and Mehdi Kamali. Numerical investigation of railway transition zones stiffened with auxiliary rails. *Proceedings of the Institution of Civil Engineers - Transport*, 173(5):299–308, October 2020. doi: 10.1680/jtran.17.00035.

[29] H. Heydari-Noghabi, J. N. Varandas, M. Esmaeili, and J. Zakeri. Investigating the influence of auxiliary rails on dynamic behavior of railway transition zone by a 3d train-track interaction model. *Latin American Journal of Solids and Structures*, 14 (11):2000–2018, 2017. doi: 10.1590/1679-78253906.

[30] Avni Jain, Andrei V. Metrikine, Michaël J. M. M. Steenbergen, and Karel N. van Dalen. Dynamic amplifications in railway transition zones: performance evaluation of sleeper configurations using energy criterion. *Frontiers in Built Environment*, 10, 2024. ISSN 2297-3362. doi: 10.3389/fbuil.2024.1285131. URL https://www.frontiersin.org/journals/built-environment/articles/10.3389/fbuil.2024.1285131. (Note: Included as Chapter 4).

[31] Cristina Alves Ribeiro, André Paixão, Eduardo Fortunato, and Rui Calçada. Under sleeper pads in transition zones at railway underpasses: numerical modelling and experimental validation. *Structure and Infrastructure Engineering*, 11(11):1432–1449, 2015. doi: 10.1080/15732479.2014.970203.

[32] Karmen Fifer Bizjak, Friderik Knez, Stanislav Lenart, and Katja Slanc. Life-cycle assessment and repair of the railway transition zones of an existing bridge using geocomposite materials. *Structure and Infrastructure Engineering*, 13(3):331–344, 2017. doi: 10.1080/15732479.2016.1158288.

[33] Wenli Jia, Valeri Markine, Mario Carvalho, David P. Connolly, and Yunlong Guo. Design of a concept wedge-shaped self-levelling railway sleeper. *Construction and Building Materials*, 386:131524, July 2023. doi: 10.1016/j.conbuildmat.2023.131524.

[34] A. Jain, A.V. Metrikine, M.J.M.M. Steenbergen, and K.N. van Dalen. Railway transition zones: evaluation of existing transition structures and a newly proposed transition structure. *International Journal of Rail Transportation*, 0(0):1–21, 2023. doi: 10.1080/23248378.2023.2272668. (Note: Included as Chapter 3).

[35] Karel N. van Dalen and Andrei V. Metrikine. Transition radiation of elastic waves at the interface of two elastic half-planes. *Journal of Sound and Vibration*, 310(3):702–717, 2008. ISSN 0022-460X. doi: https://doi.org/10.1016/j.jsv.2007.06.007. URL https://www.sciencedirect.com/science/article/pii/S0022460X07004397. EUROMECH Colloquium 484 on Wave Mechanics and Stability of Long Flexible Structures Subject to Moving Loads and Flows.

[36] Karel N. van Dalen, Apostolos Tsouvalas, Andrei V. Metrikine, and Jeroen S. Hoving. Transition radiation excited by a surface load that moves over the interface of two elastic layers. *International Journal of Solids and Structures*, 73-74:99–112, 2015. ISSN 0020-7683. doi: https://doi.org/10.1016/j.ijsolstr.2015.07.001. URL https://www.sciencedirect.com/science/article/pii/S0020768315002978.

[37] Karel van Dalen and Michael Steenbergen. Modeling of train-induced transitional wavefields. In J Pombo, editor, *Proceedings of the 3rd international conference on railway technology*, pages 1–16, United Kingdom, 2016. Civil-Comp Press. ISBN 978-1-905088-65-2. doi: 10.4203/ccp.110.199. URL http://www.civil-comp.com/conf/rw2016/rw2016_flyer.pdf.

[38] A. Jain, K.N. van Dalen, M.J.M.M. Steenbergen, and A.V. Metrikine. Dynamic amplifications in railway transition zones: investigation of key phenomena. *Journal of Physics: Conference Series*, 2647(15):152002, jun 2024. doi: 10.1088/1742-6596/2647/15/152002. URL https://dx.doi.org/10.1088/1742-6596/2647/15/152002. (Note: Included as Chapter 5).

[39] Avni Jain, Yuriy Marykovskiy, Andrei V. Metrikine, and Karel N. van Dalen. Quantifying the impact of stiffness distributions on the dynamic behaviour of railway transition zones. *Transportation Geotechnics*, 45:101211, 2024. ISSN 2214-3912. doi: https://doi.org/10.1016/j.trgeo.2024.101211. URL https://www.sciencedirect.com/science/article/pii/S2214391224000321. (Note: Included as Chapter 6).

[40] *ABAQUS/Standard User's Manual, Version 6.9*. Dassault Systèmes Simulia Corp, United States.

[41] Haoyu Wang and Valeri Markine. Modelling of the long-term behaviour of transition zones: Prediction of track settlement. *Engineering Structures*, 156:294–304, 2018. ISSN 0141-0296. doi: https://doi.org/10.1016/j.engstruct.2017.11.038. URL https://www.sciencedirect.com/science/article/pii/S0141029617315110.

[42] Haoyu Wang, Valeri Markine, and Xiangming Liu. Experimental analysis of railway track settlement in transition zones. *Proceedings of the Institution of Mechanical Engineers, Part F: Journal of Rail and Rapid Transit*, 232(6):1774–1789, 2018. doi: 10.1177/0954409717748789. PMID: 30662168.

[43] Haoyu Wang and Valeri Markine. Dynamic behaviour of the track in transitions zones considering the differential settlement. *Journal of Sound and Vibration*, 459:114863, 2019. ISSN 0022-460X. doi: https://doi.org/10.1016/j.jsv.2019.114863. URL https://www.sciencedirect.com/science/article/pii/S0022460X19304171.

[44] *ABAQUS Online Documentation: Version 6.6-1*. Dassault Systèmes Simulia Corp, United States.

[45] A. Jain, K.N. van Dalen, A.V. Metrikine, A.B. Faragau, and M.J.M.M. Steenbergen. Comparative analysis of the dynamic amplifications due to inhomogeneities at railway transition zones. In J. Pombo, editor, *Proceedings of The Fifth International Conference on Railway Technology: Research, Development and Maintenance*, volume CCC 1 of *Civil-Comp Conferences*, United Kingdom, 2023. Civil-Comp Press. doi: 10.4203/ccc.1.19.1.

[46] A. Jain, A.V. Metrikine, M.J.M.M. Steenbergen, and K.N. van Dalen. Evaluation of a novel mitigation measure for two different types of railway transition zones. In

Proceedings of the Sixth International Conference on Railway Technology: Research, Development and Maintenance, volume 7 of *RAILWAYS 2024*, page 1–11. Civil-Comp Press. doi: 10.4203/ccc.7.17.1.

REFERENCES FOR CHAPTER 8

[1] P Hölscher and P Meijers. Literature study of knowledge and experience of transition zones. *Delft: report*, (415990-0011), 2007.

[2] Buddhima Indraratna, Muhammad Babar Sajjad, Trung Ngo, António Gomes Correia, and Richard Kelly. Improved performance of ballasted tracks at transition zones: A review of experimental and modelling approaches. *Transportation Geotechnics*, 21:100260, December 2019. doi: 10.1016/j.trgeo.2019.100260.

[3] R. Sañudo, L. dell'Olio, J.A. Casado, I.A. Carrascal, and S. Diego. Track transitions in railways: A review. *Construction and Building Materials*, 112:140–157, June 2016. doi: 10.1016/j.conbuildmat.2016.02.084.

[4] André Paixão, Eduardo Fortunato, and Rui Calçada. Transition zones to railway bridges: Track measurements and numerical modelling. *Engineering Structures*, 80: 435–443, December 2014. doi: 10.1016/j.engstruct.2014.09.024.

[5] *Design of Track Transitions*. Transportation Research Board, October 2006. ISBN 9780309436670. doi: 10.17226/23228. URL `http://dx.doi.org/10.17226/23228`.

[6] A. Jain, Andrei V. Metrikine, Michael J.M.M. Steenbergen, and Karel N. van Dalen. Design of railway transition zones: a novel energy-based criterion. *Transportation Geotechnics*, page 101223, 2024. ISSN 2214-3912. doi: https://doi.org/10.1016/j.trgeo.2024.101223. (Note: Included as Chapter 2).

[7] Avni Jain, Yuriy Marykovskiy, Andrei V. Metrikine, and Karel N. van Dalen. Quantifying the impact of stiffness distributions on the dynamic behaviour of railway transition zones. *Transportation Geotechnics*, 45:101211, 2024. ISSN 2214-3912. doi: https://doi.org/10.1016/j.trgeo.2024.101211. (Note: Included as Chapter 6).

[8] A. Jain, A.V. Metrikine, M.J.M.M. Steenbergen, and K.N. van Dalen. Evaluation of a novel mitigation measure for two different types of railway transition zones. In *Proceedings of the Sixth International Conference on Railway Technology: Research, Development and Maintenance*, volume 7 of *RAILWAYS 2024*, page 1–11. Civil-Comp Press. doi: 10.4203/ccc.7.17.1. (Note: Included as Chapter 9).

[9] A. I. Vesnitskii and A. V. Metrikin. Transition radiation in one-dimensional elastic systems. *Journal of Applied Mechanics and Technical Physics*, 33(2):202–207, 1992. ISSN 1573-8620. doi: 10.1007/bf00851588.

[10] Andrei V. Metrikine and A.C.W.M. Vrouwenvelder. Surface ground vibration due to a moving train in a tunnel: Two-dimensional model. *Journal of Sound and Vibration*, 234(1):43–66, June 2000. ISSN 0022-460X. doi: 10.1006/jsvi.1999.2853.

[11] A.V. Metrikine, A.R.M. Wolfert, and H.A. Dieterman. Transition radiation in an elastically supported string. abrupt and smooth variations of the support stiffness. *Wave Motion*, 27(4):291–305, May 1998. ISSN 0165-2125. doi: 10.1016/s0165-2125(97)00055-3.

[12] Karel N. van Dalen and Andrei V. Metrikine. Transition radiation of elastic waves at the interface of two elastic half-planes. *Journal of Sound and Vibration*, 310(3):702–717, 2008. ISSN 0022-460X. doi: https://doi.org/10.1016/j.jsv.2007.06.007.

[13] Karel N. van Dalen, Apostolos Tsouvalas, Andrei V. Metrikine, and Jeroen S. Hoving. Transition radiation excited by a surface load that moves over the interface of two elastic layers. *International Journal of Solids and Structures*, 73-74:99–112, 2015. ISSN 0020-7683. doi: https://doi.org/10.1016/j.ijsolstr.2015.07.001.

[14] H. A. Dieterman and A. Metrikine. Equivalent stiffness of a half-space interacting with a beam. critical velocities of a moving load along the beam. *European Journal of Mechanics, A/Solids*, 15(1):67–90, January 1996. ISSN 0997-7538.

[15] Z. Dimitrovová and A.F.S. Rodrigues. Critical velocity of a uniformly moving load. *Advances in Engineering Software*, 50:44–56, 2012. ISSN 0965-9978. doi: https://doi.org/10.1016/j.advengsoft.2012.02.011. CIVIL-COMP.

[16] Kausel Eduardo, Estaire José, and Crespo-Chacón Inés. Proof of critical speed of high-speed rail underlain by stratified media. *Proceedings of the Royal Society A: Mathematical, Physical and Engineering Sciences*, 476(2240), August 2020. ISSN 1471-2946. doi: 10.1098/rspa.2020.0083.

[17] Z. Dimitrovová and J.N. Varandas. Critical velocity of a load moving on a beam with a sudden change of foundation stiffness: Applications to high-speed trains. *Computers Structures*, 87(19):1224–1232, 2009. ISSN 0045-7949. doi: https://doi.org/10.1016/j.compstruc.2008.12.005. Civil-Comp Special Issue.

[18] William Powrie, Louis Le Pen, David Milne, and David Thompson. Train loading effects in railway geotechnical engineering: Ground response, analysis, measurement and interpretation. *Transportation Geotechnics*, 21:100261, 2019. ISSN 2214-3912. doi: https://doi.org/10.1016/j.trgeo.2019.100261.

[19] Pranjal Mandhaniya, J. T. Shahu, and Sarvesh Chandra. Analysis of dynamic response of ballasted rail track under a moving load to determine the critical speed of motion. *Journal of Vibration Engineering & Technologies*, 11(7):3197–3213, October 2022. ISSN 2523-3939. doi: 10.1007/s42417-022-00741-3.

[20] Pranjal Mandhaniya, J. T. Shahu, and Sarvesh Chandra. An assessment of dynamic impact factors for ballasted track using finite element method and multivariate regression. *Journal of Vibration Engineering & Technologies*, 10(7):2609–2623, April 2022. ISSN 2523-3939. doi: 10.1007/s42417-022-00507-x.

[21] Ana Ramos, Rui Calçada, and António Gomes Correia. Influence of train speed and its mitigation measures in the short- and long-term performance of a ballastless transition zone. *Railway Engineering Science*, 31(4):309–324, July 2023. ISSN 2662-4753. doi: 10.1007/s40534-023-00314-4.

[22] Ana Ramos, António Gomes Correia, and Rui Calçada. Influence of the train speed on the long term performance of the subgrade of the ballasted and ballastless tracks. In Honghua Dai, editor, *Computational and Experimental Simulations in Engineering*, pages 13–25, Cham, 2023. Springer International Publishing.

[23] X Lei and B Zhang. Influence of track stiffness distribution on vehicle and track interactions in track transition. *Proceedings of the Institution of Mechanical Engineers, Part F: Journal of Rail and Rapid Transit*, 224(6):592–604, June 2010. ISSN 2041-3017. doi: 10.1243/09544097jrrt318.

[24] Ricardo Insa, Pablo Salvador, Javier Inarejos, and Alejandro Roda. Analysis of the influence of under sleeper pads on the railway vehicle/track dynamic interaction in transition zones. *Proceedings of the Institution of Mechanical Engineers, Part F: Journal of Rail and Rapid Transit*, 226(4):409–420, December 2011. ISSN 2041-3017. doi: 10.1177/0954409711430174.

[25] Haoyu Wang and Valeri Markine. Corrective countermeasure for track transition zones in railways: Adjustable fastener. *Engineering Structures*, 169:1–14, August 2018. ISSN 0141-0296. doi: 10.1016/j.engstruct.2018.05.004.

[26] Miriam Labrado Palomo, Jesús Herminio Alcañiz Martínez, Adrian Zornoza Arnoa, and Juan José Catalán Medina. Structural and vibration performance in different scenarios of a prefabricated wedge for railway transition zones. *Journal of Vibration Engineering & Technologies*, 9(7):1657–1668, May 2021. ISSN 2523-3939. doi: 10.1007/s42417-021-00319-5.

[27] Miriam Labrado Palomo, Fernando Roca Barceló, Fran Ribes Llario, and Julia Real Herráiz. Effect of vehicle speed on the dynamics of track transitions. *Journal of Vibration and Control*, page 107754631774525, December 2017. ISSN 1741-2986. doi: 10.1177/1077546317745254.

[28] A. Jain, Andrei V. Metrikine, Michael J.M.M. Steenbergen, and Karel N. van Dalen. Railway transition zones: evaluation of existing transition structures and a newly proposed transition structure. *International Journal of Rail Transportation*, 0(0): 1–21, 2023. doi: 10.1080/23248378.2023.2272668. (Note: Included as Chapter 3).

[29] A. Jain, A.V. Metrikine, and K.N. Dalen. Energy redistribution in railway transition zones by geometric optimisation of a novel transition structure. *Transportation Geotechnics*, page 101383, 2024. ISSN 2214-3912. doi: https://doi.org/10.1016/j.trgeo.2024.101383. (Note: Included as Chapter 7).

[30] H E M HUNT. Settlement of railway track near bridge abutments. *Proceedings of the Institution of Civil Engineers - Transport*, 123(1):68–73, February 1997. ISSN 1751-7710. doi: 10.1680/itran.1997.29182.

[31] Jens CO Nielsen, Eric G Berggren, Anders Hammar, Fredrik Jansson, and Rikard Bolmsvik. Degradation of railway track geometry – correlation between track stiffness gradient and differential settlement. *Proceedings of the Institution of Mechanical Engineers, Part F: Journal of Rail and Rapid Transit*, 234(1):108–119, December 2018. ISSN 2041-3017. doi: 10.1177/0954409718819581.

[32] Meysam Banimahd, Peter K. Woodward, Justin Kennedy, and Gabriela M. Medero. Behaviour of train–track interaction in stiffness transitions. *Proceedings of the Institution of Civil Engineers - Transport*, 165(3):205–214, August 2012. ISSN 1751-7710. doi: 10.1680/tran.10.00030.

[33] Jennifer Elizabeth Nicks. *The bump at the end of the railway bridge*, volume 71. 2009.

[34] Avni Jain, Andrei V. Metrikine, Michaël J. M. M. Steenbergen, and Karel N. van Dalen. Dynamic amplifications in railway transition zones: performance evaluation of sleeper configurations using energy criterion. *Frontiers in Built Environment*, 10, 2024. ISSN 2297-3362. doi: 10.3389/fbuil.2024.1285131. (Note: Included as Chapter 4).

[35] A. Jain, Karel N. van Dalen, Andrei V. Metrikine, Andrei B. Faragau, and Michael J.M.M. Steenbergen. Comparative analysis of the dynamic amplifications due to inhomogeneities at railway transition zones. In J. Pombo, editor, *Proceedings of The Fifth International Conference on Railway Technology: Research, Development and Maintenance*, volume CCC 1 of *Civil-Comp Conferences*, United Kingdom, 2023. Civil-Comp Press. doi: 10.4203/ccc.1.19.1.

[36] Mykola Sysyn, Michal Przybylowicz, Olga Nabochenko, and Lei Kou. Identification of sleeper support conditions using mechanical model supported data-driven approach. *Sensors*, 21(11):3609, May 2021. ISSN 1424-8220. doi: 10.3390/s21113609.

[37] A Lundqvist and T Dahlberg. Load impact on railway track due to unsupported sleepers. *Proceedings of the Institution of Mechanical Engineers, Part F: Journal of Rail and Rapid Transit*, 219(2):67–77, March 2005. ISSN 2041-3017. doi: 10.1243/095440905x8790.

[38] Y Bezin, S D Iwnicki, M Cavalletti, E de Vries, F Shahzad, and G Evans. An investigation of sleeper voids using a flexible track model integrated with railway multi-body dynamics. *Proceedings of the Institution of Mechanical Engineers, Part F: Journal of Rail and Rapid Transit*, 223(6):597–607, June 2009. ISSN 2041-3017. doi: 10.1243/09544097jrrt276.

[39] Mykola Sysyn, Olga Nabochenko, and Vitalii Kovalchuk. Experimental investigation of the dynamic behavior of railway track with sleeper voids. *Railway Engineering Science*, 28(3):290–304, August 2020. ISSN 2662-4753. doi: 10.1007/s40534-020-00217-8.

[40] J. Y. Zhu, D. J. Thompson, and C. J.C. Jones. On the effect of unsupported sleepers on the dynamic behaviour of a railway track. *Vehicle System Dynamics*, 49(9):1389–1408, September 2011. ISSN 1744-5159. doi: 10.1080/00423114.2010.524303.

[41] Ryutaro Takahashi, Kimitoshi Hayano, Takahisa Nakamura, and Yoshitsugu Momoya. Integrated risk of rail buckling in ballasted tracks at transition zones and its countermeasures. *Soils and Foundations*, 59(2):517–531, April 2019. ISSN 0038-0806. doi: 10.1016/j.sandf.2018.12.013.

[42] Andrei B. Fărăgău, Traian Mazilu, Andrei V. Metrikine, Tao Lu, and Karel N. vanDalen. Transition radiation in an infinite one-dimensional structure interacting with a moving oscillator—the green's function method. *Journal of Sound and Vibration*, 492:115804, February 2021. ISSN 0022-460X. doi: 10.1016/j.jsv.2020.115804.

[43] *ABAQUS Online Documentation: Version 6.6-1*. Dassault Systèmes Simulia Corp, United States, .

[44] *ABAQUS/Standard User's Manual, Version 6.9*. Dassault Systèmes Simulia Corp, United States, .

[45] Haoyu Wang and Valeri Markine. Dynamic behaviour of the track in transitions zones considering the differential settlement. *Journal of Sound and Vibration*, 459: 114863, 2019. ISSN 0022-460X. doi: https://doi.org/10.1016/j.jsv.2019.114863.

[46] Simon Iwnick. Manchester benchmarks for rail vehicle simulation. *Vehicle System Dynamics*, 30(3–4):295–313, September 1998. ISSN 1744-5159. doi: 10.1080/00423119808969454.

[47] Emil Aggestam, Jens C.O. Nielsen, Karin Lundgren, Kamyab Zandi, and Anders Ekberg. Optimisation of slab track design considering dynamic train–track interaction and environmental impact. *Engineering Structures*, 254:113749, March 2022. ISSN 0141-0296. doi: 10.1016/j.engstruct.2021.113749.

REFERENCES FOR CHAPTER 9

[1] Buddhima Indraratna, Muhammad Babar Sajjad, Trung Ngo, António Gomes Correia, and Richard Kelly. Improved performance of ballasted tracks at transition zones: A review of experimental and modelling approaches. *Transportation Geotechnics*, 21: 100260, December 2019. doi: 10.1016/j.trgeo.2019.100260. URL https://doi.org/10.1016/j.trgeo.2019.100260.

[2] R. Sañudo, L. dell'Olio, J.A. Casado, I.A. Carrascal, and S. Diego. Track transitions in railways: A review. *Construction and Building Materials*, 112:140–157, June 2016. doi: 10.1016/j.conbuildmat.2016.02.084. URL https://doi.org/10.1016/j.conbuildmat.2016.02.084.

[3] A. Jain, Andrei V. Metrikine, Michael J.M.M. Steenbergen, and Karel N. van Dalen. Design of railway transition zones: a novel energy-based criterion. *Transportation Geotechnics*, page 101223, 2024. ISSN 2214-3912. doi: https://doi.org/10.1016/j.trgeo.2024.101223. URL https://www.sciencedirect.com/science/article/pii/S2214391224000448. (Note: Included as Chapter 2).

[4] A. Jain, Andrei V. Metrikine, Michael J.M.M. Steenbergen, and Karel N. van Dalen. Railway transition zones: evaluation of existing transition structures and a newly proposed transition structure. *International Journal of Rail Transportation*, 0(0):1–21, 2023. doi: 10.1080/23248378.2023.2272668. (Note: Included as Chapter 3).

[5] A. Jain, Andrei V. Metrikine, Michael J.M.M. Steenbergen, and Karel N. van Dalen. Dynamic amplifications in railway transition zones: performance evaluation of sleeper configurations using energy criterion. *Frontiers in Built Environment*, 2024. (Note: Included as Chapter 4).

[6] Avni Jain, Yuriy Marykovskiy, Andrei V. Metrikine, and Karel N. van Dalen. Quantifying the impact of stiffness distributions on the dynamic behaviour of railway transition zones. *Transportation Geotechnics*, 45:101211, 2024. ISSN 2214-3912. doi: https://doi.org/10.1016/j.trgeo.2024.101211. URL https://www.sciencedirect.com/science/article/pii/S2214391224000321. (Note: Included as Chapter 6).

[7] Avni Jain, Andrei V. Metrikine, and Karel N. van Dalen. Energy redistribution in railway transition zones by geometric optimisation of a novel transition structure. 2024. doi: 10.2139/ssrn.4830921. URL http://dx.doi.org/10.2139/ssrn.4830921. (Note: Included as Chapter 7).

REFERENCES FOR CHAPTER 10

[1] Fernando Pardo de Santayana, José Estaire Gepp, and José Luis García de la Oliva. Activities of the laboratorio de geotecnia – cedex in railway engineering. https://www.capacity4rail.eu/IMG/pdf/21_cedex_lab_geotecrailwayactivities.pdf. [Accessed 10-07-2024].